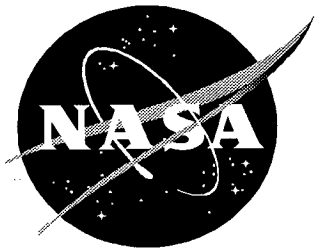

NASA Technical Memorandum 4649

Low-Speed Wind-Tunnel Investigation of the Stability and Control Characteristics of a Series of Flying Wings With Sweep Angles of 60°

Thomas M. Moul
Langley Research Center • Hampton, Virginia

Scott P. Fears
Lockheed Engineering & Sciences Company • Hampton, Virginia

Holly M. Ross and John V. Foster
Langley Research Center • Hampton, Virginia

National Aeronautics and Space Administration
Langley Research Center • Hampton, Virginia 23681-0001

August 1995

Available electronically at the following URL address: http://techreports.larc.nasa.gov/ltrs/ltrs.html

Printed copies available from the following:

NASA Center for AeroSpace Information
800 Elkridge Landing Road
Linthicum Heights, MD 21090-2934
(301) 621-0390

National Technical Information Service (NTIS)
5285 Port Royal Road
Springfield, VA 22161-2171
(703) 487-4650

Summary

A wind-tunnel investigation was conducted in the Langley 12-Foot Low-Speed Tunnel to study the low-speed stability and control characteristics of a series of four flying wings over an extended range of angle of attack (–8° to 48°). Because of the current emphasis on reducing the radar cross section (RCS) of new military aircraft, the planform of each wing was composed of lines swept at a relatively high angle of 60°, and all the trailing-edge lines were aligned with one of the two leading edges. Three arrow planforms with different aspect ratios and one diamond planform were tested. The models incorporated leading-edge flaps for improved pitching-moment characteristics and lateral stability and had three sets of trailing-edge flaps that were deflected differentially for roll control, symmetrically for pitch control, and in a split fashion for yaw control. Top bodies of three widths and twin vertical tails of various sizes and locations were also tested on each model. A large aerodynamic database was compiled that could be used to evaluate some of the trade-offs involved in the design of a configuration with a reduced RCS and good flight dynamic characteristics.

The results of the investigation indicate that the three arrow wings experienced a pitch-up that became more severe as aspect ratio was increased. This pitch-up could be reduced by deflecting the leading-edge flaps. When deflected symmetrically, the trailing-edge flaps produced relatively small pitching moments on all the wings. These pitch-control increments were more linear with deflection angle in the nose-up direction than in the nose-down direction. Also, the nose-down control effectiveness was less than the nose-up effectiveness at the higher angles of attack. Although all the configurations would require small changes in longitudinal stability, each of them could be statically trimmed at angles of attack up to maximum lift by using the inboard and middle flaps together. However, additional control power may be needed to provide a control margin for dynamic situations such as maneuvering or countering turbulence. Another limit on the trim capability of these wings may be imposed by the need to budget the amount of flap deflection available for each type of control (pitch, roll, or yaw). The combination of pitch-up and reduced nose-down control effectiveness resulted in a hung stall (trim condition at which there is insufficient nose-down control for recovery) for some of the configurations.

When the vertical tails were not used, each of the wings exhibited neutral or unstable directional stability for most of the angles of attack tested. These configurations were laterally stable at low and high angles of attack, but the three arrow wings typically exhibited a region of lateral instability near maximum lift. Directional and lateral stability were both improved when the twin vertical tails were added, and lateral stability was also improved by leading-edge flap deflections. In general, directional and lateral stability were both reduced by adding the wide top body.

The trailing-edge flaps were deflected differentially for roll control and were split on one side for yaw control. Differential deflections of the outboard trailing-edge flaps produced less adverse yaw than the middle flaps and thus were an attractive candidate for primary roll control. The roll control of a configuration could be increased by deflecting more than one set of trailing-edge flaps. The side force produced by split deflection of the trailing-edge flaps was highly dependent on the direction of the sweep of the flap hinge line. On the forward-swept outboard flaps, the side force produced a yawing-moment increment that opposed the yawing moment produced by the drag of the flap. In contrast, the side force generated by split deflection of the rearward-swept middle flaps produced yawing-moment increments in the same direction as the drag, and the middle flaps therefore provided more effective yaw control than the outboard flaps. Deflection of the all-moving twin vertical tails was significantly more effective at providing yaw control for the diamond wing than for the three arrow wings.

Introduction

Recent advances in low-observables technology, which increase the effectiveness and survivability of military aircraft, have strongly influenced most new designs. When attempting to achieve low observability, some or all of the aircraft signatures (radar, infrared, visual, or acoustic) may be considered, depending on mission requirements. One primary method of reducing radar observability is to decrease the radar cross section (RCS) of the aircraft by appropriately tailoring the external contours of the configuration. However, when these reduced-RCS shaping constraints are emphasized, the resulting aircraft may have an unconventional forebody shape, wing planform, or tail geometry. Each of these design features can have a large influence on the stability and control characteristics of a configuration; thus, a potential conflict exists between achieving a reduced RCS and achieving good flight dynamic characteristics. If the aircraft is a fighter, effective maneuverability during close-in engagements will require good stability and control characteristics for angles of attack up to and beyond maximum lift. As a result, designers will be required to balance the attributes of maneuverability and low observability to create a fighter that will be successful in both close-in and beyond-visual-range engagements. For other types of aircraft, the stability and control requirements may be less stringent, and the

designs may be more strongly influenced by low-observability considerations.

This study consists of an investigation of flying wing candidates for aircraft with reduced RCS. The wing planforms have highly swept leading and trailing edges, with the trailing edges aligned with one of the two leading edges (fig. 1). The wings are divided into three groups corresponding to the sweep angles of the leading and trailing edges (50°, 60°, and 70°). Each group consists of a diamond planform and three arrow planforms of different aspect ratio (fig. 2). As a result of the high sweep angles, some of the planforms are somewhat unconventional in appearance.

This report presents the results of a static low-speed wind-tunnel investigation of the group of flying wings with sweep angles of 60°. The results for the wings with sweep angles of 50° are reported in reference 1, and the results for the wings with sweep angles of 70° are reported in reference 2. Tests were conducted to determine the low-speed stability and control characteristics of the basic wing planforms over a wide range of angle of attack. In addition, a number of different control concepts, a broad matrix of control settings, differences in top body width, and variations in vertical tail size and location were also tested. The data obtained on these wing planforms contribute to an aerodynamic database that could be used in defining some of the trade-offs associated with designing for both reduced RCS and good stability and control characteristics.

Symbols

All longitudinal forces and moments are referred to the stability-axis system, and all lateral-directional forces and moments are referred to the body-axis system (fig. 1). The longitudinal location of the moment reference center (MRC) varied among the different wings. This position was chosen such that each configuration would have neutral longitudinal stability at low angles of attack when all the controls were undeflected (table I). The MRC vertical position was fixed at 1.87 in. (3.7 percent of the root chord) below the wing horizontal plane on all the configurations. The total planform area (table I) was used to nondimensionalize the force and moment data.

b wingspan, ft

C_D drag coefficient, $\frac{\text{Drag force}}{\bar{q}S}$

C_L lift coefficient, $\frac{\text{Lift force}}{\bar{q}S}$

C_l rolling-moment coefficient, $\frac{\text{Rolling moment}}{\bar{q}Sb}$

C_m pitching-moment coefficient, $\frac{\text{Pitching moment}}{\bar{q}S\bar{c}}$

C_n yawing-moment coefficient, $\frac{\text{Yawing moment}}{\bar{q}Sb}$

C_Y side-force coefficient, $\frac{\text{Side force}}{\bar{q}S}$

$\bar{c}$ mean aerodynamic chord (based on entire planform), ft

$\bar{q}$ free-stream dynamic pressure, lb/ft^2

S reference area (based on entire planform), ft^2

X, Y, Z longitudinal, lateral, and vertical body axis, respectively

α angle of attack, deg

β angle of sideslip, deg

ΔC_l incremental rolling-moment coefficient, $C_{l,\text{control deflected}} - C_{l,\text{control undeflected}}$

ΔC_n incremental yawing-moment coefficient, $C_{n,\text{control deflected}} - C_{n,\text{control undeflected}}$

ΔC_Y incremental side-force coefficient, $C_{Y,\text{control deflected}} - C_{Y,\text{control undeflected}}$

$\delta_{a,\text{IB}}$ differential deflection angle of inboard trailing-edge flaps based on equal and opposite deflection, positive with trailing edge down on right wing, measured normal to hinge line, deg

$\delta_{a,\text{MID}}$ differential deflection angle of middle trailing-edge flaps based on equal and opposite deflection, positive with trailing edge down on right wing, measured normal to hinge line, deg

$\delta_{a,\text{OB}}$ differential deflection angle of outboard trailing-edge flaps based on equal and opposite deflection, positive with trailing edge down on right wing, measured normal to hinge line, deg

δ_{bf} symmetric deflection angle of body flaps, positive with trailing edge down, measured normal to hinge line, deg

$\delta_{f,\text{IB}}$ symmetric deflection angle of inboard trailing-edge flaps, positive with trailing edge down, measured normal to hinge line, deg

$\delta_{f,\text{MID}}$ symmetric deflection angle of middle trailing-edge flaps, positive with trailing edge down, measured normal to hinge line, deg

$\delta_{f,\text{OB}}$ symmetric deflection angle of outboard trailing-edge flaps, positive with trailing edge down, measured normal to hinge line, deg

δ_{LEF} leading-edge flap deflection angle, positive with leading edge down, measured normal to hinge line, deg

δ_r symmetric vertical tail deflection angle, positive with trailing edge left, deg

$\delta_{s,\,MID}$ split deflection angle of middle trailing-edge flaps, positive when deployed on left wing, measured normal to hinge line, deg

$\delta_{s,\,OB}$ split deflection angle of outboard trailing-edge flaps, positive when deployed on left wing, measured normal to hinge line, deg

Derivatives:

C_{l_β} lateral stability parameter, $\frac{\partial C_l}{\partial \beta}$, $\frac{(C_l)_{\beta=5} - (C_l)_{\beta=0}}{5°}$, per deg

C_{n_β} directional stability parameter, $\frac{\partial C_n}{\partial \beta}$, $\frac{(C_n)_{\beta=5} - (C_n)_{\beta=0}}{5°}$, per deg

C_{Y_β} side-force parameter, $\frac{\partial C_Y}{\partial \beta}$, $\frac{(C_Y)_{\beta=5} - (C_Y)_{\beta=0}}{5°}$, per deg

Abbreviations:

MRC moment reference center

RCS radar cross section

Model Description

Four flying-wing models (three arrow-wing planforms and one diamond planform) with leading- and trailing-edge sweep angles of 60° (fig. 2) were tested. Given the relatively high sweep angle, initial sizing analysis indicated that arrow wings with aspect ratios between 2.0 and 3.0 could produce viable configurations. As a result, aspect ratios of 3.0 (Wing 1), 2.5 (Wing 2), and 2.0 (Wing 3) were chosen for the arrow planforms (figs. 3 to 5). Unlike the aerodynamic data that were nondimensionalized with the entire planform area, these aspect ratios were computed by using the trapezoidal areas shown in figure 2(b). For Wing 1, the three aftmost points on the planform extended back the same distance (fig. 3). During formulation of the remaining planforms, the overall length was held constant, and the trapezoidal areas of Wings 2 and 3 were made approximately equal to that of Wing 1. Consequently, as aspect ratio was decreased on the arrow wings, the span was reduced and the tip chord was increased to maintain approximately the same trapezoidal area. The dimensions of the diamond wing (fig. 6) were dictated by the overall length and the leading- and trailing-edge sweep angles, and this wing had a resulting aspect ratio of 1.15. From a geometric point of view, the arrow planforms can be considered to be built up from the diamond planform by the addition of outboard panels having the same sweep angles as the diamond planform (fig. 2). Flat plate models of the basic planforms were constructed from 3/4-in. plywood, and the leading and trailing edges were beveled at a 9° half-angle. Table I shows the geometric characteristics for each wing.

All four wings incorporated leading-edge flaps for improved longitudinal characteristics and increased roll stability at high angles of attack. The chord length of these flaps was the same for all the wings, and the hinge line was located along the wing leading-edge bevel line (fig. 2). These flaps were tested at deflection angles of 15°, 30°, and 45°. There were three sets of trailing-edge flaps, designated inboard (IB), middle (MID), and outboard (OB), on each wing for roll, pitch, and yaw control (figs. 3 to 6). For the arrow wings, the chord length of the trailing-edge flaps was 30 percent of the distance between the leading and trailing edges on the outboard section of the wing. For the diamond wing, the trailing-edge flaps had the same chord length as those on the arrow wing with the lowest aspect ratio (Wing 3). The total trailing-edge flap area was approximately 18 percent of the wing area for each of the wings. The trailing-edge flaps were deflected symmetrically (–30°, –15°, 15°, and 30°) for pitch control and differentially (–15° and –30°) for roll control. Split deflection of these flaps (to be discussed subsequently) was examined as a means to provide yaw control.

To provide supplemental nose-down pitch control, body flaps were tested using model parts constructed of sheet metal (fig. 7). The body flaps were mounted on the underside of the wing inboard of the trailing-edge flaps. The inboard corners of the undeflected body flaps were positioned on the centerline with their hinge line coinciding with the hinge line of the trailing-edge flaps (fig. 8). A symmetric downward deflection of 69° was tested on each wing. The sheet metal part modeled the bottom surface of a beveled body flap (fig. 8). Because these models had a trailing-edge bevel half-angle of 9°, the 60° bend in the sheet metal part represented a 69° deflection of the simulated beveled flap (fig. 8).

As noted previously, split deflections of the trailing-edge flaps to provide yaw control were tested. This concept involves a given flap separating into top and bottom halves such that the top half deflects upward and the bottom half deflects downward. These deflections would be made on either the right wing or the left wing, thereby creating an unbalanced drag force and an associated yawing moment. During these tests, sheet metal pieces were

mounted on the underside of the wing beneath the middle or outboard trailing-edge flaps to represent the lower half of a split deflection. The upper half was simulated by deflecting the trailing-edge flap upward at the same angle (fig. 9). The tested deflection angles (39°, 69°, and 84°) were measured similar to the body flap deflection angles. For the arrow wings (Wings 1, 2, and 3), the split trailing-edge flaps were tested on the right wing. For the diamond wing (Wing 4), the split deflections were tested on the left wing.

Three top body shapes were tested on the upper surface of each wing in conjunction with a single bottom body that covered the balance (fig. 10). A photograph of the bodies is shown in figure 11. Some testing was done without a top body, but the bottom body was always on the wing to shield the balance from the airflow. The length and height of the top bodies were kept constant, but the width was varied to obtain the three top shapes (wide, medium, and narrow). The resulting cross-sectional shapes were semielliptical for the wide and narrow bodies and semicircular for the medium body (fig. 10). When installed, the front tip of the top bodies was 5 in. (9.9 percent of the root chord) aft of the leading edge of the wing, and the rear tip was the same distance forward of the wing trailing edge. The front tip of the bottom body was also 5 in. behind the leading edge, and the rear tip was 15.5 in. (30.7 percent of the root chord) forward of the wing trailing edge.

Three sets of vertical tails (small, medium, and large) were tested (fig. 12). The planform of each tail was a 30°-60°-90° triangle with the leading edge swept 60° (fig. 13). The tails were sized such that the large tail had twice the area of the medium tail and four times the area of the small tail (table I). They were mounted in a twin tail configuration with zero cant and toe angle, and were deflected as all-moving tails for directional control about a vertical axis located at one-half the vertical tail root chord. On some reduced-RCS aircraft (F-117, YF-22, and YF-23), the tails are canted to reduce their contributions to the total aircraft RCS. However, during this study, the tails were uncanted so that the maximum levels of directional stability and control available from the triangular planforms could be determined. On Wing 1, all three tails were tested at an inboard location, and only the small tails were tested in an outboard location (fig. 14). The inboard location was longitudinally positioned so that the aftmost point of the small tail was located over the hinge line of the inboard trailing-edge flap. The medium and large tails were mounted such that the rotation point was in the same location as for the small tails. The outboard location was longitudinally positioned so that the aftmost point of the small tail was at the juncture of the hinge lines of the middle and outboard trailing-edge flaps. For Wings 2, 3, and 4, only the medium tails were tested at the inboard location (fig. 15).

Test Techniques and Conditions

The aerodynamic testing was performed in the Langley 12-Foot Low-Speed Tunnel. The model and balance were mounted in the test section on a sting and C-strut arrangement (fig. 16). Figures 17 to 20 show photographs of the four wings mounted in the test section with the wide top body attached. The tests were conducted at a free-stream dynamic pressure of 4 lb/ft^2, which corresponds to a test Reynolds number of 0.88×10^6 for Wing 1, 0.92×10^6 for Wing 2, 0.96×10^6 for Wing 3, and 1.03×10^6 for Wing 4 based on the mean aerodynamic chord of each wing. A six-component, internally mounted strain gauge balance was used to measure the aerodynamic loads. The static force and moment data were measured over an angle-of-attack range of −8° to 48° and over a sideslip range of −15° to 15°. The data at sideslip angles of 0° and 5° were used to calculate the lateral-directional stability derivatives (C_{l_β}, C_{n_β}, and C_{Y_β}) by means of a linear calculation between these two angles. Flow upwash corrections were included during the angle-of-attack calibration, but no corrections were made for flow sidewash, wall effects, or test section blockage.

Results and Discussion

Longitudinal Stability Characteristics

The longitudinal stability characteristics of the four flying wings are presented in the following figures.

Wing planform. Comparisons of the longitudinal characteristics of the four wings with various leading-edge flap deflections and top bodies are presented in figures 21 to 24. In general, the maximum lift coefficient for these wings was about 1.1, which occurred at an angle of attack of approximately 32° for the arrow wings (Wings 1, 2, and 3) and about 36° for the diamond wing (Wing 4). The lift curve slopes of the arrow wings (trapezoidal aspect ratios of 3.0, 2.5, and 2.0) were similar and higher than the lift curve slope of the diamond wing (aspect ratio of 1.15). Consequently, the arrow wings produced more lift at a given angle of attack than the diamond wing for angles of attack below maximum lift.

As mentioned previously, the moment reference centers were chosen so that each configuration with the wide top body on (fig. 23) would have neutral longitudinal stability at angles of attack near 0° when all the controls were undeflected. The arrow wings experienced a pitch-up for angles of attack between 10° and 20° (depending on planform and leading-edge flap deflection), that became larger as the aspect ratio was increased. For these planforms, larger aspect ratios were obtained by adding outboard wing panels of increasing size to the basic diamond shape. Previous studies have shown that the onset of separation on the outboard portions of swept wings can result in a pitch-up (refs. 3 and 4), and that these effects will be more pronounced when the outboard portions of the swept wings are located farther behind the moment reference center. For these reasons, the wings with the higher aspect ratios were more susceptible to pitch-up effects because the outboard portions of the wings were larger and further aft. In contrast, the diamond wing, which did not have these outboard wing panels, actually experienced a slight pitch-down at comparable angles of attack.

Top bodies. The effect of the various top bodies (fig. 10) on the longitudinal characteristics of the different wings is shown in figures 25 to 32. With the leading-edge flaps undeflected, the models were tested with the top body off and with the wide top body on (figs. 25 to 28). Adding the wide top body reduced lift for angles of attack just below maximum lift, but the angle of attack for maximum lift was slightly increased. Adding the wide top body also resulted in a nose-down increment in pitching moment, and this effect was intensified with increases in wing aspect ratio.

With the leading-edge flaps deflected 45°, the models were tested with each of the three top bodies and with the top body removed (figs. 29 to 32). In general, the effects of the top bodies for $\delta_{LEF} = 45°$ were similar to, but smaller in magnitude than those for $\delta_{LEF} = 0°$. As the width of the top body was increased, the nose-down pitching-moment increment increased. These effects were most noticeable for the higher aspect ratios.

Leading-edge flaps. The effect of deflections of the leading-edge flaps on the longitudinal characteristics of the different wings is shown in figures 33 to 40. Data are shown for the four planforms with the top body removed in figures 33 to 36 and with the wide top body on in figures 37 to 40. For the arrow wings, the data show some typical effects of leading-edge flap deflections. Deflections of these flaps increased the angle of attack for maximum lift (ref. 5), but they resulted in lift losses at the lower angles of attack, where they caused the flow to separate from the lower surface of the wing. On an actual aircraft, these lift losses would be minimized by appropriately scheduling the leading-edge flap deflections with angle of attack. For the diamond wing, leading-edge flap deflections generally degraded lift throughout the tested angle-of-attack range because they most likely reduced any vortex lift that the diamond wing was experiencing.

The most significant longitudinal effect of deflecting the leading-edge flaps was an expected reduction in the pitch-up that occurred over a large range of angle of attack on each of the wings. Leading-edge flap deflections reduced the pitch-up by improving the flow over the upper surfaces of the wings at the higher angles of attack and thereby reducing the tendency of the flow to separate. As a result, the onset of separation on the outboard portions of the wings occurred at a higher angle of attack, and the pitch-up was delayed.

Vertical tails. Figures 41 to 44 show the effect of the twin medium vertical tails (figs. 13 to 15) on the

longitudinal characteristics of the four configurations with the narrow top body on and the leading-edge flaps deflected 45°. Adding the medium vertical tails reduced lift coefficient near maximum lift for each of the wings. This lift reduction was possibly due to the tails interfering with the leading-edge vortical flow on the wing upper surfaces, causing these vortices to burst earlier. A flow field investigation (flow visualization, laser Doppler velocimeter, pressure measurements, etc.) would be required to make this determination.

The effects of changes in tail size were tested on Wing 1 by mounting the different tails at the inboard location (figs. 13 and 14). As shown in figure 45, all three tails reduced lift coefficient near maximum lift, and this effect was intensified as vertical tail size increased.

In addition to the inboard location, the small vertical tails were also mounted in an outboard location on Wing 1 (fig. 14). Figure 46 shows the effects of the location of the small tails on the longitudinal characteristics. The small tails did not result in as large a reduction in lift in the outboard location as they did in the inboard location. If the tails were interfering with the leading-edge vortices on the wing upper surfaces, this result would indicate that moving the tails outboard would position them farther from the paths of the vortices, thereby diminishing their effects on these vortices.

Longitudinal Control Characteristics

The longitudinal control characteristics of the four flying wings are presented in the following figures.

Inboard trailing-edge flaps. The longitudinal control effectiveness of symmetric deflections of the inboard trailing-edge flaps is presented in figures 47 to 52. For many of the cases, trailing-edge-down deflections (subsequently called nose-down deflections because they produce nose-down pitching-moment increments) were somewhat more effective than trailing-edge-up (nose-up) deflections at the lower angles of attack. In contrast, the nose-down effectiveness was reduced to negligible values at the higher angles of attack, where the nose-up deflections became more effective. These results indicated a potential pitch-up problem for some of these configurations. The aforementioned conditions can result in a deep stall, stable trim condition (fig. 47) where adequate nose-down control is not available for recovery (hung stall). The lack of linearity of these controls with deflection angle is illustrated in the intermediate deflection angles shown in figure 49 for Wing 1 where a 15° deflection provided almost as much control effectiveness as a 30° deflection. A comparison of figures 47 and 49 indicates that adding the wide top body to Wing 1 reduced the effectiveness of the inboard trailing-edge flaps for angles of attack up to maximum lift. This result is thought to occur because the wide body, located in front of the inboard trailing-edge flaps (fig. 10), interfered with the flow over the flaps and reduced their effectiveness.

Middle trailing-edge flaps. Figures 53 to 58 show the longitudinal control effectiveness of symmetric deflections of the middle trailing-edge flaps. Unlike the inboard flaps, the nose-up and nose-down control effectiveness of the middle flaps for the arrow wings was similar at the lower angles of attack. At lower angles of attack, nose-down deflections of the middle flaps were more effective than nose-up deflections for the diamond wing. However, as with the inboard flaps, the nose-down control effectiveness of the middle flaps was reduced to small levels at the higher angles of attack for all the wings. On Wing 1 (fig. 55), intermediate nose-up deflections of the middle flaps produced linear control effectiveness, but nose-down deflections did not. For the

arrow wings with the wide body on, the middle flaps (figs. 55 to 57) were more effective than the inboard flaps (figs. 49 to 51) at angles of attack below about 24°. This is attributed to the larger size and longer longitudinal moment arm of the middle flaps. In contrast, the middle flaps on the diamond wing were not as effective as the inboard flaps, despite their similar size, because the moment arm of the middle flaps was shorter.

Inboard and middle trailing-edge flaps. The longitudinal control effectiveness produced when the inboard and middle trailing-edge flaps were deflected symmetrically is shown in figures 59 to 62. The nose-up control effectiveness and the nose-down control effectiveness produced by the multiple deflections were fairly similar at the lower angles of attack for the arrow wings. However, as noted previously for the individual deflections, the nose-down control was reduced at the higher angles of attack. On Wings 2 and 3, intermediate multiple deflections showed that the nose-up control was linear with deflection angle. However, the nose-down control was not linear, and most of the available effectiveness was generated by the 15° deflection. This indicates that large downward flap deflection angles most likely caused the flow over the upper surfaces of the flaps to separate, reducing their effectiveness. As noted previously for the individual flap deflections on the diamond wing, the nose-down control was higher at the lower angles of attack, and the nose-up control was greater at the higher angles of attack.

The longitudinal control effectiveness produced by multiple deflections of the inboard and middle trailing-edge flaps was not very large, despite the movement of a significant portion of the total wing area allocated for controls. Even so, if the longitudinal stability of Wings 2, 3, and 4 was decreased slightly, these wings could be statically trimmed up to maximum lift. For Wing 1 to be trimmable up to maximum lift, a slight increase in stability would be required to eliminate the hung stall trim point ($\alpha = 44°$). If dynamic factors are considered, more pitch control power may be needed to provide these wings with a control margin for use during situations such as maneuvering or countering turbulence (ref. 6). An additional limit on the trim capability of these wings may be imposed by the need to budget the amount of flap deflection available for each type of control (pitch, roll, or yaw). If some portion of the total flap travel must be reserved for roll or yaw control, the remaining amount available for pitch control will be less than the maximum, and the trim capability will be correspondingly reduced.

Outboard trailing-edge flaps. Isolated symmetric deflections of the outboard trailing-edge flaps were tested on Wing 3 only (fig. 63). The nose-down deflections became ineffective at a lower angle of attack (20°) than for any of the previously discussed flap deflections. In contrast, the nose-up deflections remained effective over the entire test angle-of-attack range, and the nose-up control effectiveness was linear with deflection angle. At angles of attack below about 24°, the outboard flaps were more effective than the inboard flaps (fig. 51) but not quite as effective as the middle flaps (fig. 57). These results were due primarily to the relationship between flap area and moment arm for the three control surfaces (fig. 5).

Maximum nose-down control. In addition to the trailing-edge flaps, each configuration also had body flaps on the bottom surface of the wing (fig. 8) that were intended to provide supplemental nose-down pitch control. The body flaps were tested in combination with nose-down deflections of the trailing-edge flaps, and the data are presented in figures 64 to 68. Small nose-down pitching moments were obtained by deflecting the body flaps down 69°. These increments were nearly constant over the test angle-of-attack range. The outboard trailing-edge flaps provided additional nose-down increments for the arrow wings at the lower angles of attack. For the diamond wing, a positive (nose-down) deflection of the outboard trailing-edge flaps actually produced a small nose-up pitching-moment increment. Because isolated symmetric deflections of the outboard trailing-edge flaps were not tested on the diamond wing, the cause of this result is unknown.

Lateral-Directional Stability Characteristics

The lateral-directional stability characteristics of the four flying wings are presented in the following figures.

Sideslip. The lateral-directional force and moment coefficients of the four wings with the wide top body on are presented in figures 69 to 84 as a function of sideslip at various angles of attack and leading-edge flap settings. When the leading-edge flaps were undeflected, the coefficients were generally a linear function of the sideslip angle at angles of attack of 0°, 12°, and 48°. At the intermediate angles of attack (16°, 20°, and 32°), where some portion of the wings was probably experiencing separated flow, the variations in the lateral-directional coefficients with sideslip were nonlinear. When the leading-edge flaps were deflected 45°, the flow over the wings was most likely improved at the intermediate angles of attack, and the lateral-directional coefficients became more linear at angles of attack of 16° and 20°. Deflecting the leading-edge flaps caused an expected separation of the flow from the lower surfaces of the wings at very low angles of attack, which accounted for the small nonlinearities in the lateral-directional coefficients at an angle of attack of 0°.

Wing planform. Comparisons of the lateral-directional stability characteristics (computed between sideslip angles of 0° and 5°) of the four wings with various leading-edge flap deflections and top bodies are presented in figures 85 to 88. Note that the data are for the configurations without vertical tails, and therefore each of these wings possessed unstable or essentially neutral values of directional stability (C_{n_β}) for most of the angles of attack tested.

Each of the wings was laterally stable (negative C_{l_β}) at the lower angles of attack and at the higher angles of attack above maximum lift, but most of these configurations exhibited significantly reduced lateral stability in a region just below maximum lift. This phenomenon is a well-documented characteristic of highly swept wings that is due primarily to asymmetric breakdown of the wing leading-edge vortices at sideslip conditions (ref. 7). At angles of attack below approximately 8° and above approximately 40°, the lateral stability was only slightly affected by changes in wing planform. However, between these angles of attack, changes in wing planform caused large variations in lateral stability that were dependent on the top body and on the leading-edge flap deflection. In fact, many of the arrow-wing configurations exhibited a region of lateral instability of significant magnitude somewhere within this range of angle of attack. In contrast, the diamond wing was laterally stable for almost all the positive angles of attack tested. In general, the diamond wing was the most laterally stable of the four wings. These results indicate that the outboard panels added to the basic diamond planform to create the arrow wings contributed to the lateral instabilities.

Top bodies. The effect of the various top bodies (figs. 10 and 11) on the lateral-directional stability characteristics of the four wings is shown in figures 89 to 96. With the leading-edge flaps undeflected, the wings were tested with the top body off and with the wide top body on (figs. 89 to 92). Each of the top bodies (wide,

medium, and narrow) was tested on the wings when the leading-edge flaps were deflected 45° (figs. 93 to 96).

When the leading-edge flaps were undeflected, addition of the wide top body reduced directional stability for most of the angles of attack tested with the largest stability loss occurring at angles of attack between approximately 20° and 40°. When the leading-edge flaps were deflected, the effects of the wide top body on the directional stability of the arrow wings were greatly reduced.

Adding the wide top body also significantly reduced lateral stability for all four wings when the leading-edge flaps were undeflected. The resulting reductions in lateral stability were particularly high for angles of attack between 16° and 40°. When the leading-edge flaps were deflected 45°, the wide and medium bodies produced minimal changes in lateral stability, but adding the narrow top body resulted in a region of lateral instability at angles of attack between approximately 28° and 40° for all four wings. The changes in lateral and directional stability produced by the various bodies indicated that the top bodies affected the separation patterns of the flow on the upper surfaces of the wings.

Leading-edge flaps. The effect of leading-edge flap deflections on the lateral-directional stability characteristics of the four wings is shown in figures 97 to 104. Data are shown for the four planforms with the top body removed in figures 97 to 100 and with the wide top body on in figures 101 to 104. With the top body off, leading-edge flap deflections had minor effects on directional stability for all four planforms. With the wide top body on, leading-edge flap deflections reduced directional instability for angles of attack between approximately 20° and 36°.

For both the body off and the wide body on, deflections of the leading-edge flaps generally improved lateral stability at the intermediate angles of attack. These improvements consisted of a reduction in the maximum level of lateral instability, a decrease in the range of angle of attack where the instability occurred, or an increase in the angle of attack where the configuration became unstable. As a result, most of the arrow wing configurations with the wide body on were laterally stable throughout the angle-of-attack range when the maximum leading-edge flap deflection (45°) was used. In general, these improvements increased with increases in deflection angle. The diamond wing was laterally stable throughout the angle-of-attack range with and without the wide top body on. At the lower angles of attack, leading-edge flap deflections actually reduced lateral stability for some of the configurations. Deflections of these flaps would be scheduled with angle of attack on an actual aircraft, thereby minimizing this detrimental effect. (See "Leading-edge flaps," p. 5.)

Vertical tails. The effect of the twin medium vertical tails (figs. 12 to 15) on the lateral-directional stability characteristics of the four wings with the narrow body on is shown in figures 105 to 108. Use of the narrow body for the tails-on testing enabled the tails to be deflected through larger angles before they interfered with the body. The leading-edge flaps were deflected 45° for all the tails-on testing.

Adding the medium tails caused an expected increase in directional stability on each of the four wings that was relatively invariant at angles of attack below approximately 40°. The effect of the tails on lateral stability was more varied. Even though they produced side forces and yawing moments, adding the tails did not significantly change the lateral stability of the arrow wings at angles of attack below 16° (figs. 105 to 107). The presence of the vertical tails probably caused an induced load on the aft sections of the wing because of an end plate effect (ref. 8). This induced load would result in a rolling moment in the opposite direction to the rolling moment generated by the vertical tails in sideslip. Because these two rolling moments are typically of similar magnitudes, they tend to cancel each other; so adding the tails has minimal effect on the lateral stability at the lower angles of attack. For the diamond wing (fig. 108), the vertical tails increased lateral stability at these lower angles of attack. The tails produced larger changes in lateral stability on this wing because the induced loads were most likely smaller on the diamond planform. At angles of attack between 28° and 40°, adding the tails significantly reduced lateral instability for all the wings. This lateral instability was shown previously to exist when the narrow body was used. These beneficial lateral stability effects could possibly be attributed to a favorable interference effect produced by the vertical tails. The tails were most likely obstructing any vortex flow on the upper surfaces of the wings at the higher angles of attack, and they thereby improved the lateral stability by causing a more symmetric bursting of these vortices. This premise is supported by the previously discussed losses in maximum lift that resulted when the vertical tails were added to the wings (figs. 41 to 44).

Three tail sizes with similar planforms were tested at the inboard location on Wing 1 (figs. 12 to 14). Figure 109 shows the effects of tail size on the lateral-directional stability characteristics. As would be expected, adding the small tails provided a slightly smaller increase in directional stability than adding the medium tails. The large tails produced larger side forces but provided only minimal increases in directional stability compared with the medium tails for most of the

angles of attack tested. The reason for this result was not determined during this study. Because of the induced effects previously discussed, changes in tail size did not affect lateral stability at the lower angles of attack. At the higher angles of attack, changes in tail size did not significantly alter the ability of the tail to produce a favorable vortex-interference effect, and each set of tails produced similar reductions in the lateral instability between angles of attack of 28° and 40°.

As discussed previously, the small vertical tails were mounted on Wing 1 in both inboard and outboard locations (fig. 14). Figure 110 shows the effect of the location of the small tails on the lateral-directional stability characteristics of Wing 1. At the inboard location, the small tails provided a greater increase in directional stability than in the outboard location for most of the angles of attack tested, even though the outboard location had a longer directional moment arm. This is probably because the flow at the outboard location was more spanwise than the flow at the inboard location, and this spanwise component of the flow reduced the effectiveness of the tails in the outboard location. In the outboard location, the small tails significantly increased lateral stability at the angles of attack between 12° and 32°.

Lateral Control Characteristics

The lateral control characteristics of the four flying wings are presented in the following figures.

The lateral controls tested on these wings consisted of differential deflections of the inboard, middle, and outboard trailing-edge flaps. Figures 111 to 116 show the lateral control effectiveness of the various trailing-edge flaps for each of the wings with the leading-edge flap deflected 45° and the wide top body on. For the arrow wings, the roll-control effectiveness of a given flap was relatively invariant with change in angle of attack. For the diamond wing, a region of increased effectiveness occurred at angles of attack just below maximum lift. The largest levels of low-angle-of-attack roll-control effectiveness were produced by the relatively large middle flaps on Wings 1 and 2. As aspect ratio was decreased, the size of the middle flaps on the arrow wings was reduced, and the outboard flaps were made larger. As a result, the roll-control effectiveness of the outboard trailing-edge flaps on the arrow wings was increased by decreasing the aspect ratio. The outboard flaps on the diamond wing (Wing 4) were very effective, and they produced the largest roll-control increments of any of the single flap deflections. The roll control could be increased by deflecting more than one set of trailing-edge flaps, and on some of the configurations the inboard and middle trailing-edge flaps were deflected in combination. For Wing 1, intermediate deflections were tested (figs. 115 and 116). These data suggest that the roll-control effectiveness produced by the inboard flaps was nonlinear with deflection angle.

On the arrow wings (Wings 1, 2, and 3), differential deflections of the inboard and outboard trailing-edge flaps yielded very small yawing moments that were predominantly proverse. However, deflections of the middle trailing-edge flaps produced adverse yawing moments that began at an angle of attack of approximately 4° and persisted to the maximum angle of attack tested. For the diamond wing (Wing 4), all the trailing-edge flap deflections produced small proverse yawing moments. These results show that the flaps with a forward-swept hinge line (inboard and outboard flaps on Wings 1, 2, and 3 and all flaps on Wing 4) produced predominantly small proverse yawing moments, but flaps with a rearward-swept hinge line (middle flaps on Wings 1, 2, and 3) produced significant adverse yawing moments. For this reason, differential deflection of the outboard flaps is an attractive candidate for primary roll control. Also, these flaps were marginally effective at producing pitch control, and using them exclusively for roll control would not significantly diminish the pitch control of the configuration.

Figure 117 shows a comparison of differential deflections of the various trailing-edge flaps on Wing 1 with the top body off. Comparisons of this data with the wide-body-on data (fig. 111) show that the primary effects of the body on roll-control effectiveness were a reduction in the effectiveness of the middle flaps and a slight increase in the effectiveness of the inboard flaps at the intermediate angles of attack. The middle flaps may have become less effective because of reduced flow over these flaps resulting from a channeling of flow around the body away from the inboard flaps, and the inboard flaps may have become more effective because they were no longer shielded by the wide body.

A comparison of differential deflections of the inboard and middle trailing-edge flaps on Wing 1 with the wide body on and the leading-edge flaps undeflected is shown in figure 118. Comparisons of these data with the data when the leading-edge flaps were deflected 45° (fig. 111) show that the primary effect of leading-edge flap deflections on the roll-control effectiveness of the middle flaps was a small decrease in effectiveness at the lower angles of attack. This decrease in effectiveness most likely resulted because a large leading-edge flap deflection actually induces the flow to separate from the lower surface of the wing at the lower angles of attack, thereby degrading the flow over the ailerons. As discussed previously, this effect could be minimized by appropriately scheduling the leading-edge flaps with angle of attack.

Directional Control Characteristics

The directional control characteristics of the four flying wings are presented in the following figures.

Two types of directional controls, split trailing-edge flaps (fig. 9) and vertical tail deflections (figs. 12 to 15), were tested on these models. As discussed in the section "Model Description" (p. 3), the split trailing-edge flaps were designed to separate into a top half that would deflect upward and a bottom half that would deflect downward at the same angle, and they would be deflected on only one wing at a time. The resulting geometry would result in an unbalanced incremental drag force on the wing that would produce an associated yawing moment. The all-moving twin vertical tails were deflected about an unswept hinge post located at the midpoint of the tail root chord.

Split trailing-edge flaps. The control effectiveness of split deflections of the outboard trailing-edge flaps for each of the wings with the wide top body on and the leading-edge flaps deflected 45° is shown in figures 119 to 122. Note that the right flaps were deflected on Wings 1, 2, and 3, and the left flaps were deflected on Wing 4. Split deflections of the outboard flaps produced negligible yawing moments that were sometimes opposite to those that would be expected to be generated by the drag of the split flaps. This result was due to the strong influence of side force on the yawing moments produced by these deflections (fig. 133). The forward sweep of the hinge line on the outboard surfaces caused these surfaces to function as a left rudder deflection when deflected on the right wing. For this reason, deflections of an aft surface with a forward-swept hinge line produced rudder-like side forces that generated yawing moments opposite to the yawing moments generated by the drag of the device, resulting in a lower net yawing moment. For most of the angles of attack tested, split deflections of the outboard flaps also produced rolling moments that were due to a spoiler-like loss of lift on the wing on which the flaps were deflected.

Figures 123 to 126 show the control effectiveness of split deflections of the middle trailing-edge flaps for each of the wings with the wide top body on and the leading-edge flaps deflected 45°. As with the outboard flaps, the right middle flaps were deflected on Wings 1, 2, and 3, and the left middle flap was deflected on Wing 4. The rearward sweep of the hinge line of the middle flaps on Wings 1, 2, and 3 caused these split deflections to function as a right rudder deflection when deflected on the right wing and vice versa (fig. 133). For this reason, split deflections of the middle flaps on these wings produced side forces that generated yawing moments in the same direction as those generated by the drag of the split flaps, resulting in higher net levels of yaw-control effectiveness that were fairly constant with angle of attack. The data for intermediate deflections on Wings 2 and 3 show that the yaw-control effectiveness was linear with deflection angle for angles of attack below approximately 24°, and the −39° deflection accounted for the majority of the available effectiveness at angles of attack above 24°. Split deflections of the middle flaps produced proverse rolling moments on Wing 1 and very small adverse rolling moments on Wings 2 and 3. In general, split

deflection of the middle flaps produced much higher yawing moments than comparable deflections of the outboard flaps. Therefore, split deflection of the middle flaps is an attractive candidate for yaw control for the arrow wings.

Because of a larger side-force moment arm, split deflections of the forward-swept middle flaps on Wing 4 produced larger yawing moments than those produced by the outboard flaps. However, these deflections of the left middle flaps actually produced a right yawing moment, which is opposite to what would be expected to be generated by the drag of the split flaps. As with the outboard flaps, the middle flaps produced adverse rolling moments on Wing 4 because of a similar spoiler-like effect on the wing on which they were deflected.

Vertical tails. Figures 127 to 130 show the control effectiveness of the twin medium vertical tails at the inboard location on each wing with the narrow top body on and the leading-edge flaps deflected 45°. The tail deflection shown corresponds to the maximum deflection that could be achieved before the tails interfered with the narrow top body. For the arrow wings, the yaw-control effectiveness was small and was relatively invariant for angles of attack below 16°. As angle of attack was increased above 16°, the yaw control gradually decreased as the tails became shielded by the wing and body, and the yaw control was negligible at angles of attack above approximately 36°. For the arrow wings, the tails were less effective at providing yaw control than were split deflections of the middle trailing-edge flaps. For the diamond wing, the yaw-control effectiveness at angles of attack below 30° was substantially larger than that for the other wings, but this control effectiveness also decreased at the higher angles of attack. The larger yaw control produced on the diamond wing was partially due to the moment reference center being farther forward, creating a longer directional moment arm. For the diamond wing, deflections of the twin vertical tails were much more effective for yaw control than were the split trailing-edge flaps at angles of attack up to 30°. For this reason, vertical tail deflection is an attractive candidate for yaw control on the diamond wing. For all four wings, vertical tail deflections produced large adverse rolling moments at angles of attack between approximately 16° and 40°. At low angles of attack, however, small proverse rolling moments were measured for the arrow wings, and adverse rolling moments were measured for the diamond wing.

The effect of changes in tail size on the control effectiveness of maximum deflections of the vertical tails at the inboard location on Wing 1 is shown in figure 131. Because of geometric interference with the narrow top body, increasing the size of the tails reduced the maximum deflection angles. Because of the differences in available deflection capability, changes in tail size did not significantly change the ability to produce control moments with vertical tail deflection.

The effect of tail location on the control effectiveness of a −30° deflection of the small tails on Wing 1 is shown in figure 132. Comparisons of these data show that moving the tails outboard increased the yaw-control effectiveness produced by the small tails at angles of attack below 16°. This result was predominantly attributed to an increase in moment arm about the yaw axis. Above 16° angle of attack, the yaw-control effectiveness at the outboard location began to decrease, and a control reversal occurred at an angle of attack of 32°. At the outboard location, deflection of the small tails produced adverse rolling moments at all angles of attack. In contrast, proverse rolling moments were produced at low angles of attack when the tails were positioned at the inboard location.

Conclusions

A wind-tunnel investigation was conducted in the Langley 12-Foot Low-Speed Tunnel to study the low-speed stability and control characteristics of a series of four flying wings over an extended range of angle of attack. Because of the current emphasis on reducing the radar cross section (RCS) of new military aircraft, the planform of each wing was composed of lines swept at a relatively high angle of 60°, and all the trailing-edge lines were aligned with one of the two leading edges. Three arrow planforms with different aspect ratios and one diamond planform were tested. The models incorporated leading-edge flaps for improved pitching-moment characteristics and lateral stability and had three sets of trailing-edge flaps that were deflected differentially for roll control, symmetrically for pitch control, and in a split fashion for yaw control. Top bodies of three widths and twin vertical tails of various sizes and locations were also tested on each model. A large aerodynamic database was compiled that could be used to evaluate some of the trade-offs involved in the design of a configuration with a reduced RCS and good flight dynamic characteristics. The primary results of this investigation may be summarized as follows:

1. The maximum lift coefficient of the four wings was approximately 1.1. This value occurred at an angle of attack of 32° for the arrow wings and 36° for the diamond wing.

2. Without vertical tails, each of the wings exhibited neutral or unstable values of directional stability at most of the angles of attack tested. The configurations were laterally stable at low and very high angles of attack, but the arrow wings exhibited a region of lateral instability

near maximum lift. In general, the diamond wing exhibited the highest levels of lateral stability of the four wings tested.

3. The outboard wing panels that were added to the basic diamond shape to create the arrow wings caused the arrow wings to experience pitch-up effects that became greater as aspect ratio was increased and the outboard panels became larger. Adding these outboard wing sections was also the primary cause of the loss in lateral stability at intermediate angles of attack.

4. When the leading-edge flaps were undeflected, adding top bodies to the wings caused a small reduction in maximum lift and resulted in lower directional and lateral stability. These effects were similar, but smaller in magnitude, when the leading-edge flaps were deflected 45°. These results indicated that the top bodies had a significant effect on the separation patterns on the upper surfaces of the wings.

5. Leading-edge flap deflections greatly improved lateral stability for all the wings. These improvements included a reduction in the maximum magnitude of the instability and a reduction in the range of angle of attack over which the instability occurred. For the arrow wings, leading-edge flap deflections improved the pitching-moment characteristics by significantly reducing the pitch-up.

6. The addition of vertical tails provided expected increases in directional stability and also improved lateral stability.

7. The inboard and middle trailing-edge flaps were deflected symmetrically for pitch control on each wing. In general, these deflections produced relatively small increments in pitching moment. The control effectiveness was more linear with deflection angle for nose-up control deflections than for nose-down deflections, and the nose-down effectiveness decreased at the higher angles of attack (where it would be most needed to trim an unstable aircraft). The combination of pitch-up and reduced nose-down control resulted in a hung stall condition for some of the configurations. All the configurations would require changes in longitudinal stability (e.g., movement of the center of gravity) to eliminate the hung stall and to achieve static trim at angles of attack up to maximum lift. Also, additional control power may be needed to provide a control margin for use during dynamic situations such as maneuvering or countering turbulence. An additional limit on the trim capability of these wings may be imposed by the need to budget the amount of flap deflection available for each type of control (pitch, roll, or yaw).

8. Differential deflections of the middle and outboard trailing-edge flaps were tested for roll control. For angles of attack below maximum lift, these deflections produced rolling moments that were relatively invariant with angle of attack. Because the flap sizes varied as wing aspect ratio changed, the level of control produced by each flap varied with wing planform. The roll control of a configuration could be increased by deflecting more than one set of trailing-edge flaps. The middle flaps (aft swept hinge line) produced significant adverse yawing moments at higher angles of attack, and the outboard flaps (forward swept hinge line) produced very small yawing moments. For this reason, the outboard flaps are a more attractive candidate for the primary roll control for these wings.

9. Split deflections of the middle and outboard trailing-edge flaps were tested for yaw control. When split, the forward-swept outboard trailing-edge flaps were not effective. This is because the yawing moment produced by the side force on these flaps opposed the yawing moment produced by the drag, resulting in a lower net moment. For the arrow wings, the middle trailing-edge flaps were swept aft, and the yawing moment from the side force and drag generated by these flaps acted in the same direction, resulting in a large net yawing moment. Therefore, split deflection of the rearward-swept middle flaps is an attractive candidate for yaw control for the arrow wings.

10. Deflection of the all-moving twin vertical tails for yaw control was also tested. The vertical tails were significantly more effective on the diamond wing than on the arrow wings at angles of attack below 30°. For the arrow wings, the vertical tails produced smaller levels of yaw control than split deflections of the middle flaps. For the diamond wing, vertical tail deflection was much more effective than the split trailing-edge flaps for angles of attack up to 30°. Therefore, vertical tail deflection is an attractive candidate for yaw control on the diamond wing. Large adverse rolling moments were created by tail deflections for angles of attack near maximum lift.

NASA Langley Research Center
Hampton, VA 23681-0001
April 27, 1995

References

1. Fears, Scott P.; Ross, Holly M.; and Moul, Thomas M.: *Low-Speed Wind-Tunnel Investigation of the Stability and Control Characteristics of a Series of Flying Wings With Sweep Angles of 50°*. NASA TM-4640, 1995.

2. Ross, Holly M.; Fears, Scott P.; and Moul, Thomas M.: *Low-Speed Wind-Tunnel Investigation of the Stability and Control Characteristics of a Series of Flying Wings With Sweep Angles of 70°*. NASA TM-4671, 1995.

3. Hom, K. W.; Morris, O. A.; and Hahne, D. E.: Low-Speed Investigation of the Maneuver Capability of Supersonic Fighter Wings. AIAA-83-0426, Jan. 1983.

4. Freeman, Delma C., Jr.: *Low Subsonic Flight and Force Investigation of a Supersonic Transport Model With a Highly Swept Arrow Wing*. NASA TN D-3887, 1967.

5. Talay, Theodore A.: *Introduction to the Aerodynamics of Flight*. NASA SP-367, 1975.

6. Ogburn, Marilyn E.; Foster, John V.; Nguyen, Luat T.; Breneman, Kevin P.; McNamara, William G.; Clark, Christopher M.; Rude, Dennis D.; Draper, Marjorie G.; Wood, Craig A.; and Hynes, Marshall S.: High-Angle-of-Attack Nose-Down Pitch Control Requirements for Relaxed Static Stability Combat Aircraft. *High-Angle-of-Attack Technology*, Volume I, Joseph R. Chambers, William P. Gilbert, and Luat T. Nguyen, eds., NASA CP-3149, Part 2, 1992, pp. 639–658.

7. Johnson, Joseph L., Jr.; Grafton, Sue B.; and Yip, Long P.: Exploratory Investigation of the Effects of Vortex Bursting on the High Angle-of-Attack Lateral-Directional Stability Characteristics of Highly-Swept Wings. *A Collection of Technical Papers—AIAA 11th Aerodynamic Testing Conference*, Mar. 1980, pp. 282–297. (Available as AIAA-80-0463.)

8. Queijo, M. J.; and Riley, Donald R.: *Calculated Subsonic Span Loads and Resulting Stability Derivatives of Unswept and 45° Sweptback Tail Surfaces in Sideslip and in Steady Roll*. NACA TN 3245, 1954.

Table I. Model Geometric Characteristics

	Wing 1	Wing 2	Wing 3	Wing 4
Wing:				
Area (reference), in^2	1073.05	1032.87	974.88	736.29
Area (trapezoidal), in^2	765.66	768.26	768.43	736.29
Span, in.	48.00	43.82	39.20	29.16
Mean aerodynamic chord, in.	28.71	29.80	31.25	33.67
Root chord, in.	50.50	50.50	50.50	50.50
Tip chord, in.	0	0	0	0
Aspect ratio (based on total planform)	2.15	1.86	1.58	1.15
Aspect ratio (based on trapezoidal area)	3.00	2.50	2.00	1.15
Leading-edge sweep, deg	60	60	60	60
Trailing-edge sweep, deg	±60	±60	±60	±60
Dihedral, deg	0	0	0	0
Incidence, deg	0	0	0	0
Moment reference centers:				
Longitudinal (X-axis), percent $\bar{c}$	36.83	33.06	32.00	26.07
Longitudinal (X-axis, back from nose), in.	25.40	23.46	22.14	17.18
Vertical (Z-axis, below wing centerline), in.	1.87	1.87	1.87	1.87
Leading-edge flaps:				
Area (per side), in^2	82.05	71.34	59.18	35.78
Span (per side), in.	18.95	16.66	14.05	9.02
Chord, in.	4.66	4.66	4.66	4.66
Trailing-edge flaps:				
Inboard:				
Area (per side), in^2	26.08	24.15	18.95	22.28
Span (per side), in.	6.42	5.74	4.72	5.19
Chord, in.	5.35	6.06	7.12	7.12
Middle:				
Area (per side), in^2	50.42	44.41	35.77	22.28
Span (per side), in.	10.97	9.08	7.08	5.19
Chord, in.	5.35	6.06	7.12	7.12
Outboard:				
Area (per side), in^2	19.32	24.76	34.20	22.28
Span (per side), in.	5.16	5.84	6.86	5.19
Chord, in.	5.35	6.06	7.12	7.12
Body flaps:				
Area (per side), in^2	14.72	16.68	19.61	20.50
Span (per side), in.	4.72	4.93	5.24	5.38
Chord, in.	5.35	6.06	7.12	7.12
Split trailing-edge flaps:				
Middle:				
Area (per side), in^2	50.42	44.41	35.77	22.28
Span (per side), in.	10.97	9.08	7.08	5.19
Chord, in.	5.35	6.06	7.12	7.12
Outboard:				
Area (per side), in^2	19.32	24.76	34.20	22.28
Span (per side), in.	5.16	5.84	6.86	5.19
Chord, in.	5.35	6.06	7.12	7.12

Table I. Concluded

	Wide top	Medium top	Narrow top	Bottom
Bodies:				
Length, in.	40.50	40.50	40.50	30.00
Width, in.	10.40	7.00	4.60	10.00
Height, in.	3.50	3.50	3.50	3.00

	Large	Medium	Small
Vertical tails:			
Area, in^2	100.98	50.47	25.27
Root chord, in.	21.60	15.27	10.80
Tip chord, in.	0	0	0
Height, in.	9.35	6.61	4.68
Aspect ratio	0.87	0.87	0.87
Leading-edge sweep, deg	60	60	60
Hinge line location, percent root chord	50	50	50

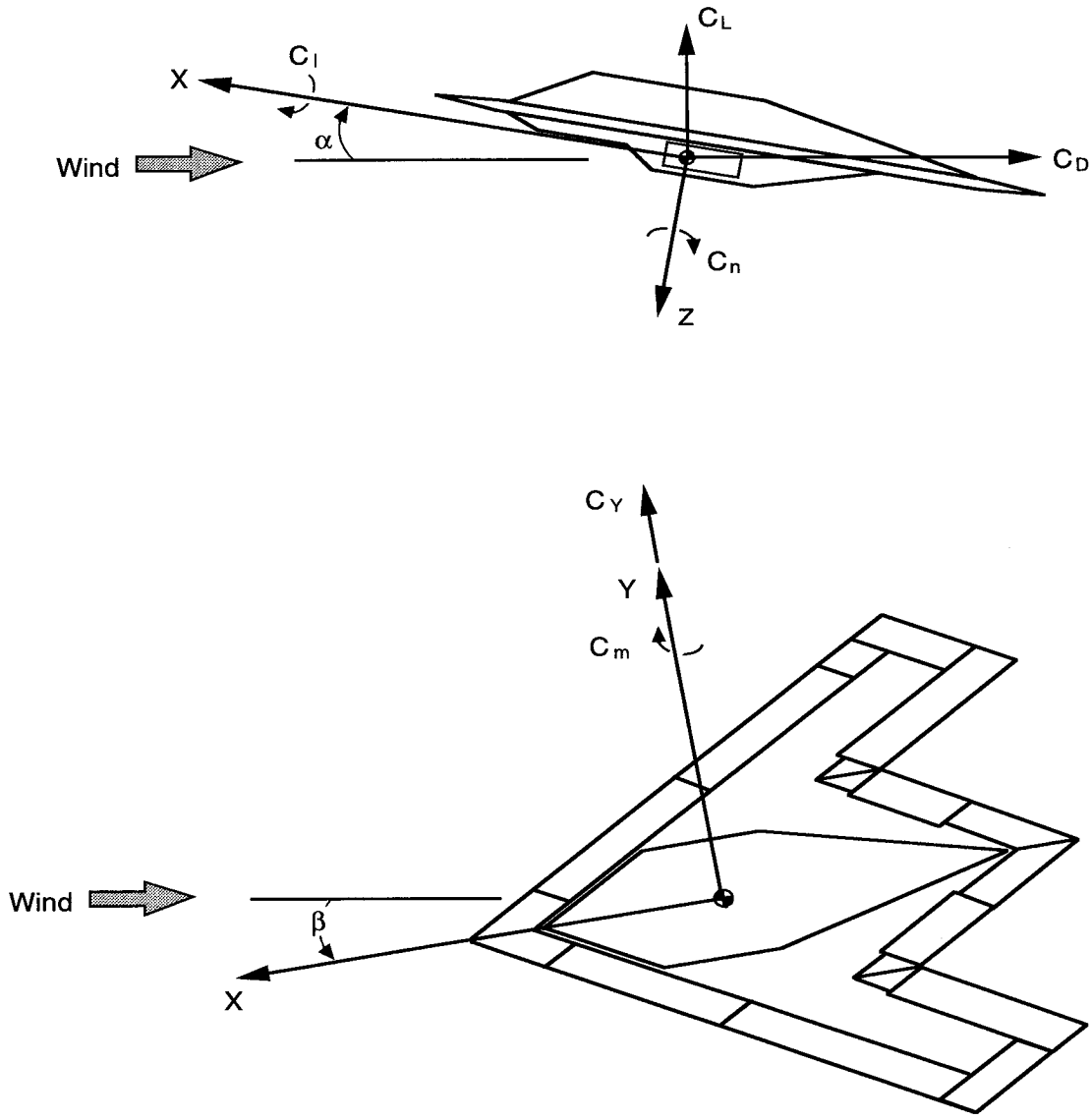

Figure 1. System of axes and angular notation.

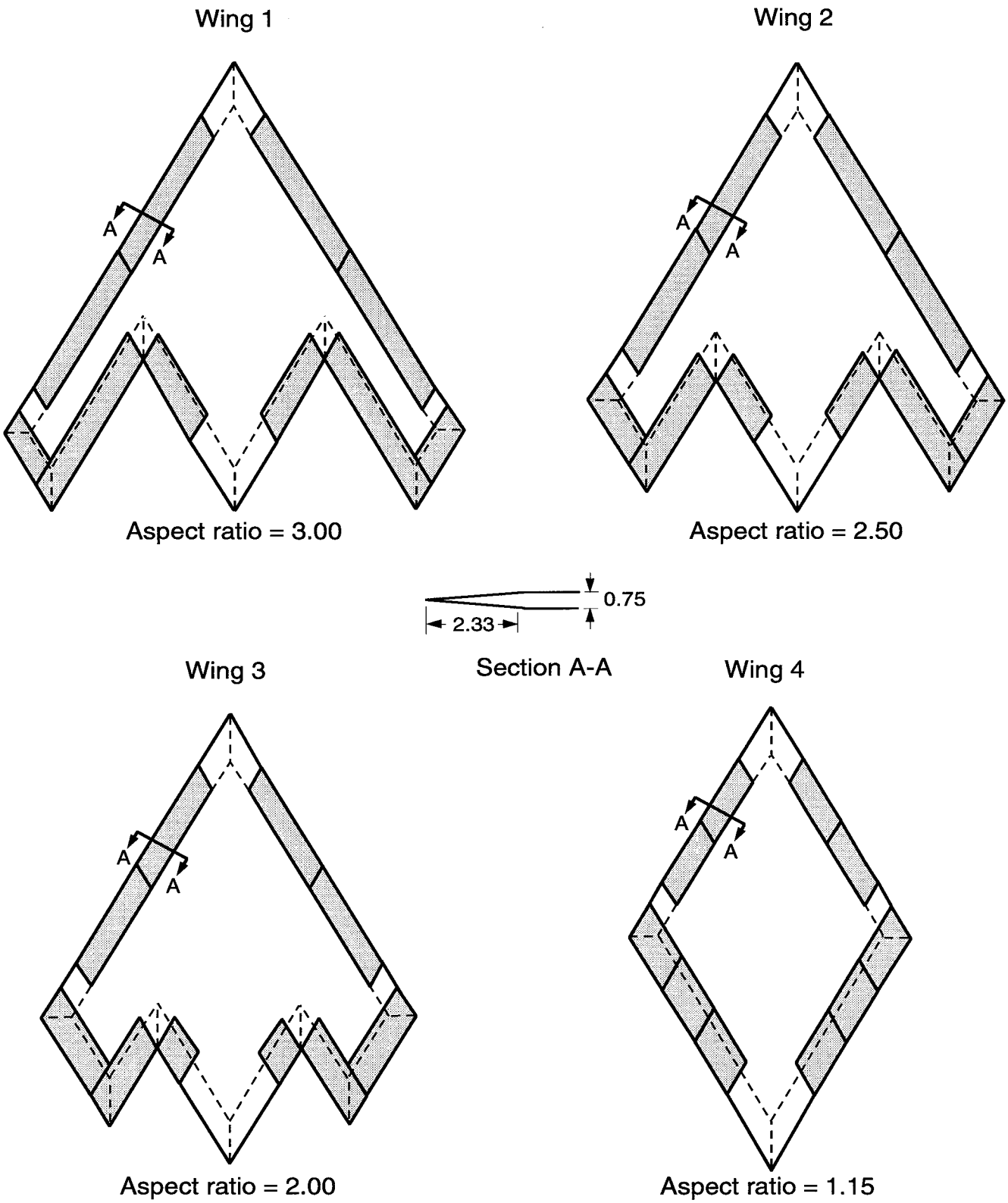

(a) Control surfaces (shaded areas) and bevel lines (dashed lines).

Figure 2. Wing planforms.

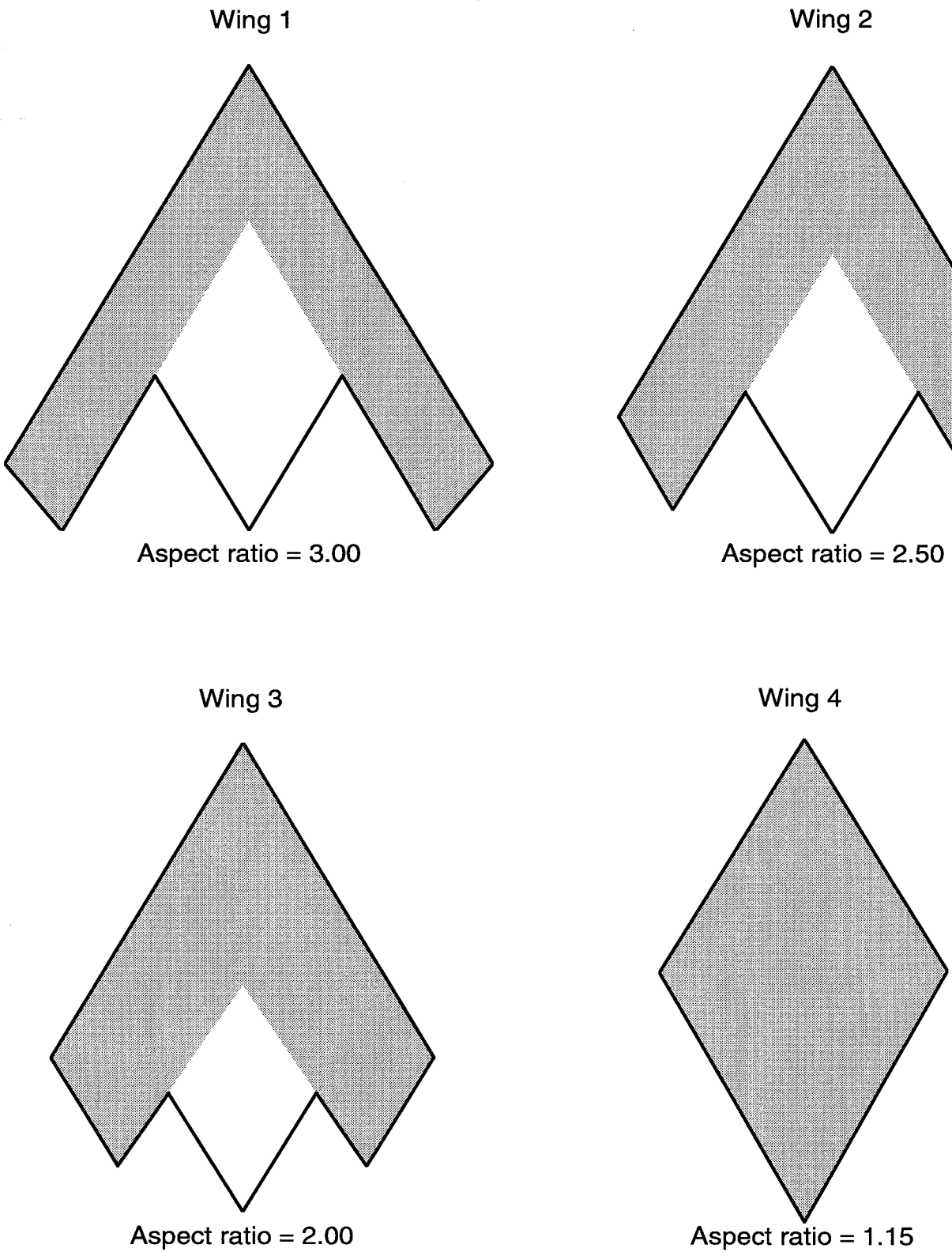

(b) Trapezoidal wing areas (shaded areas).

Figure 2. Concluded.

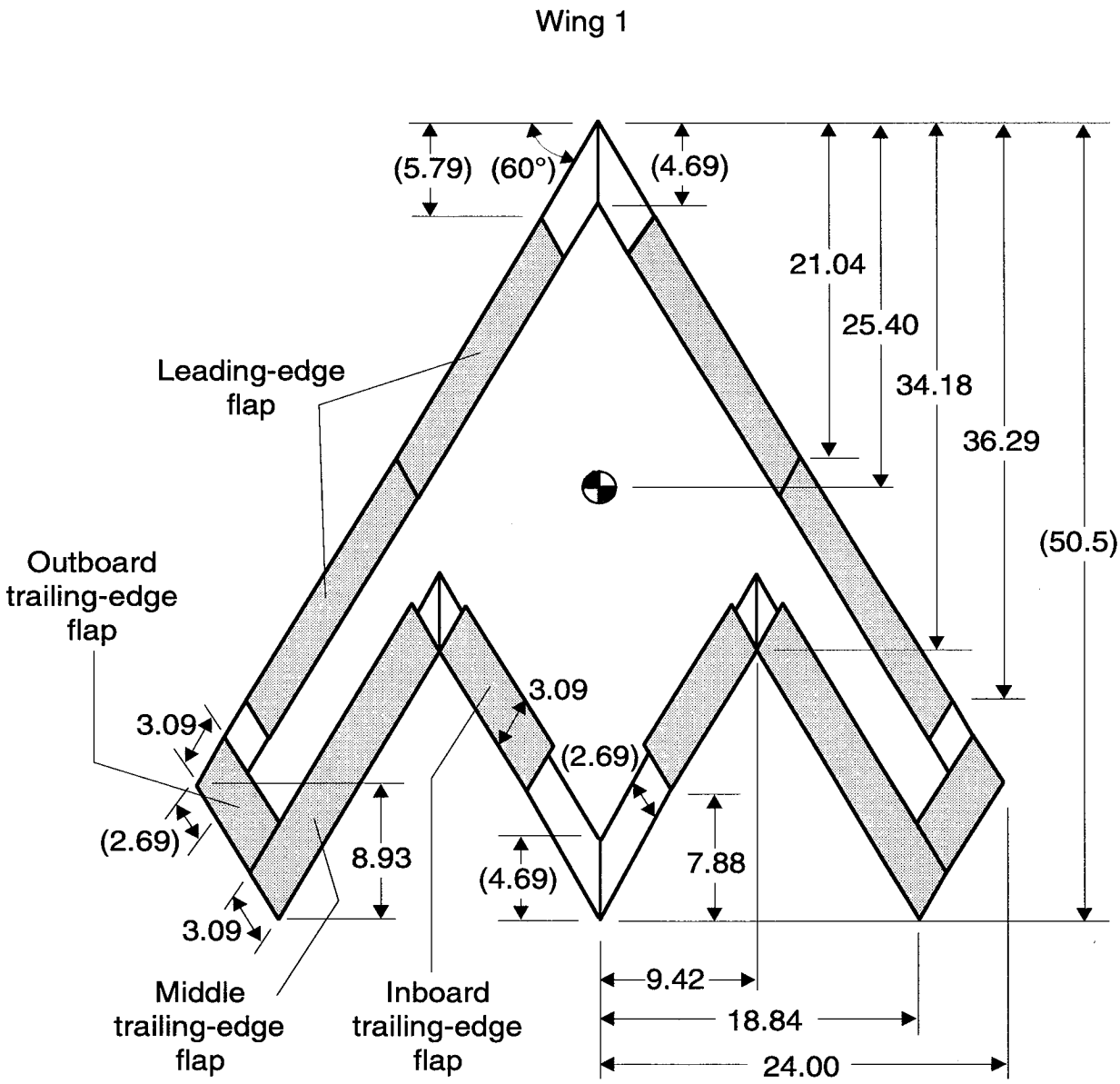

Figure 3. Wing 1. Linear dimensions are in inches. Dimensions in parentheses are common for all wings. Shaded areas indicate control surfaces.

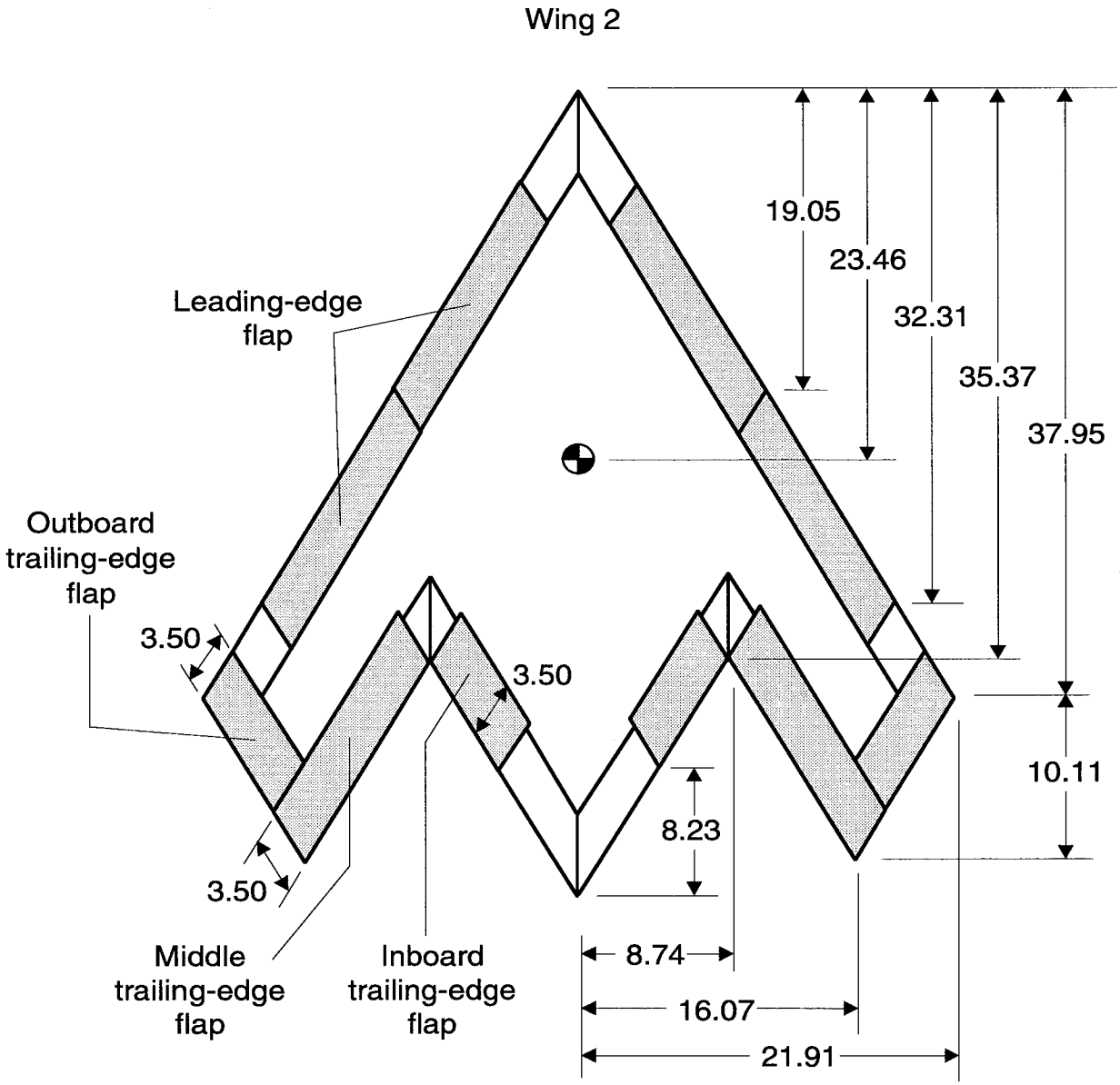

Figure 4. Wing 2. All dimensions are in inches. Shaded areas indicate control surfaces.

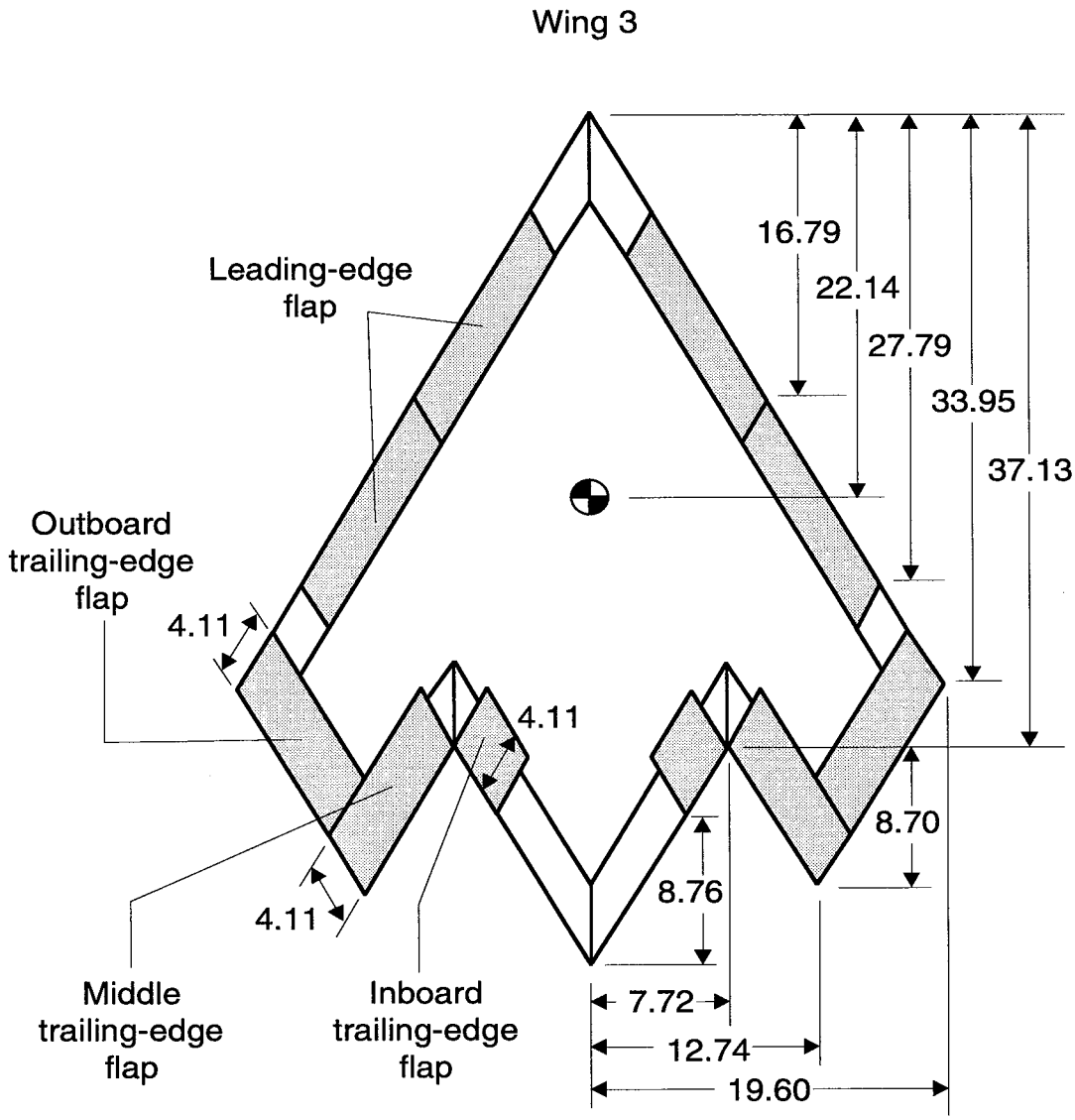

Figure 5. Wing 3. All dimensions are in inches. Shaded areas indicate control surfaces.

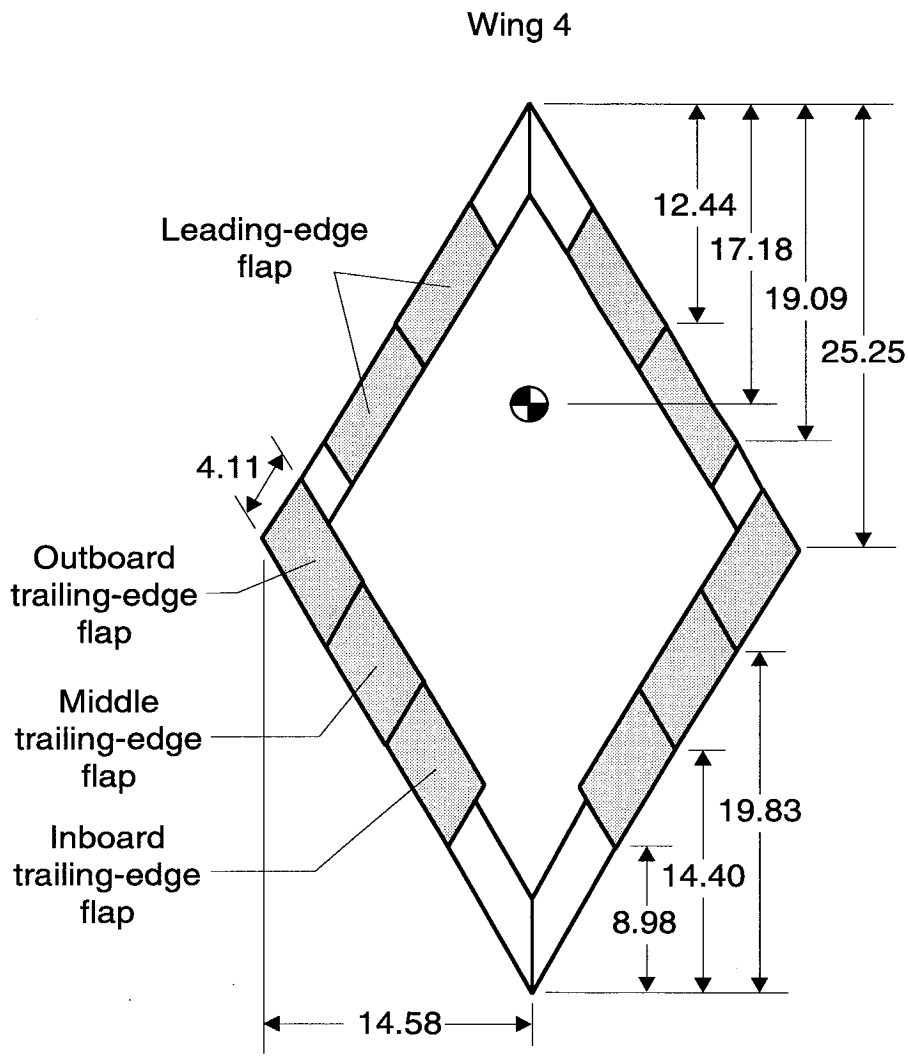

Figure 6. Wing 4. All dimensions are in inches. Shaded areas indicate control surfaces.

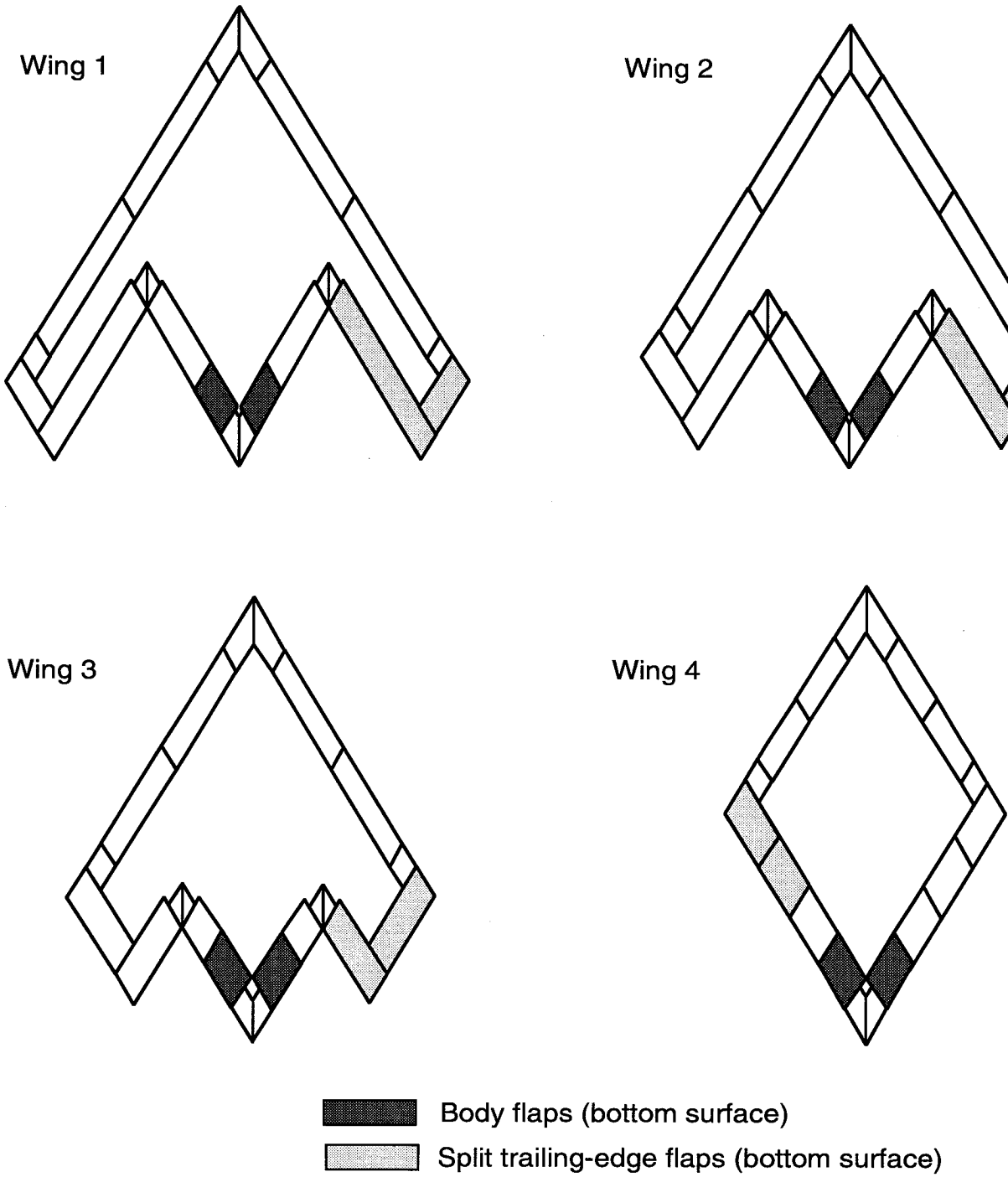

Figure 7. Top view showing locations of undeflected body flaps and split trailing-edge flaps on bottom surfaces of wings.

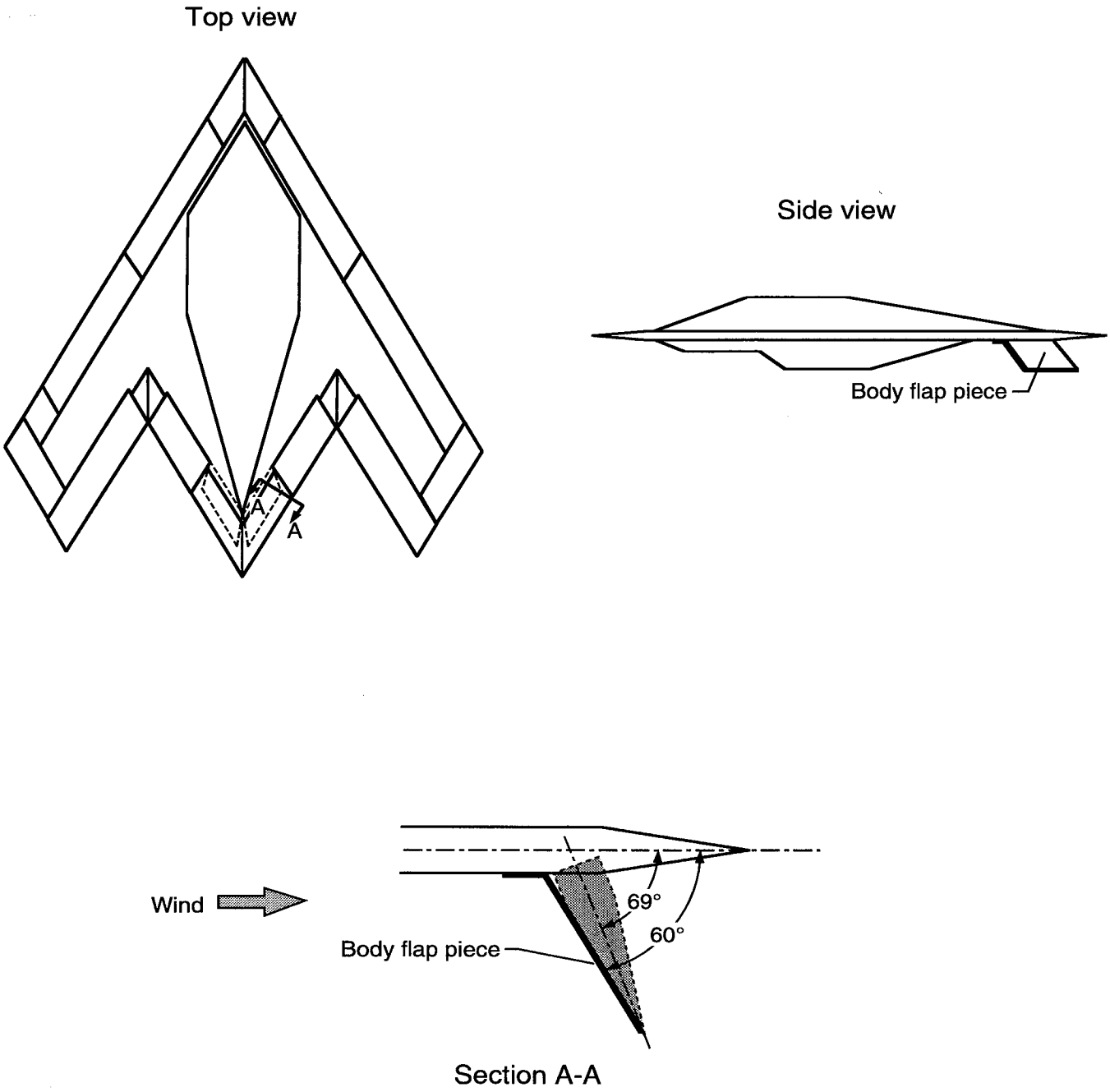

(a) Typical body flap location and mounting for deflection angle of 69°. Shaded area represents simulated flap.

Figure 8. Body flap locations, dimensions, and deflection angles.

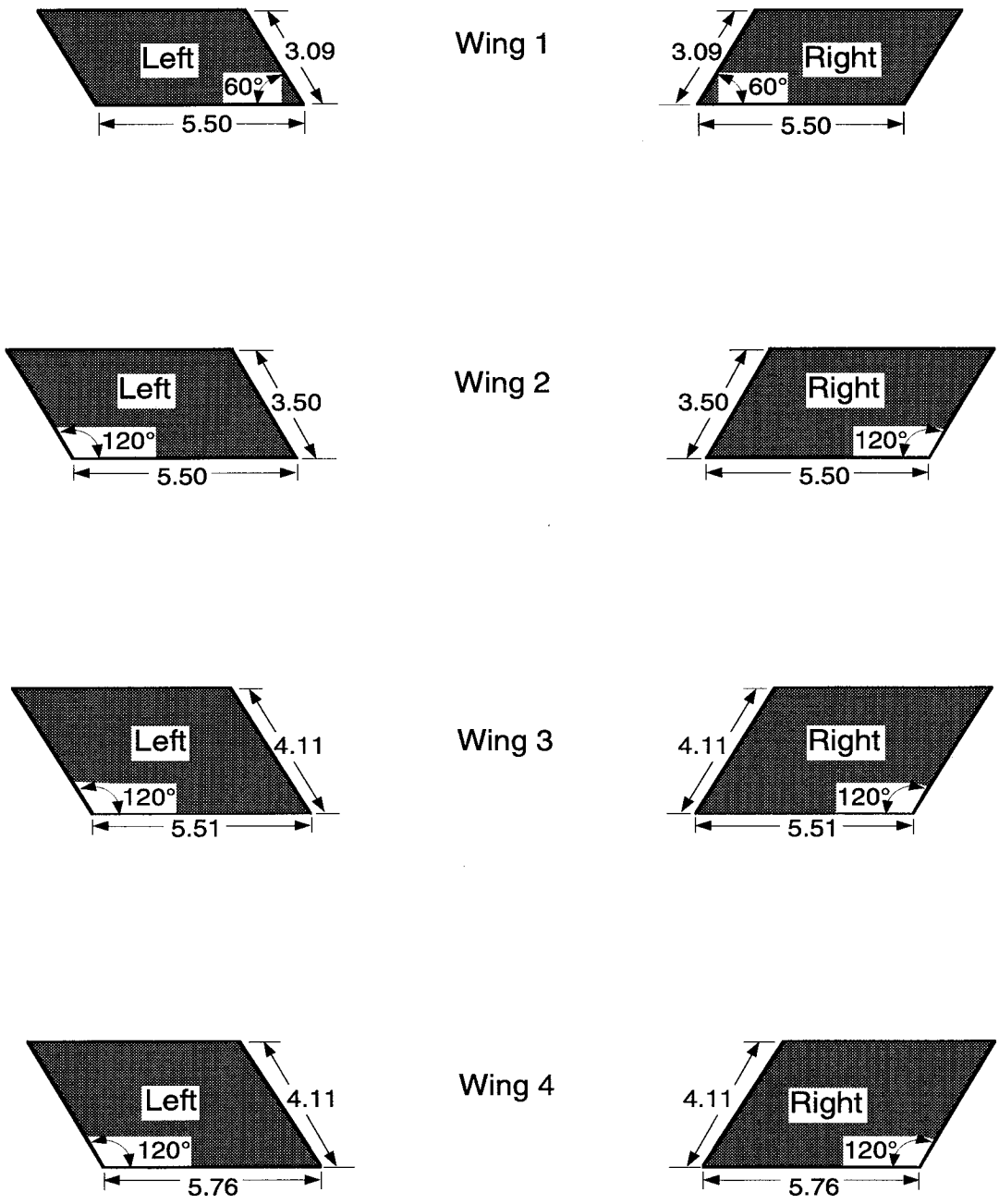

(b) Planforms of body flaps. All dimensions are in inches.

Figure 8. Concluded.

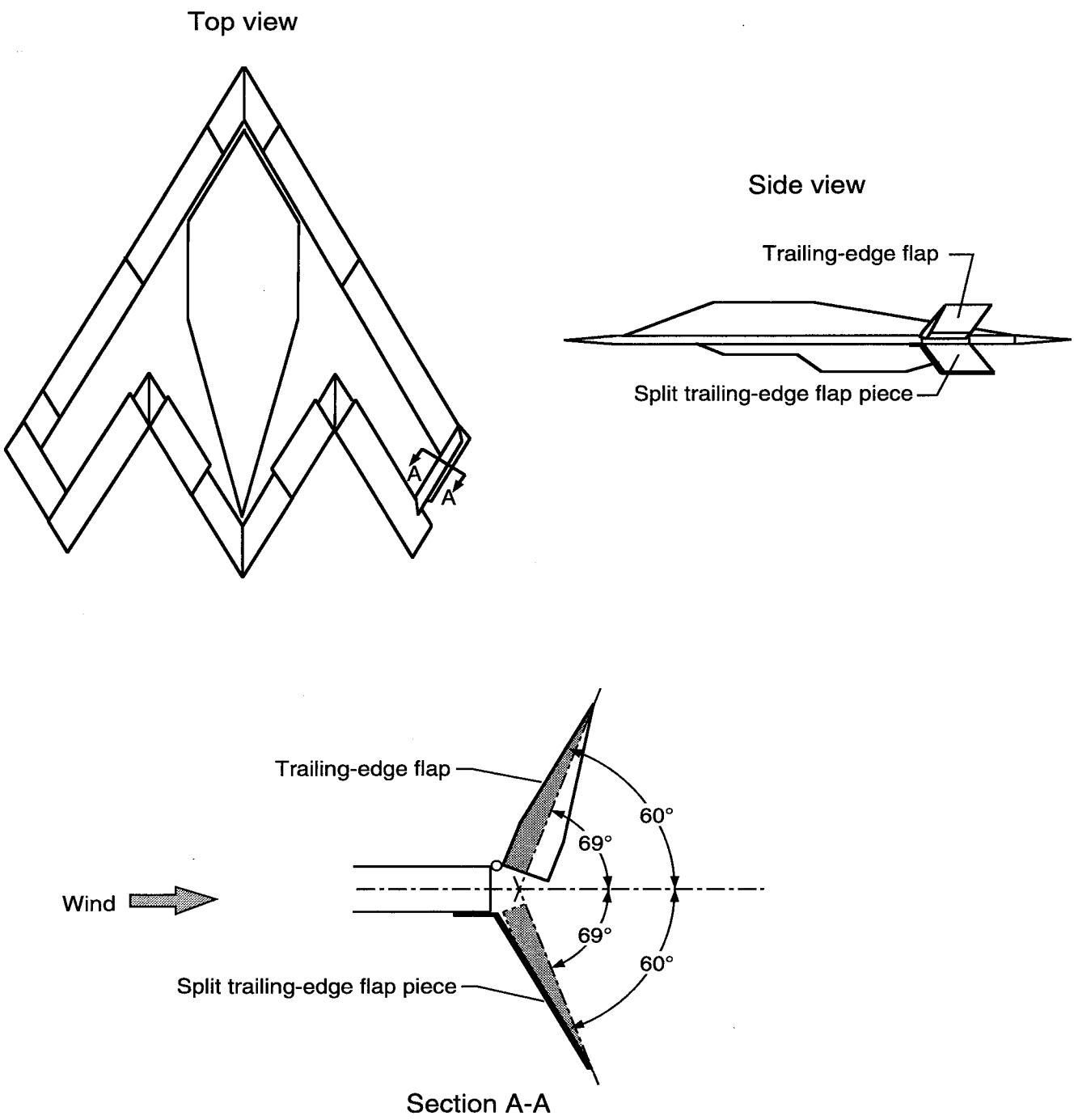

(a) Typical split trailing-edge flap location and mounting for deflection angle of 69°. Shaded areas represent simulated upper and lower halves of split flaps.

Figure 9. Split trailing-edge flap locations, dimensions, and deflection angles.

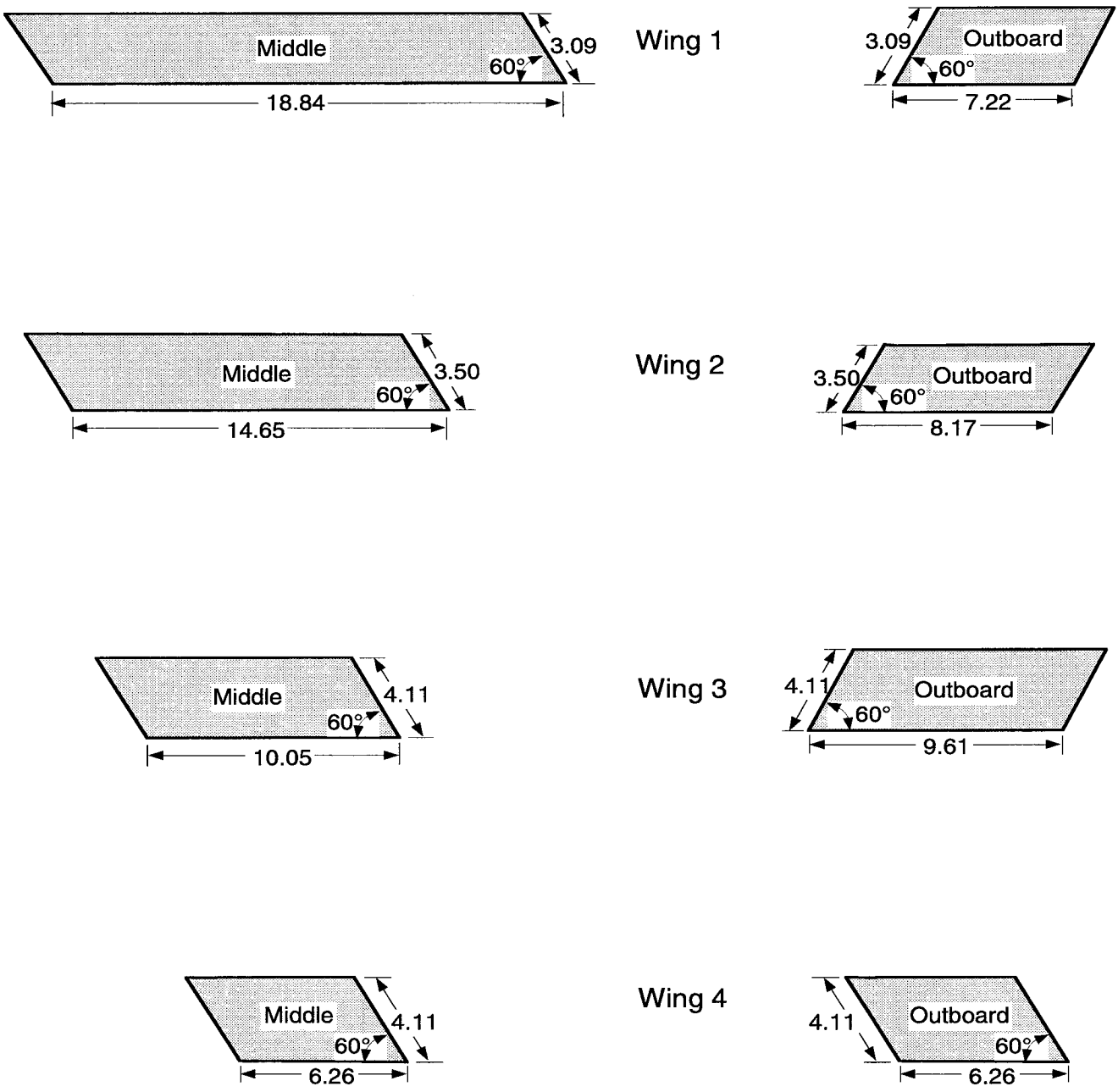

(b) Planforms of split trailing-edge flaps. All dimensions are in inches.

Figure 9. Concluded.

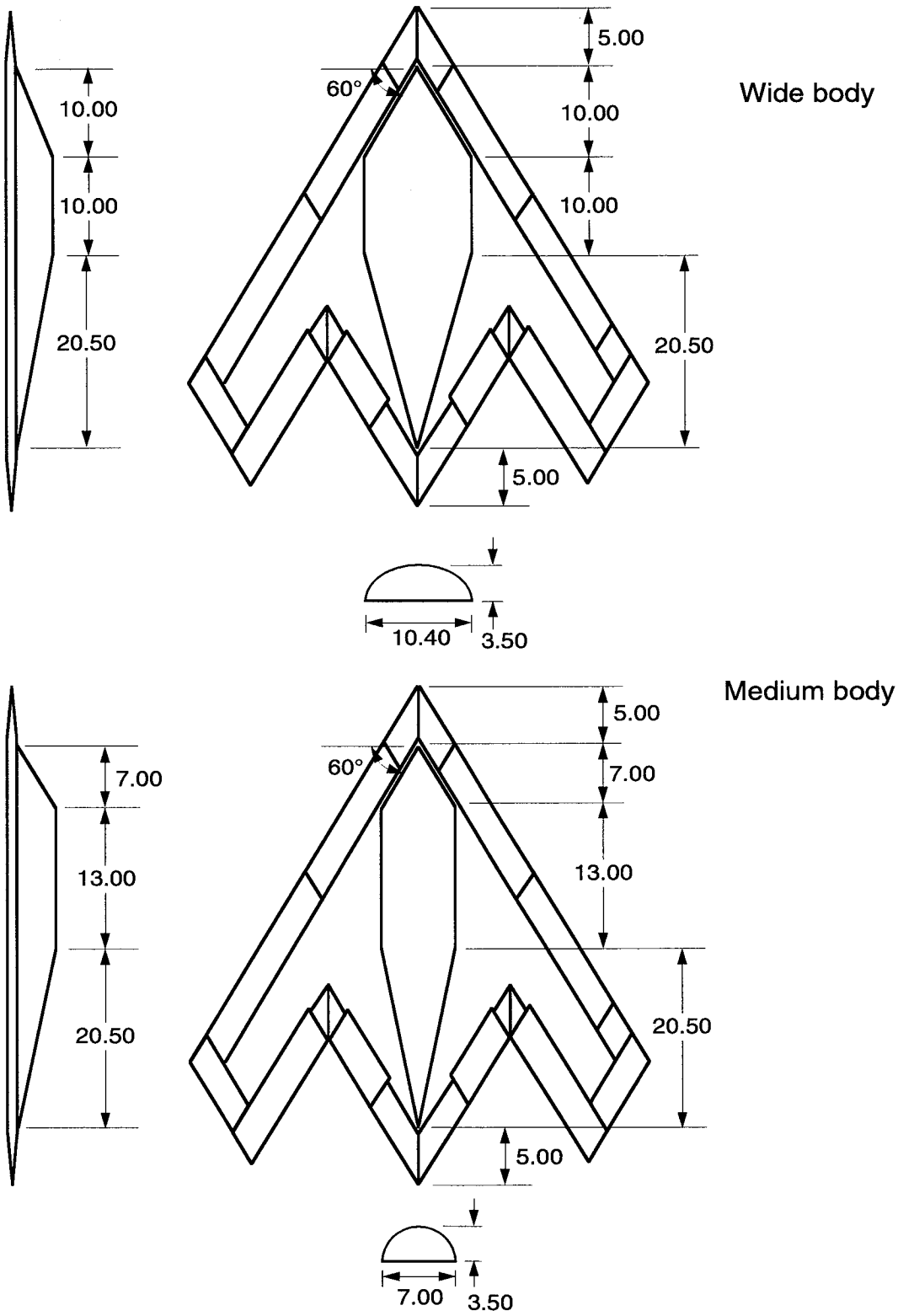

(a) Wide and medium top bodies.

Figure 10. Top bodies and bottom balance cover. All dimensions are in inches.

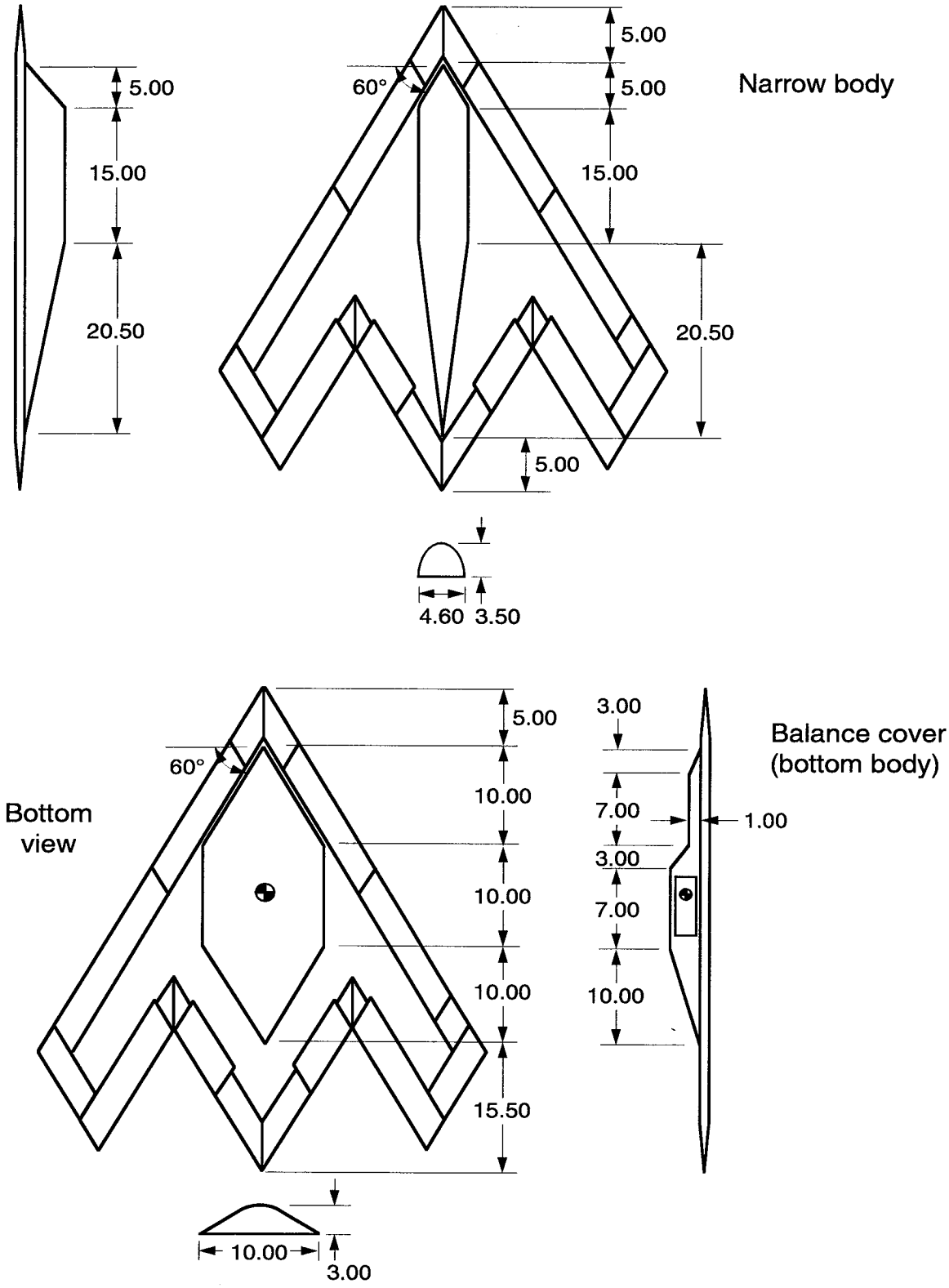

(b) Narrow top body and bottom balance cover.

Figure 10. Concluded.

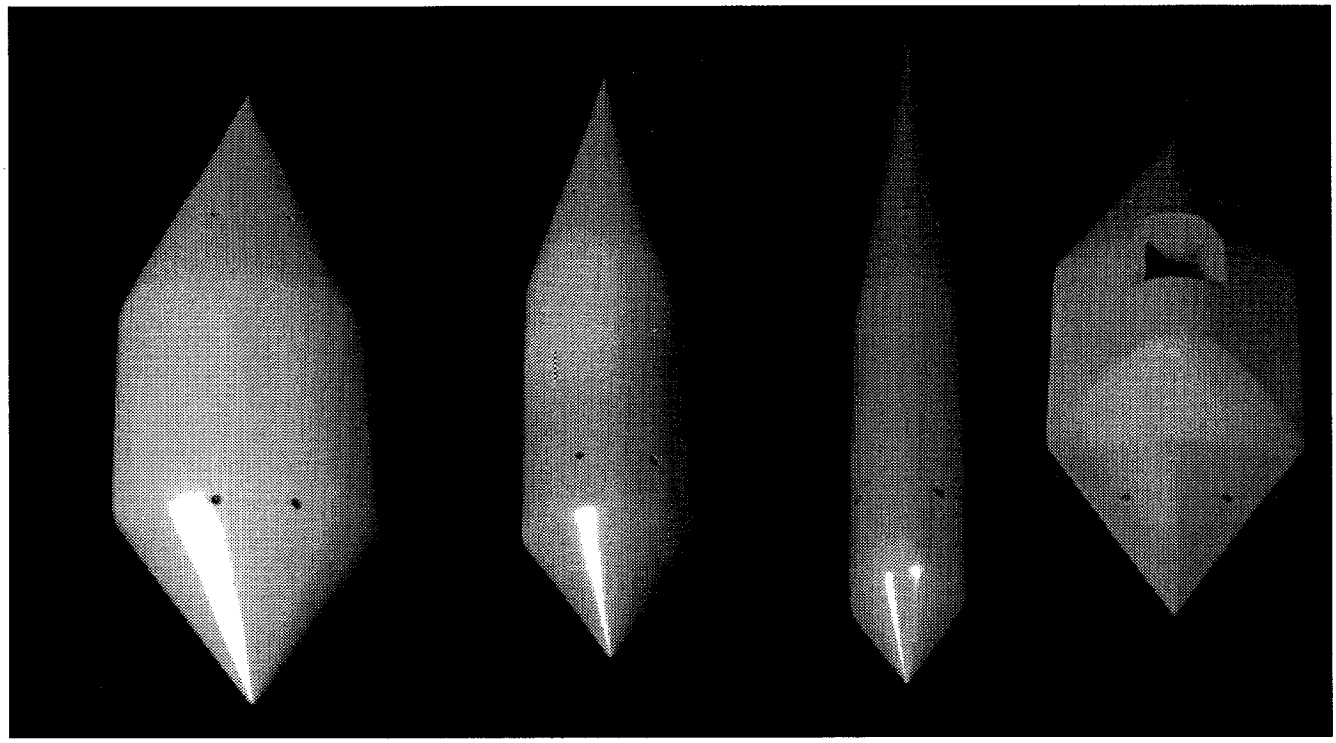

Figure 11. Top bodies and bottom balance cover.

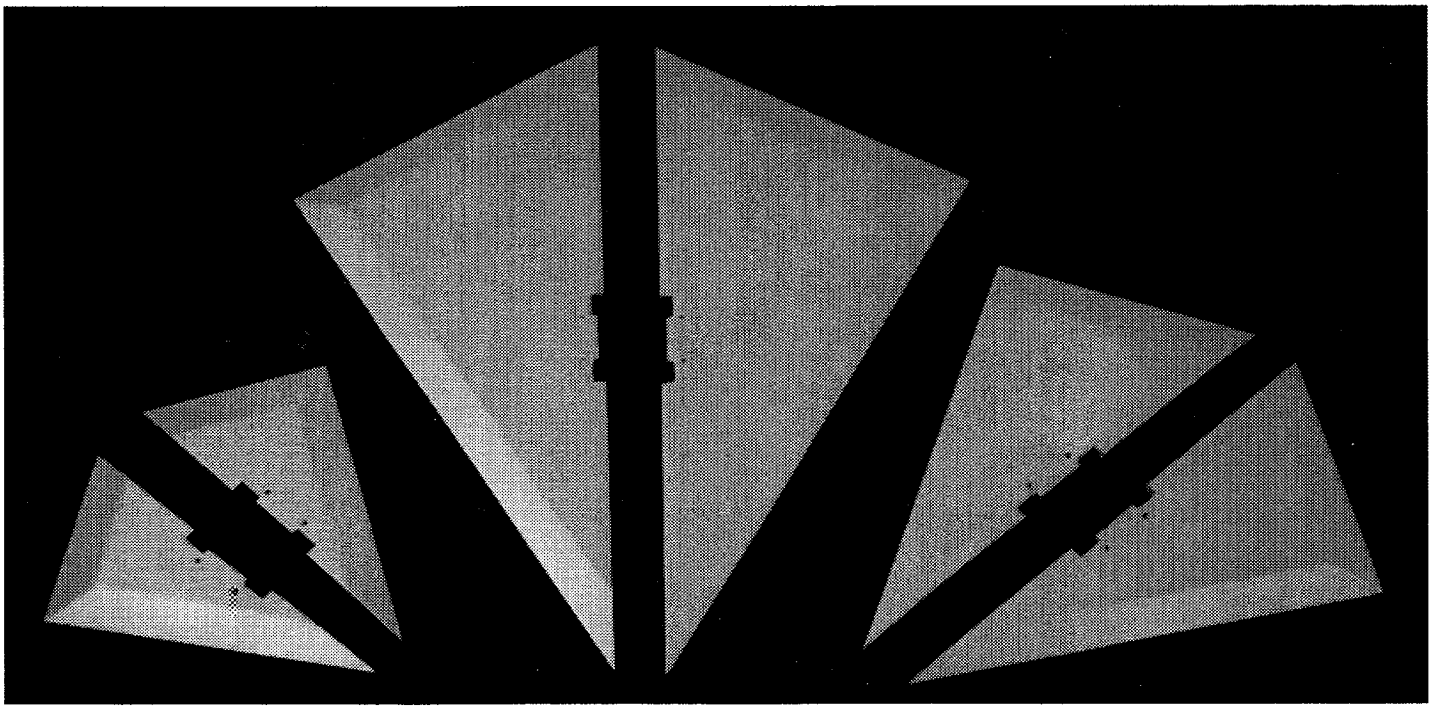

Figure 12. Large, medium, and small vertical tails.

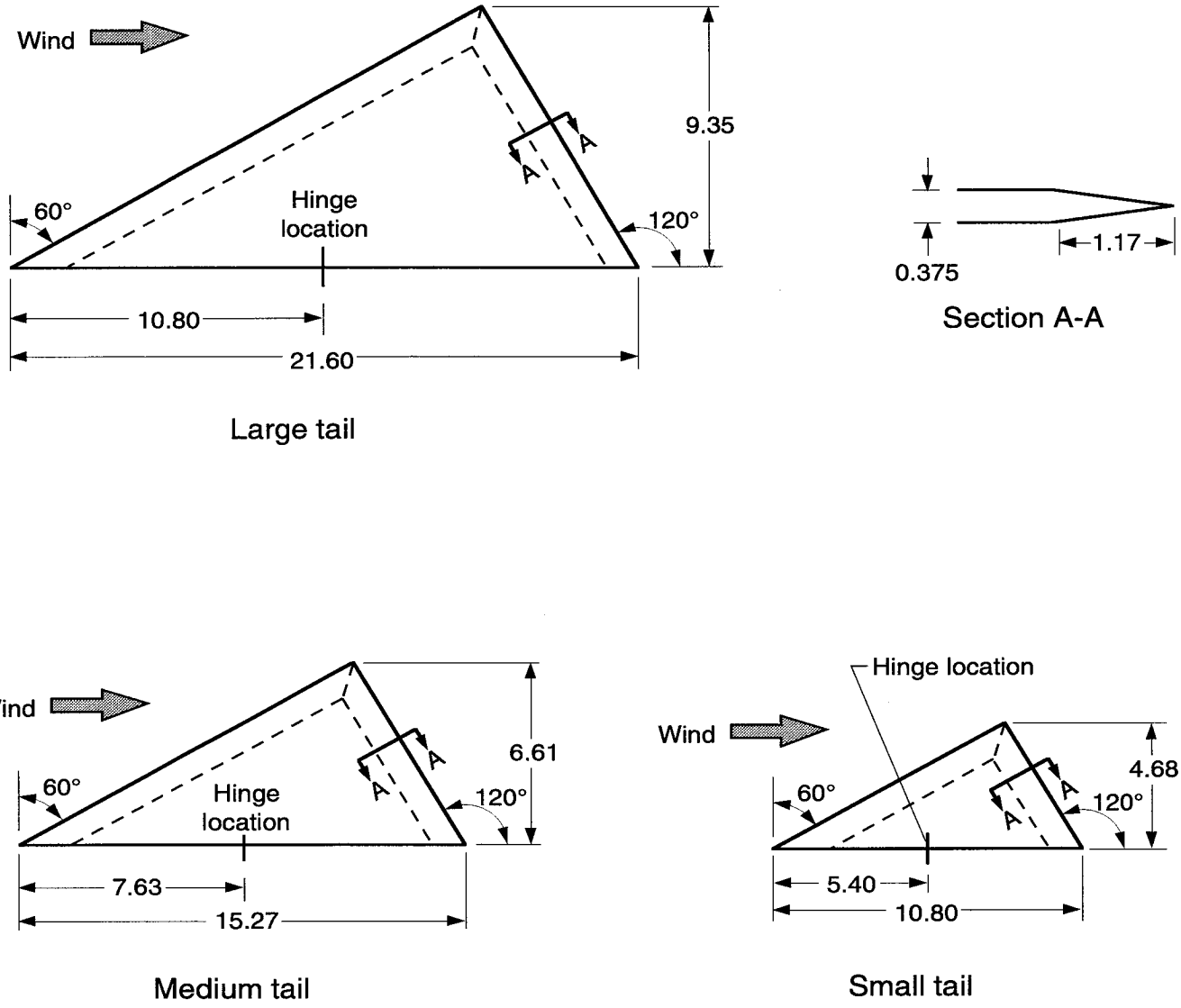

Figure 13. Large, medium, and small vertical tails. All dimensions are in inches. Dashed lines indicate bevel lines.

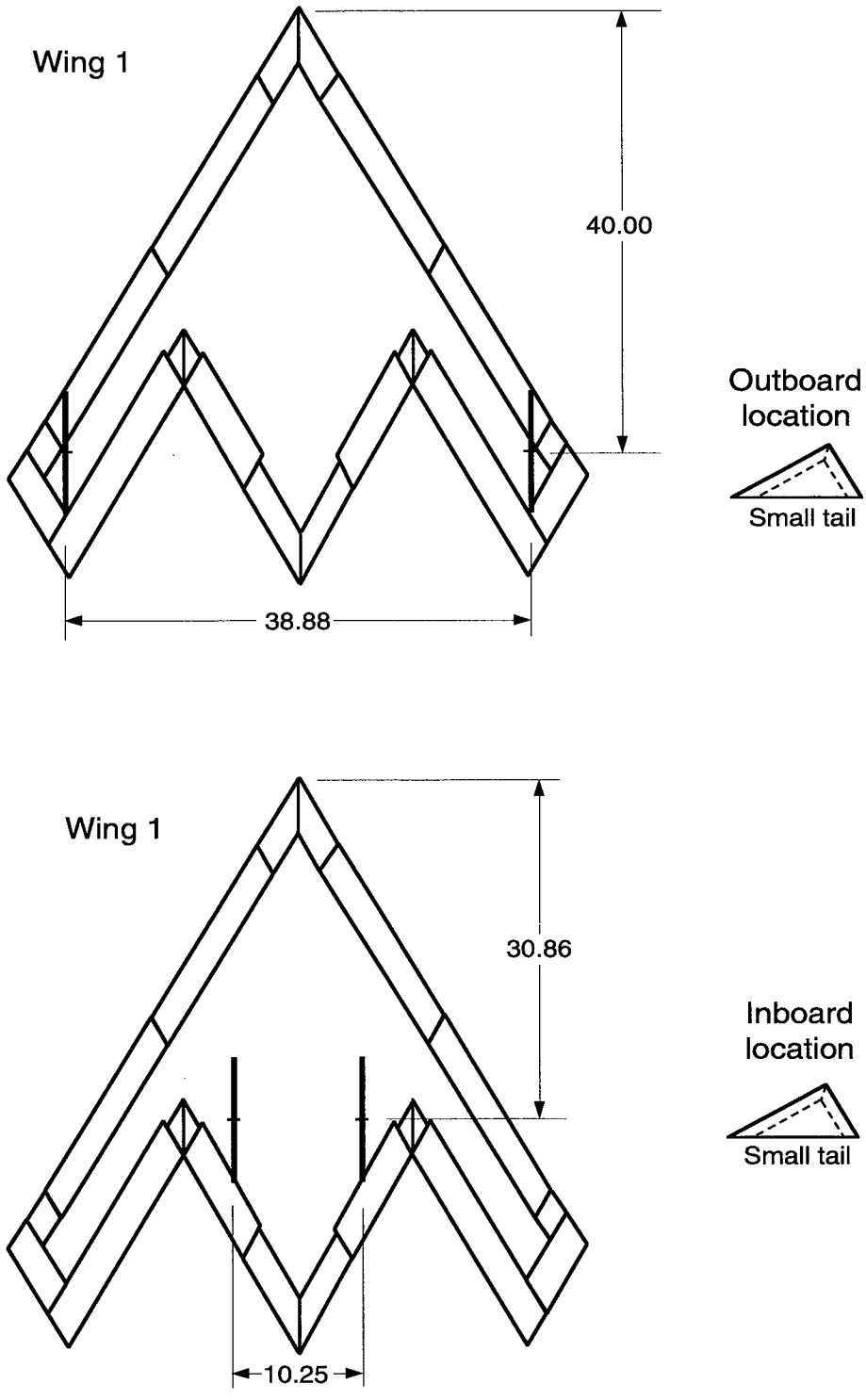

(a) Small tails at outboard and inboard locations on Wing 1.

Figure 14. Locations for small, medium, and large vertical tails on Wing 1. All dimensions are in inches.

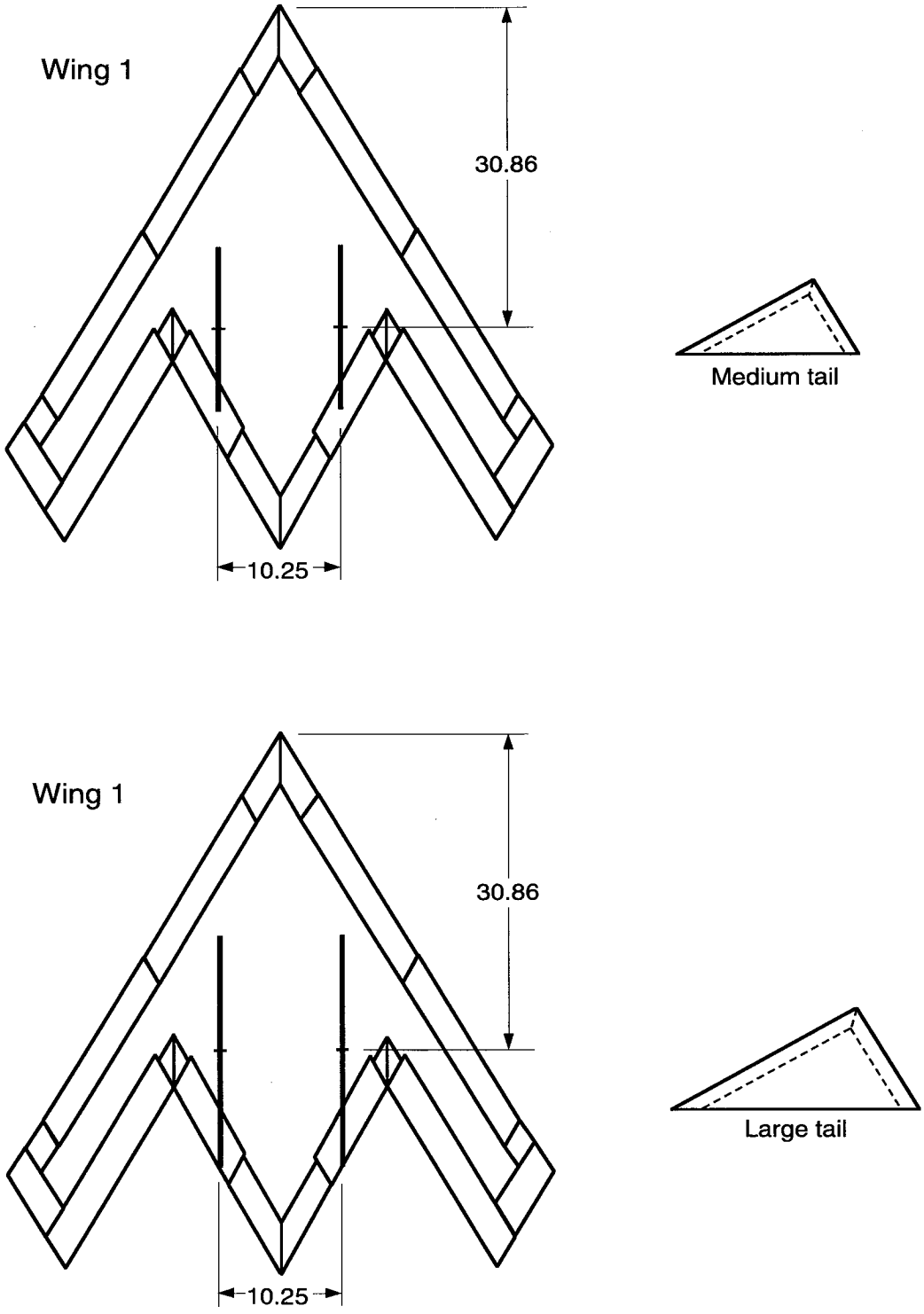

(b) Medium and large tails at inboard location on Wing 1.

Figure 14. Concluded.

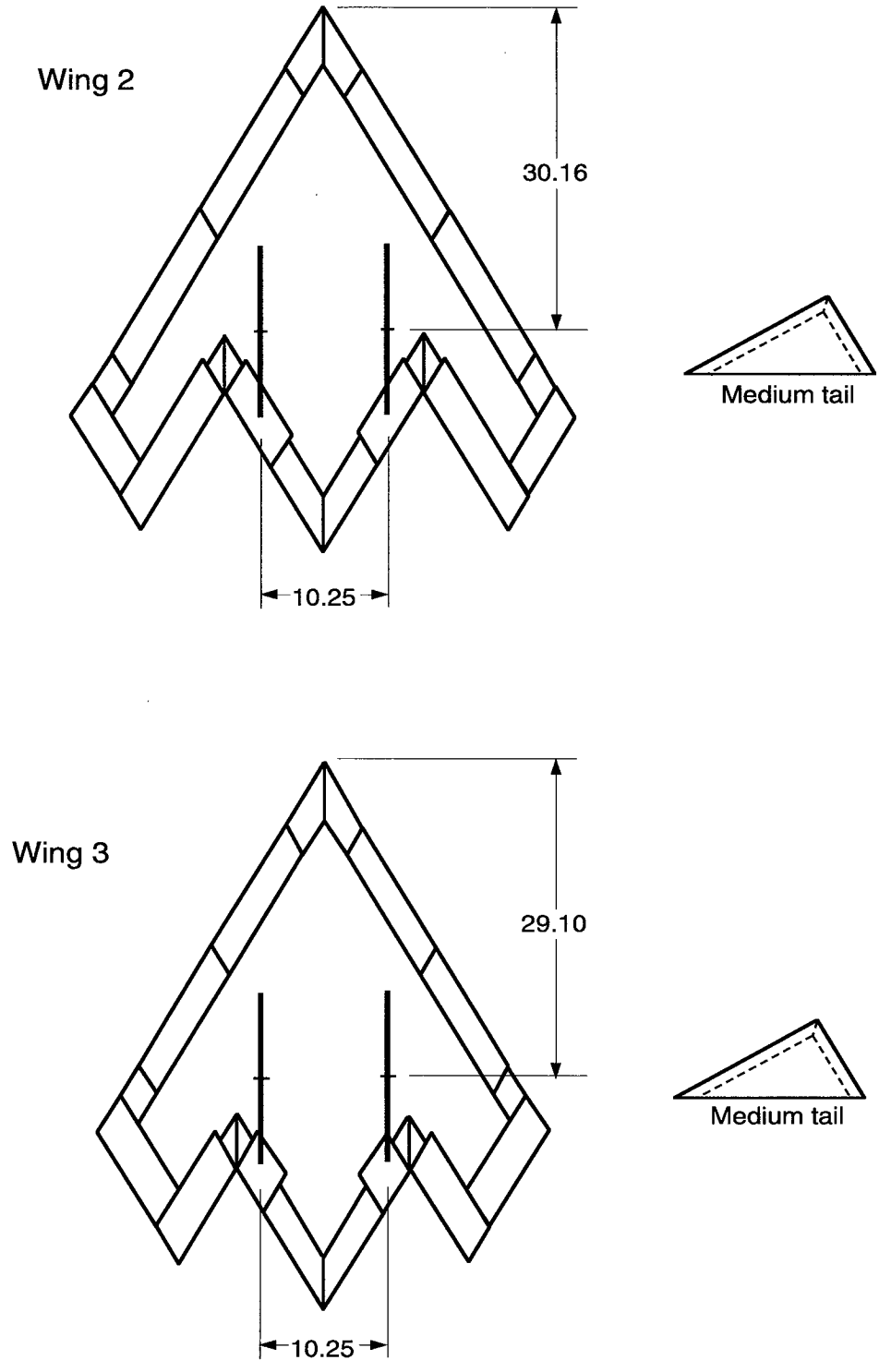

(a) Medium tails at inboard location on Wing 2 and Wing 3.

Figure 15. Inboard vertical tail locations for medium tails on Wings 2, 3, and 4. All dimensions are in inches.

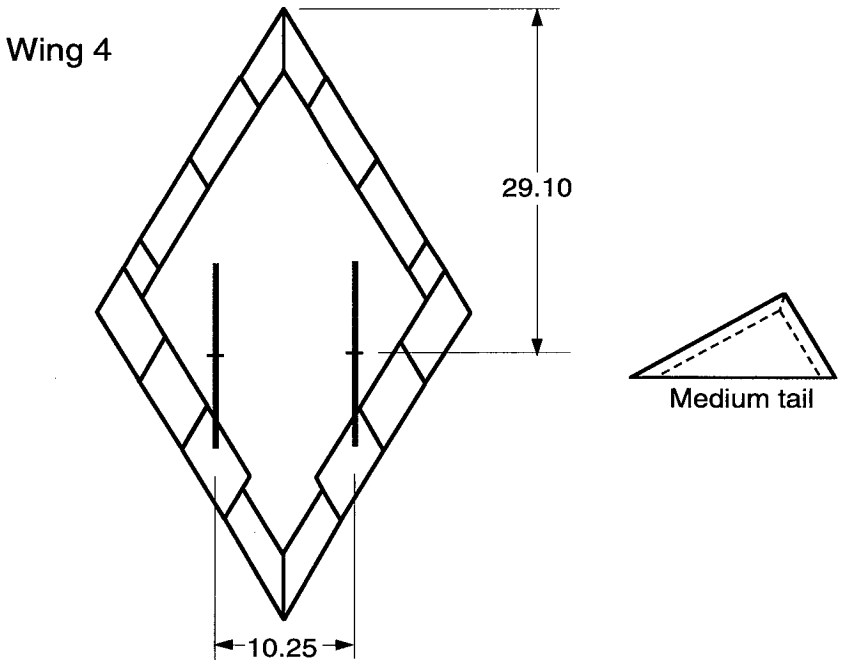

(b) Medium tails at inboard location on Wing 4.

Figure 15. Concluded.

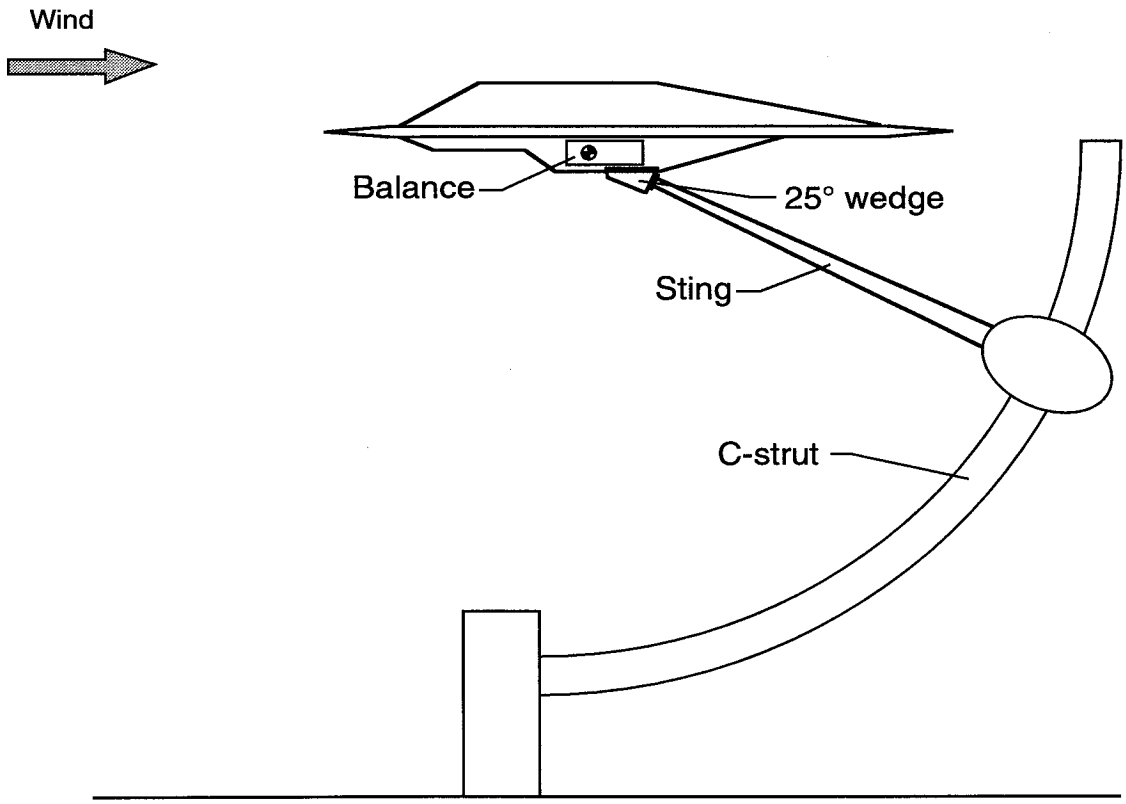

Figure 16. Typical configuration mounted on sting and C-strut arrangement in wind-tunnel test section. Not to scale.

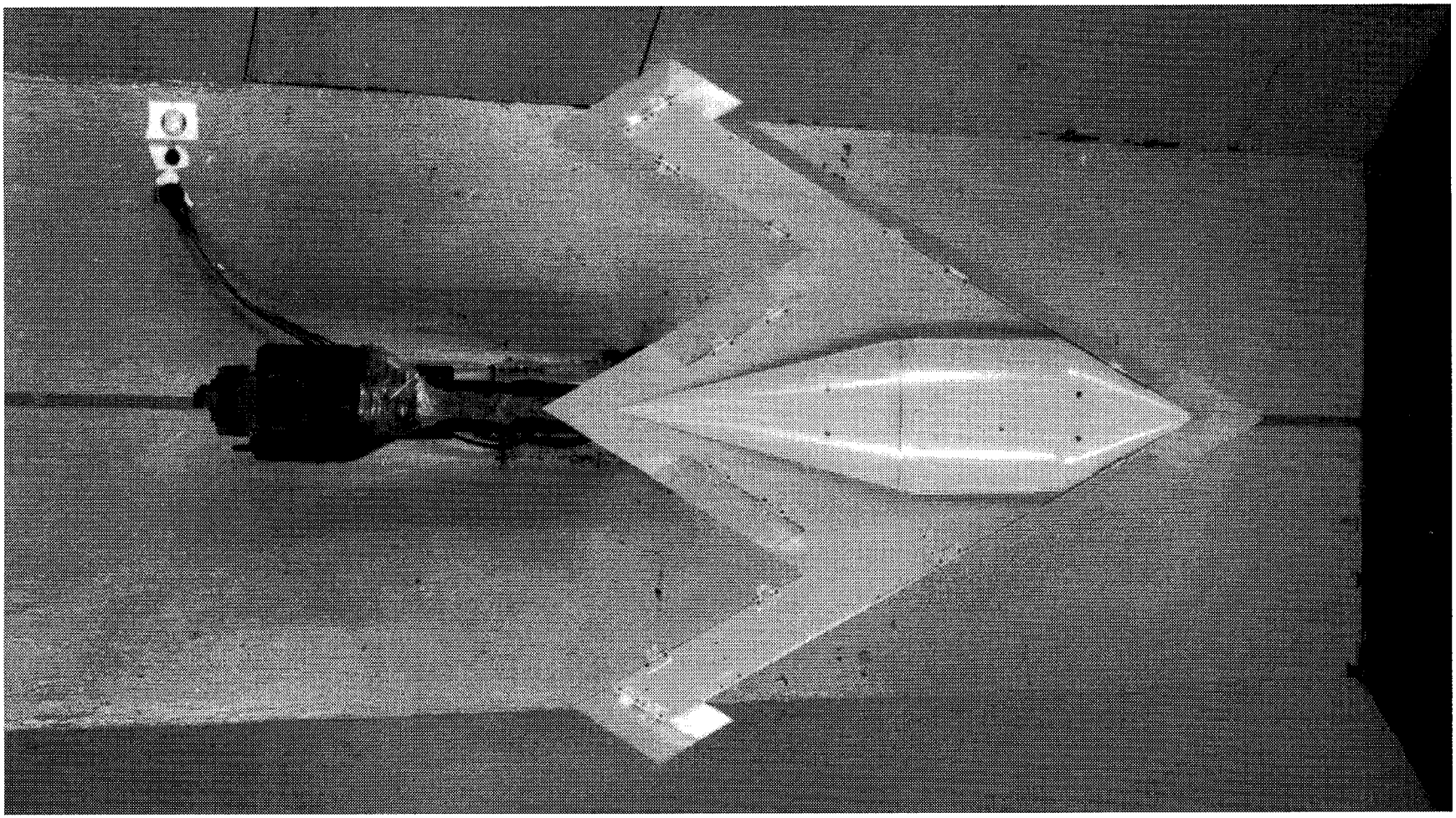

(a) Top view.

Figure 17. Wing 1 mounted in wind tunnel. Leading-edge flaps are deflected, trailing-edge flaps undeflected.

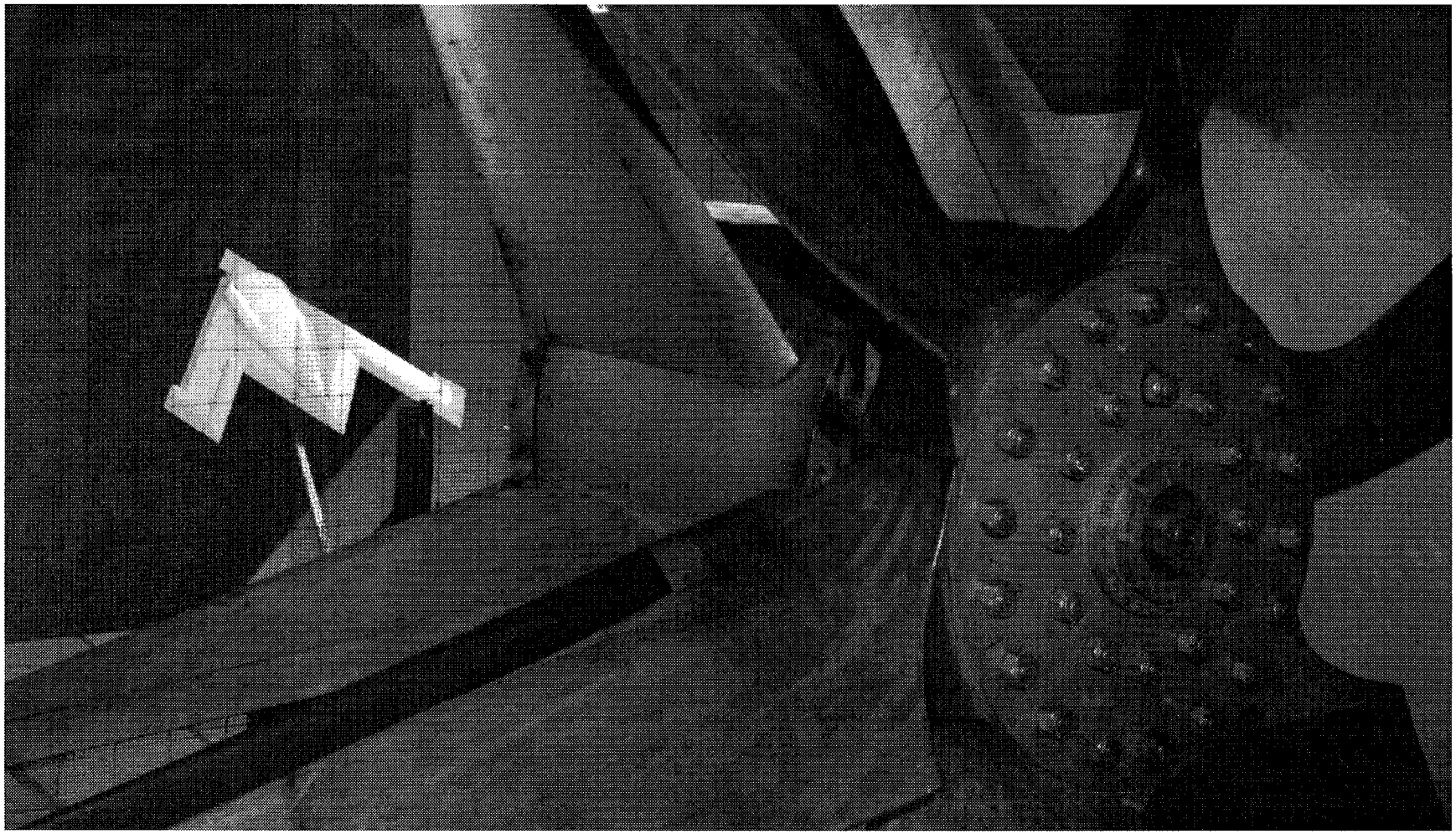

(b) Three-quarter rear view.

Figure 17. Concluded.

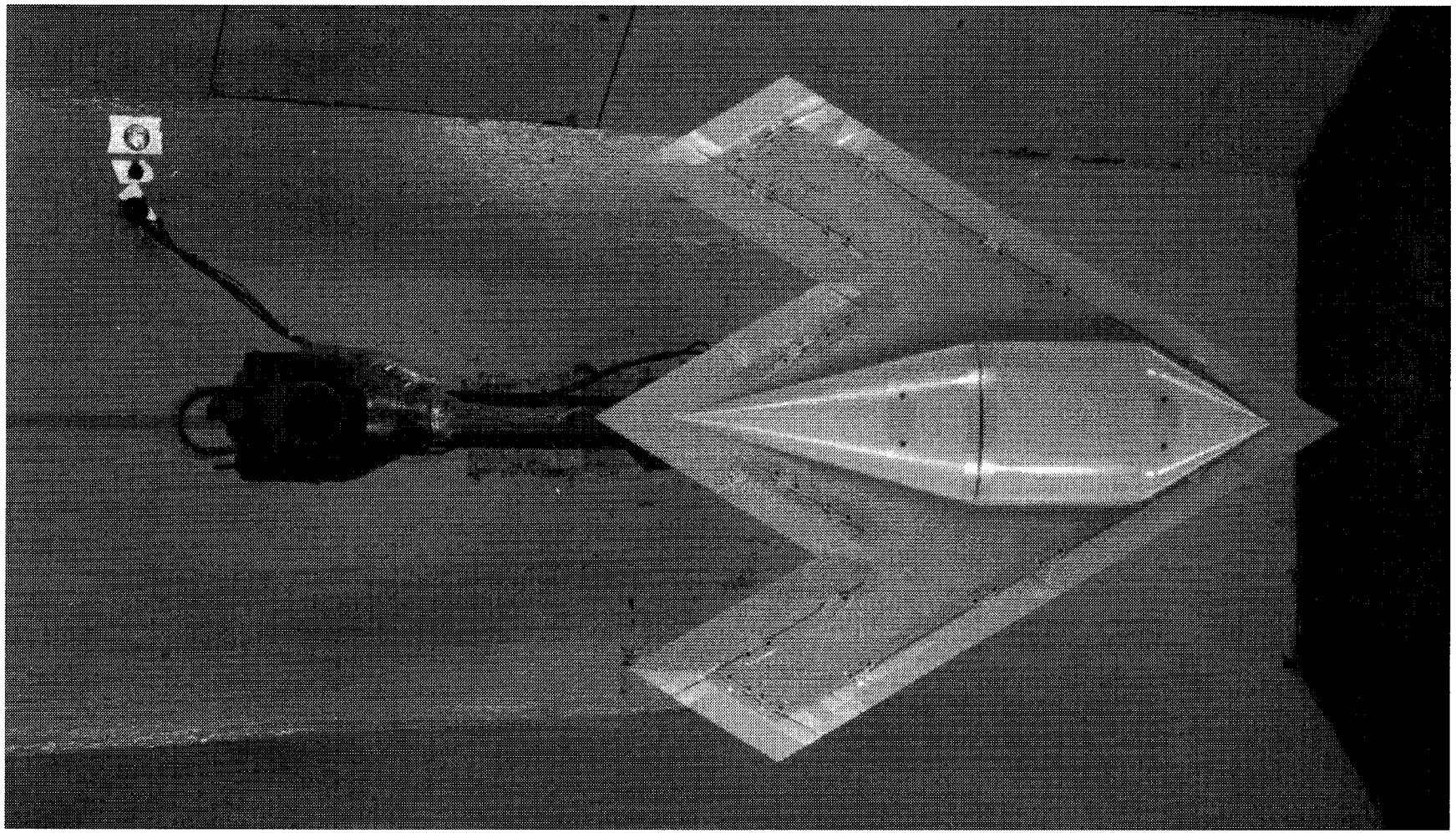

Figure 18. Wing 2 mounted in wind tunnel. Leading-edge and trailing-edge flaps undeflected.

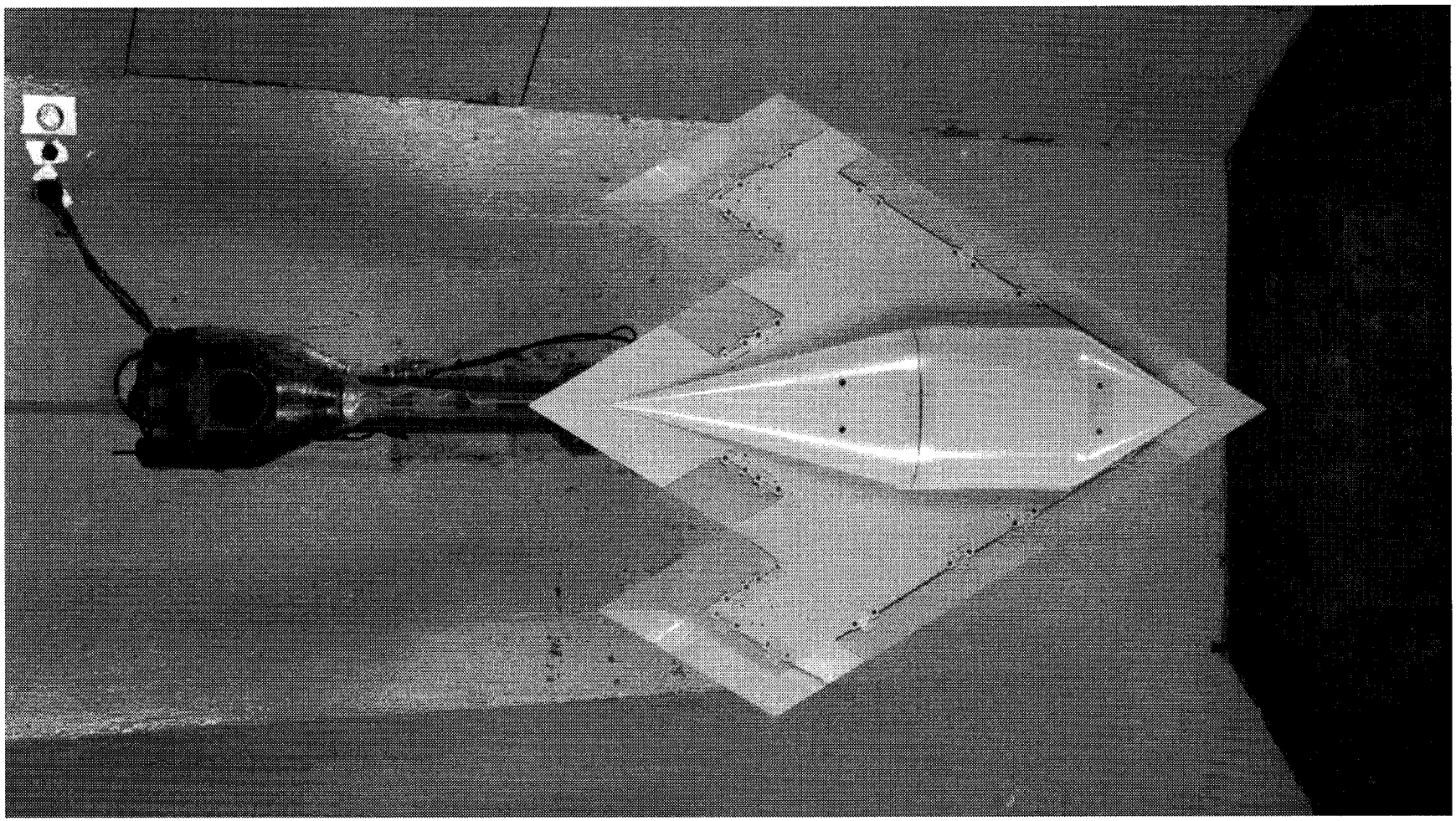

Figure 19. Wing 3 mounted in wind tunnel. Leading-edge and trailing-edge flaps undeflected.

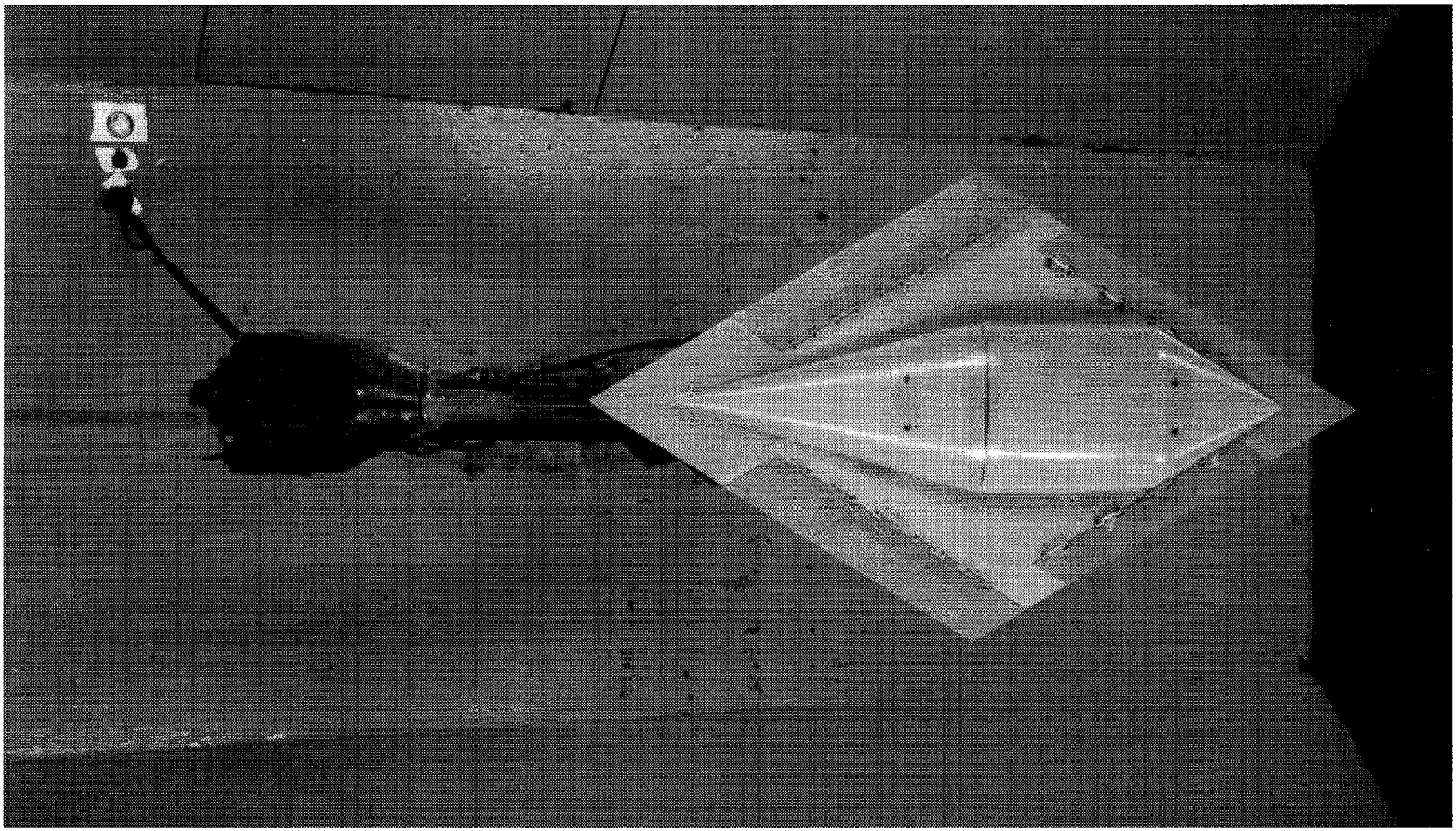

Figure 20. Wing 4 mounted in wind tunnel. Leading-edge and trailing-edge flaps undeflected.

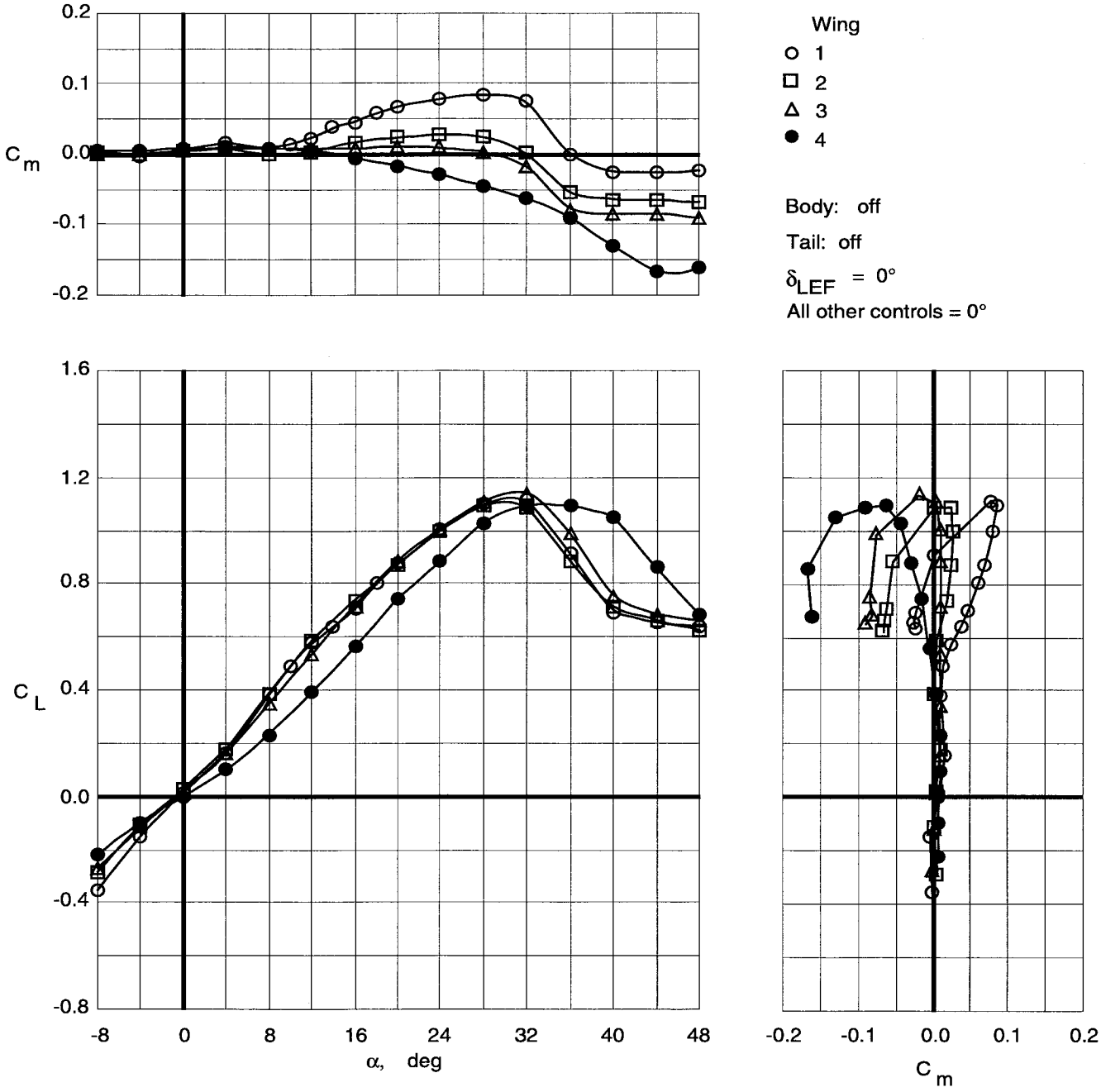

Figure 21. Longitudinal characteristics of wing planforms with top body off.

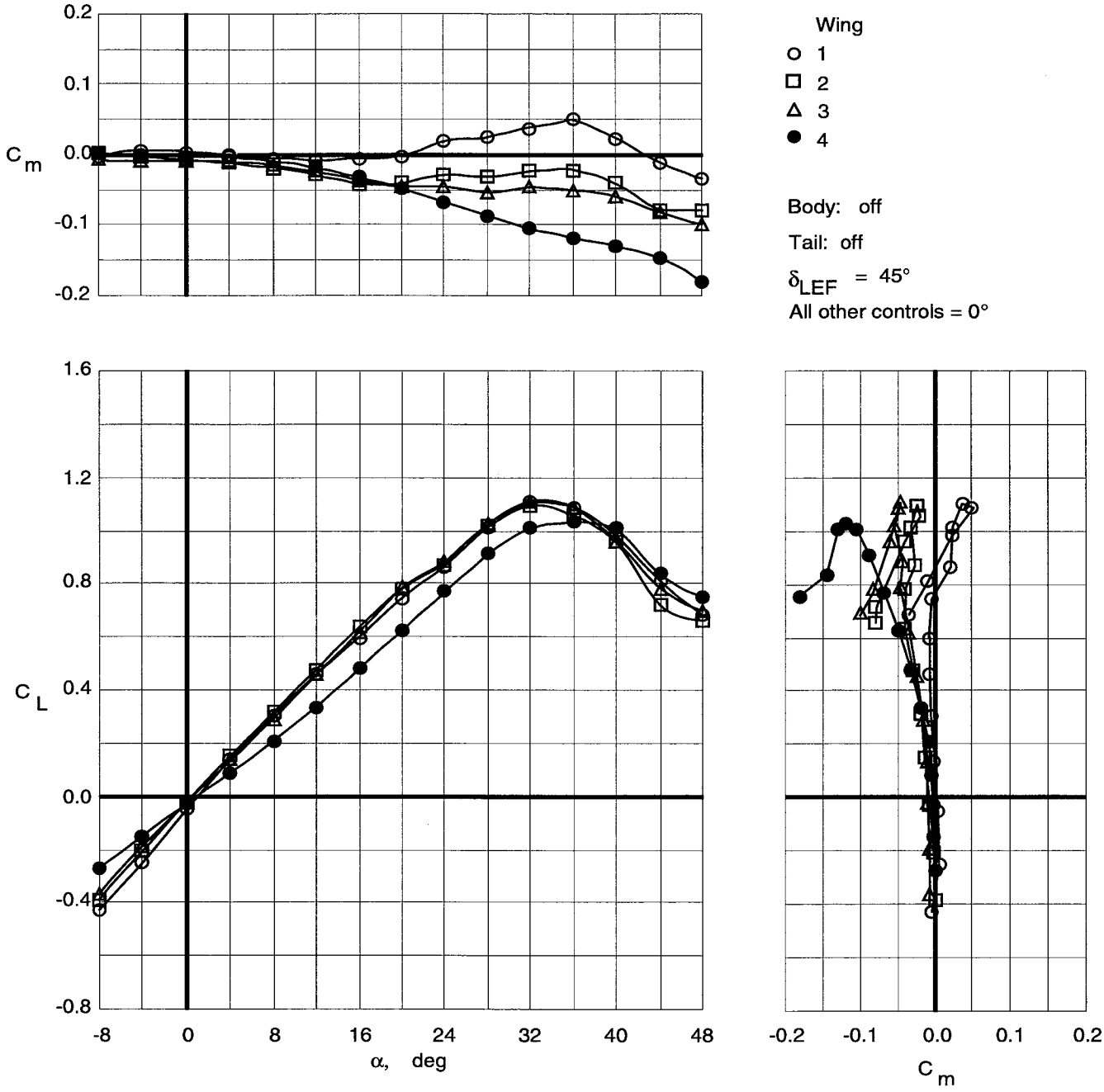

Figure 22. Longitudinal characteristics of wing planforms with top body off and leading-edge flaps deflected.

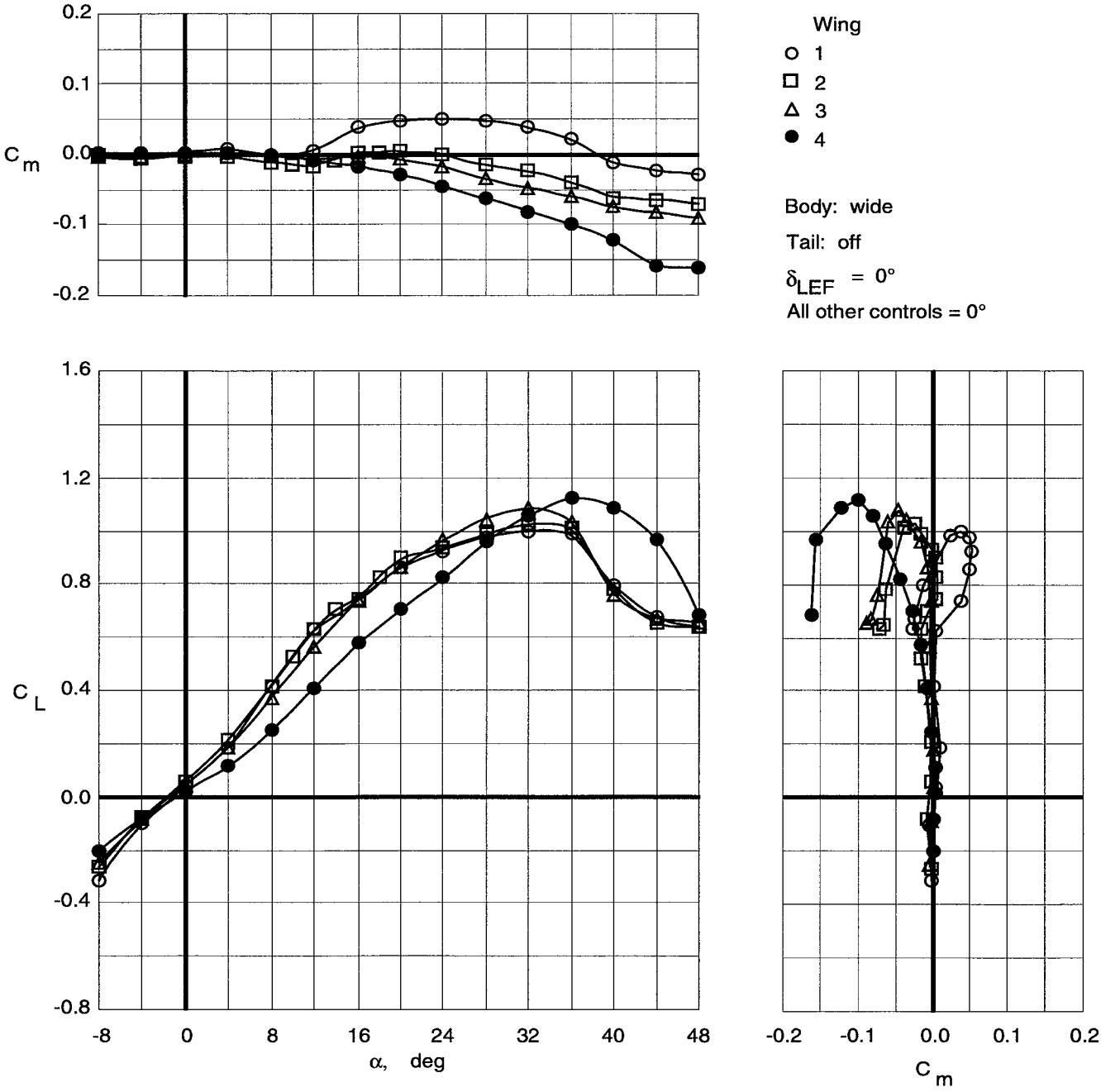

Figure 23. Longitudinal characteristics of wing planforms with wide top body on.

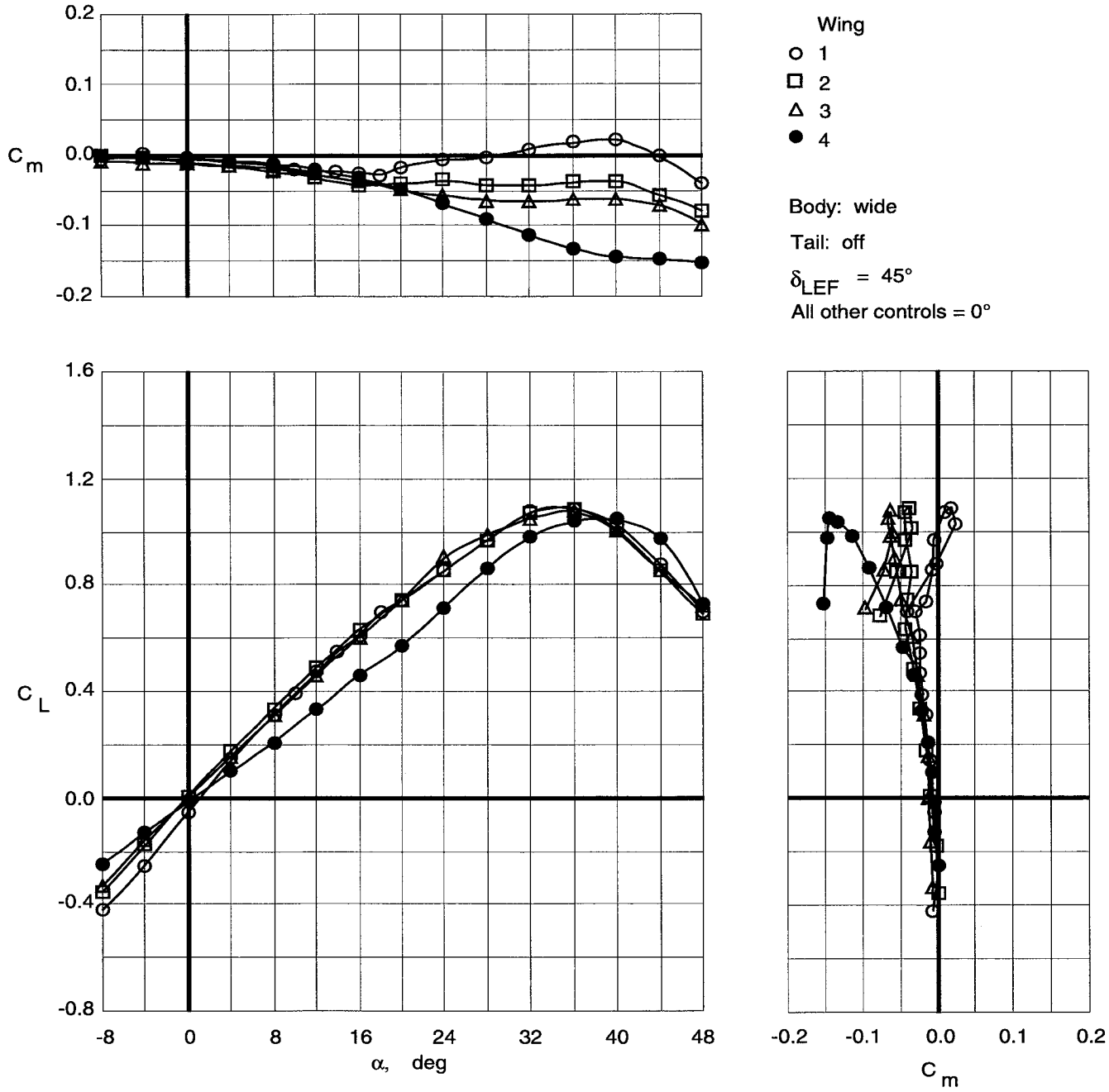

Figure 24. Longitudinal characteristics of wing planforms with wide top body on and leading-edge flaps deflected.

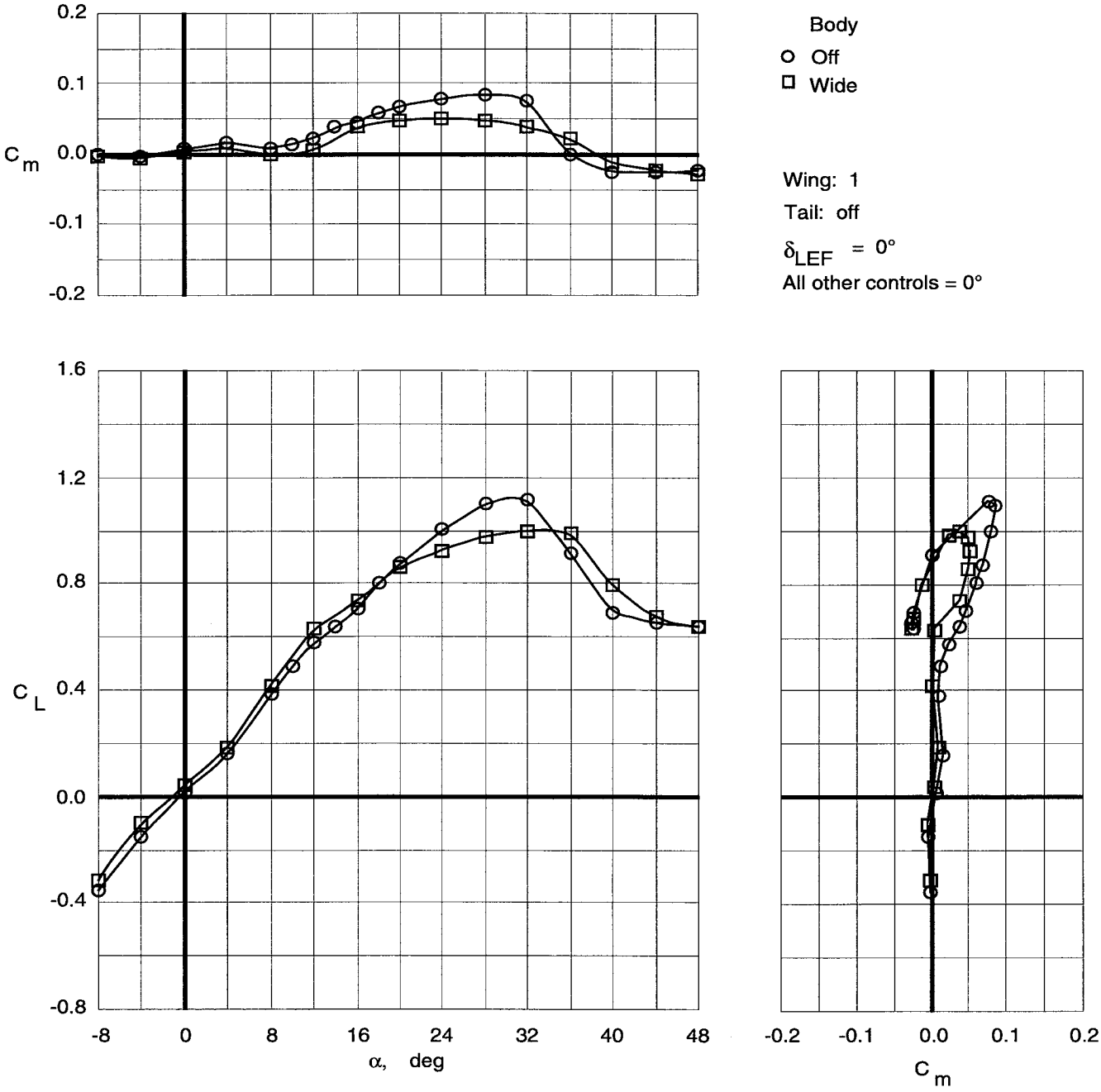

Figure 25. Effect of wide top body on longitudinal characteristics of Wing 1.

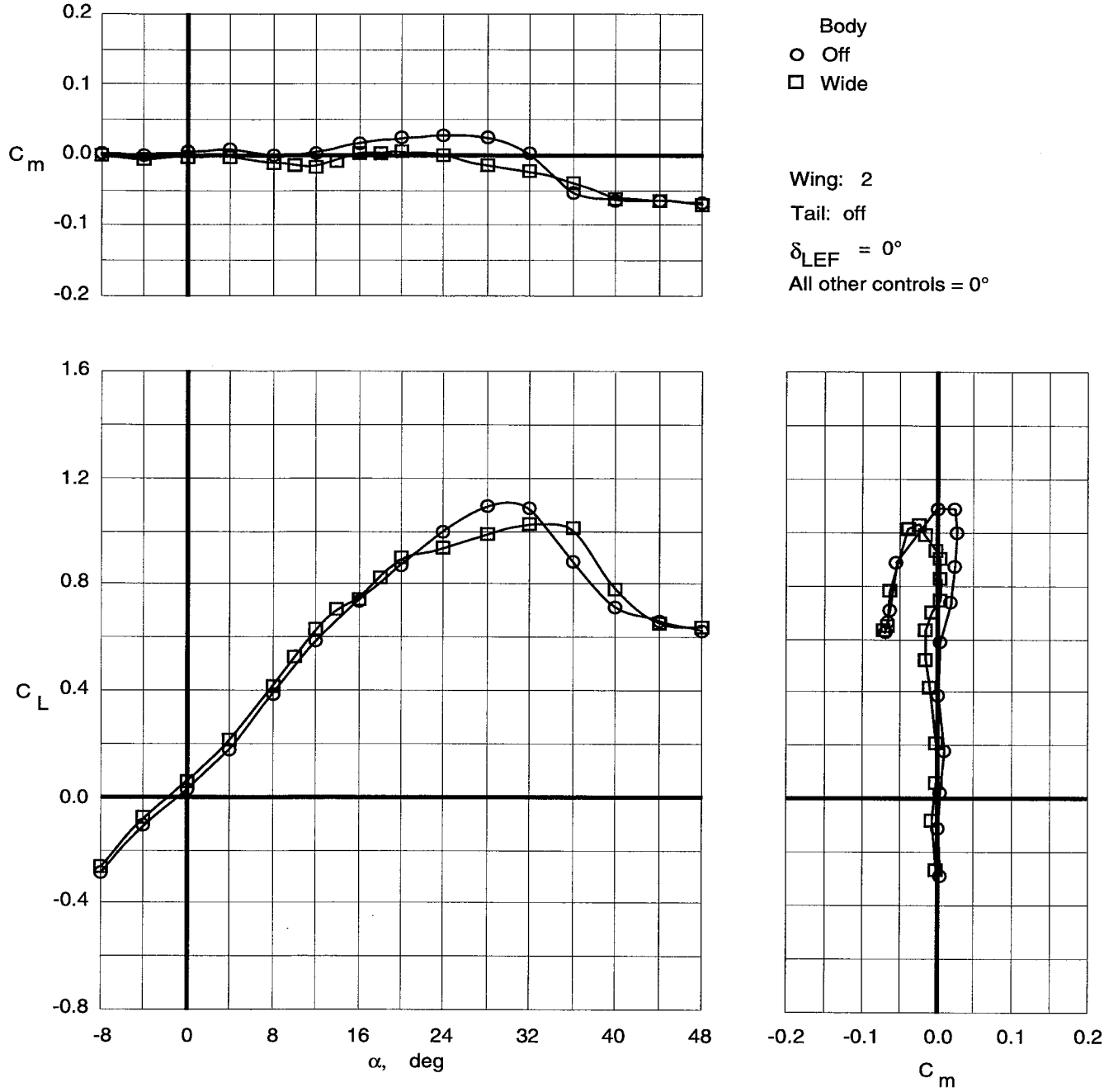

Figure 26. Effect of wide top body on longitudinal characteristics of Wing 2.

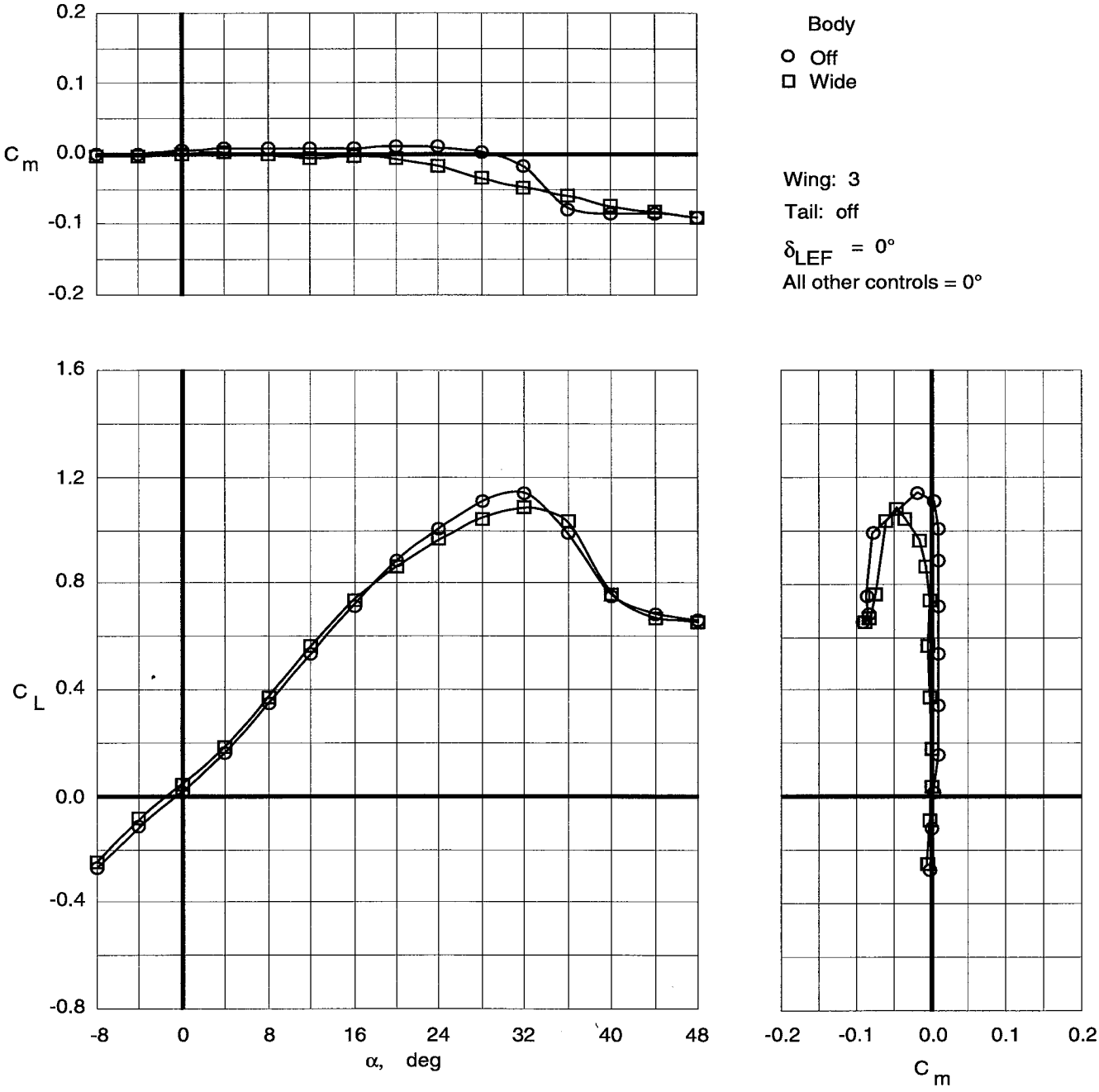

Figure 27. Effect of wide top body on longitudinal characteristics of Wing 3.

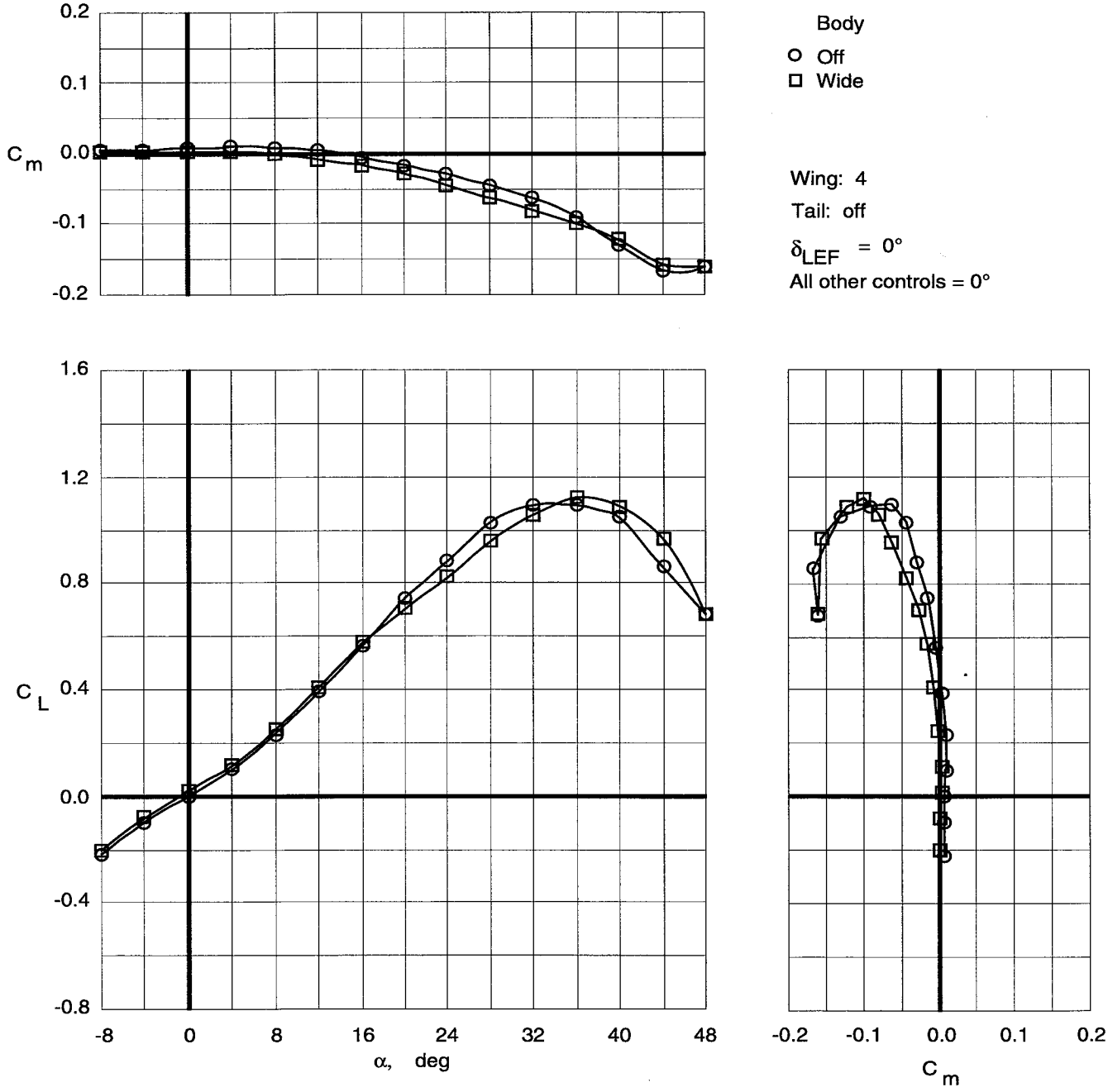

Figure 28. Effect of wide top body on longitudinal characteristics of Wing 4.

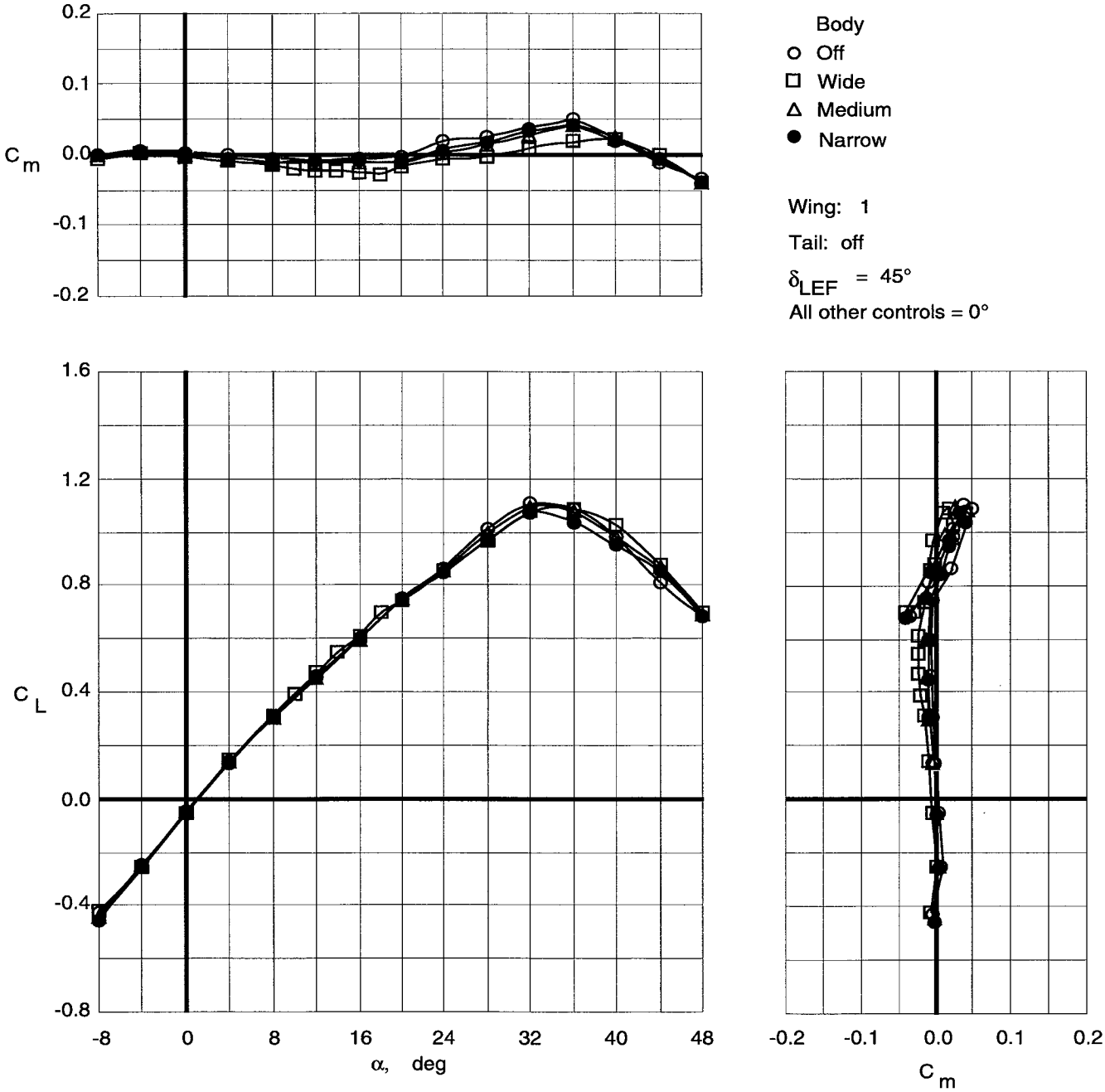

Figure 29. Effect of top body width on longitudinal characteristics of Wing 1 with leading-edge flaps deflected.

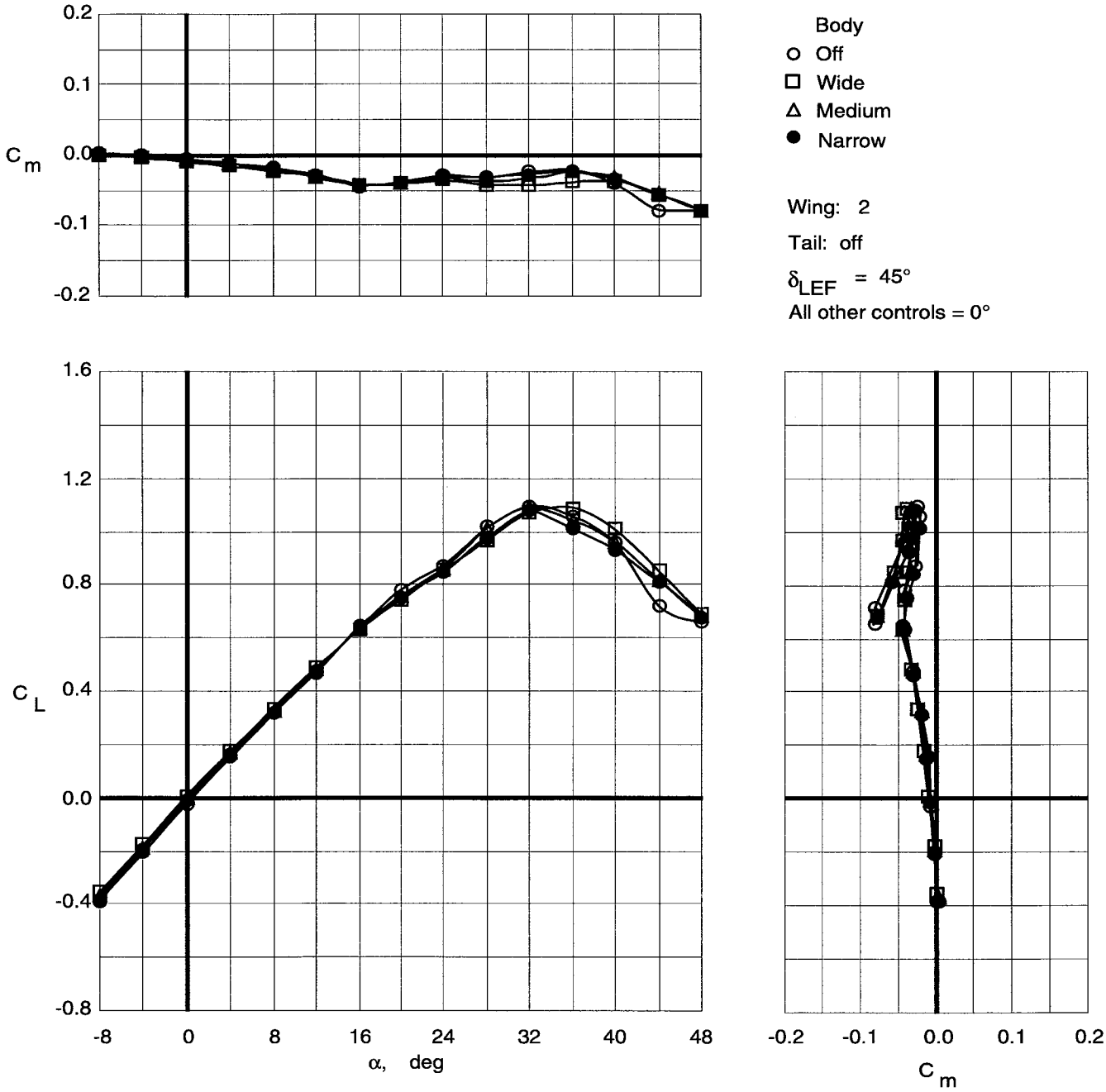

Figure 30. Effect of top body width on longitudinal characteristics of Wing 2 with leading-edge flaps deflected.

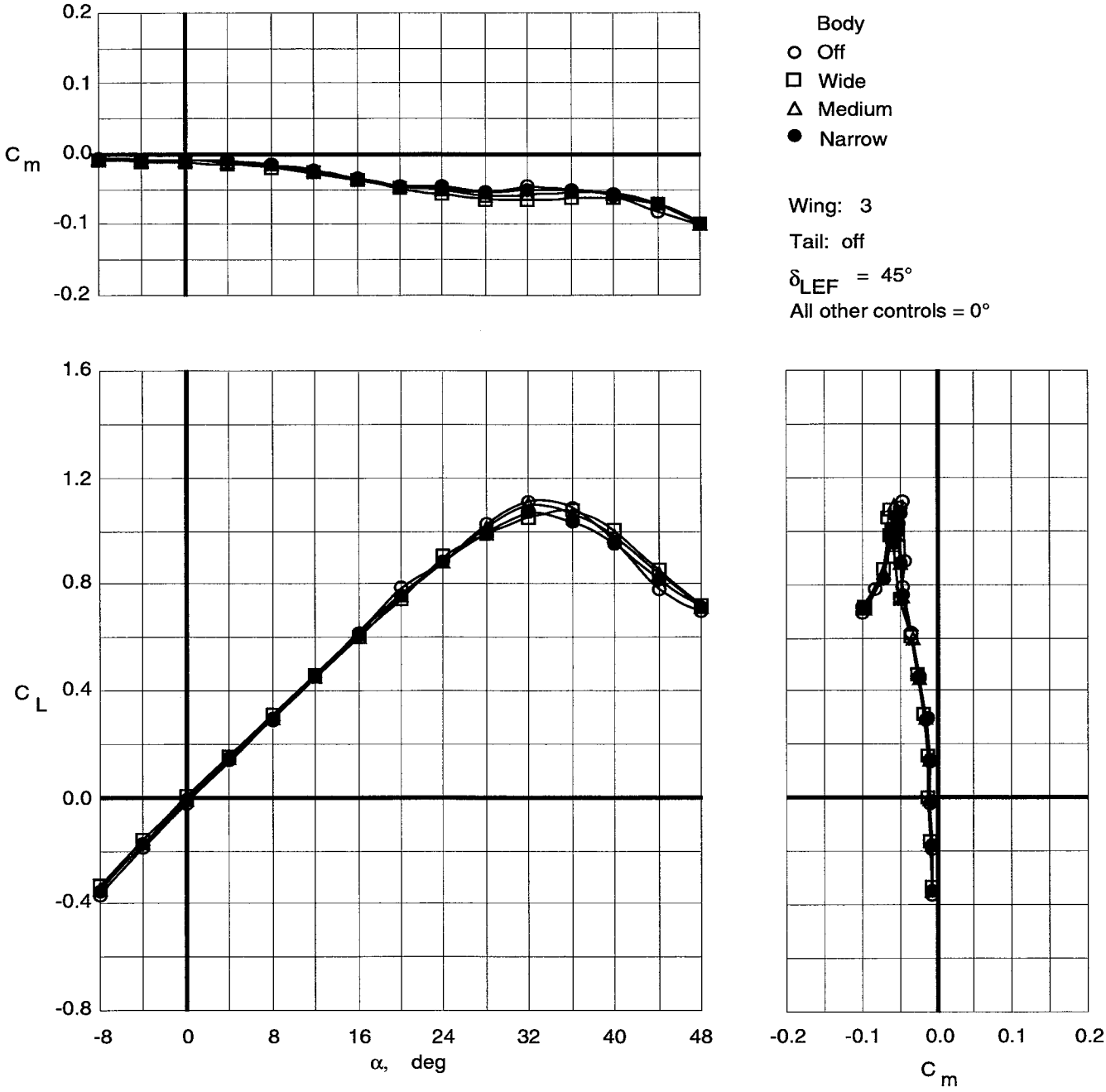

Figure 31. Effect of top body width on longitudinal characteristics of Wing 3 with leading-edge flaps deflected.

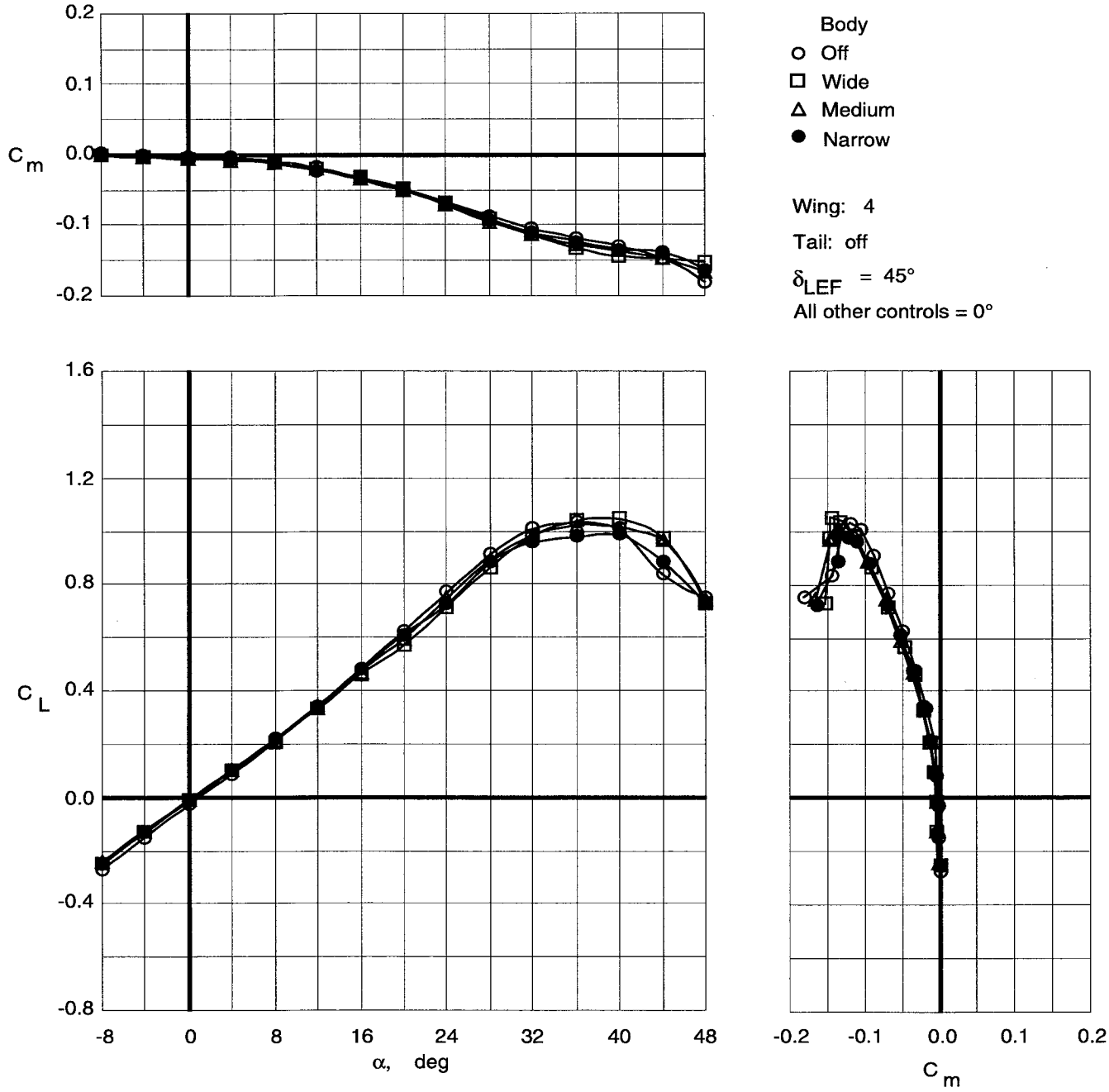

Figure 32. Effect of top body width on longitudinal characteristics of Wing 4 with leading-edge flaps deflected.

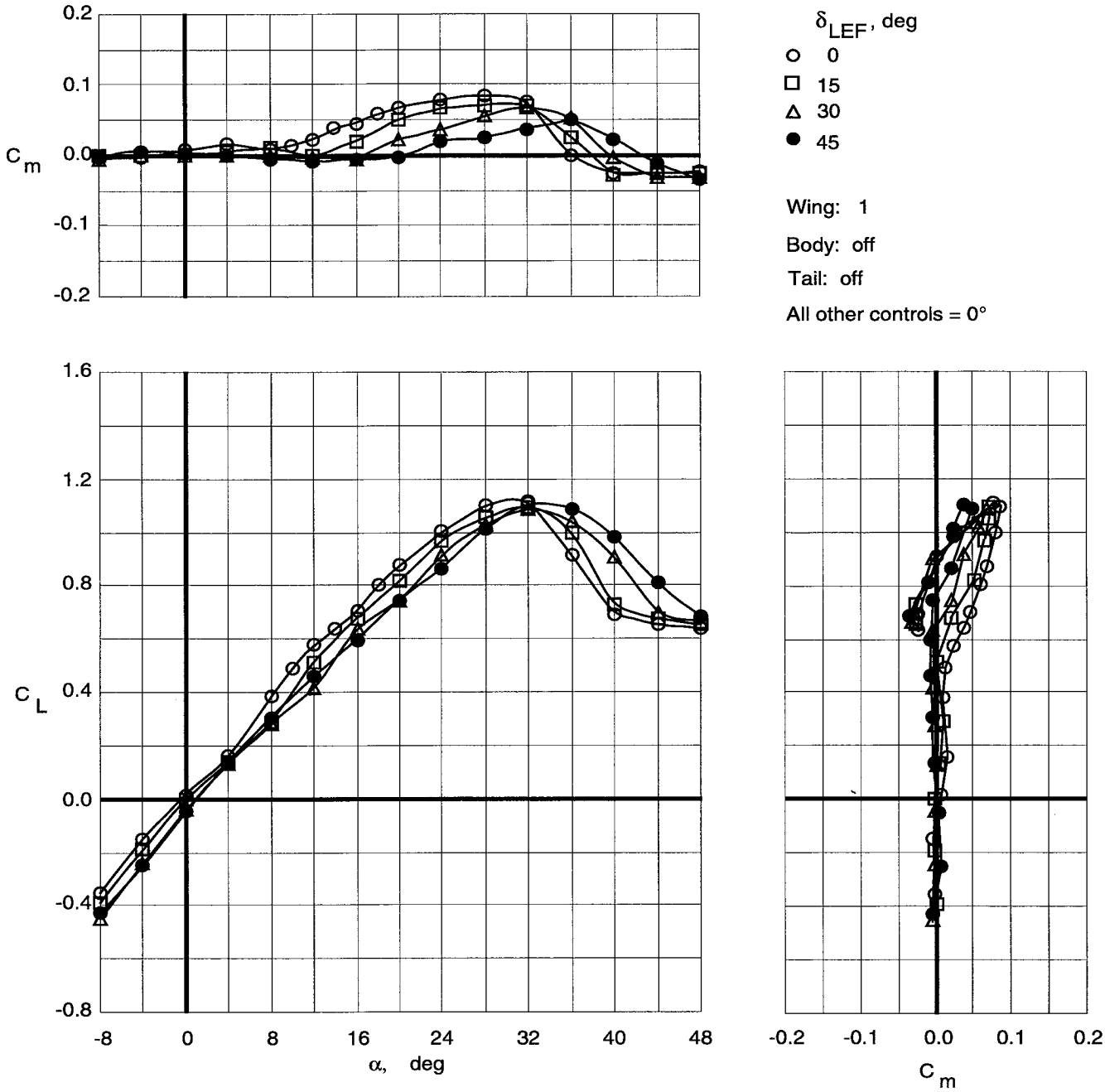

Figure 33. Effect of leading-edge flap deflections on longitudinal characteristics of Wing 1 with top body off.

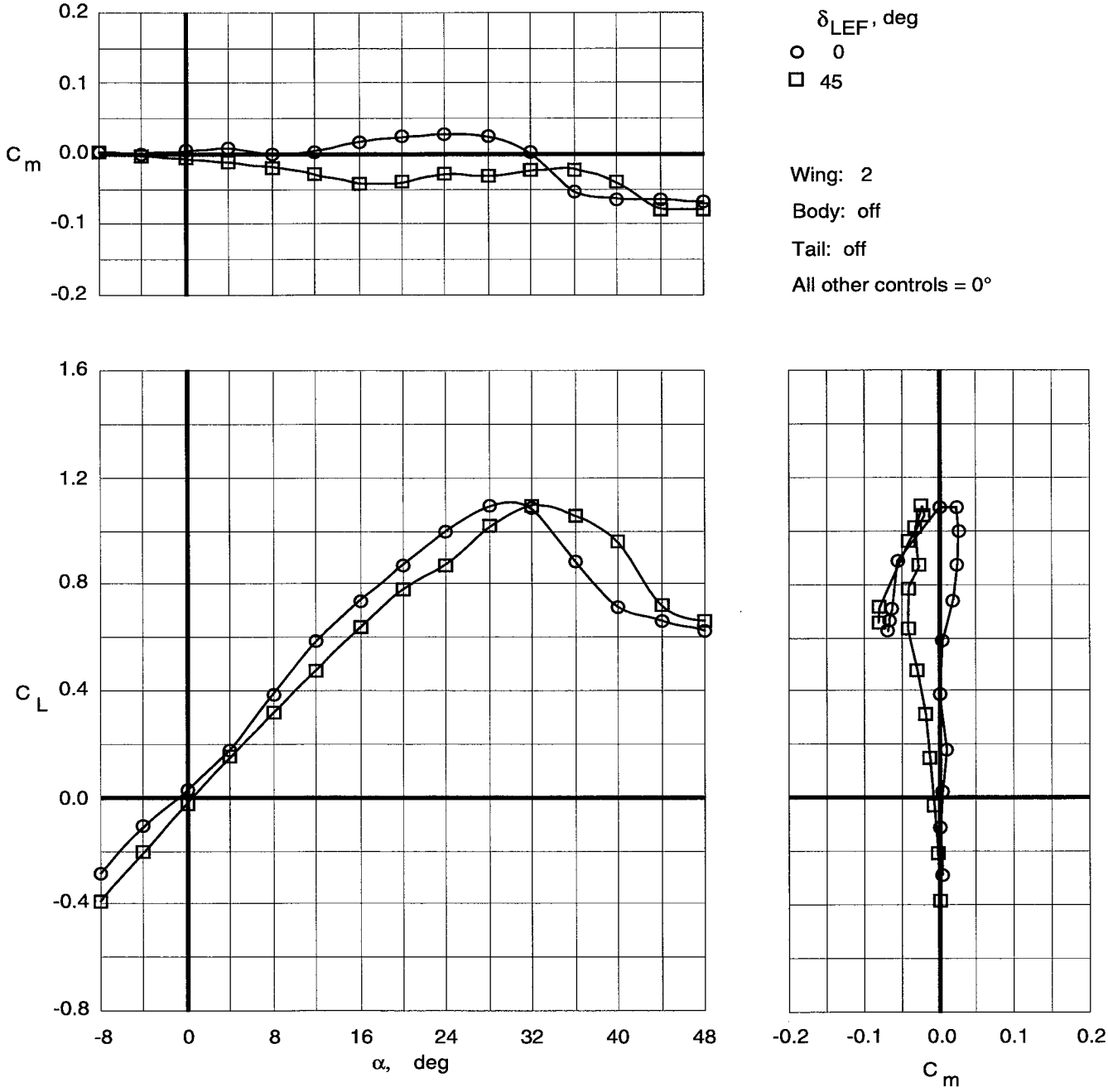

Figure 34. Effect of leading-edge flap deflection on longitudinal characteristics of Wing 2 with top body off.

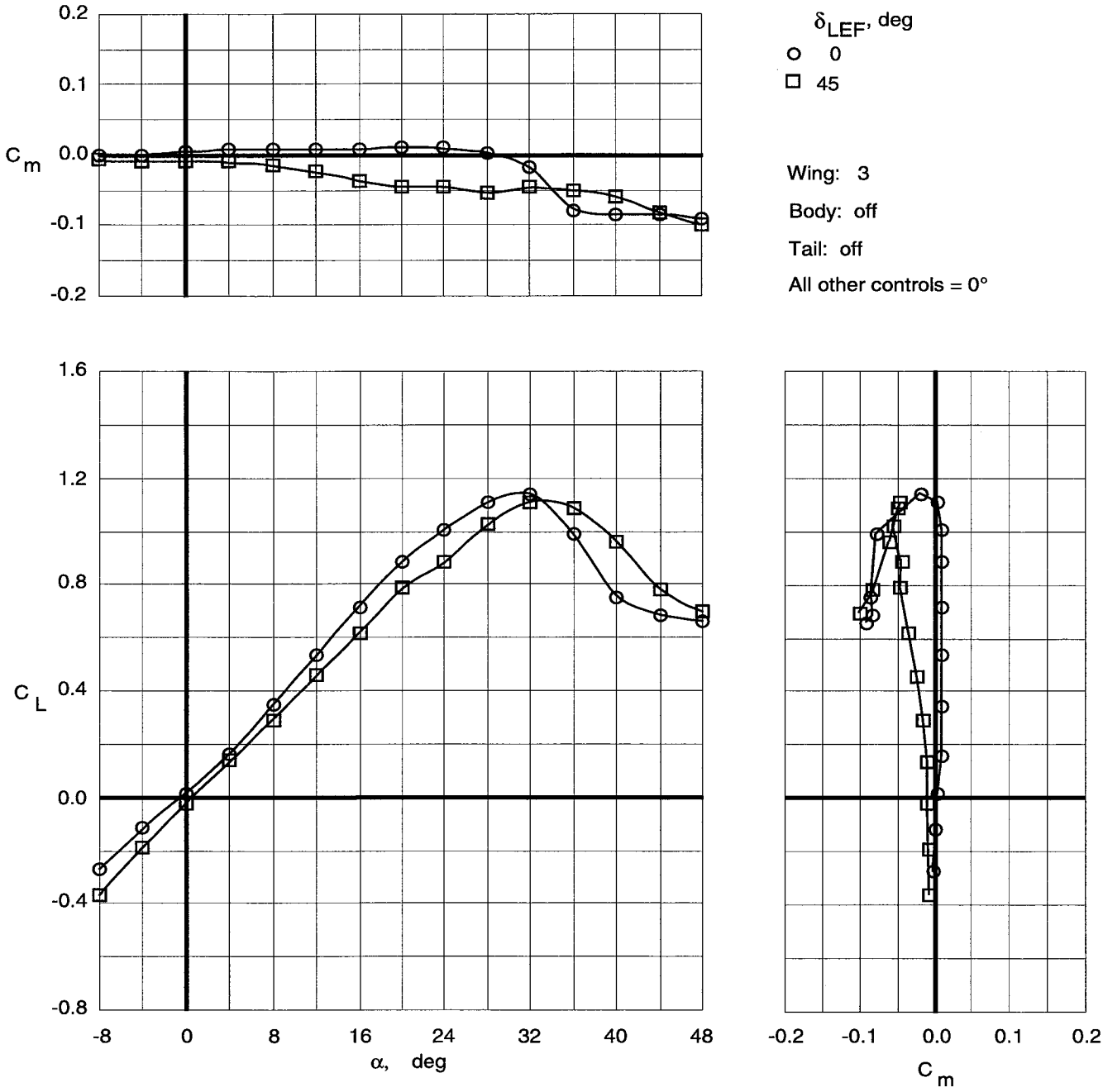

Figure 35. Effect of leading-edge flap deflection on longitudinal characteristics of Wing 3 with top body off.

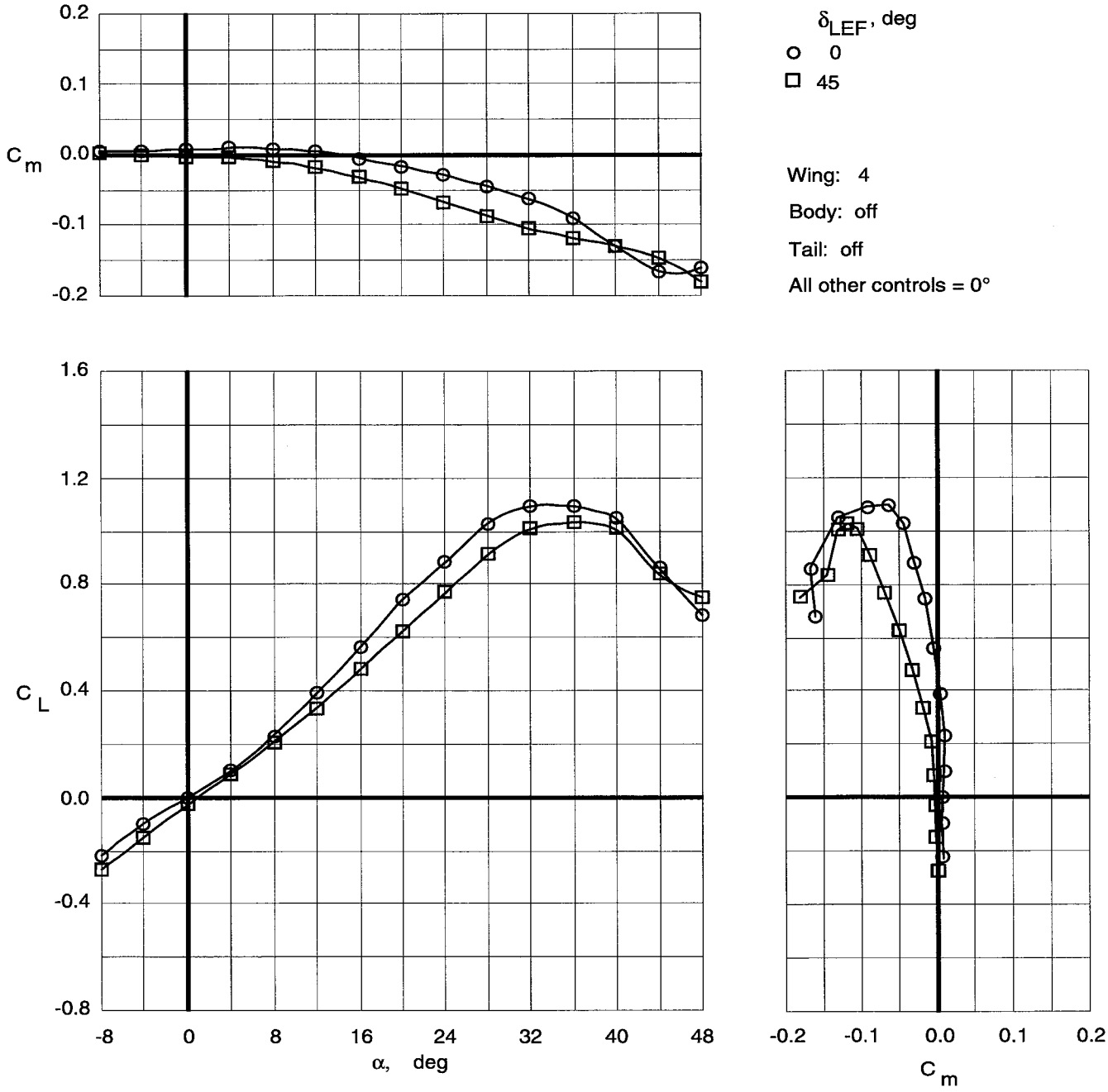

Figure 36. Effect of leading-edge flap deflection on longitudinal characteristics of Wing 4 with top body off.

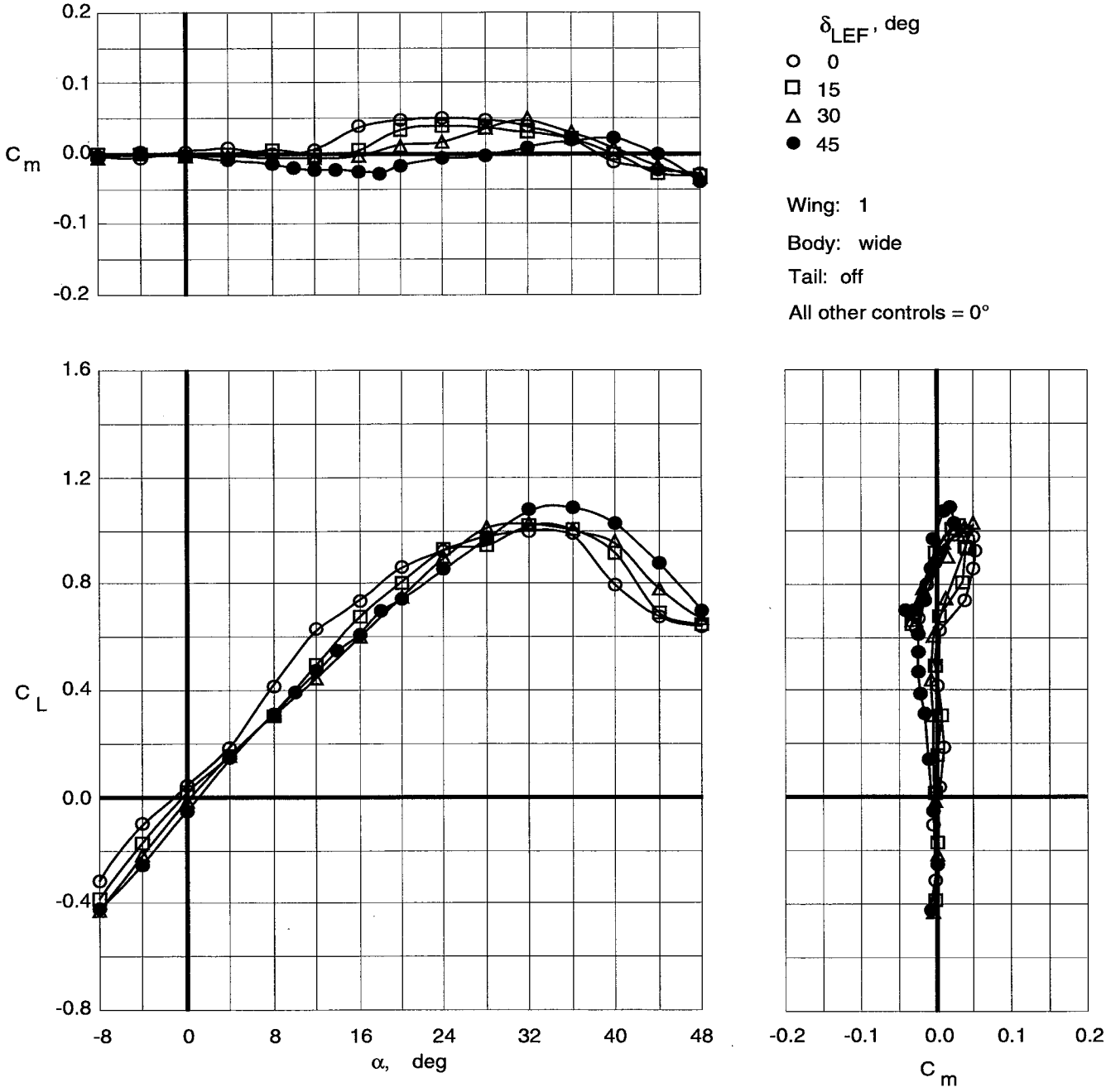

Figure 37. Effect of leading-edge flap deflections on longitudinal characteristics of Wing 1 with wide top body on.

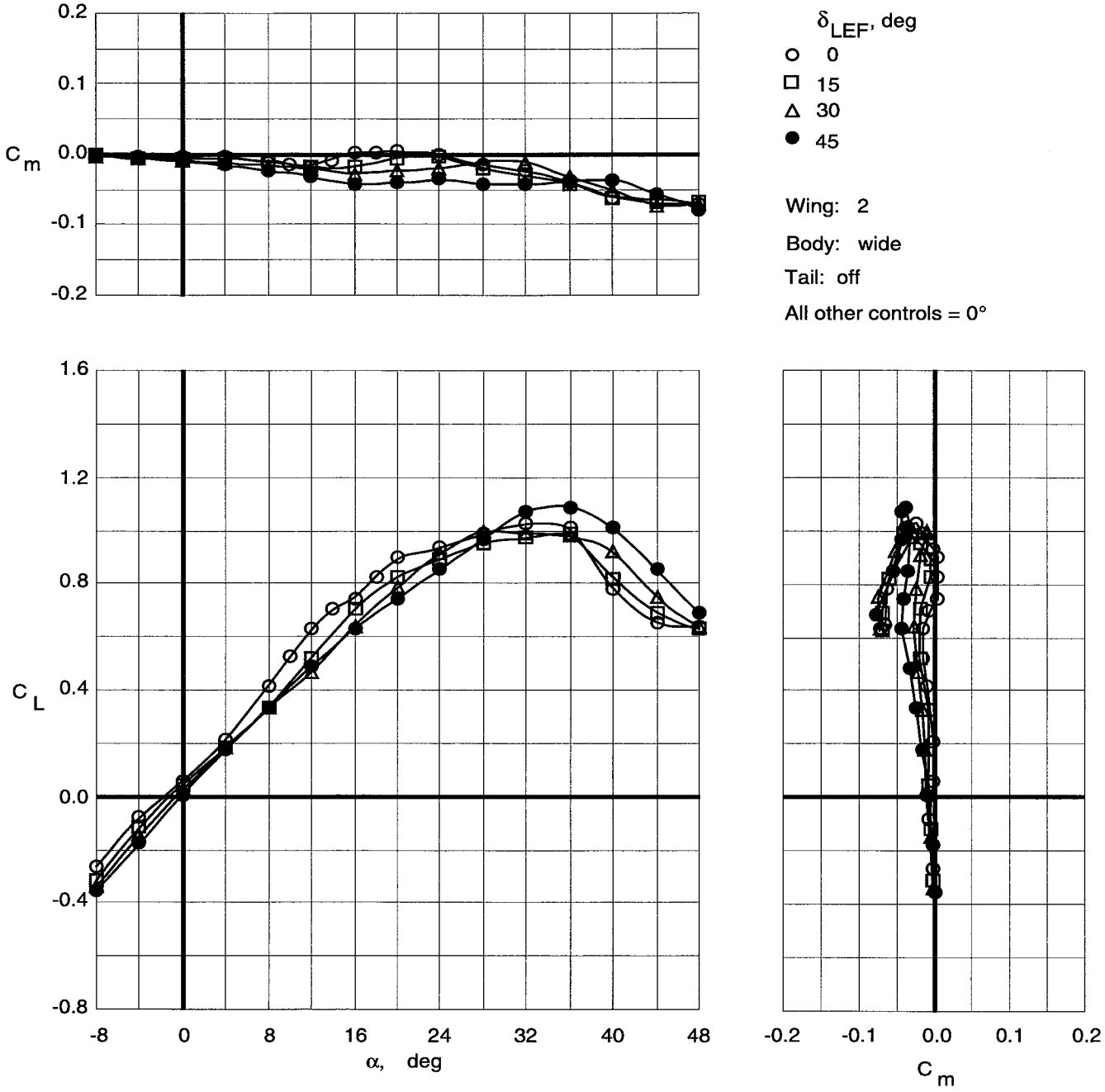

Figure 38. Effect of leading-edge flap deflections on longitudinal characteristics of Wing 2 with wide top body on.

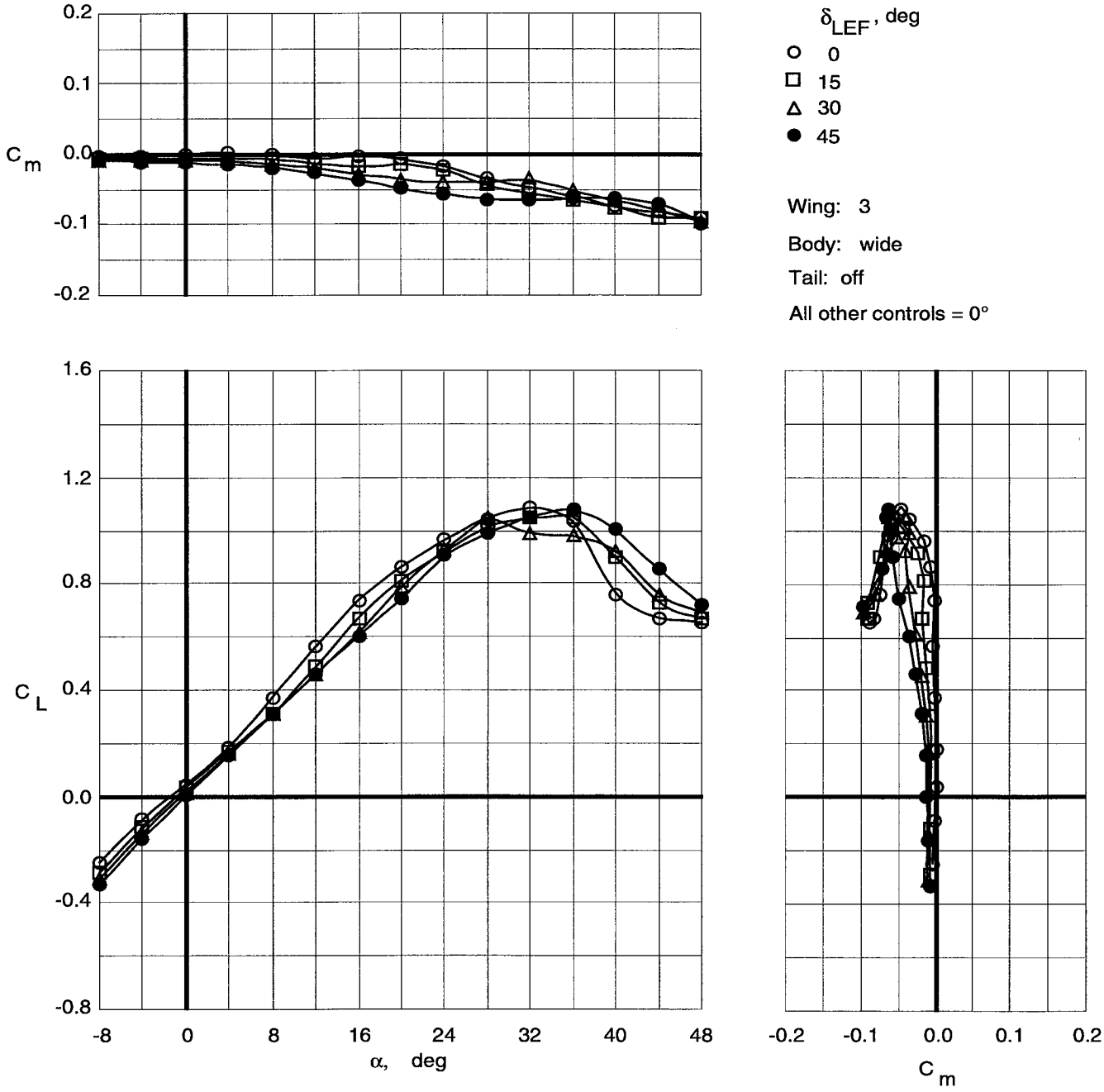

Figure 39. Effect of leading-edge flap deflections on longitudinal characteristics of Wing 3 with wide top body on.

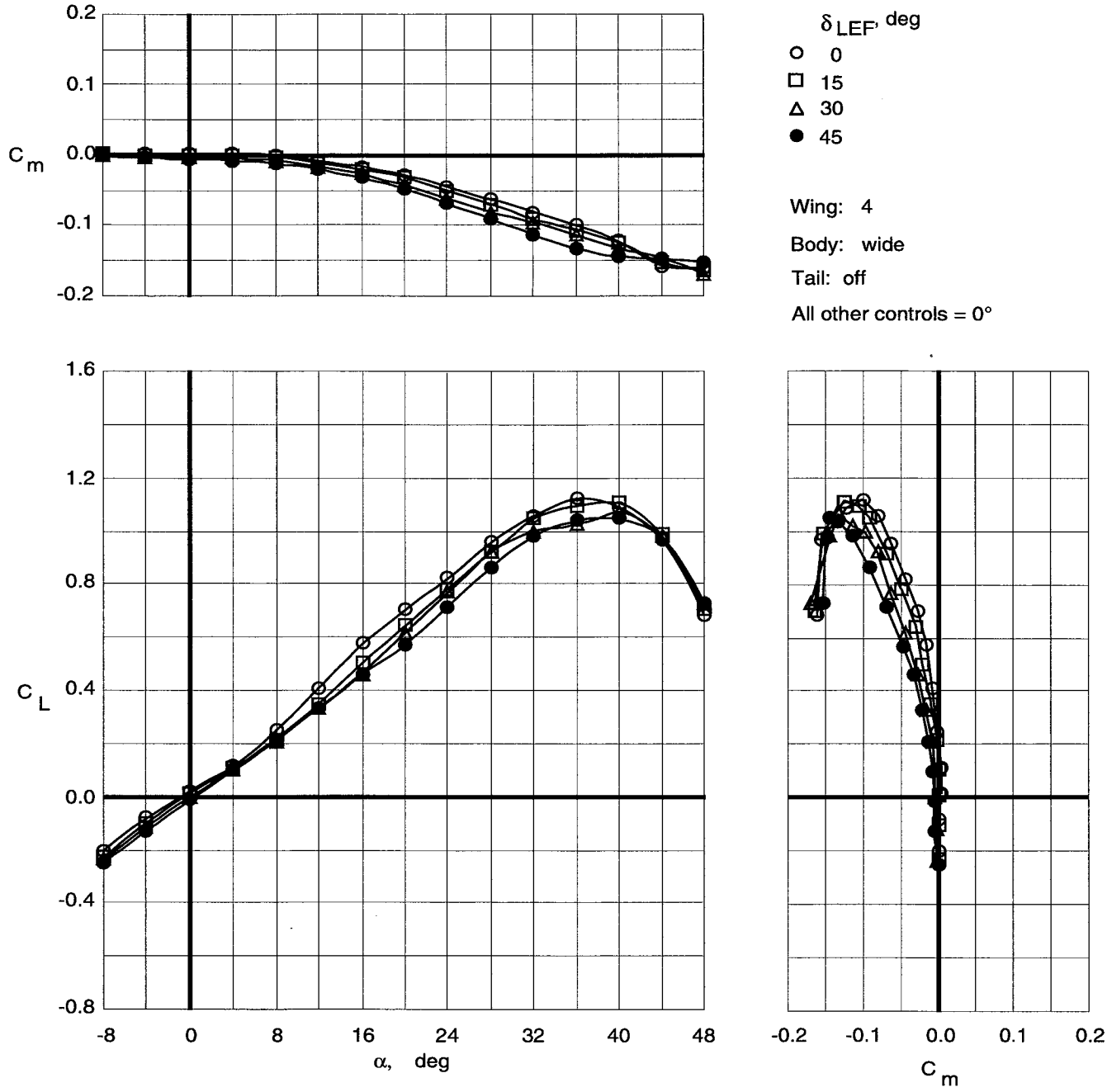

Figure 40. Effect of leading-edge flap deflections on longitudinal characteristics of Wing 4 with wide top body on.

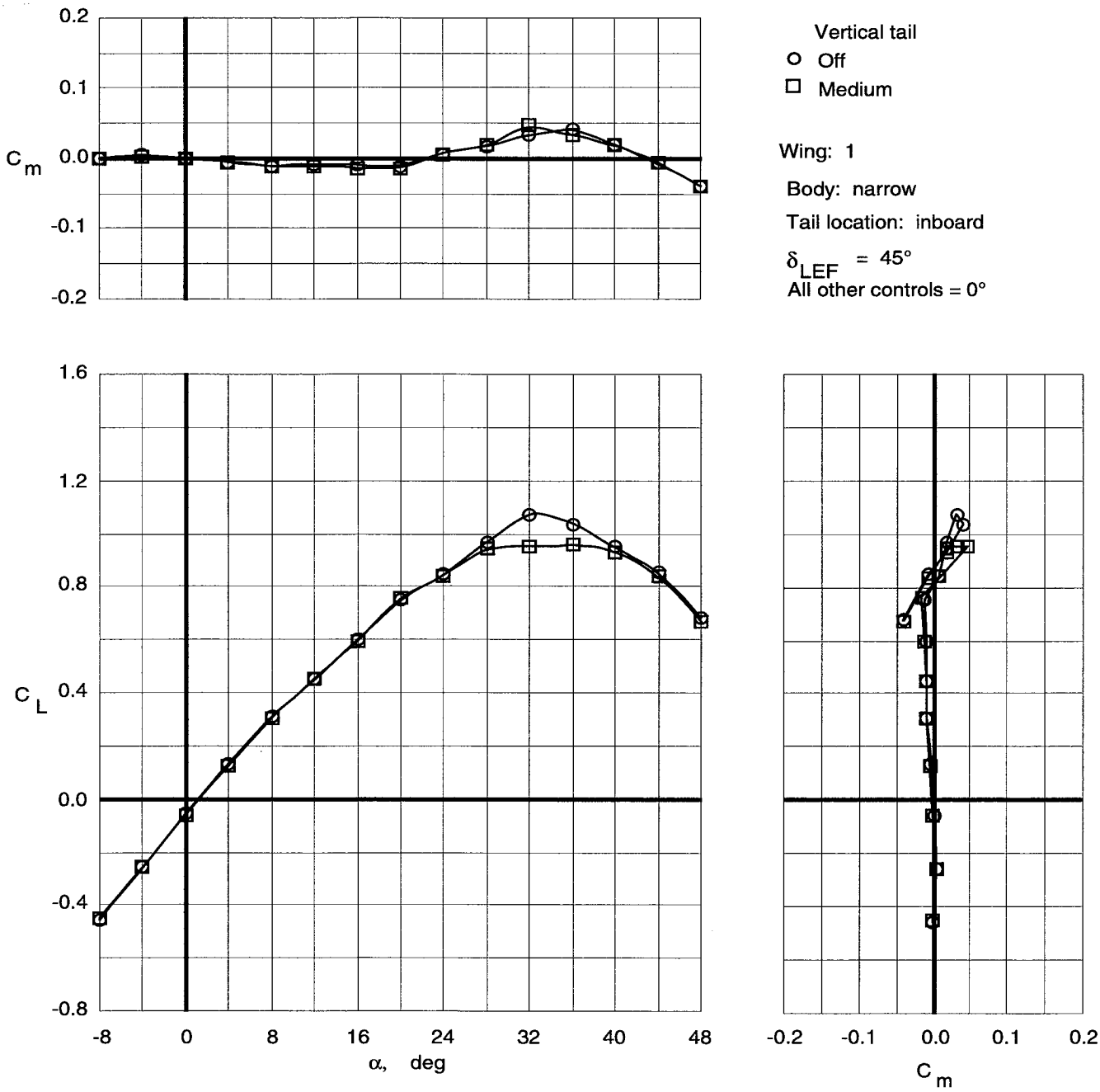

Figure 41. Effect of medium vertical tails on longitudinal characteristics of Wing 1 with narrow top body on and leading-edge flaps deflected.

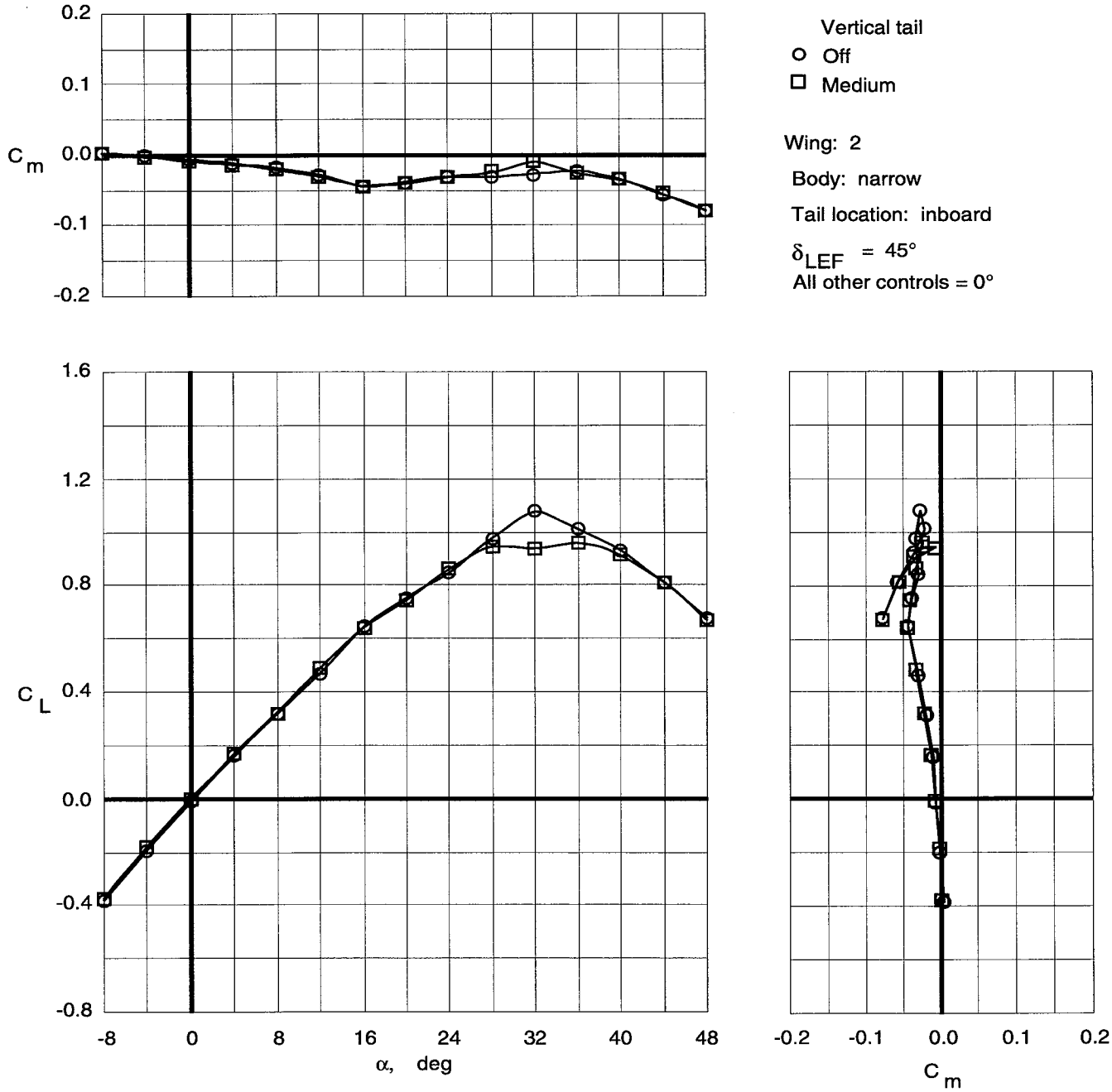

Figure 42. Effect of medium vertical tails on longitudinal characteristics of Wing 2 with narrow top body on and leading-edge flaps deflected.

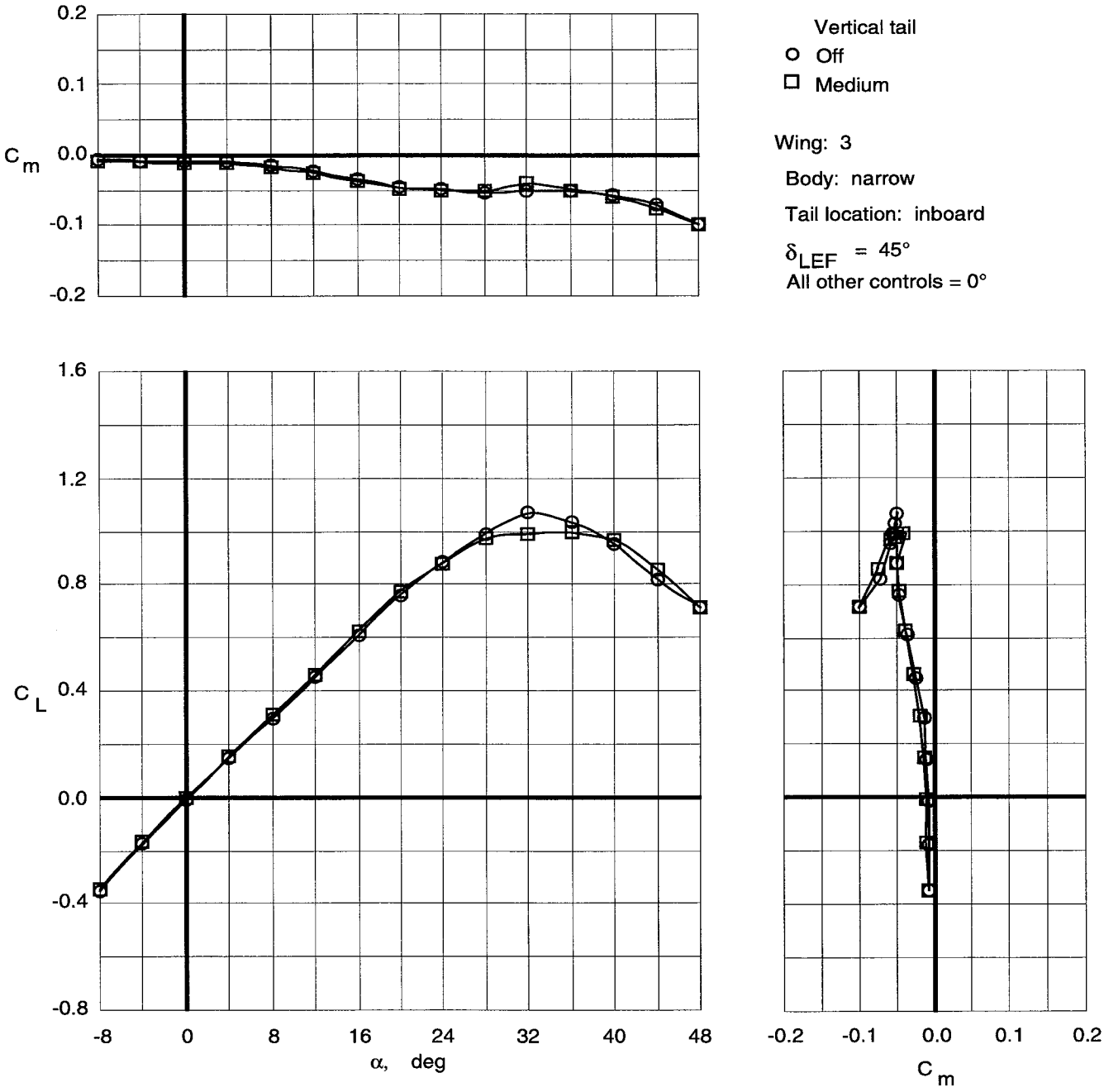

Figure 43. Effect of medium vertical tails on longitudinal characteristics of Wing 3 with narrow top body on and leading-edge flaps deflected.

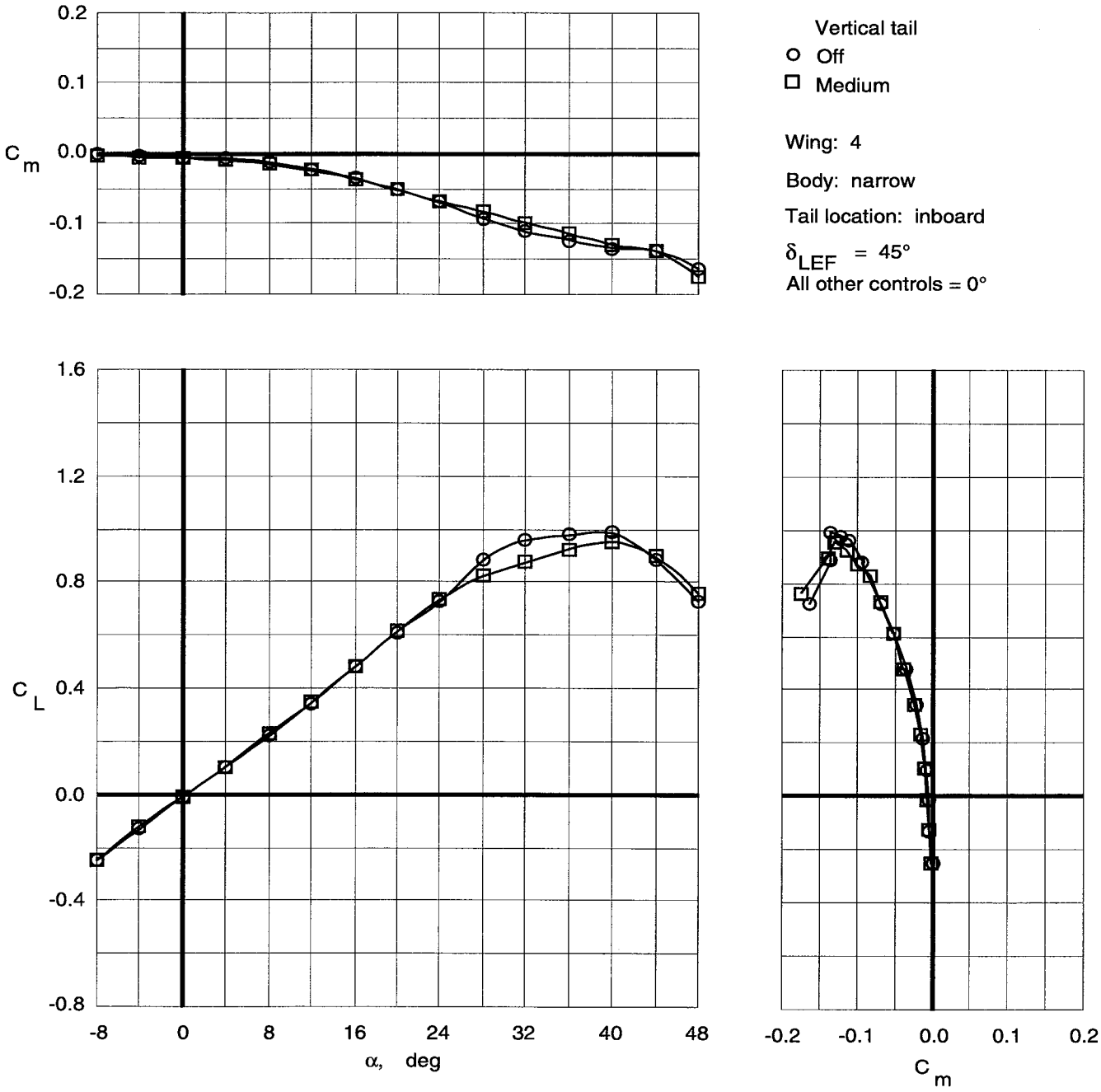

Figure 44. Effect of medium vertical tails on longitudinal characteristics of Wing 4 with narrow top body on and leading-edge flaps deflected.

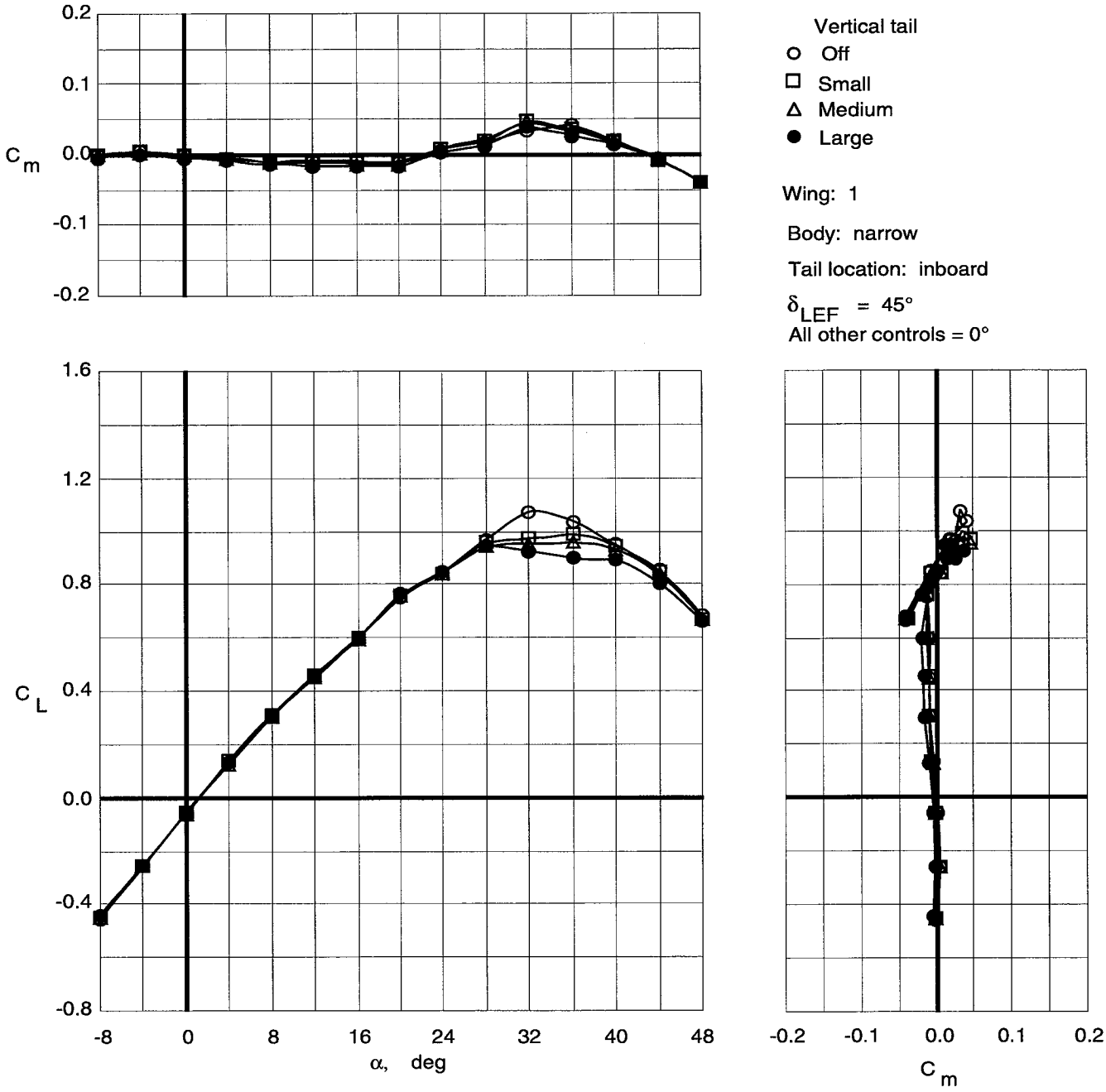

Figure 45. Effect of vertical tail size on longitudinal characteristics of Wing 1 with narrow top body on and leading-edge flaps deflected.

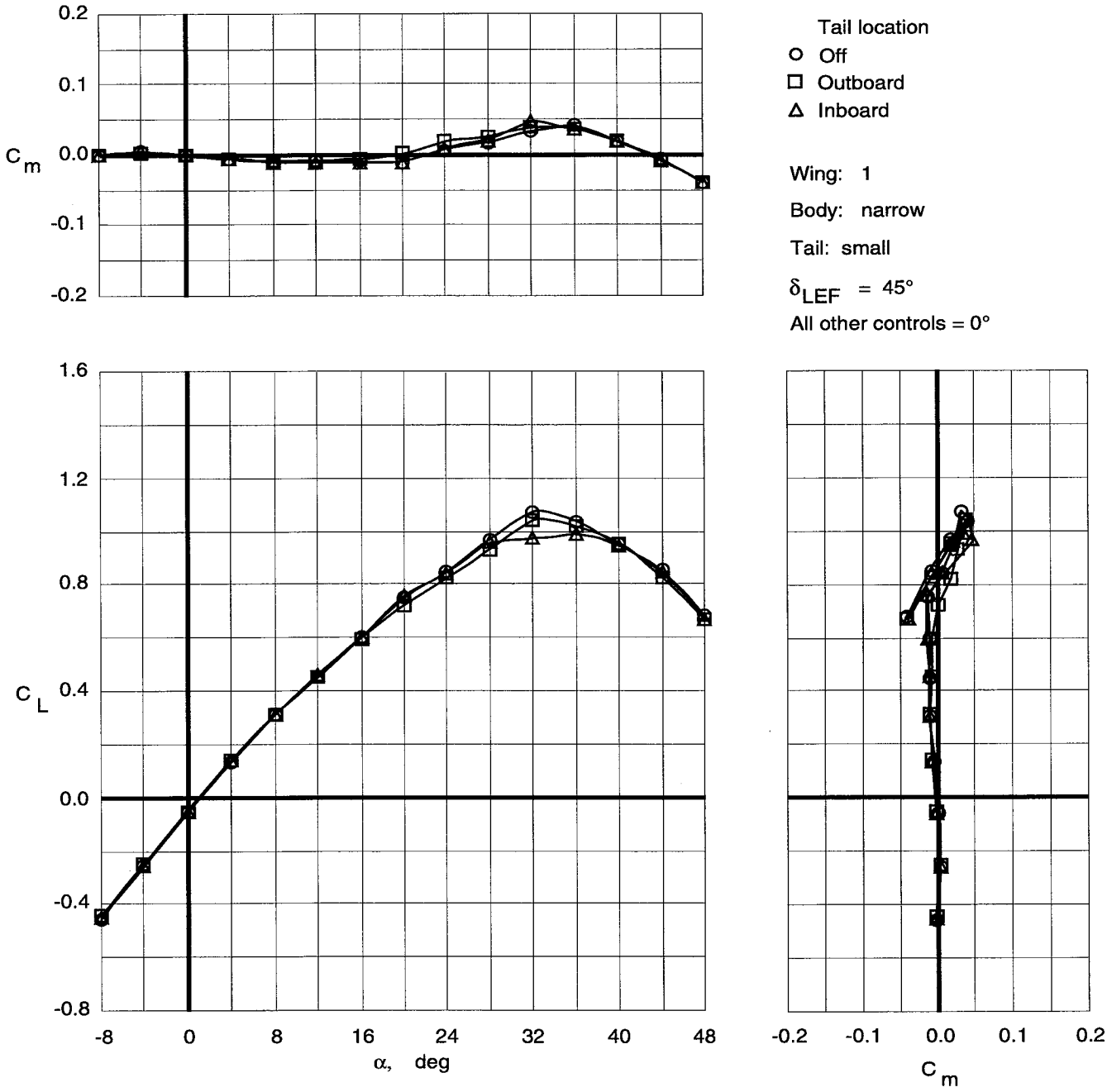

Figure 46. Effect of location of small vertical tails on longitudinal characteristics of Wing 1 with narrow top body on and leading-edge flaps deflected.

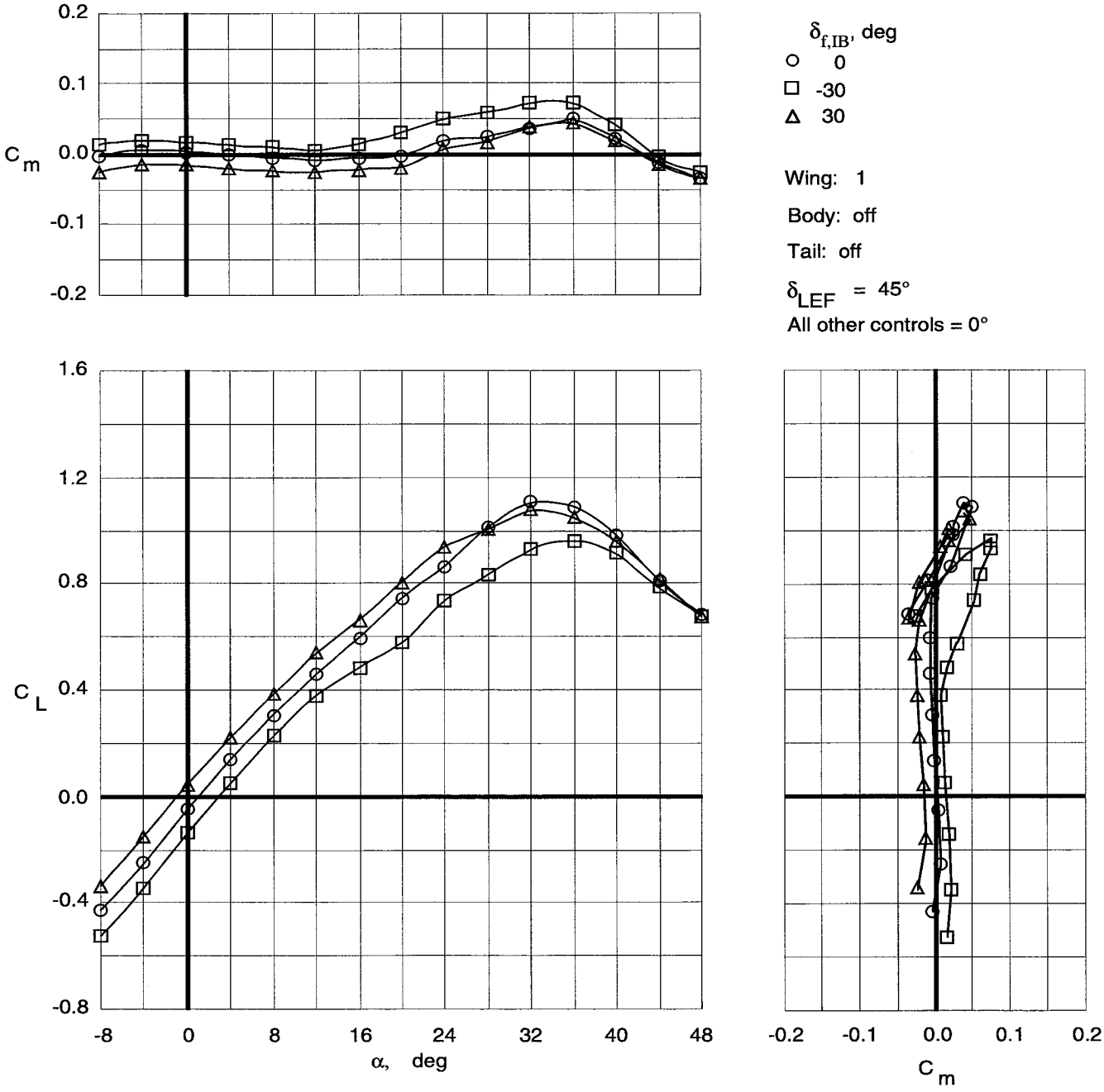

Figure 47. Control effectiveness of symmetric deflections of inboard trailing-edge flaps on Wing 1 with top body off and leading-edge flaps deflected.

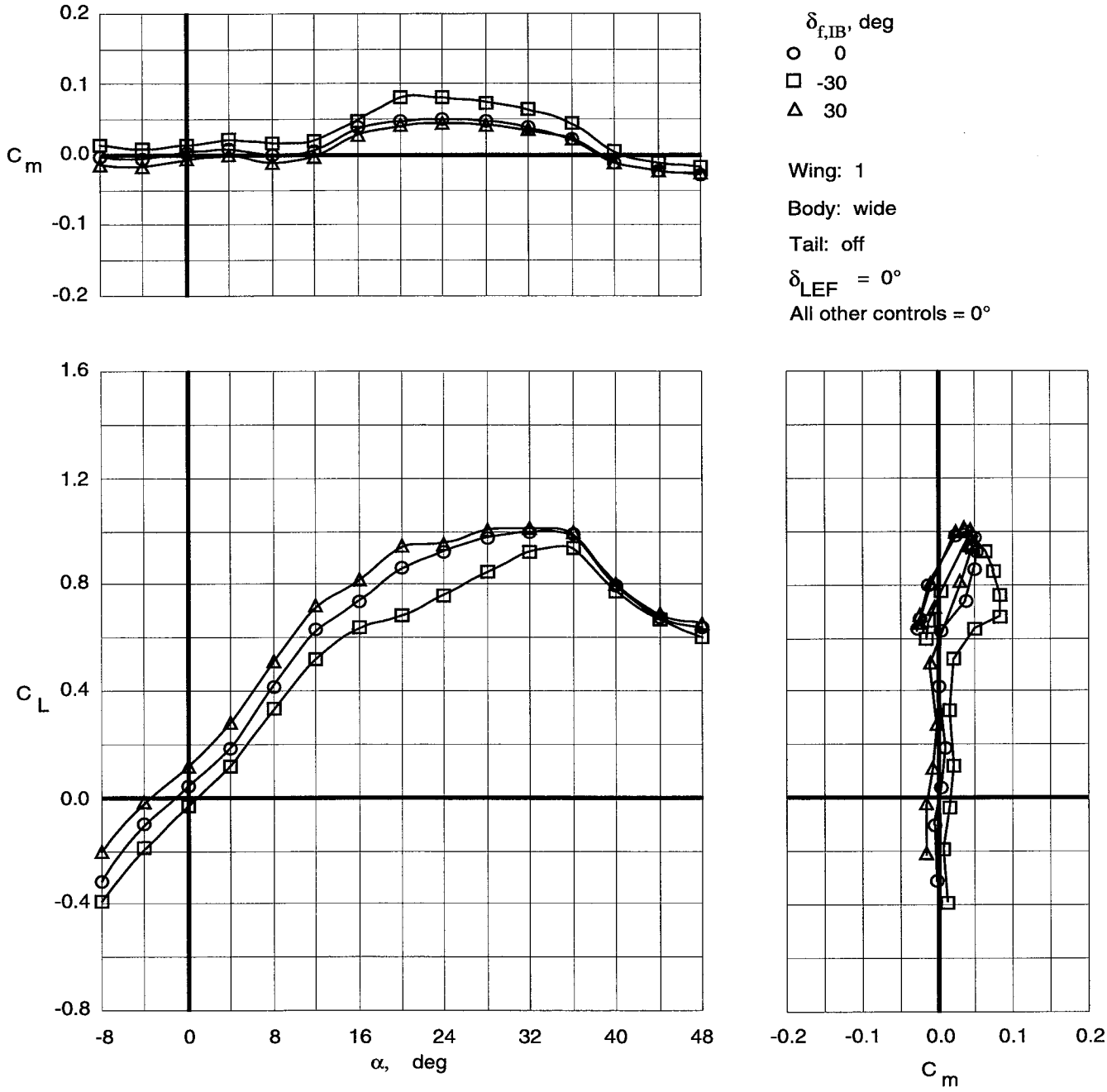

Figure 48. Control effectiveness of symmetric deflections of inboard trailing-edge flaps on Wing 1 with wide top body on.

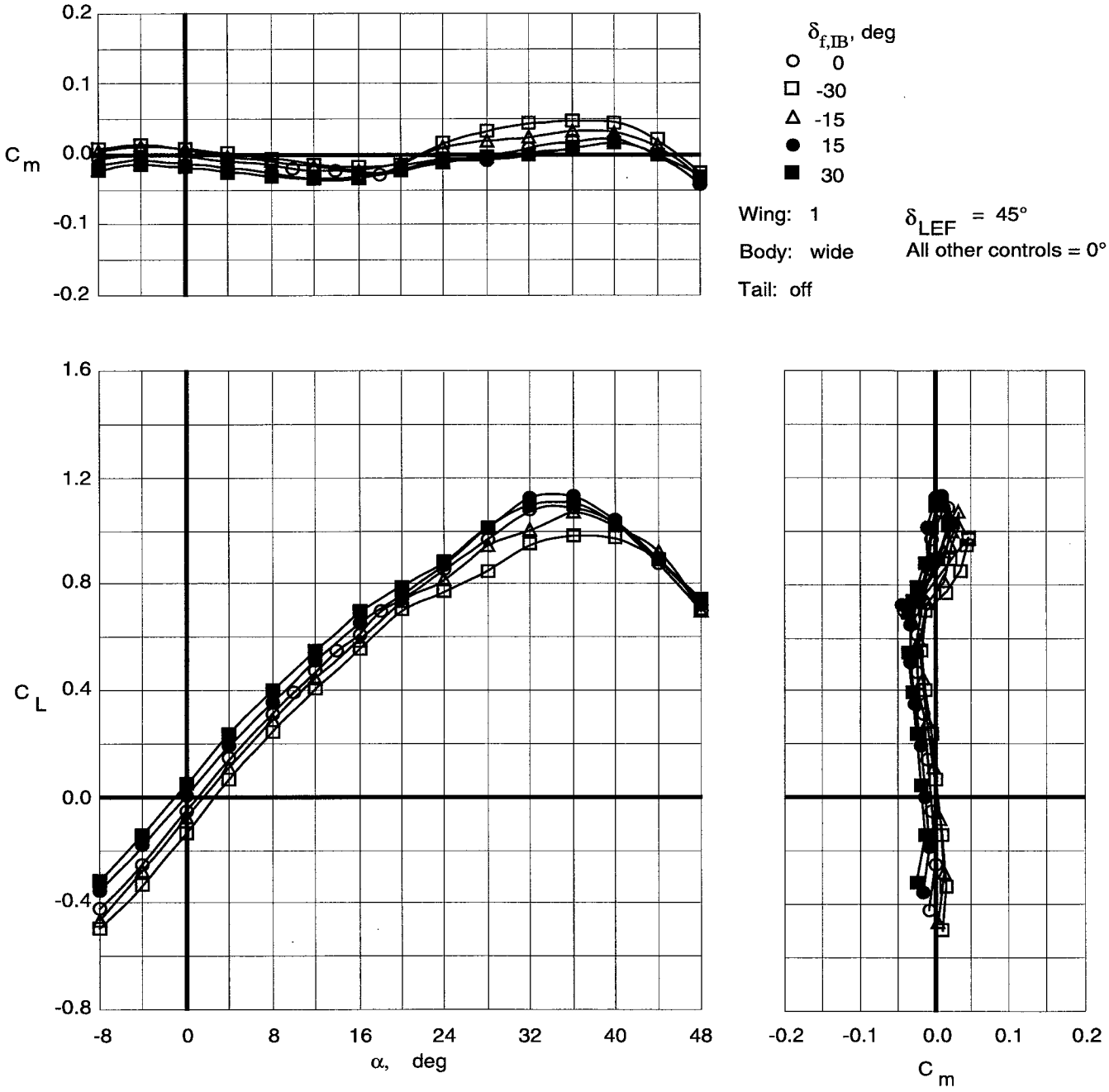

Figure 49. Control effectiveness of symmetric deflections of inboard trailing-edge flaps on Wing 1 with wide top body on and leading-edge flaps deflected.

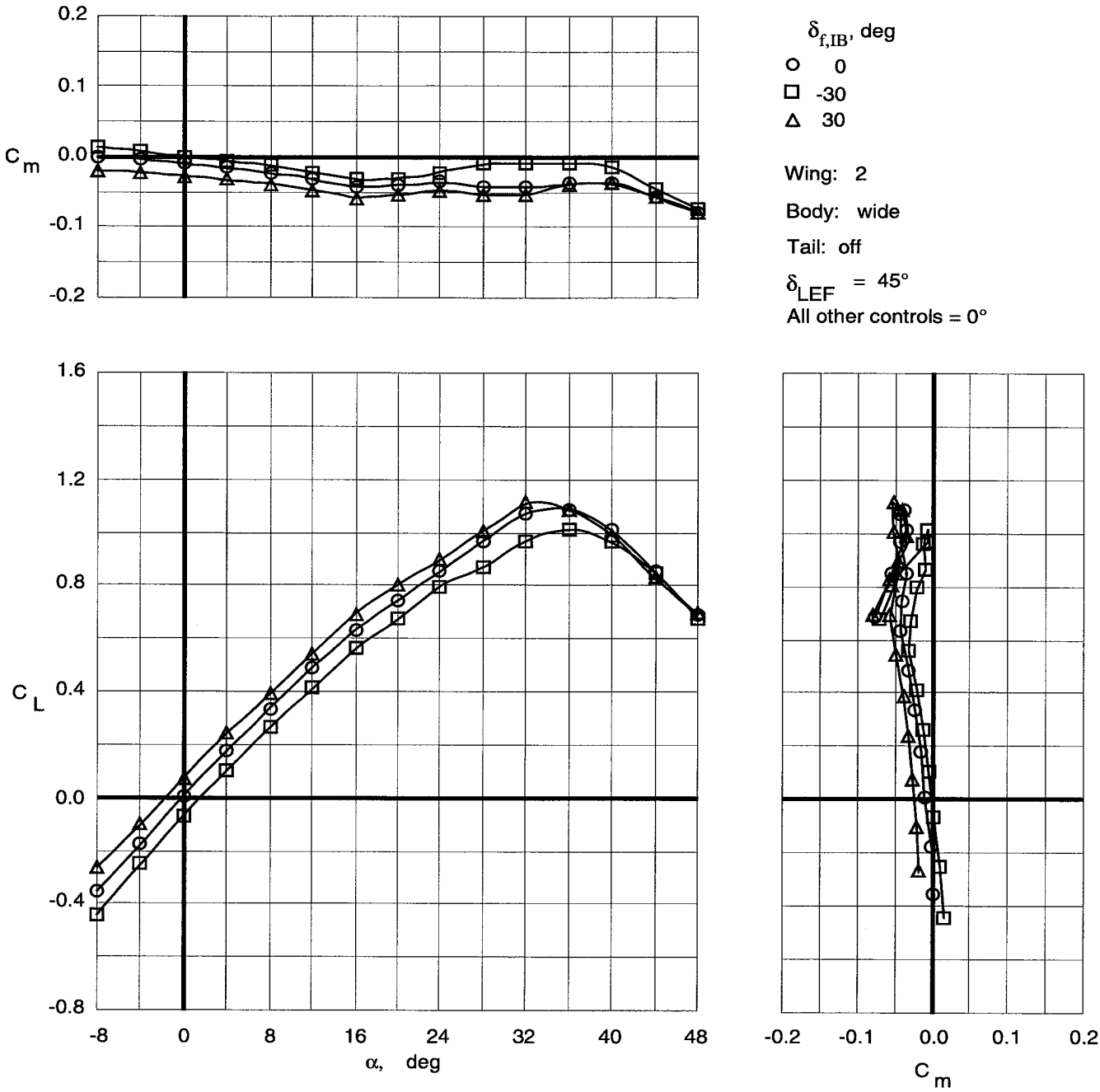

Figure 50. Control effectiveness of symmetric deflections of inboard trailing-edge flaps on Wing 2 with wide top body on and leading-edge flaps deflected.

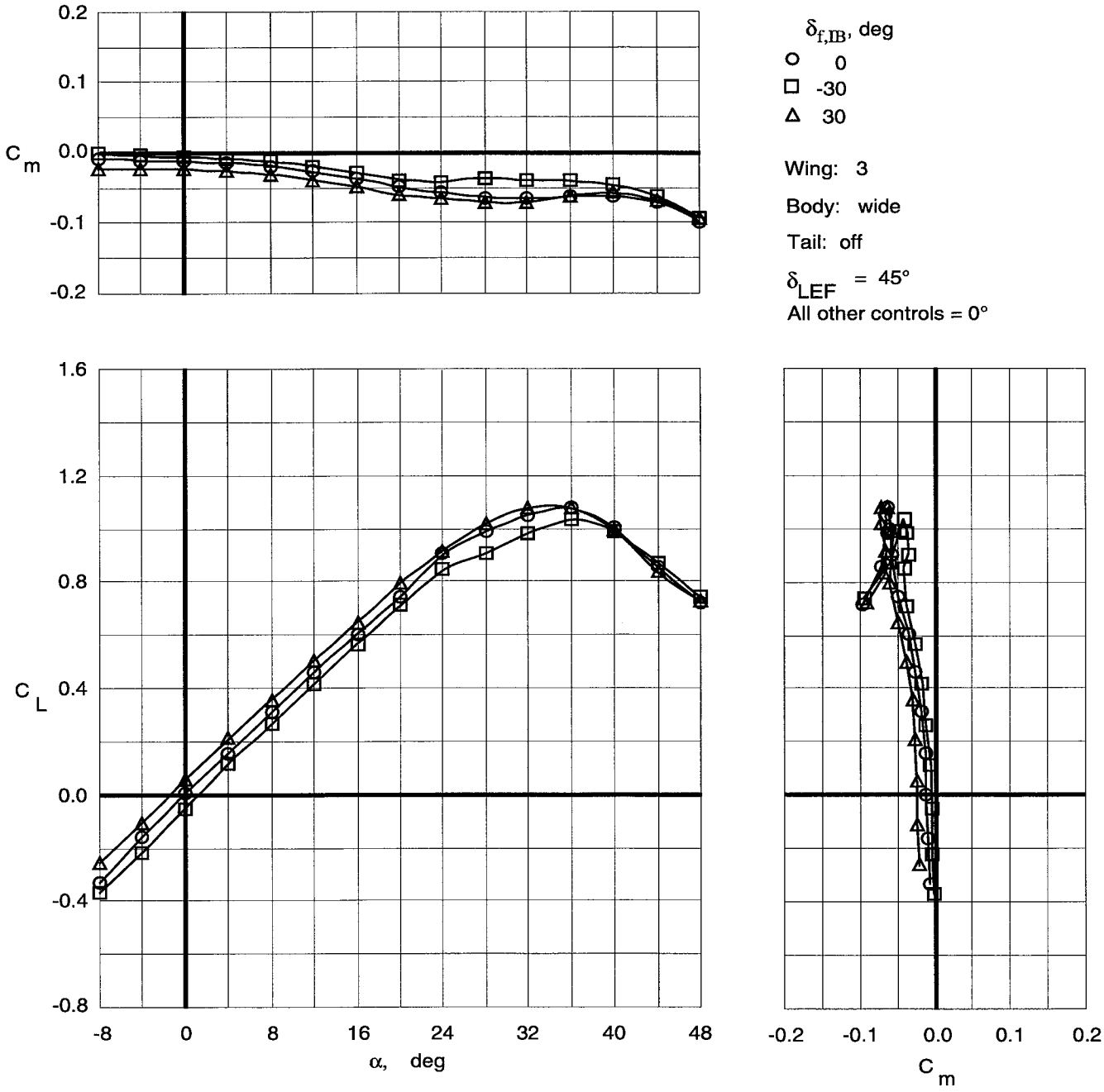

Figure 51. Control effectiveness of symmetric deflections of inboard trailing-edge flaps on Wing 3 with wide top body on and leading-edge flaps deflected.

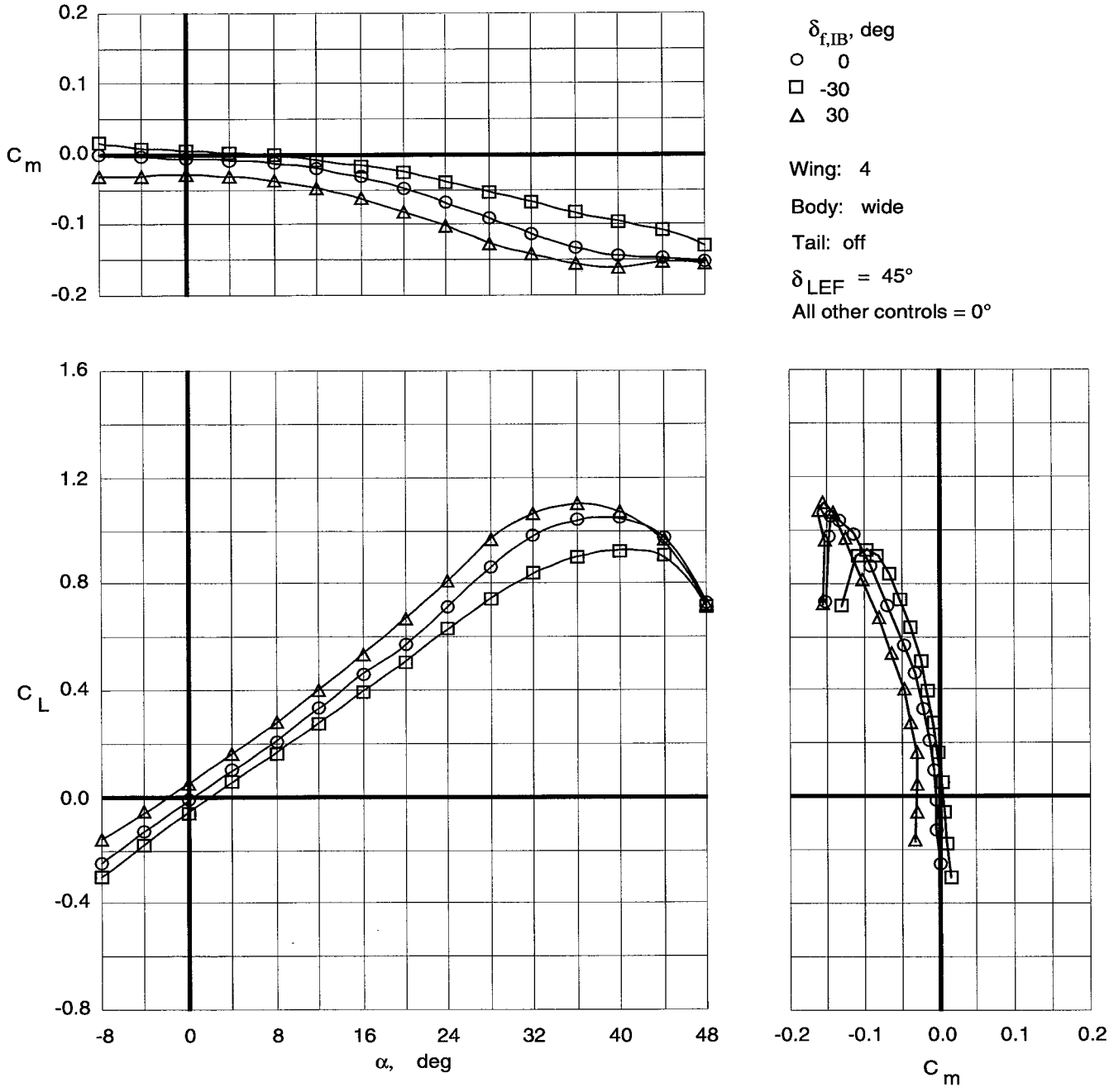

Figure 52. Control effectiveness of symmetric deflections of inboard trailing-edge flaps on Wing 4 with wide top body on and leading-edge flaps deflected.

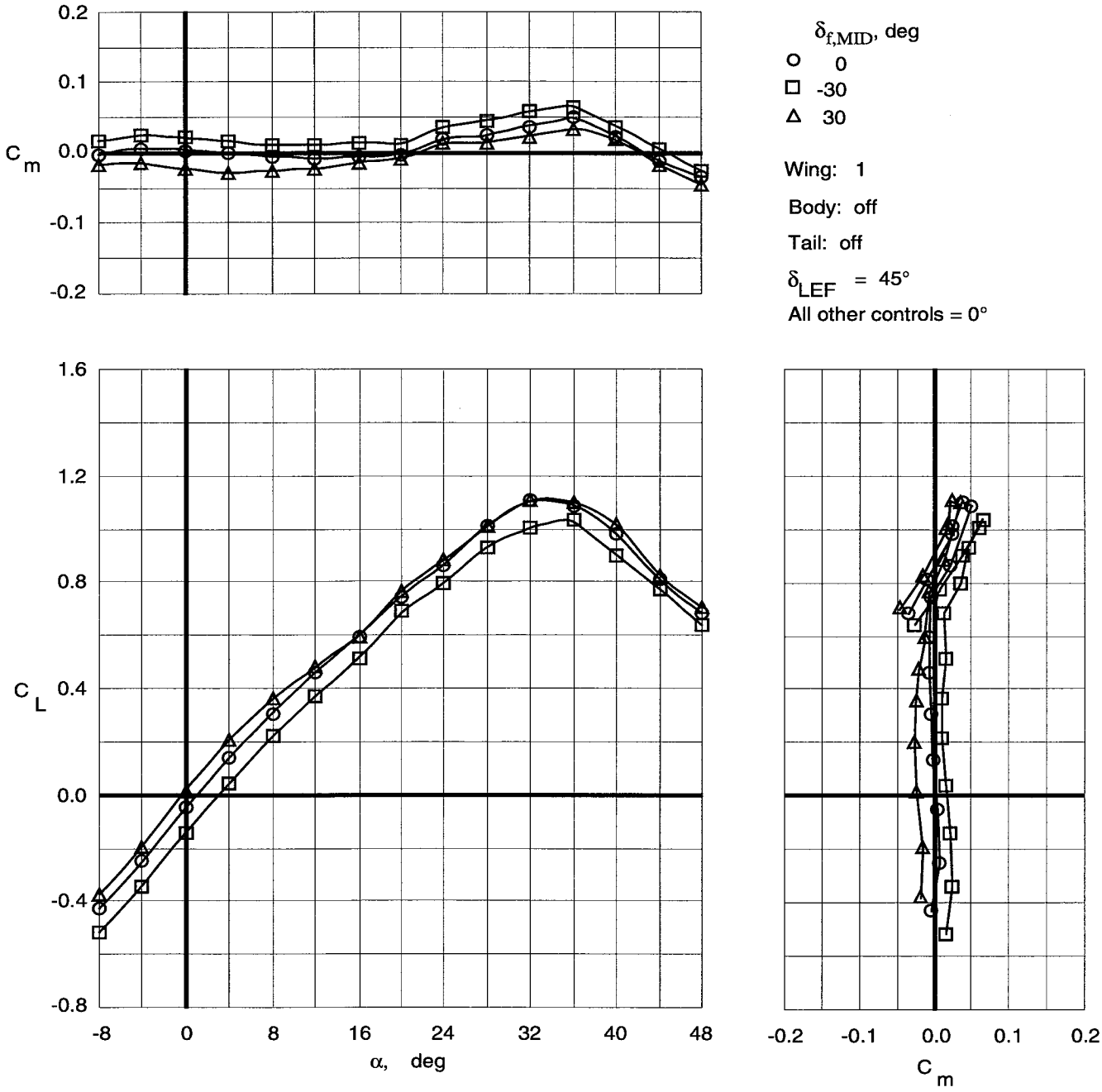

Figure 53. Control effectiveness of symmetric deflections of middle trailing-edge flaps on Wing 1 with top body off and leading-edge flaps deflected.

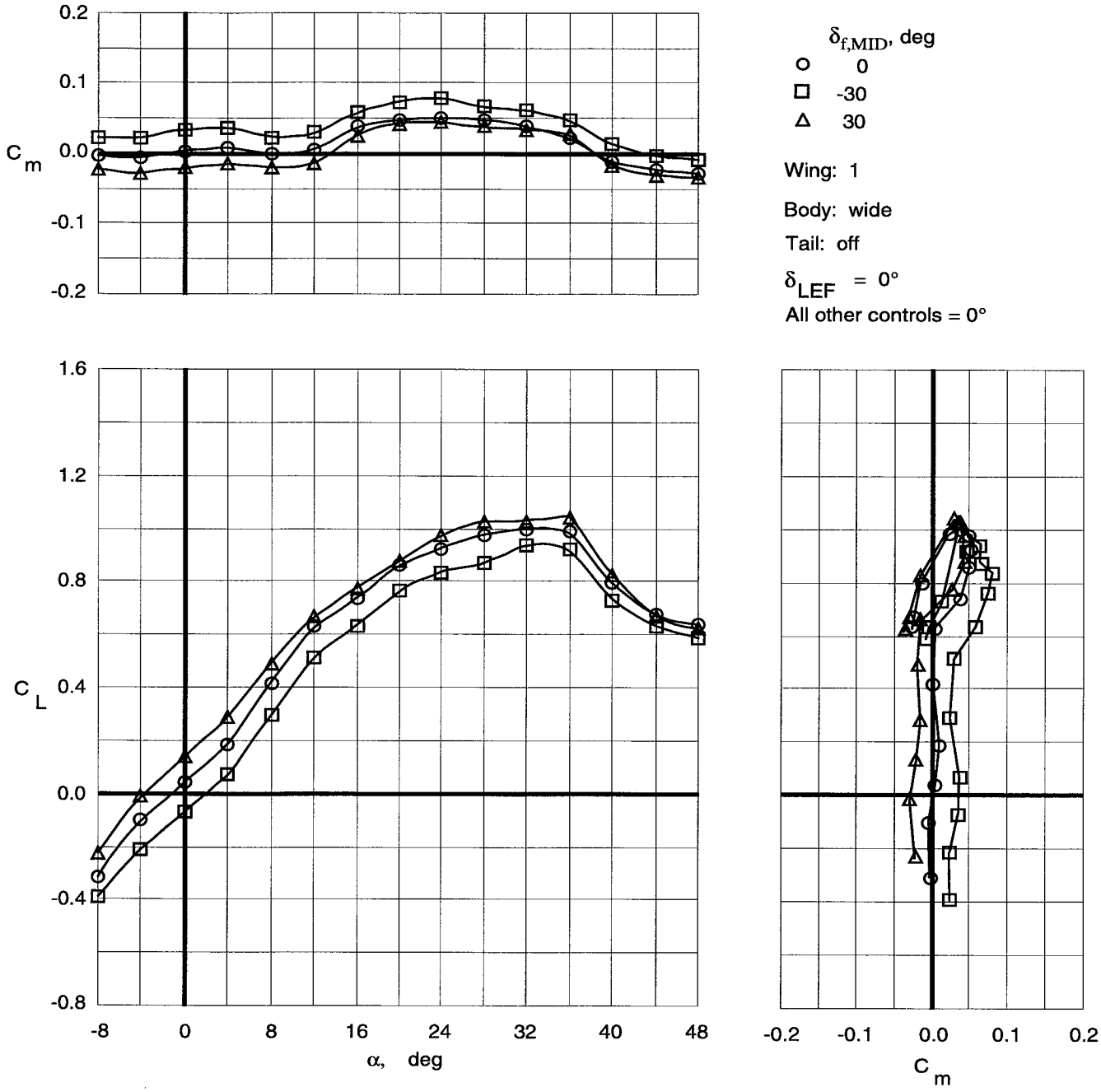

Figure 54. Control effectiveness of symmetric deflections of middle trailing-edge flaps on Wing 1 with wide top body on.

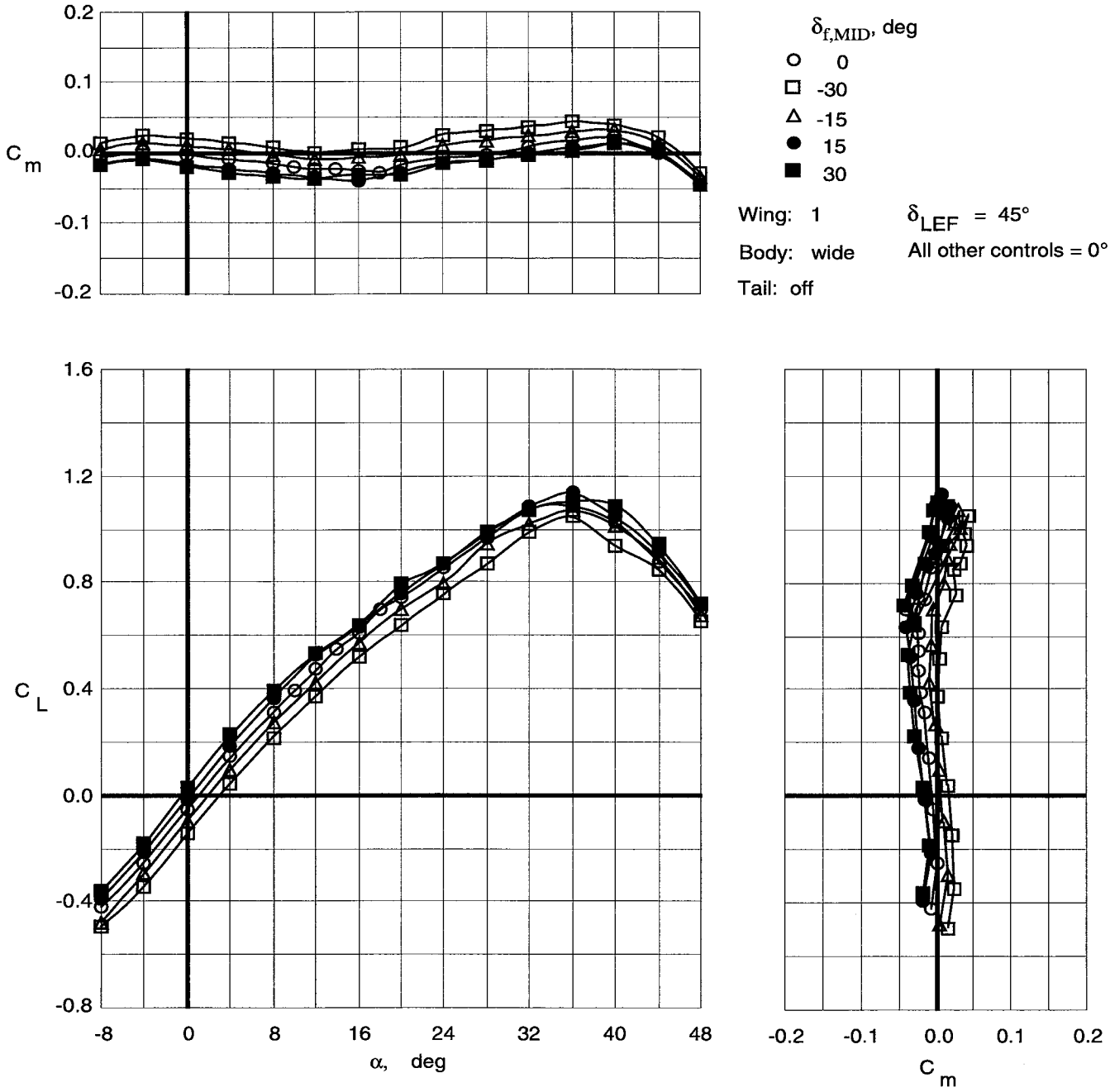

Figure 55. Control effectiveness of symmetric deflections of middle trailing-edge flaps on Wing 1 with wide top body on and leading-edge flaps deflected.

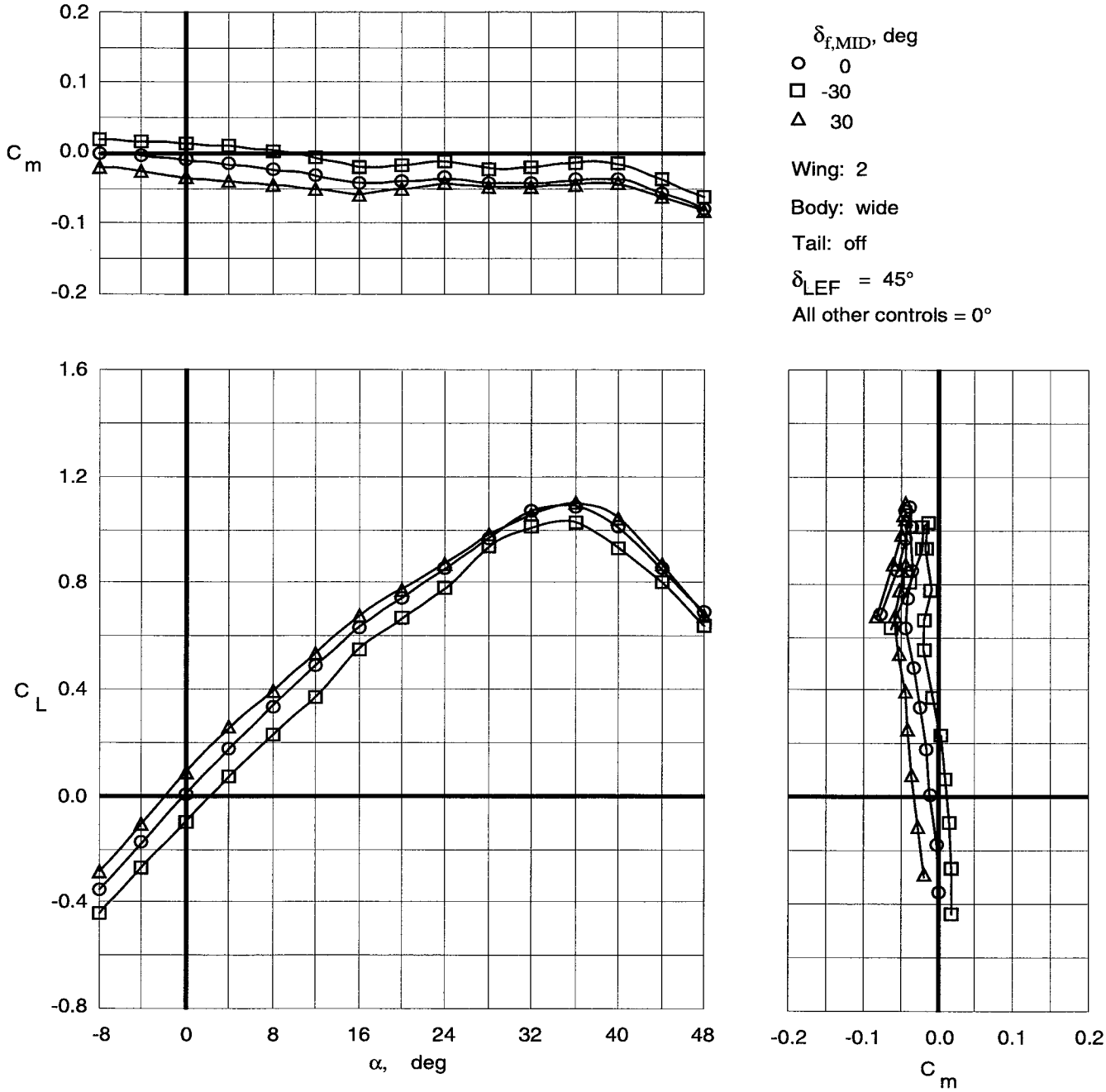

Figure 56. Control effectiveness of symmetric deflections of middle trailing-edge flaps on Wing 2 with wide top body on and leading-edge flaps deflected.

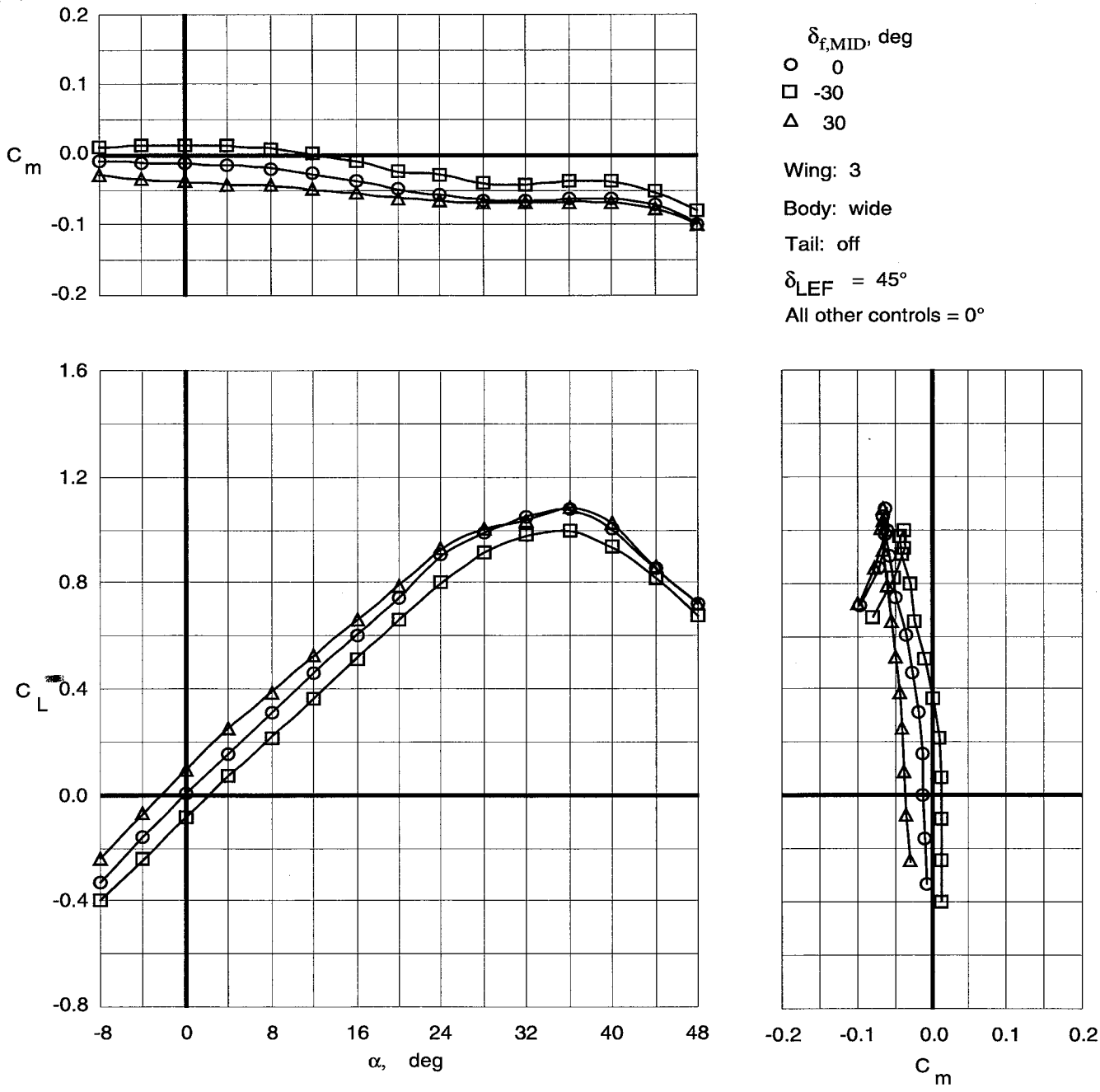

Figure 57. Control effectiveness of symmetric deflections of middle trailing-edge flaps on Wing 3 with wide top body on and leading-edge flaps deflected.

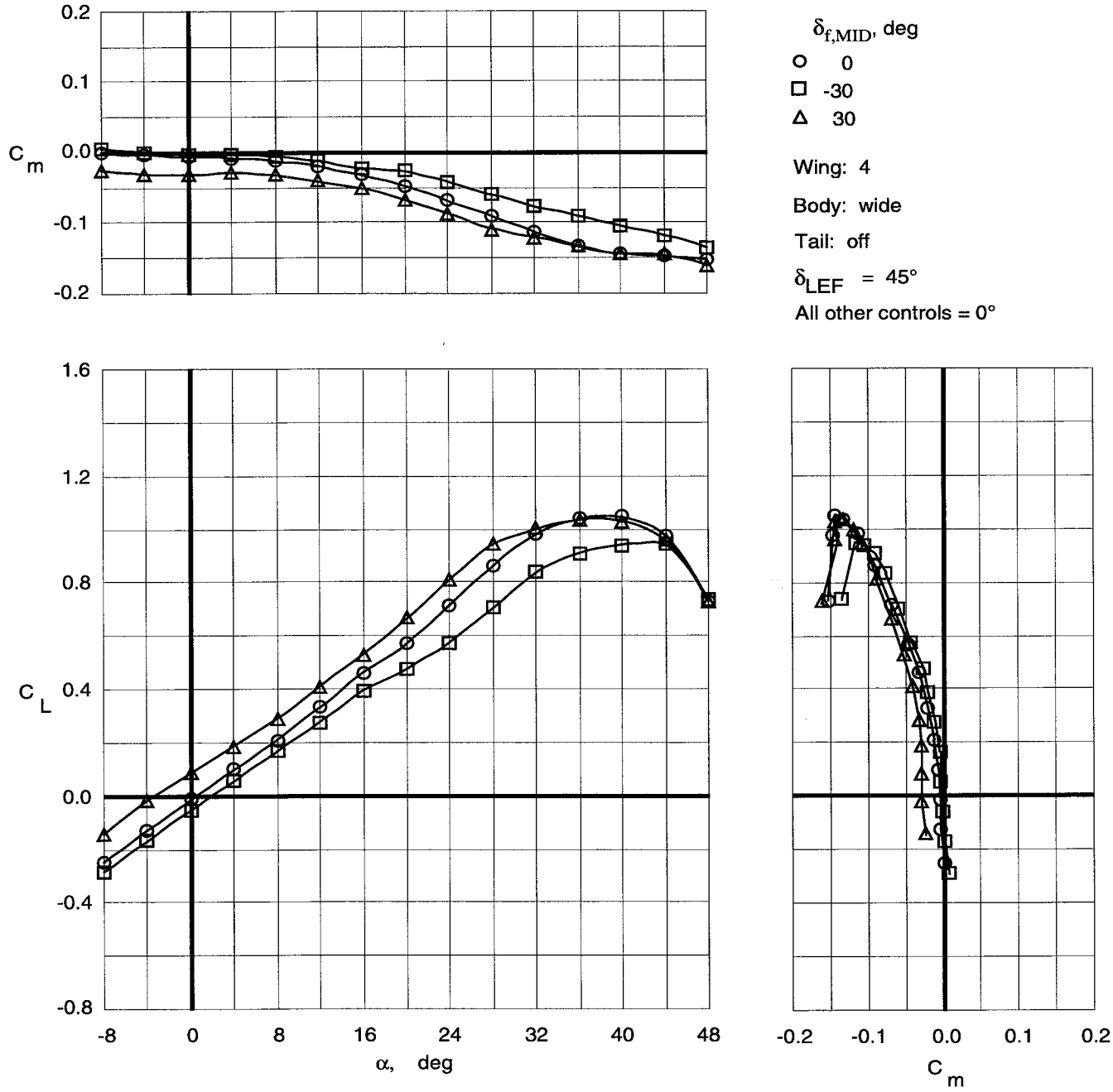

Figure 58. Control effectiveness of symmetric deflections of middle trailing-edge flaps on Wing 4 with wide top body on and leading-edge flaps deflected.

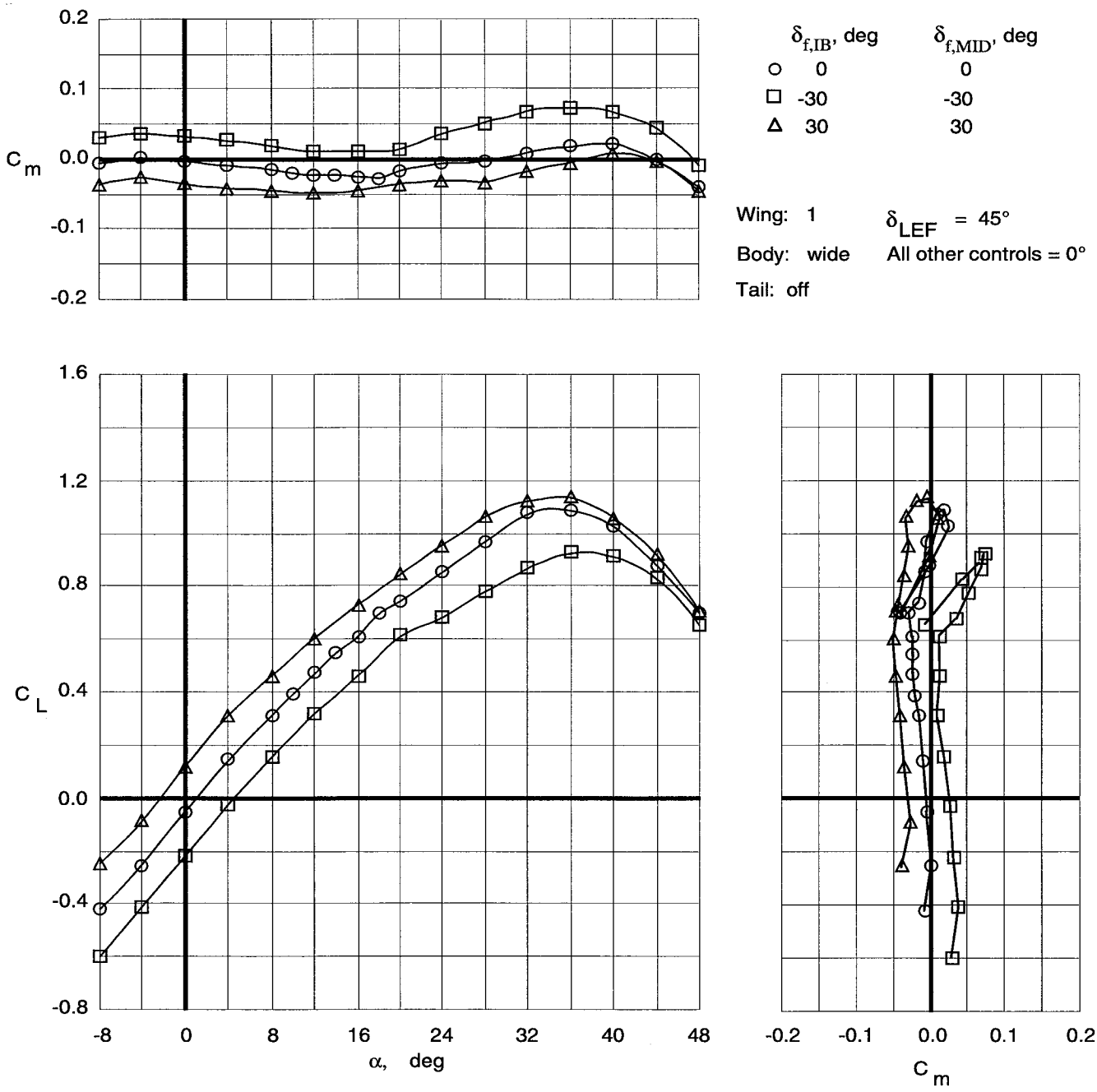

Figure 59. Control effectiveness of symmetric deflections of inboard and middle trailing-edge flaps on Wing 1 with wide top body on and leading-edge flaps deflected.

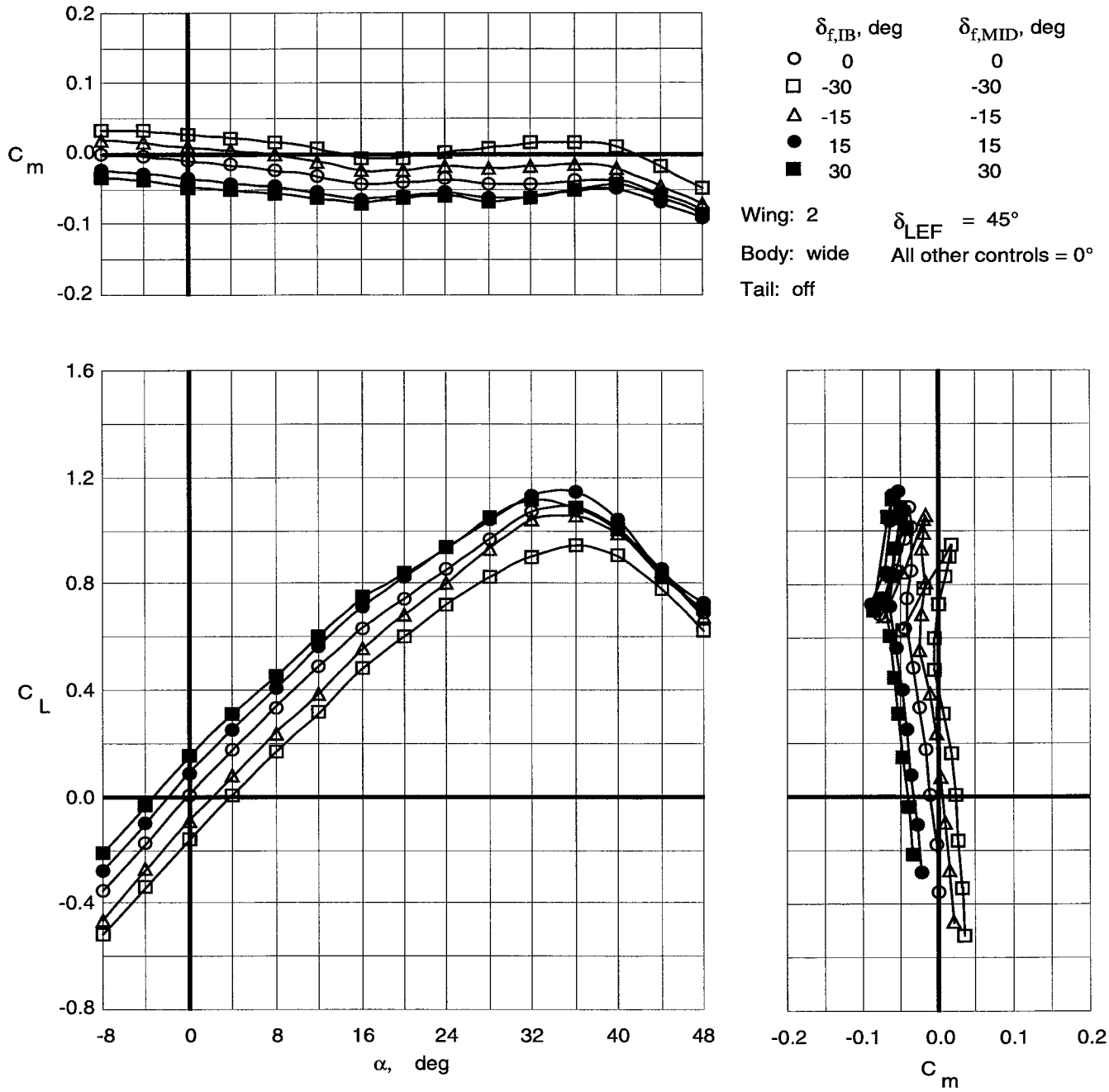

Figure 60. Control effectiveness of symmetric deflections of inboard and middle trailing-edge flaps on Wing 2 with wide top body on and leading-edge flaps deflected.

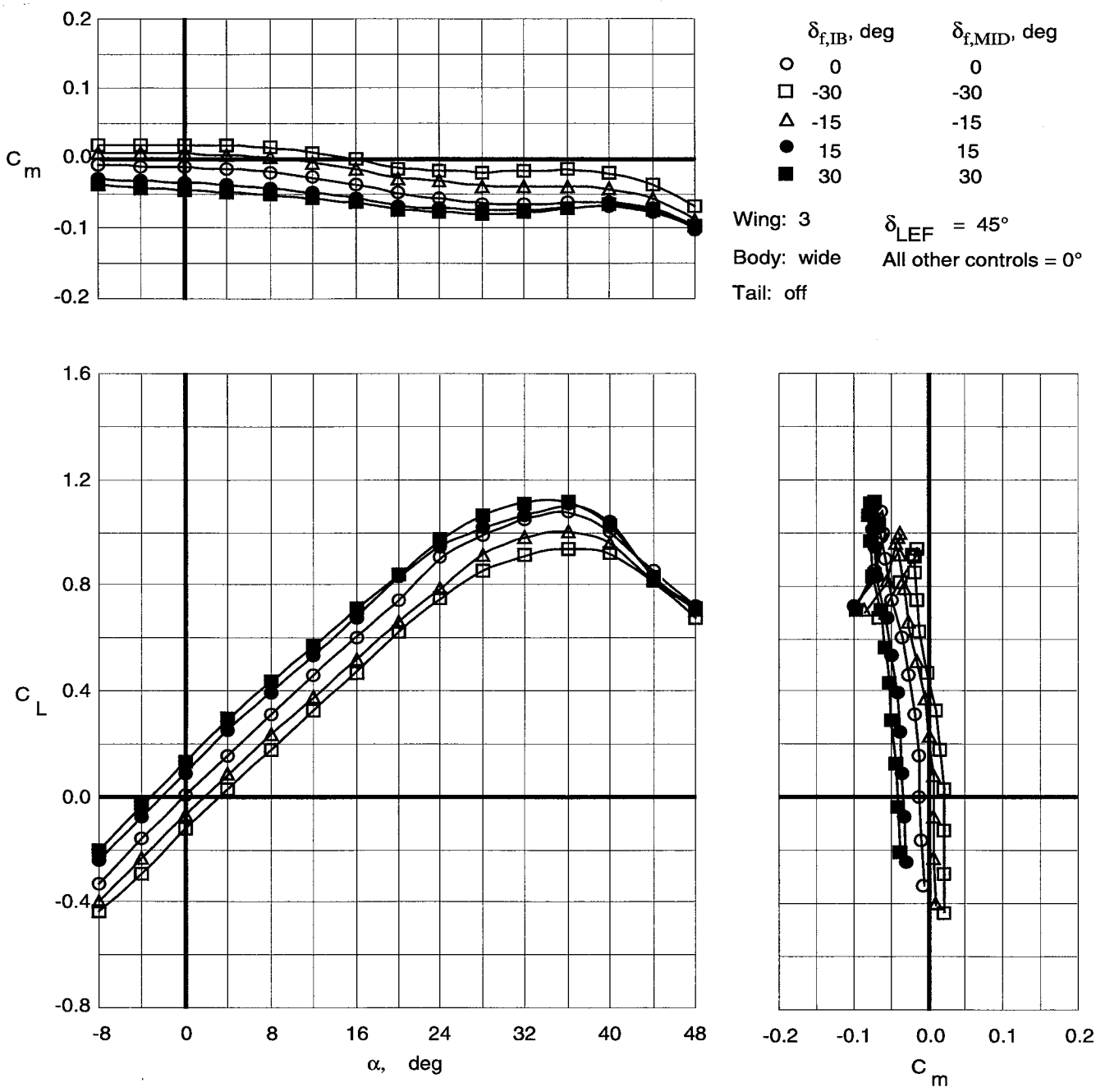

Figure 61. Control effectiveness of symmetric deflections of inboard and middle trailing-edge flaps on Wing 3 with wide top body on and leading-edge flaps deflected.

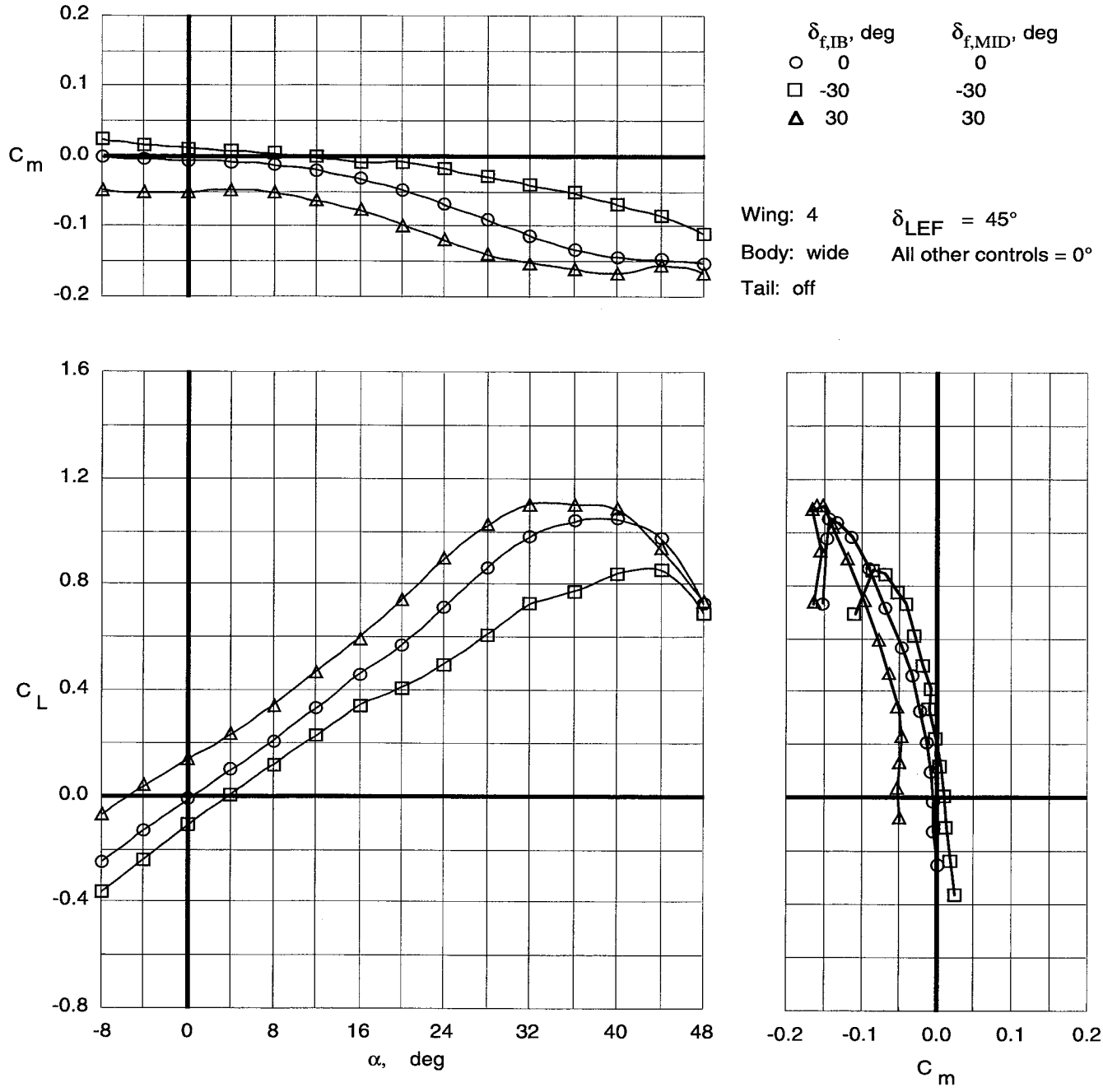

Figure 62. Control effectiveness of symmetric deflections of inboard and middle trailing-edge flaps on Wing 4 with wide top body on and leading-edge flaps deflected.

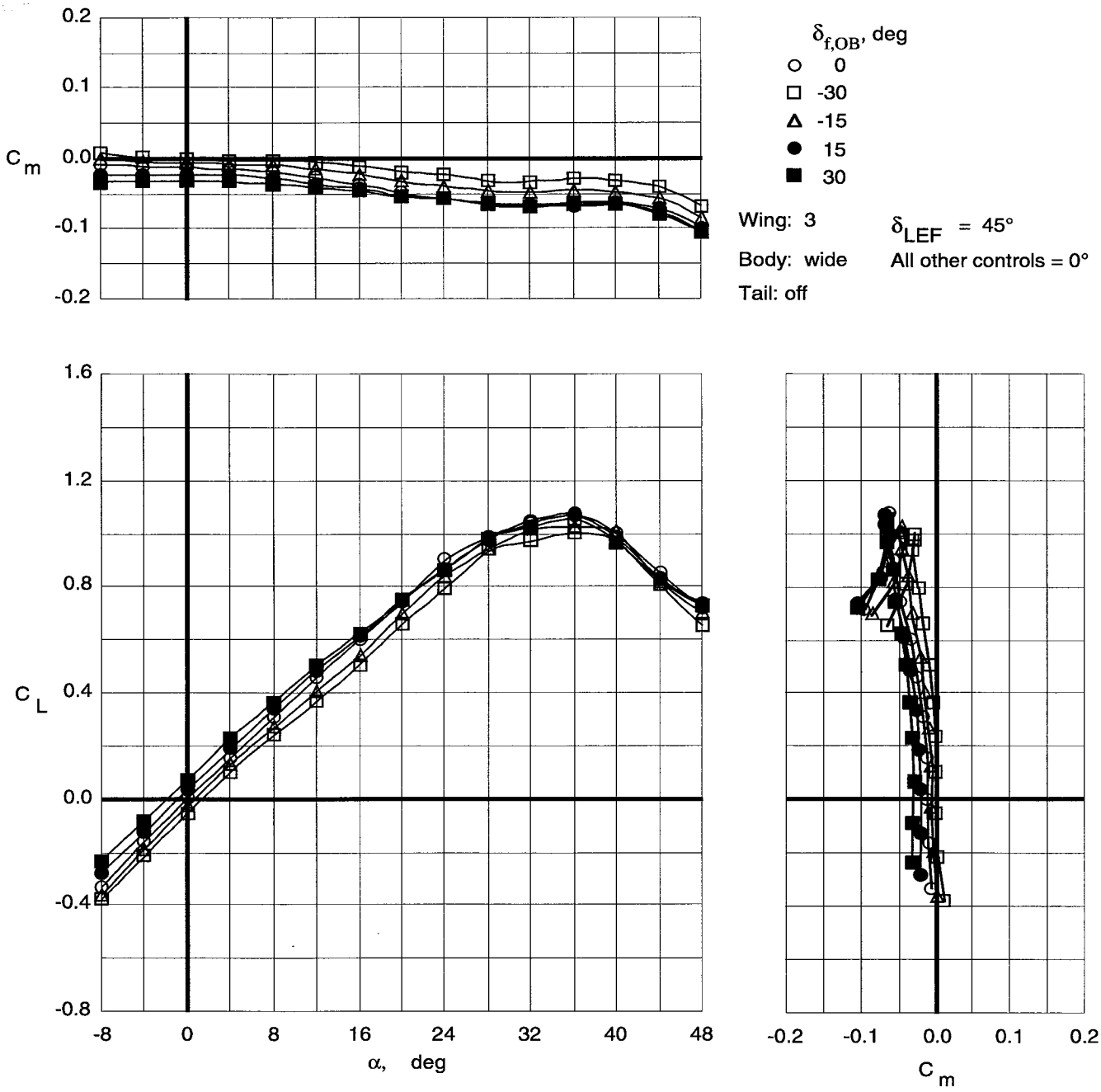

Figure 63. Control effectiveness of symmetric deflections of outboard trailing-edge flaps on Wing 3 with wide top body on and leading-edge flaps deflected.

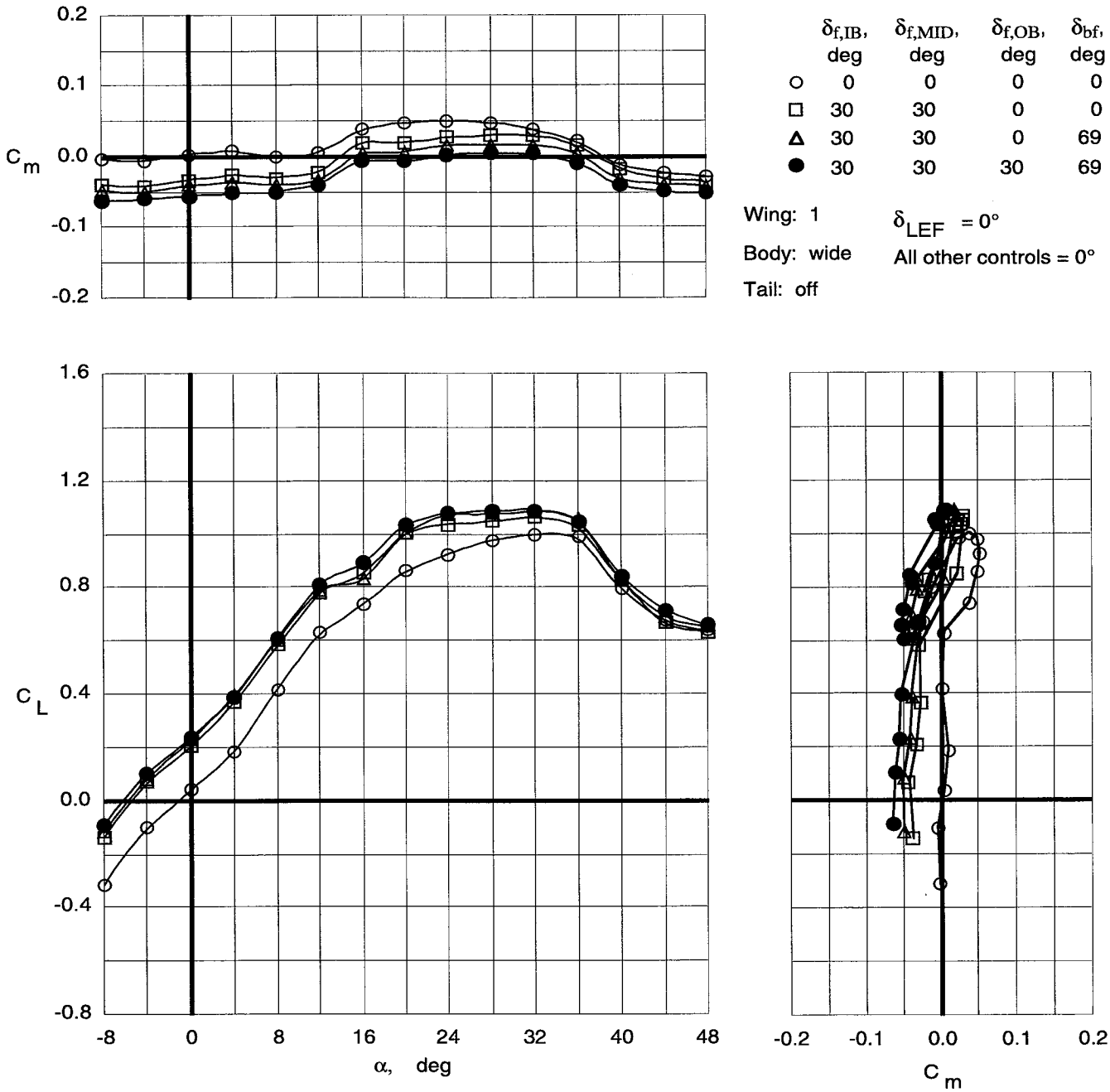

Figure 64. Control effectiveness of symmetric deflections of trailing-edge flaps and body flaps on Wing 1 with wide top body on.

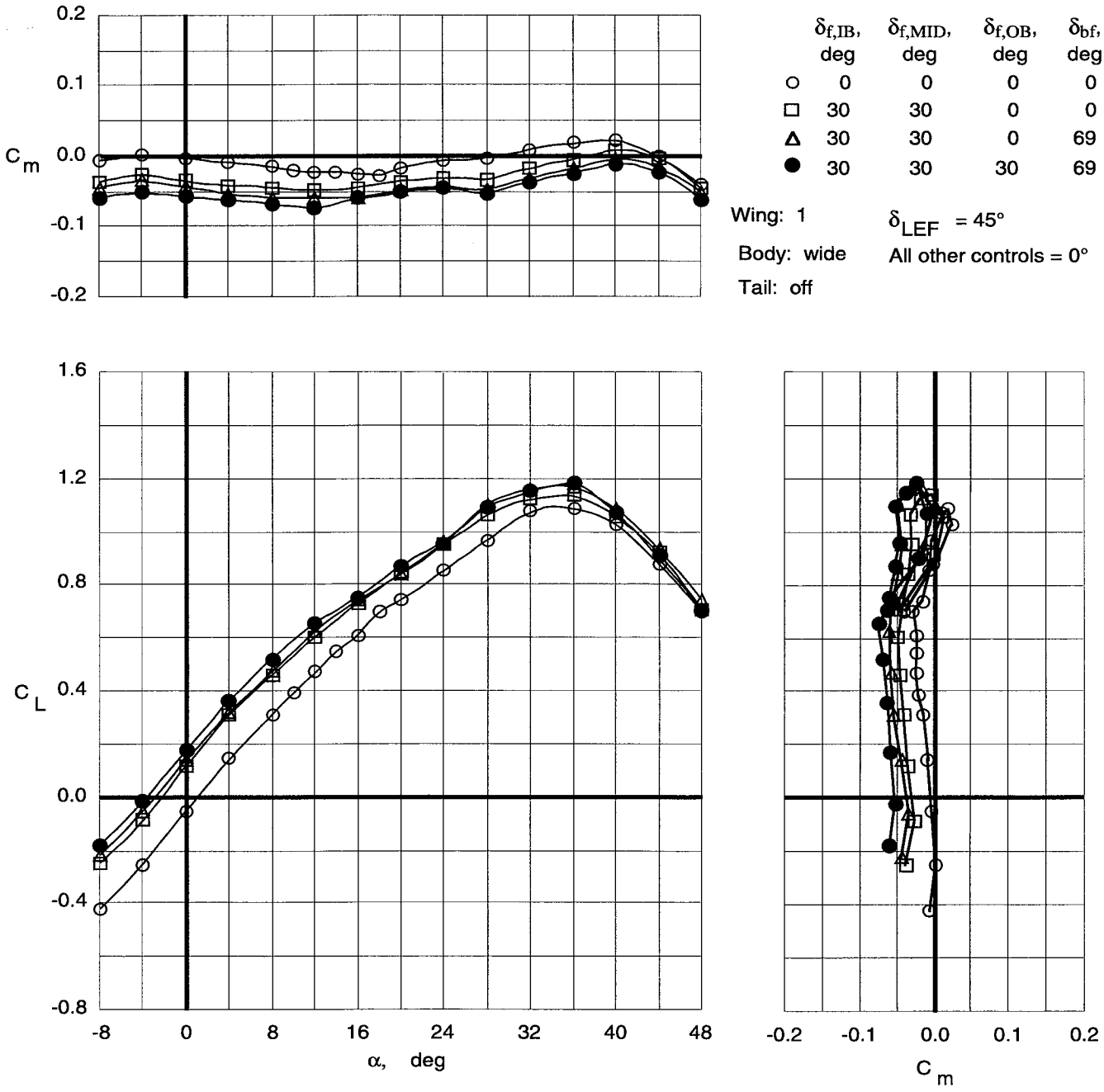

Figure 65. Control effectiveness of symmetric deflections of trailing-edge flaps and body flaps on Wing 1 with wide top body on and leading-edge flaps deflected.

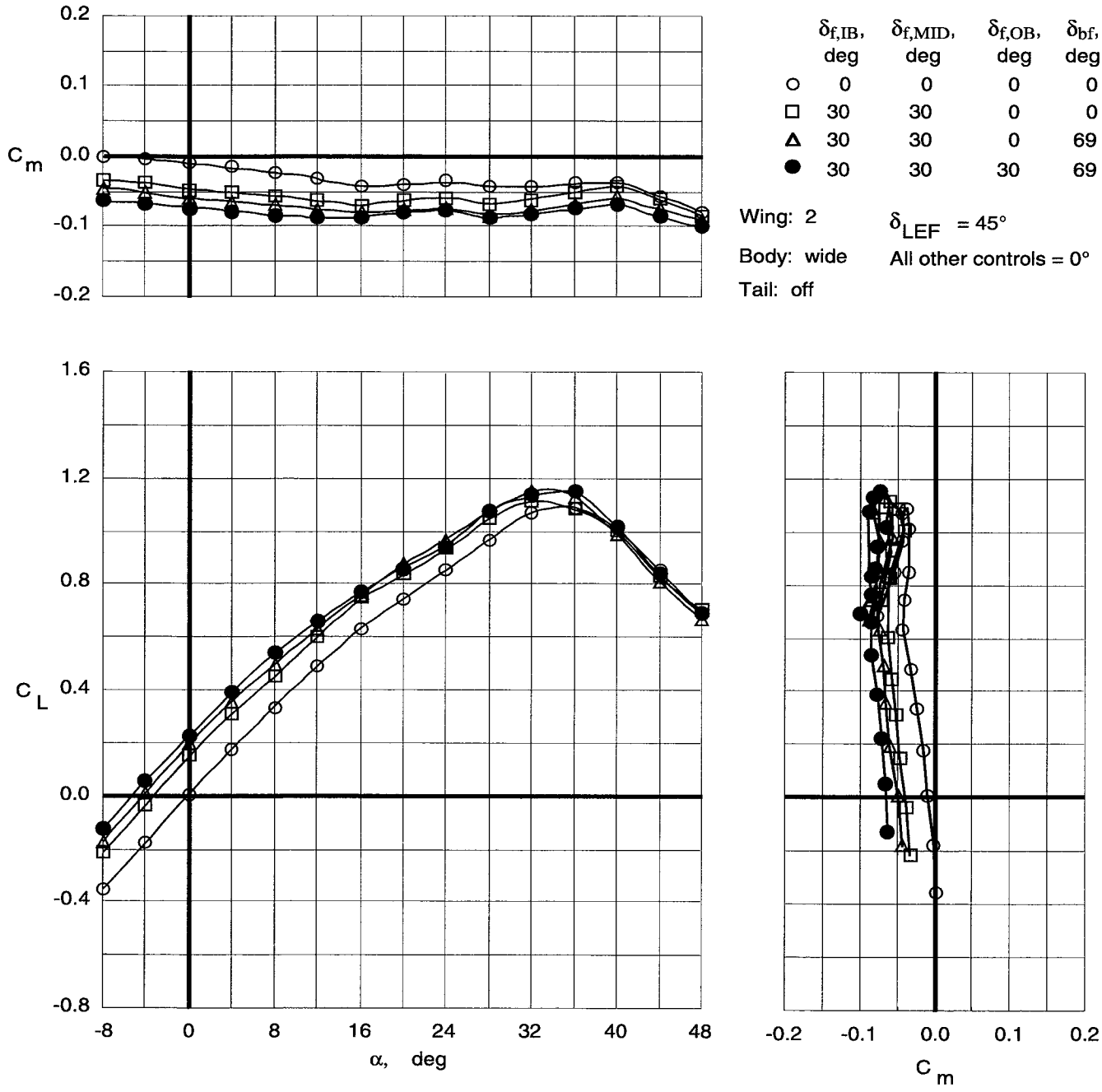

Figure 66. Control effectiveness of symmetric deflections of trailing-edge flaps and body flaps on Wing 2 with wide top body on and leading-edge flaps deflected.

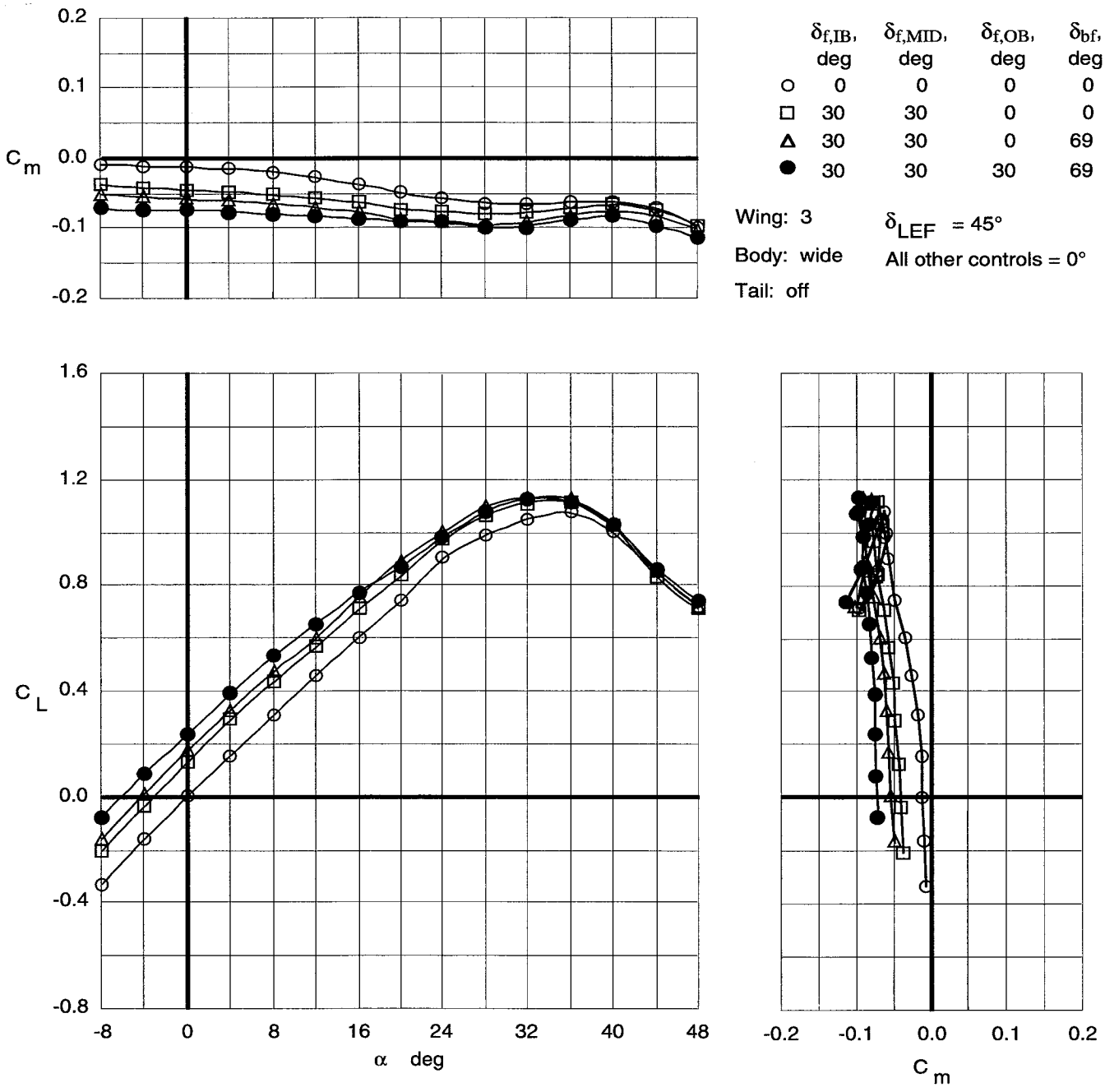

Figure 67. Control effectiveness of symmetric deflections of trailing-edge flaps and body flaps on Wing 3 with wide top body on and leading-edge flaps deflected.

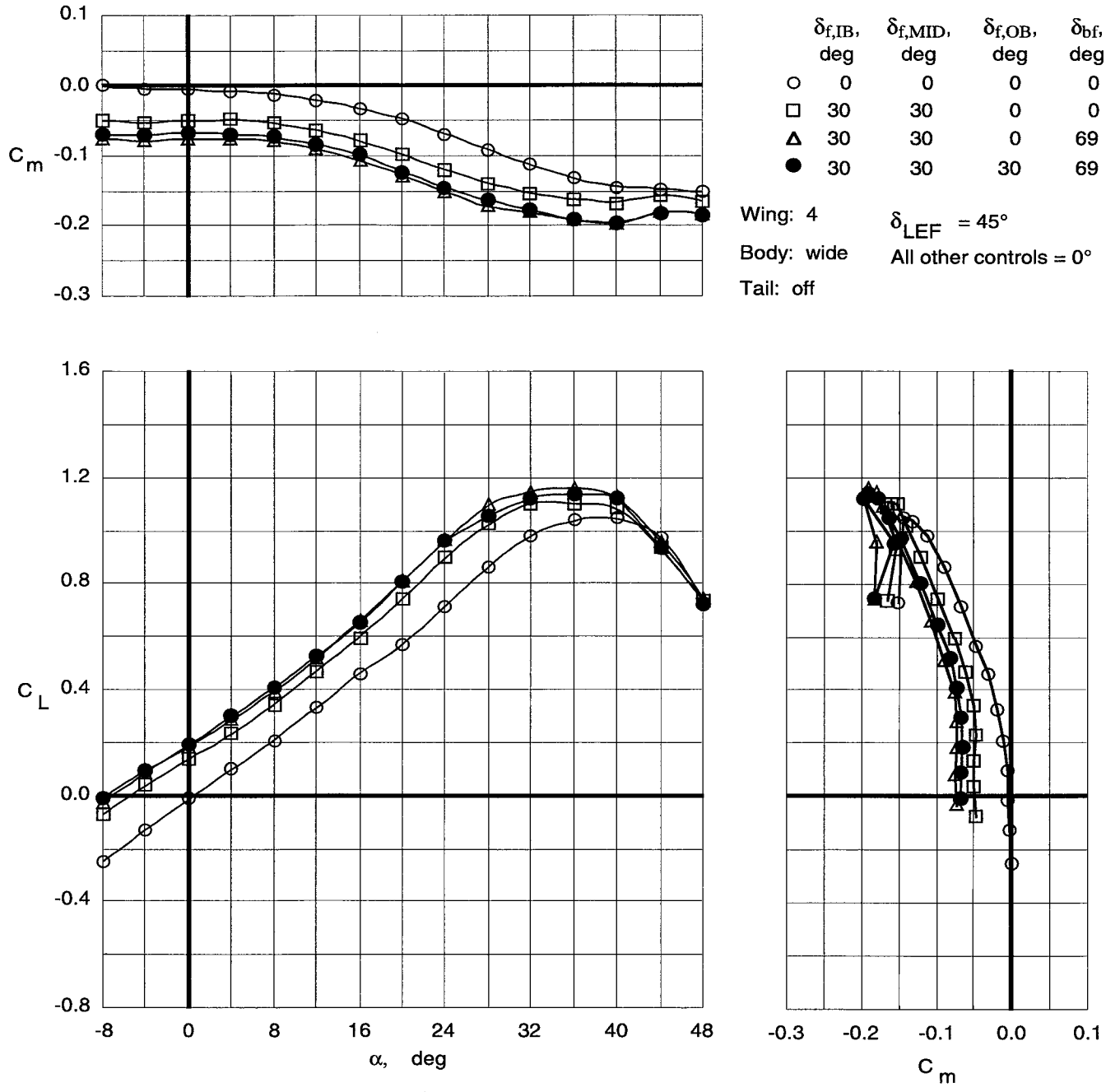

Figure 68. Control effectiveness of symmetric deflections of trailing-edge flaps and body flaps on Wing 4 with wide top body on and leading-edge flaps deflected.

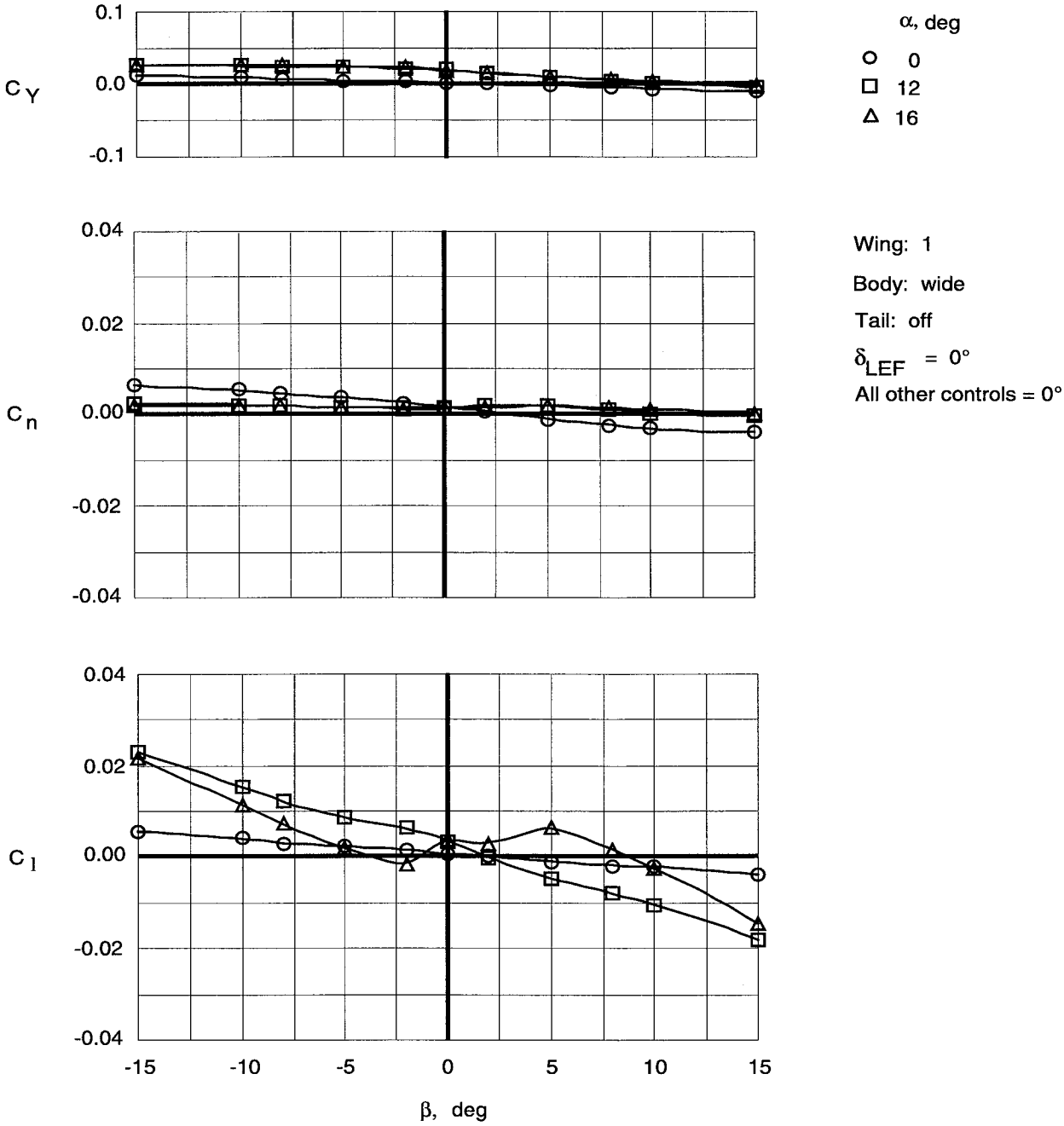

Figure 69. Variation of lateral-directional coefficients with sideslip at low angles of attack for Wing 1 with wide top body on.

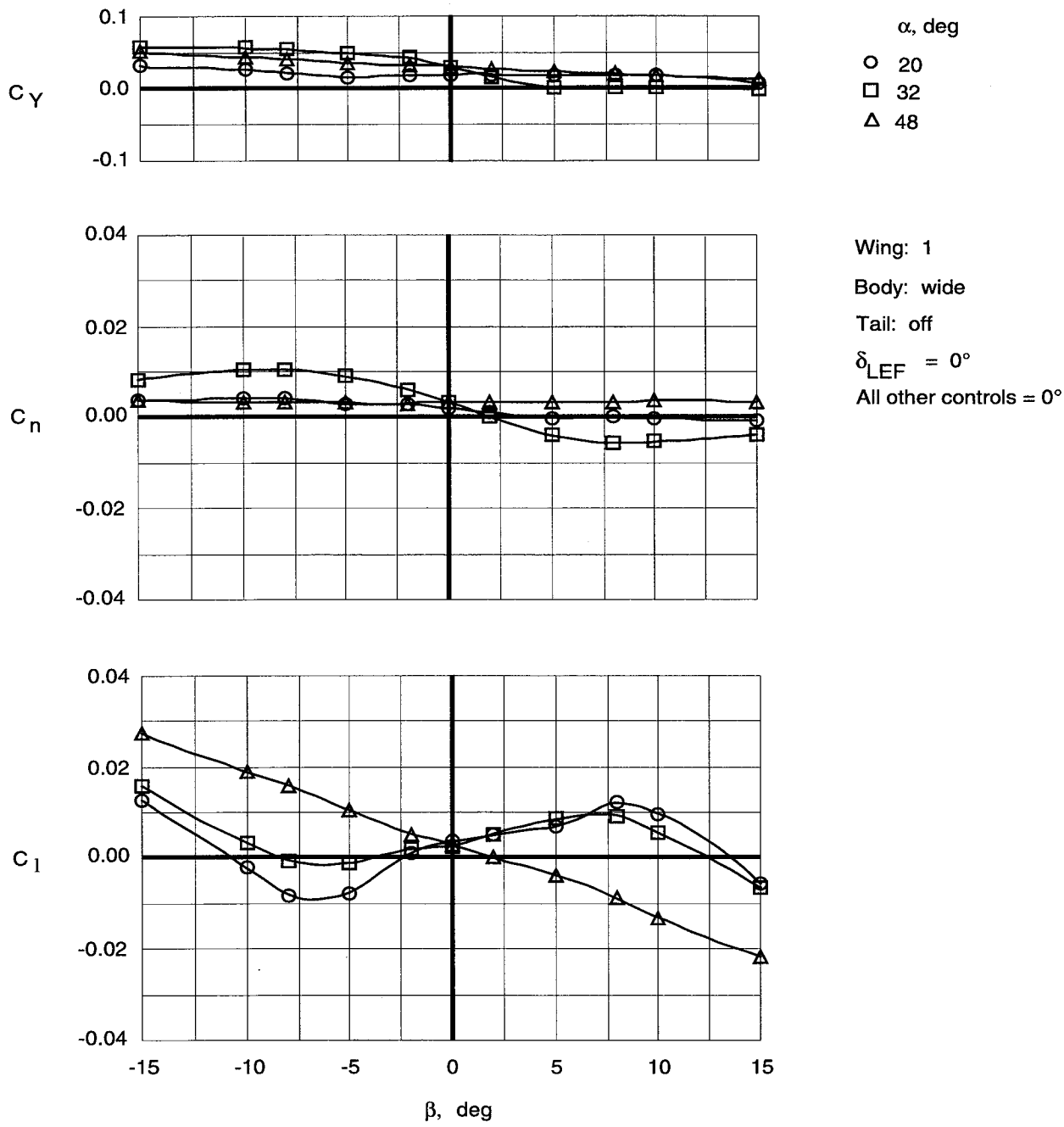

Figure 70. Variation of lateral-directional coefficients with sideslip at high angles of attack for Wing 1 with wide top body on.

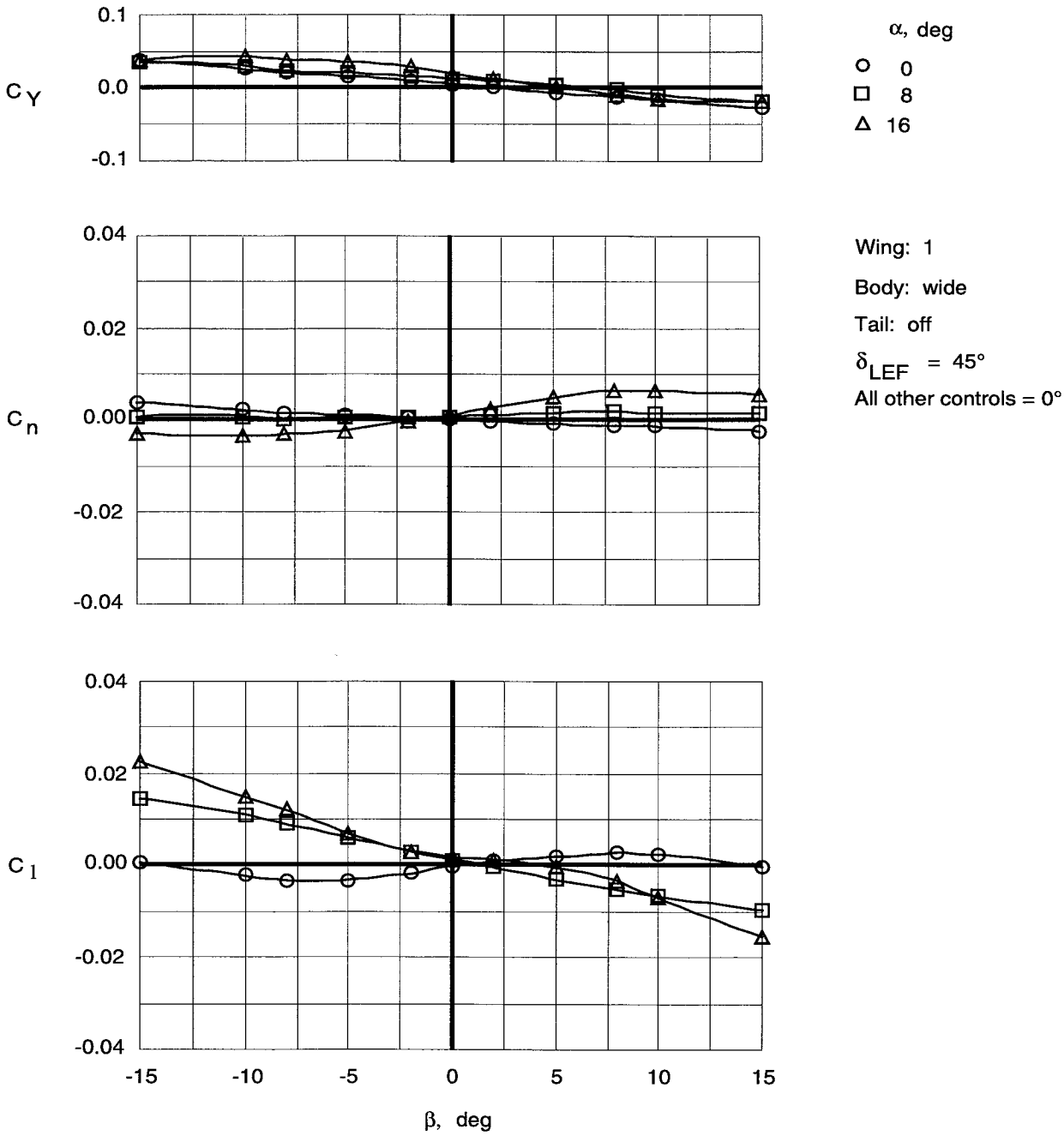

Figure 71. Variation of lateral-directional coefficients with sideslip at low angles of attack for Wing 1 with wide top body on and leading-edge flaps deflected.

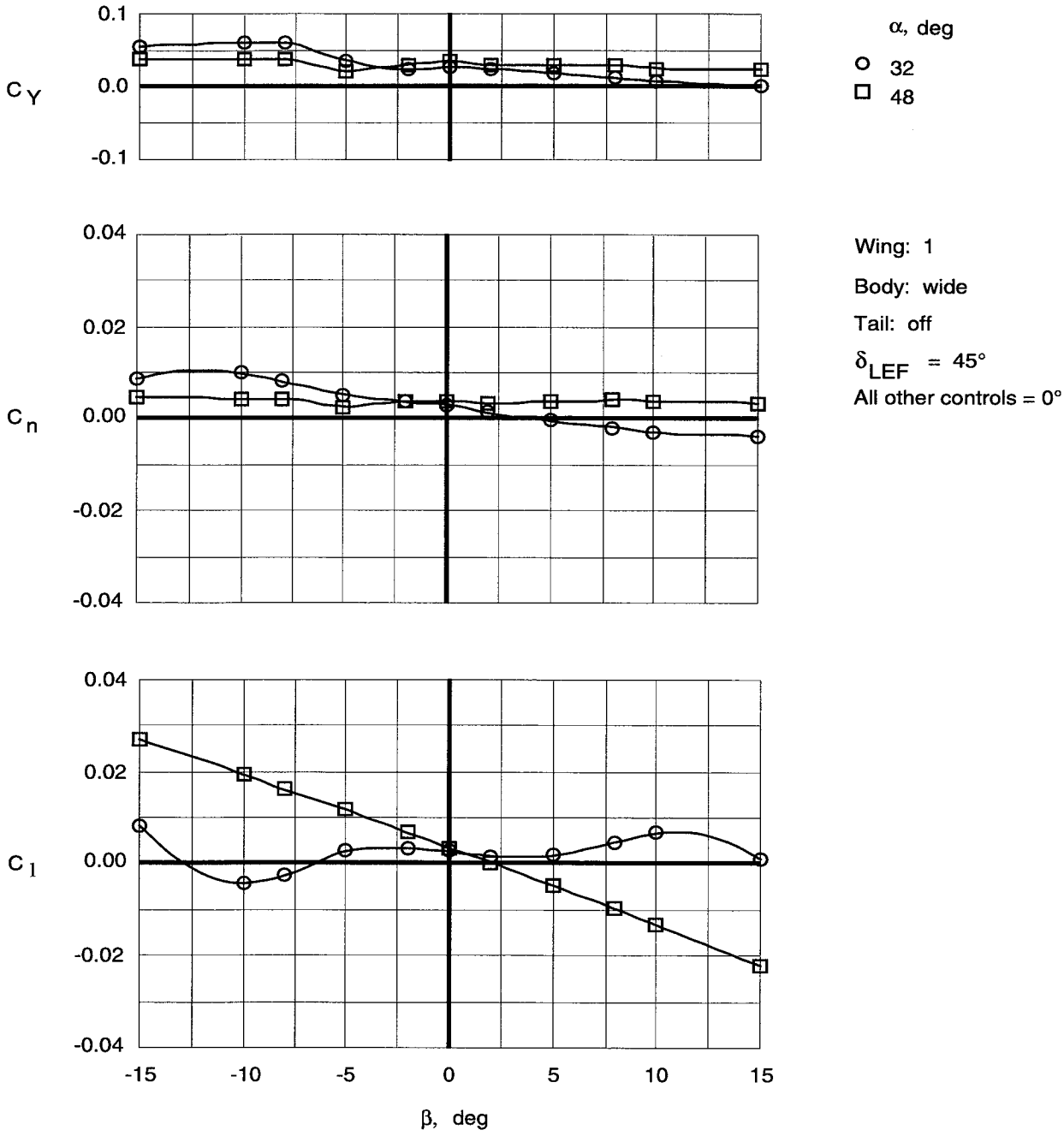

Figure 72. Variation of lateral-directional coefficients with sideslip at high angles of attack for Wing 1 with wide top body on and leading-edge flaps deflected.

C-2

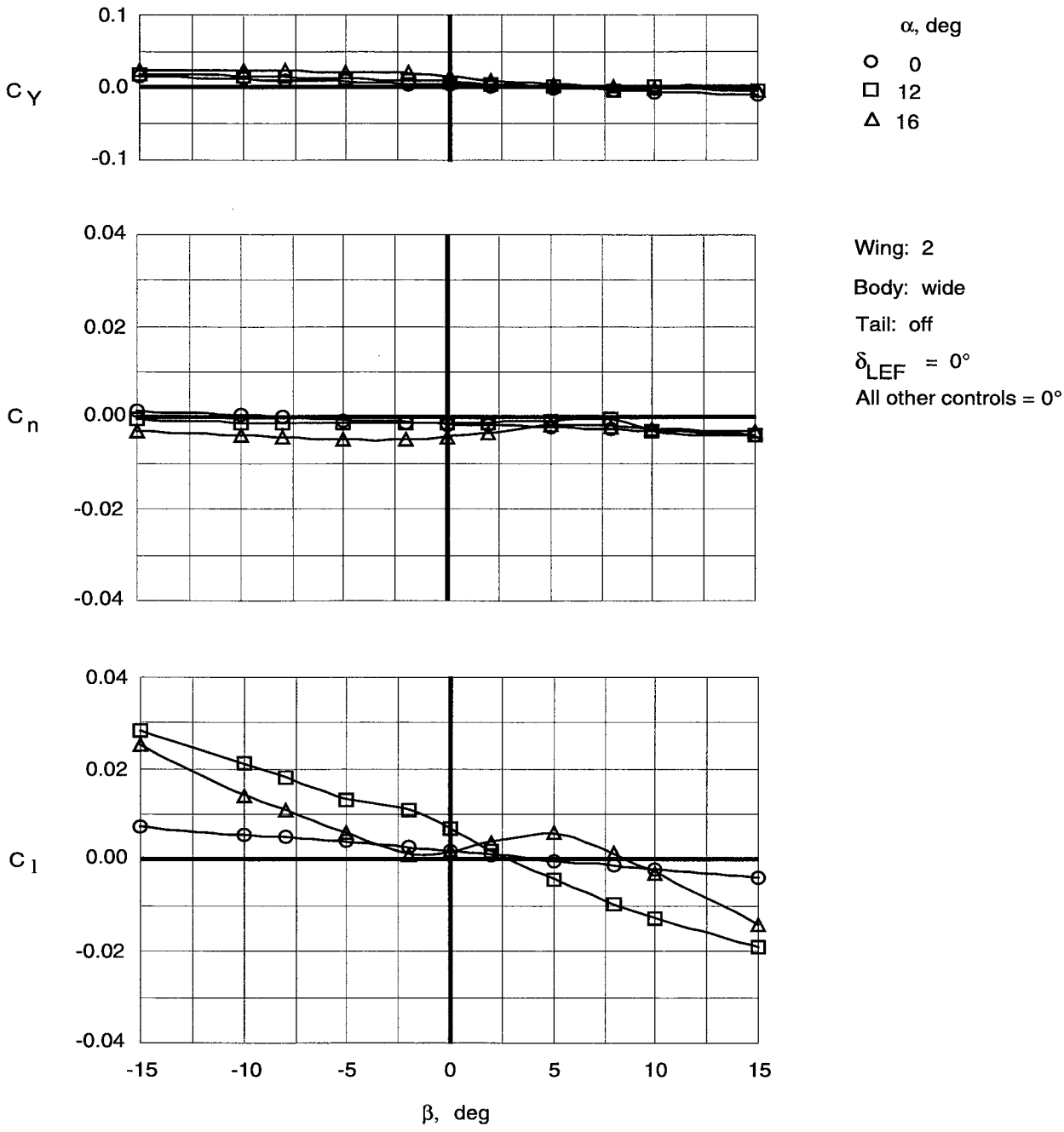

Figure 73. Variation of lateral-directional coefficients with sideslip at low angles of attack for Wing 2 with wide top body on.

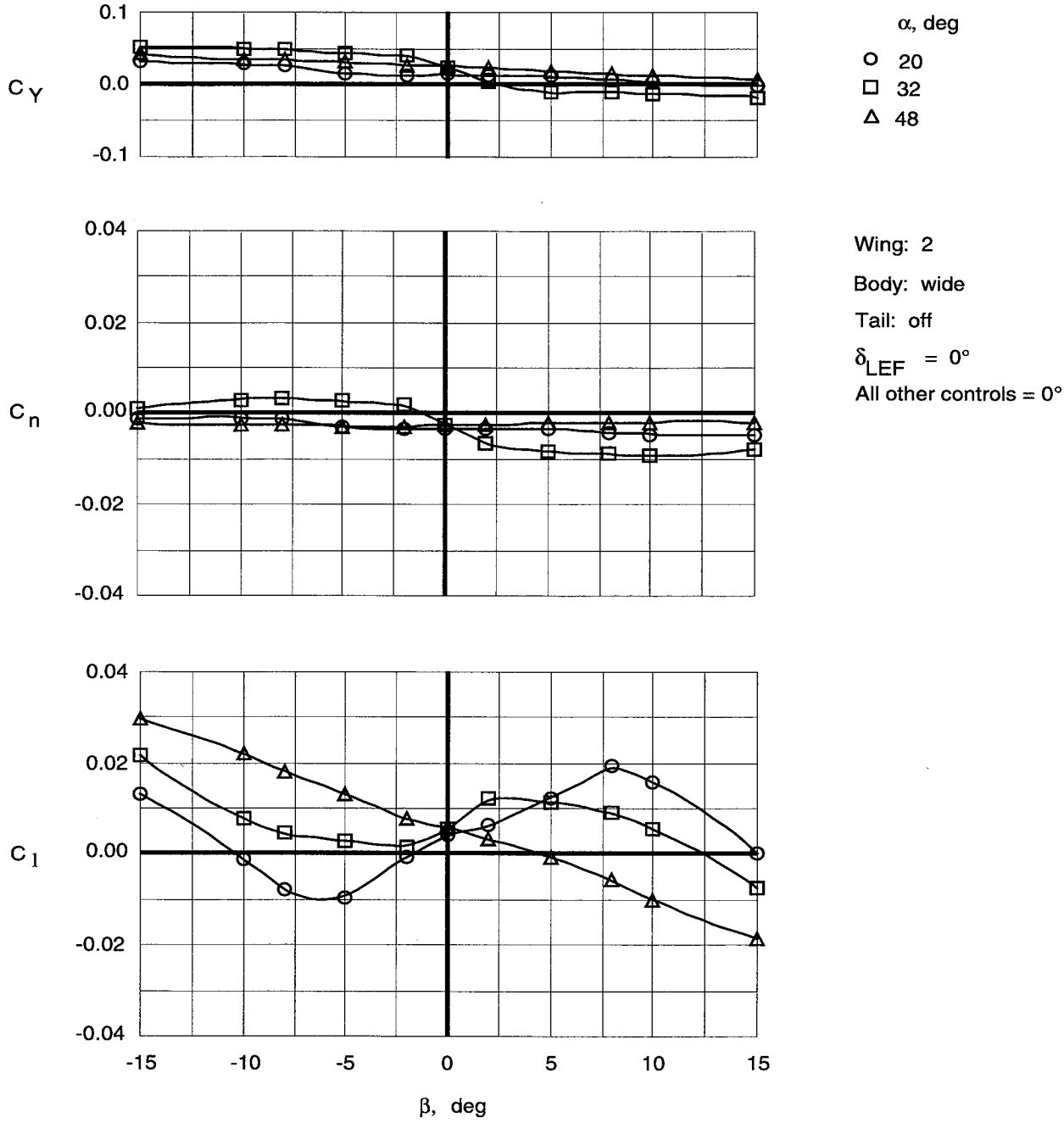

Figure 74. Variation of lateral-directional coefficients with sideslip at high angles of attack for Wing 2 with wide top body on.

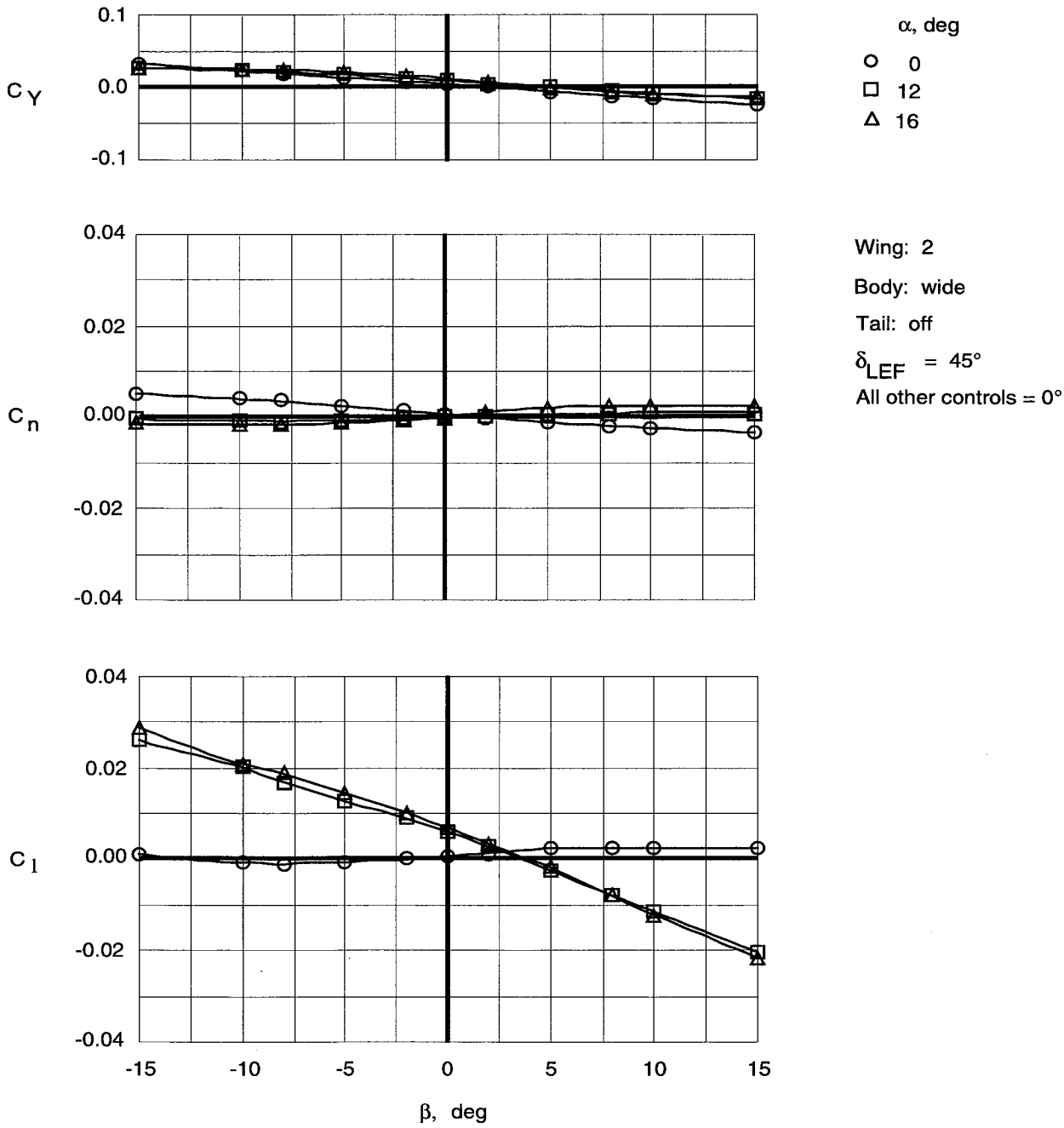

Figure 75. Variation of lateral-directional coefficients with sideslip at low angles of attack for Wing 2 with wide top body on and leading-edge flaps deflected.

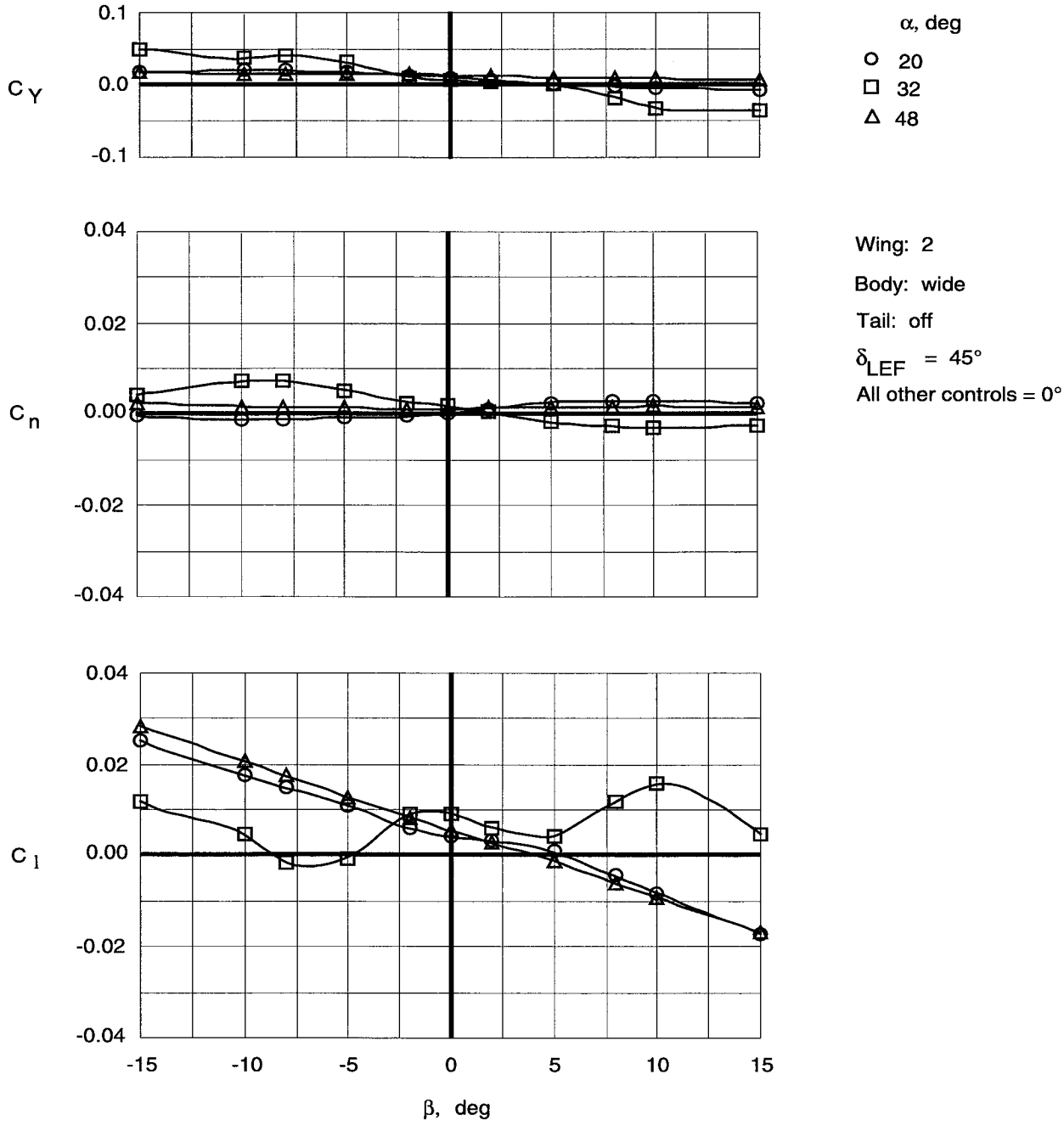

Figure 76. Variation of lateral-directional coefficients with sideslip at high angles of attack for Wing 2 with wide top body on and leading-edge flaps deflected.

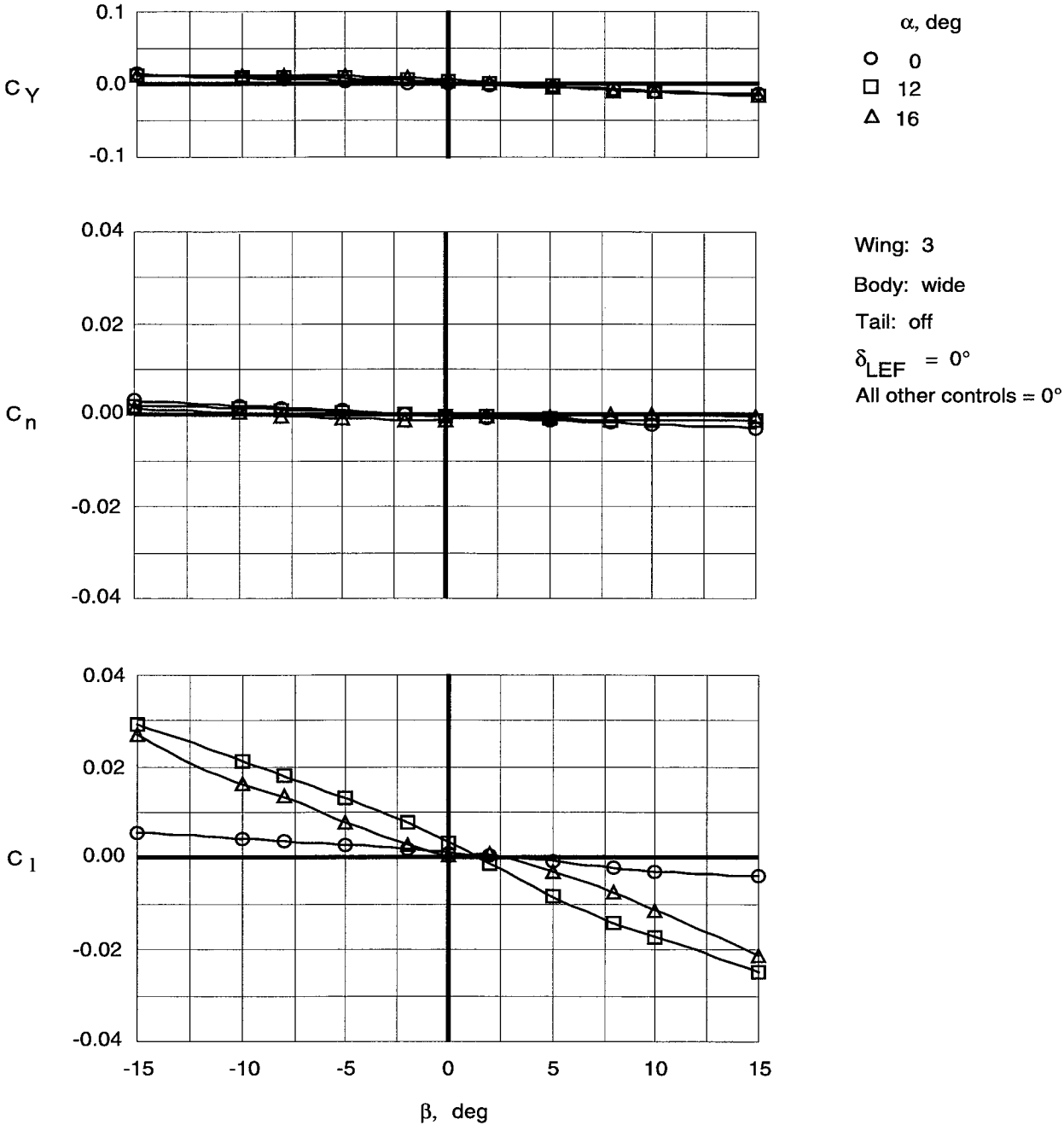

Figure 77. Variation of lateral-directional coefficients with sideslip at low angles of attack for Wing 3 with wide top body on.

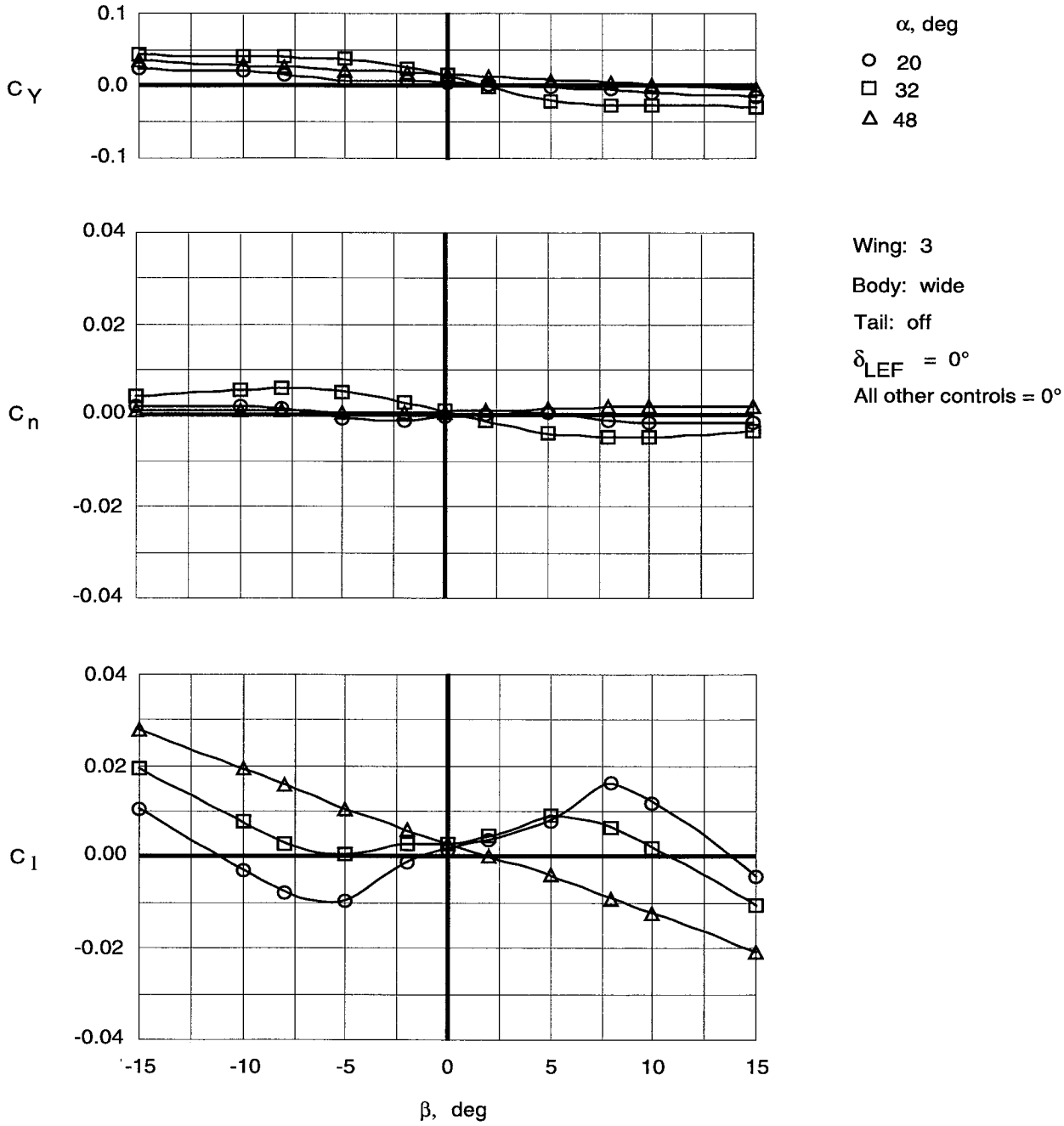

Figure 78. Variation of lateral-directional coefficients with sideslip at high angles of attack for Wing 3 with wide top body on.

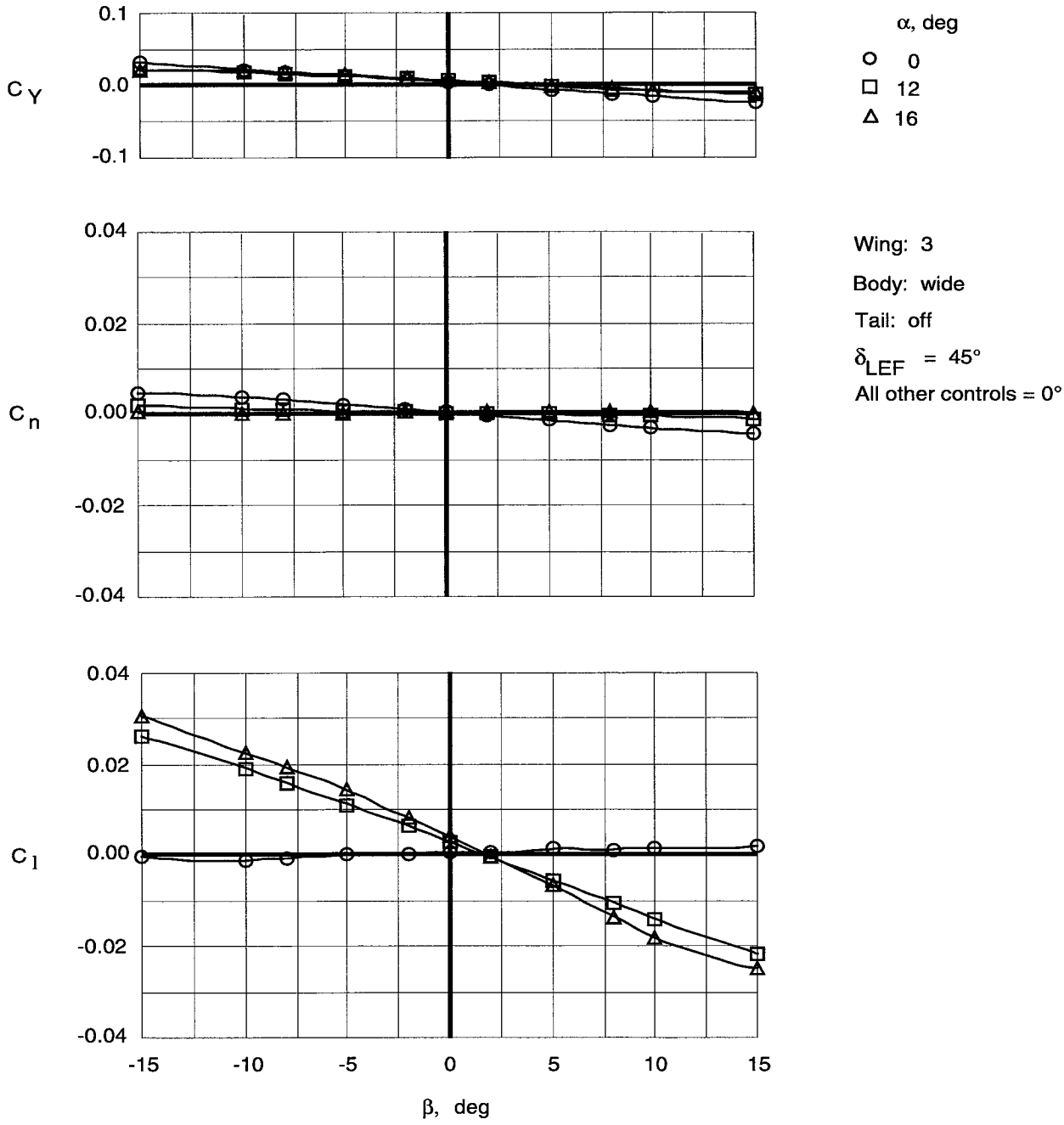

Figure 79. Variation of lateral-directional coefficients with sideslip at low angles of attack for Wing 3 with wide top body on and leading-edge flaps deflected.

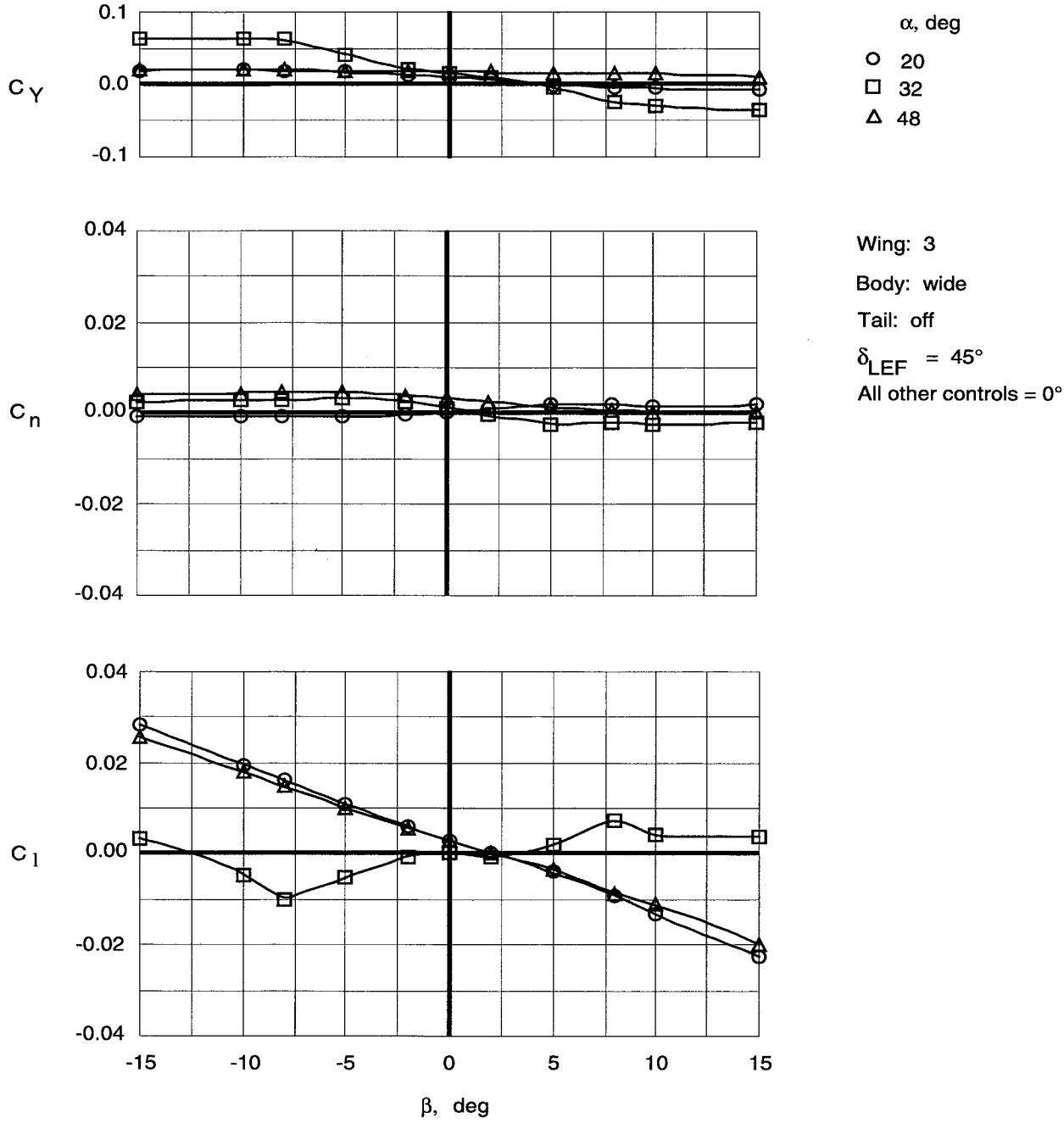

Figure 80. Variation of lateral-directional coefficients with sideslip at high angles of attack for Wing 3 with wide top body on and leading-edge flaps deflected.

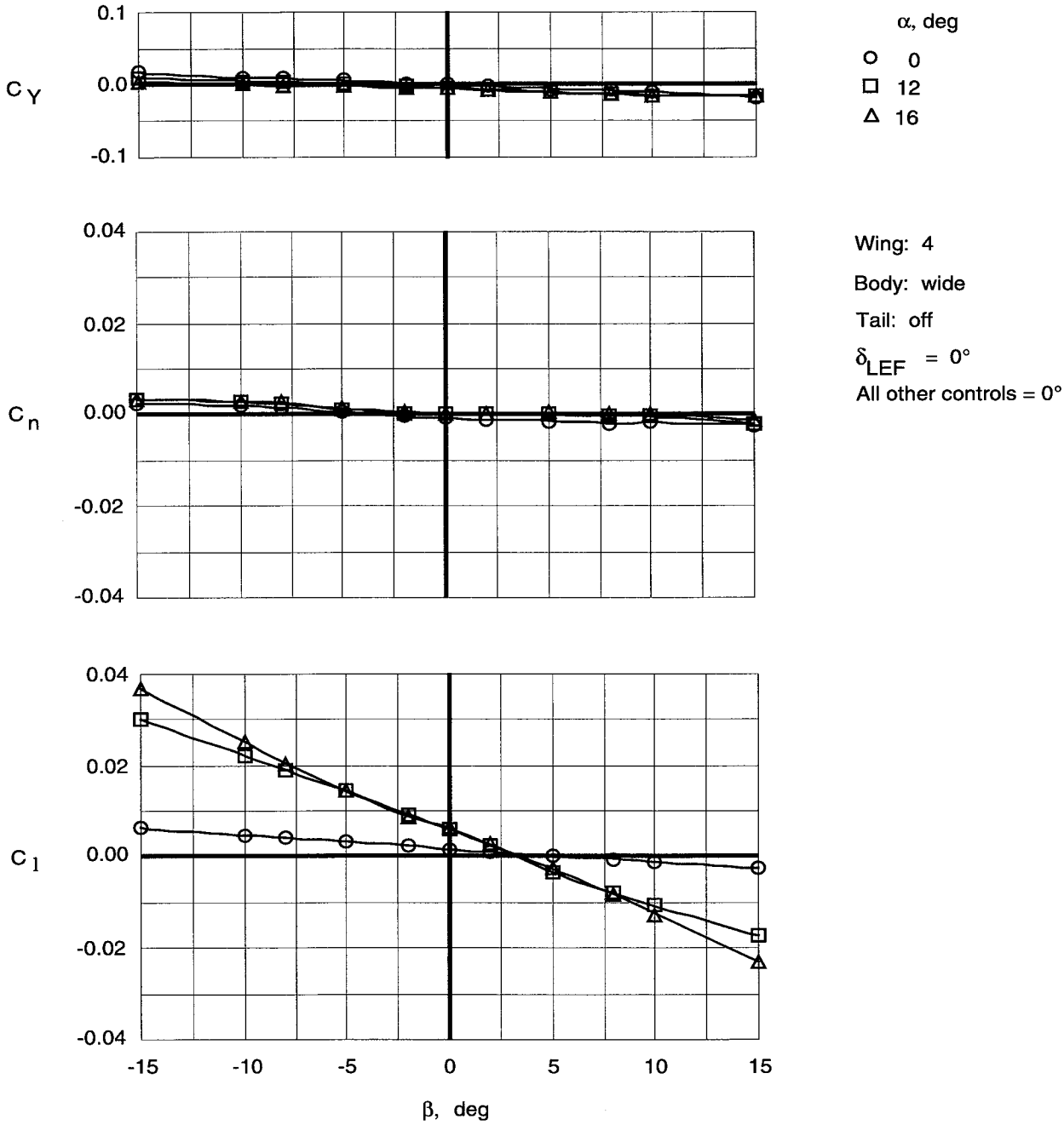

Figure 81. Variation of lateral-directional coefficients with sideslip at low angles of attack for Wing 4 with wide top body on.

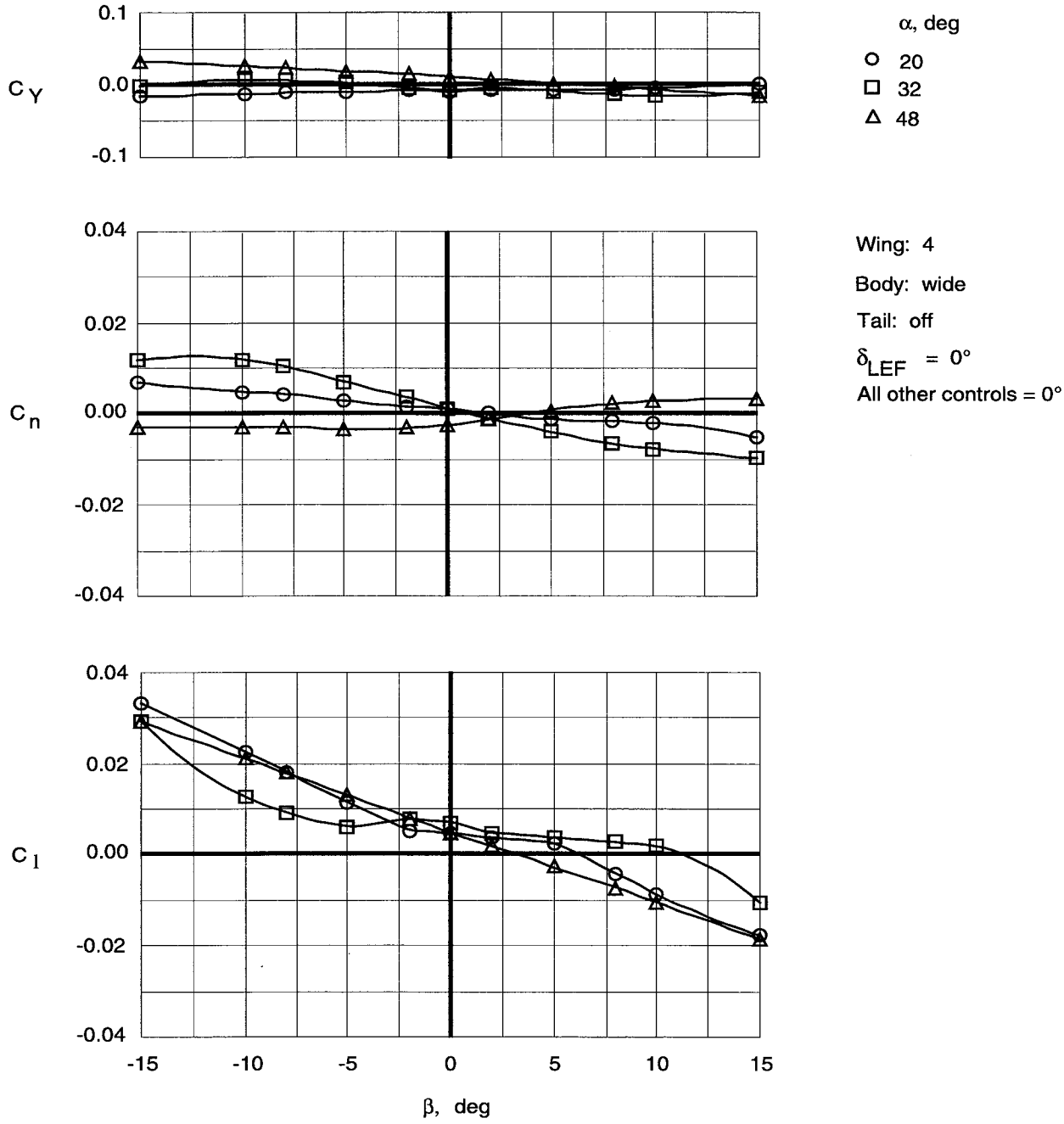

Figure 82. Variation of lateral-directional coefficients with sideslip at high angles of attack for Wing 4 with wide top body on.

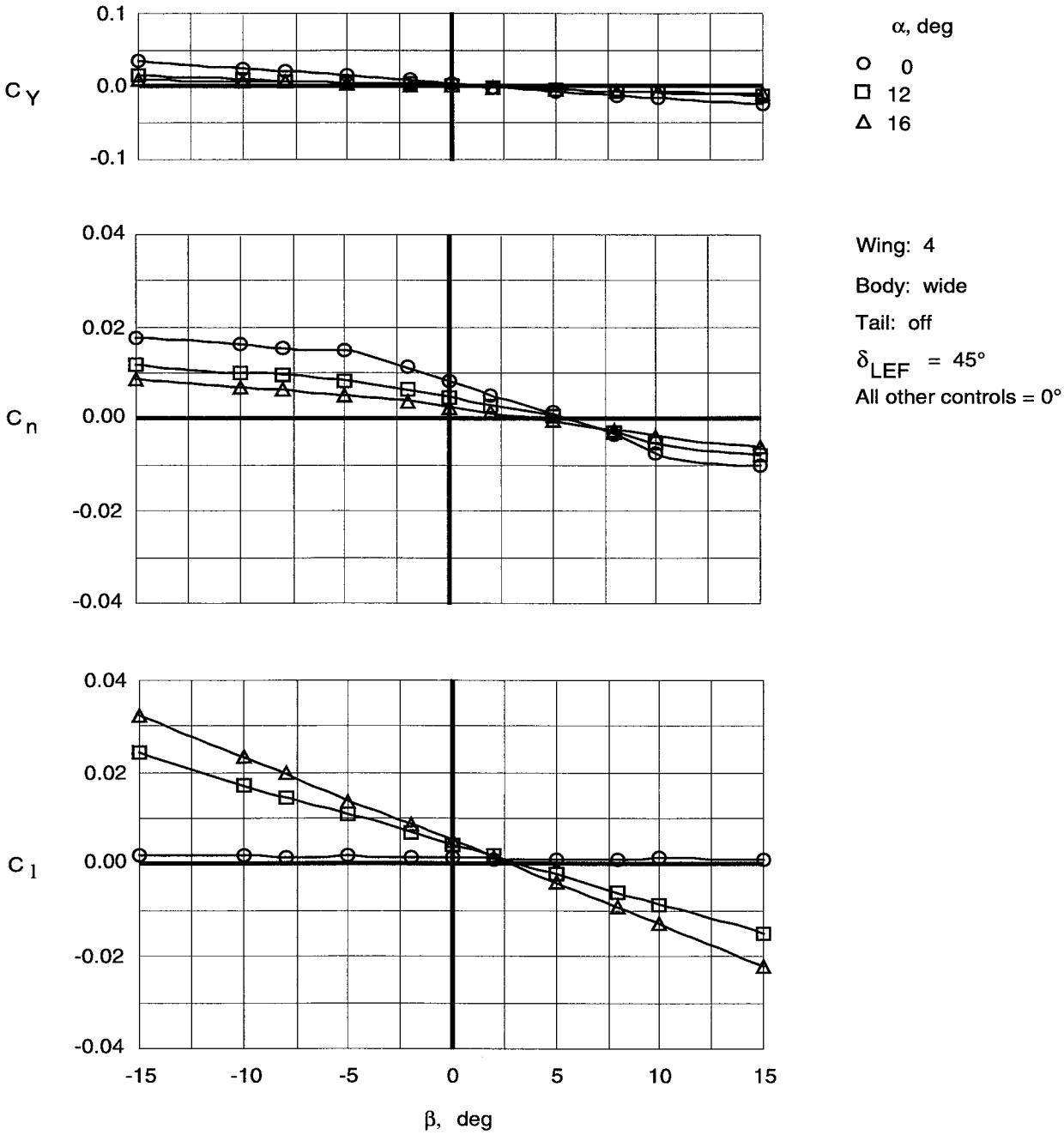

Figure 83. Variation of lateral-directional coefficients with sideslip at low angles of attack for Wing 4 with wide top body on and leading-edge flaps deflected.

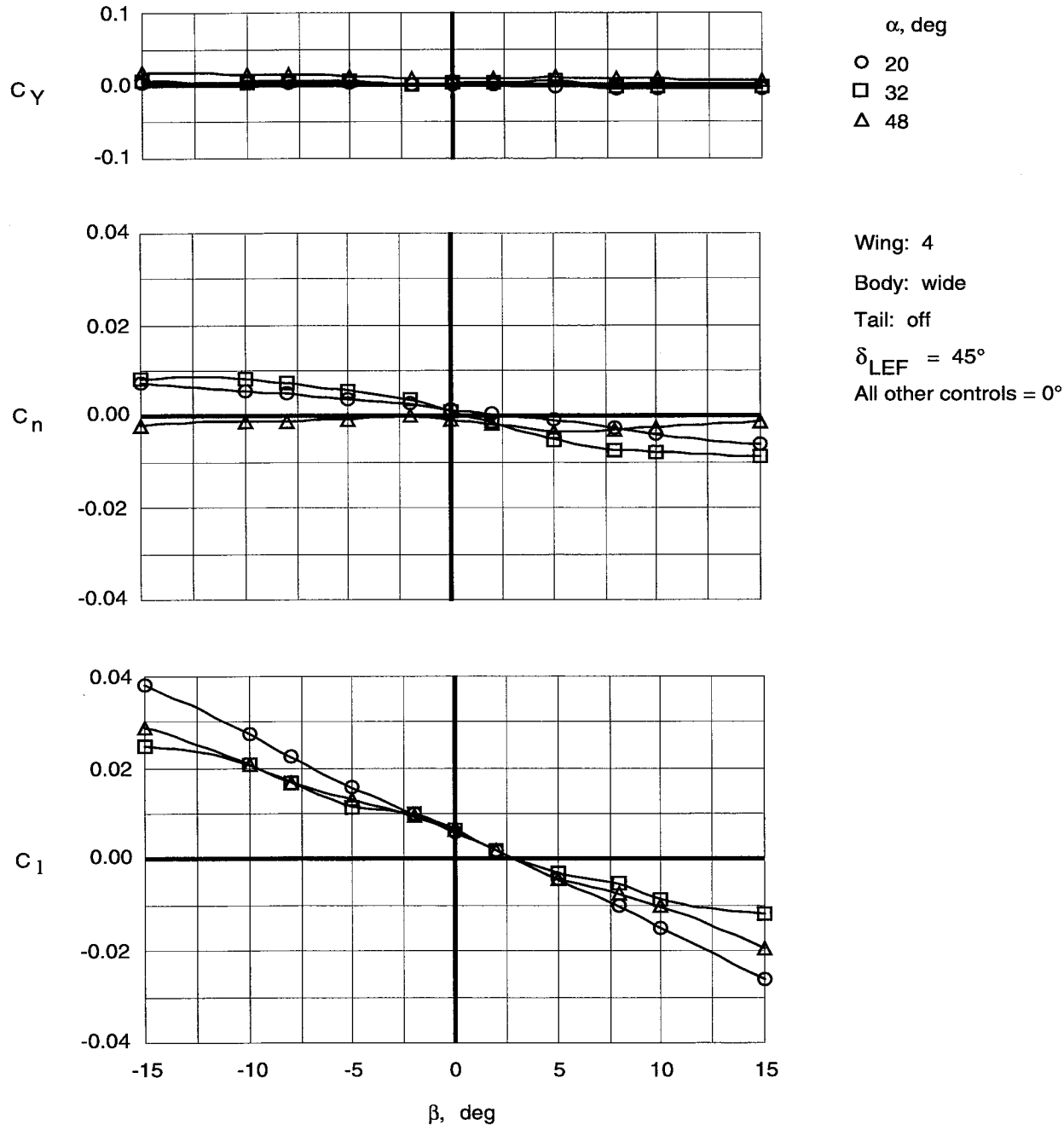

Figure 84. Variation of lateral-directional coefficients with sideslip at high angles of attack for Wing 4 with wide top body on and leading-edge flaps deflected.

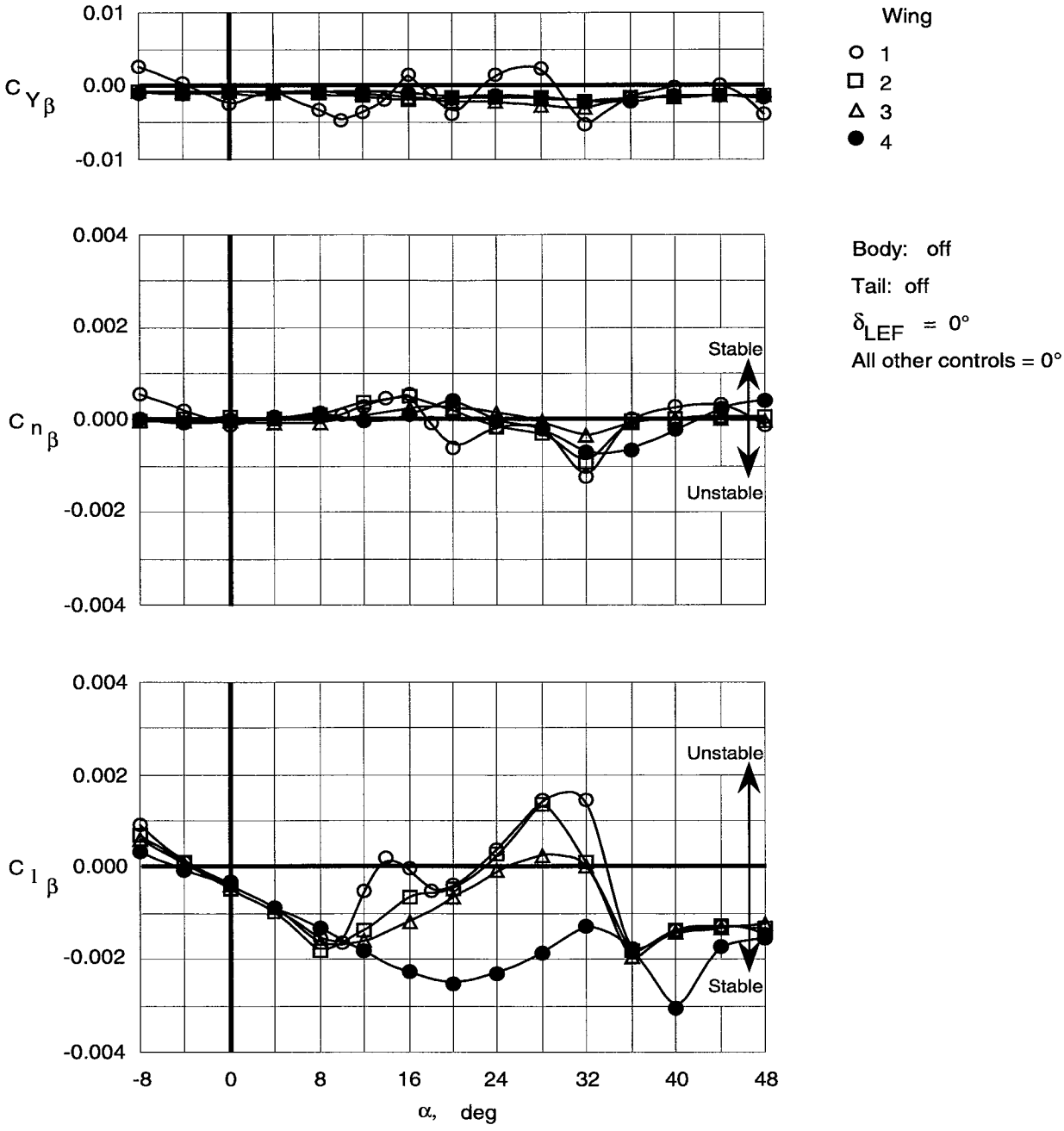

Figure 85. Lateral-directional stability characteristics of wing planforms with top body off.

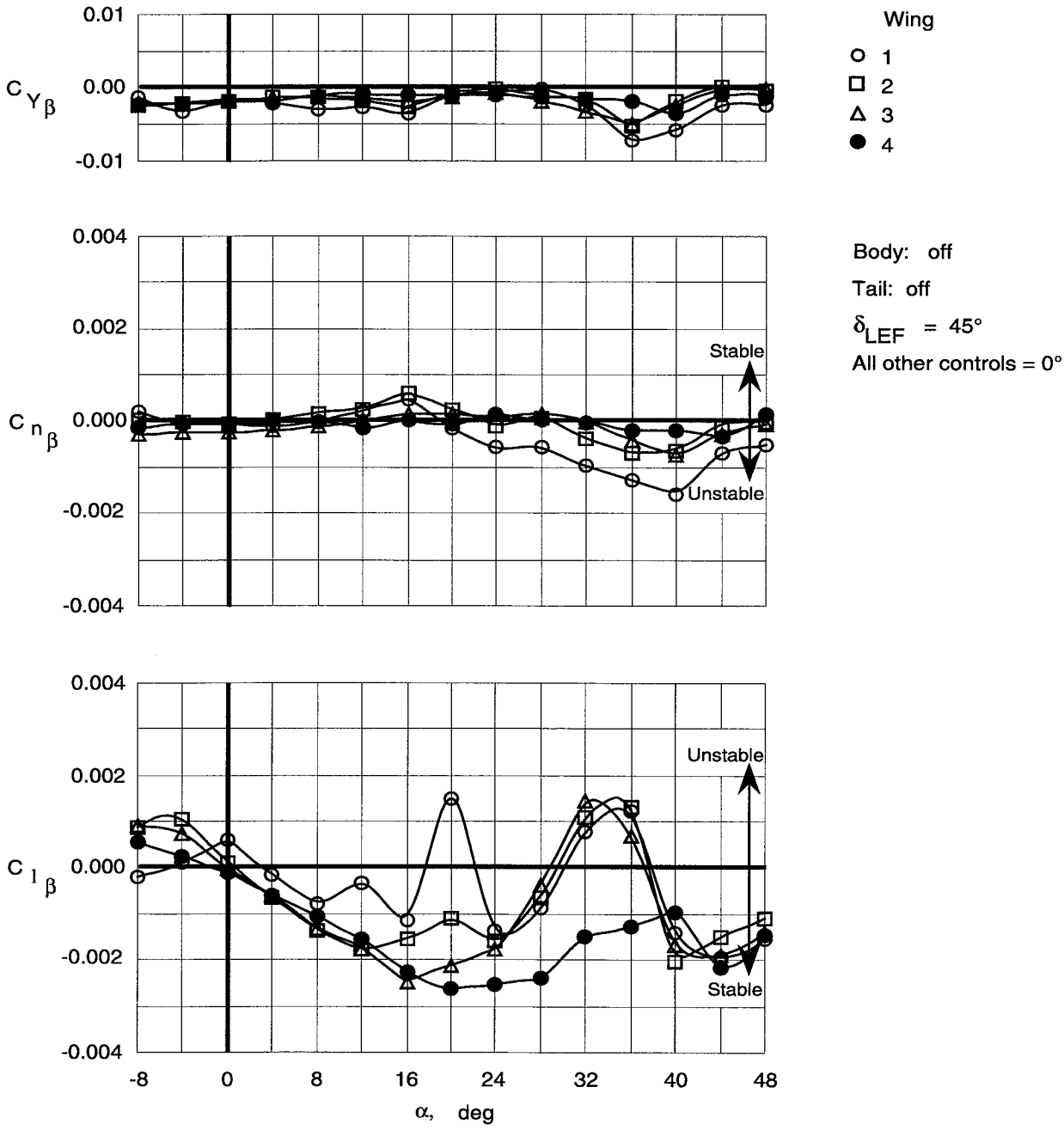

Figure 86. Lateral-directional stability characteristics of wing planforms with top body off and leading-edge flaps deflected.

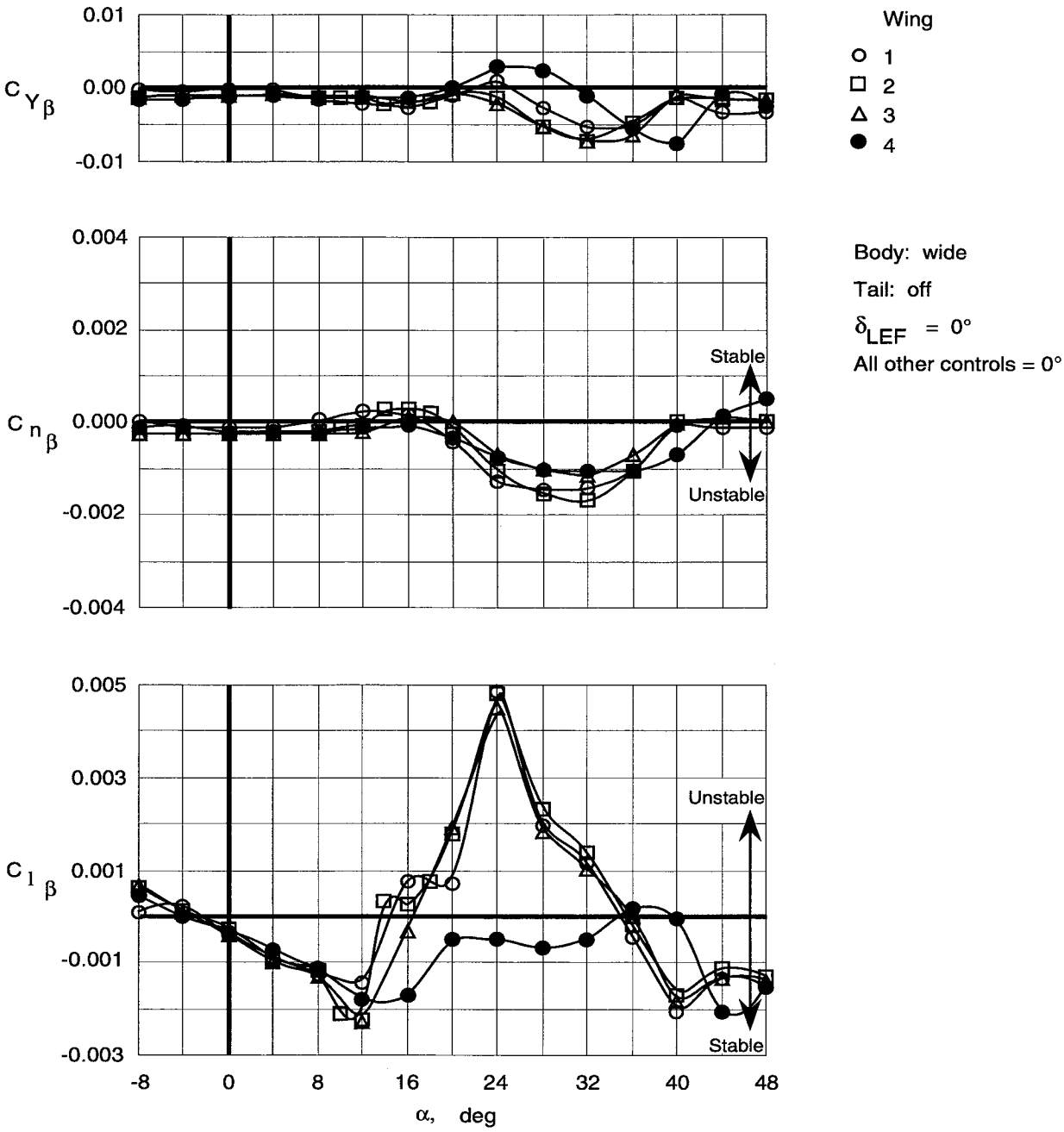

Figure 87. Lateral-directional stability characteristics of wing planforms with wide top body on.

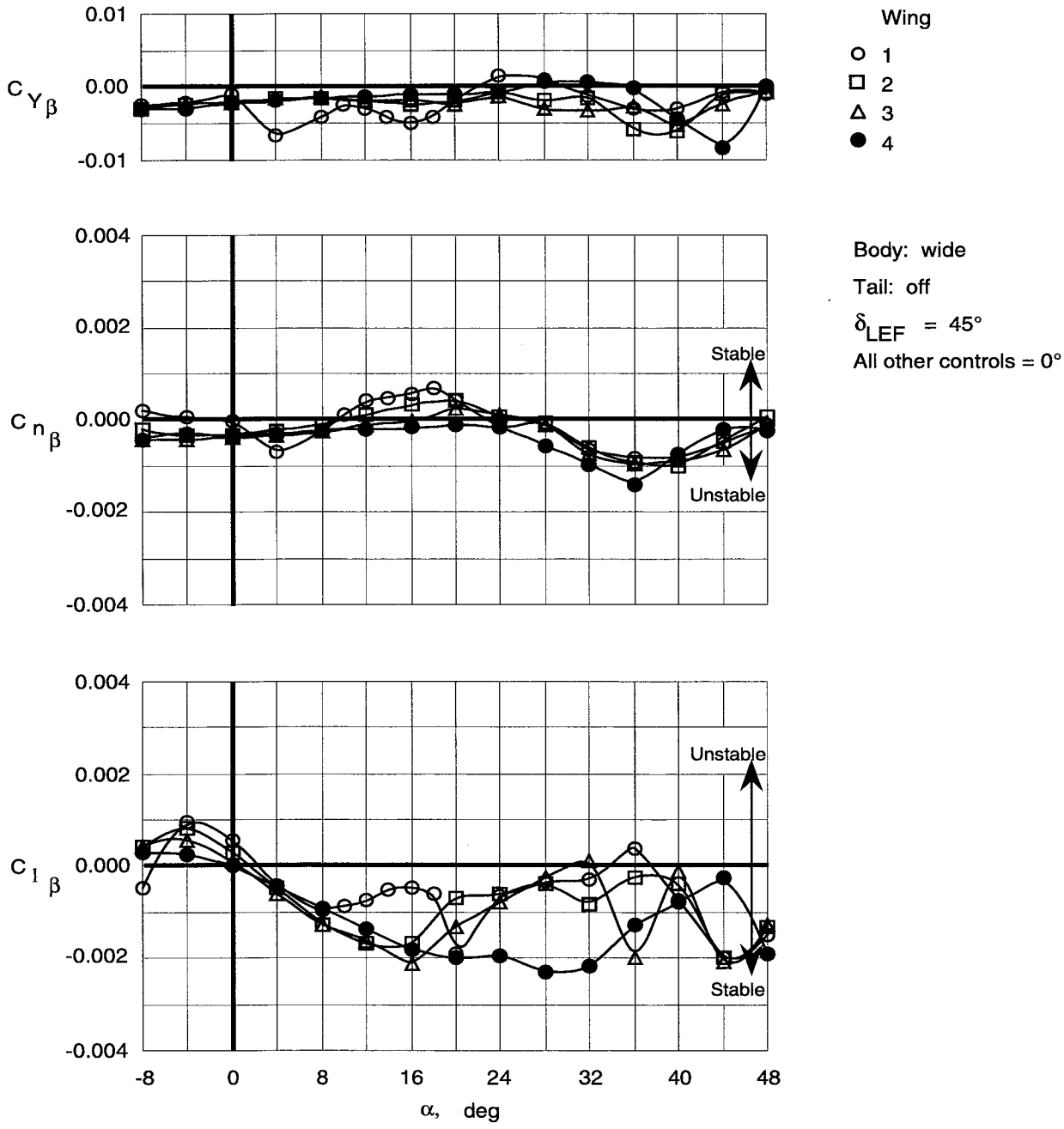

Figure 88. Lateral-directional stability characteristics of wing planforms with wide top body on and leading-edge flaps deflected.

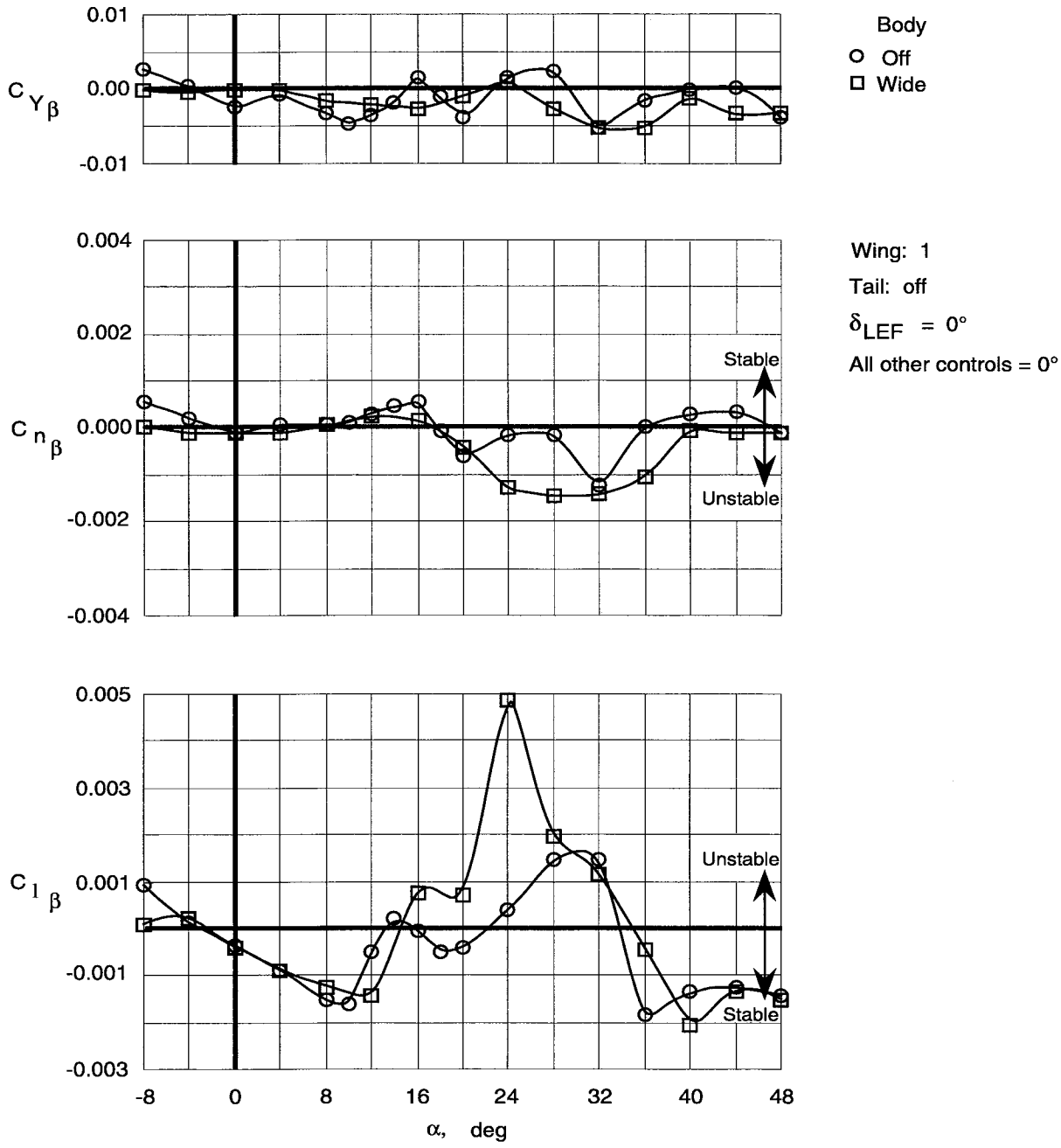

Figure 89. Effect of wide top body on lateral-directional stability characteristics of Wing 1.

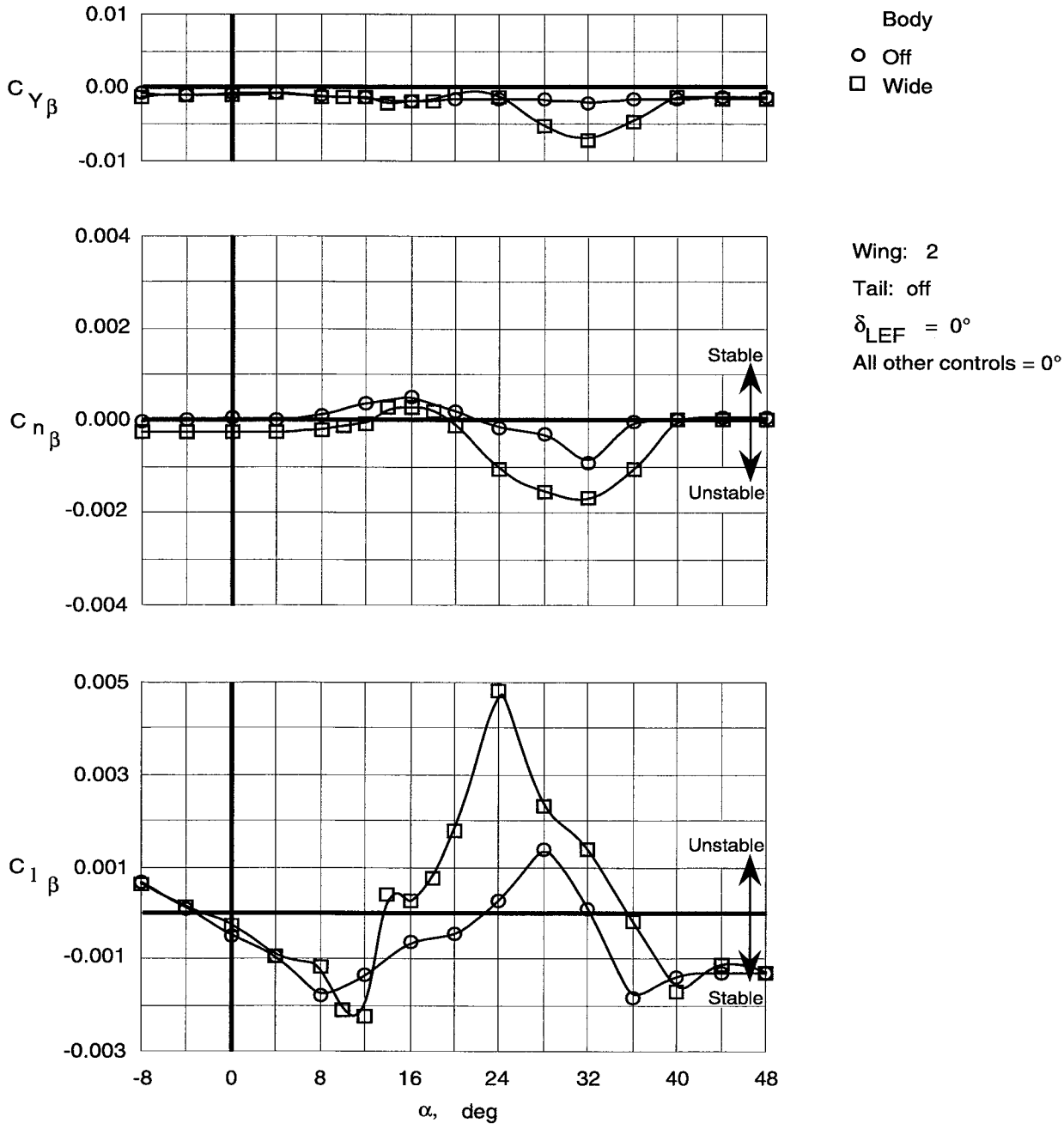

Figure 90. Effect of wide top body on lateral-directional stability characteristics of Wing 2.

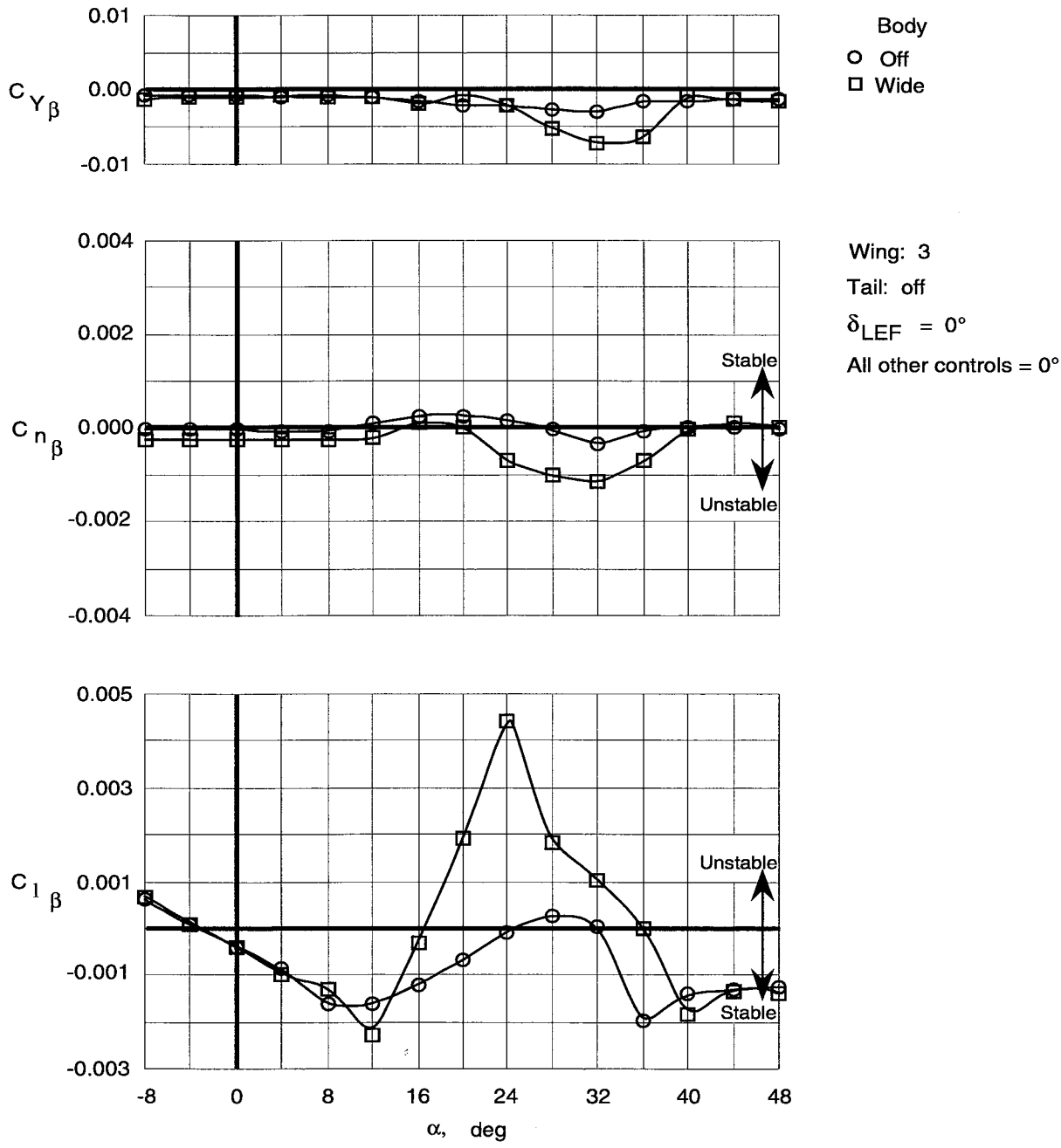

Figure 91. Effect of wide top body on lateral-directional stability characteristics of Wing 3.

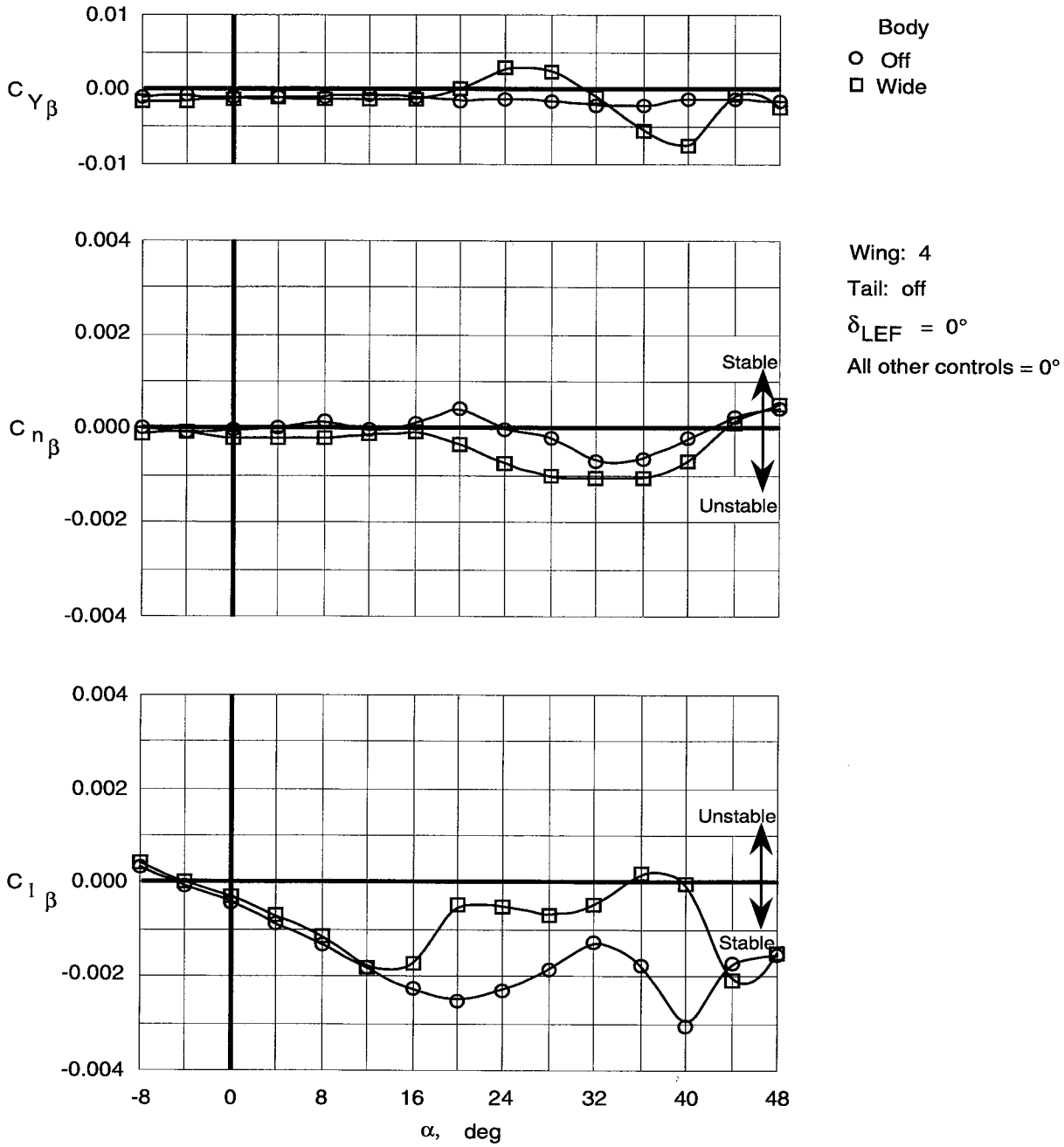

Figure 92. Effect of wide top body on lateral-directional stability characteristics of Wing 4.

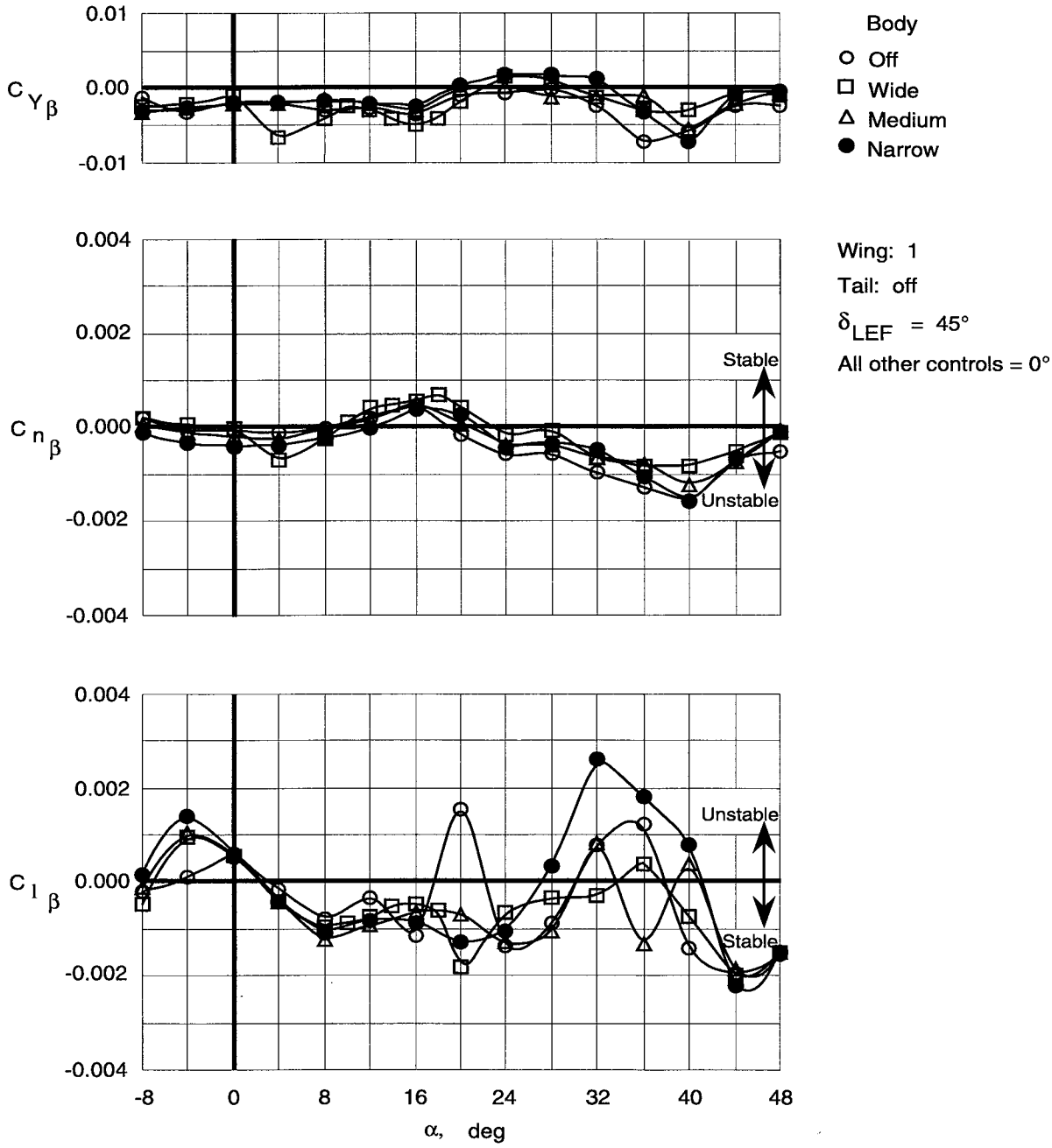

Figure 93. Effect of top body width on lateral-directional stability characteristics of Wing 1 with leading-edge flaps deflected.

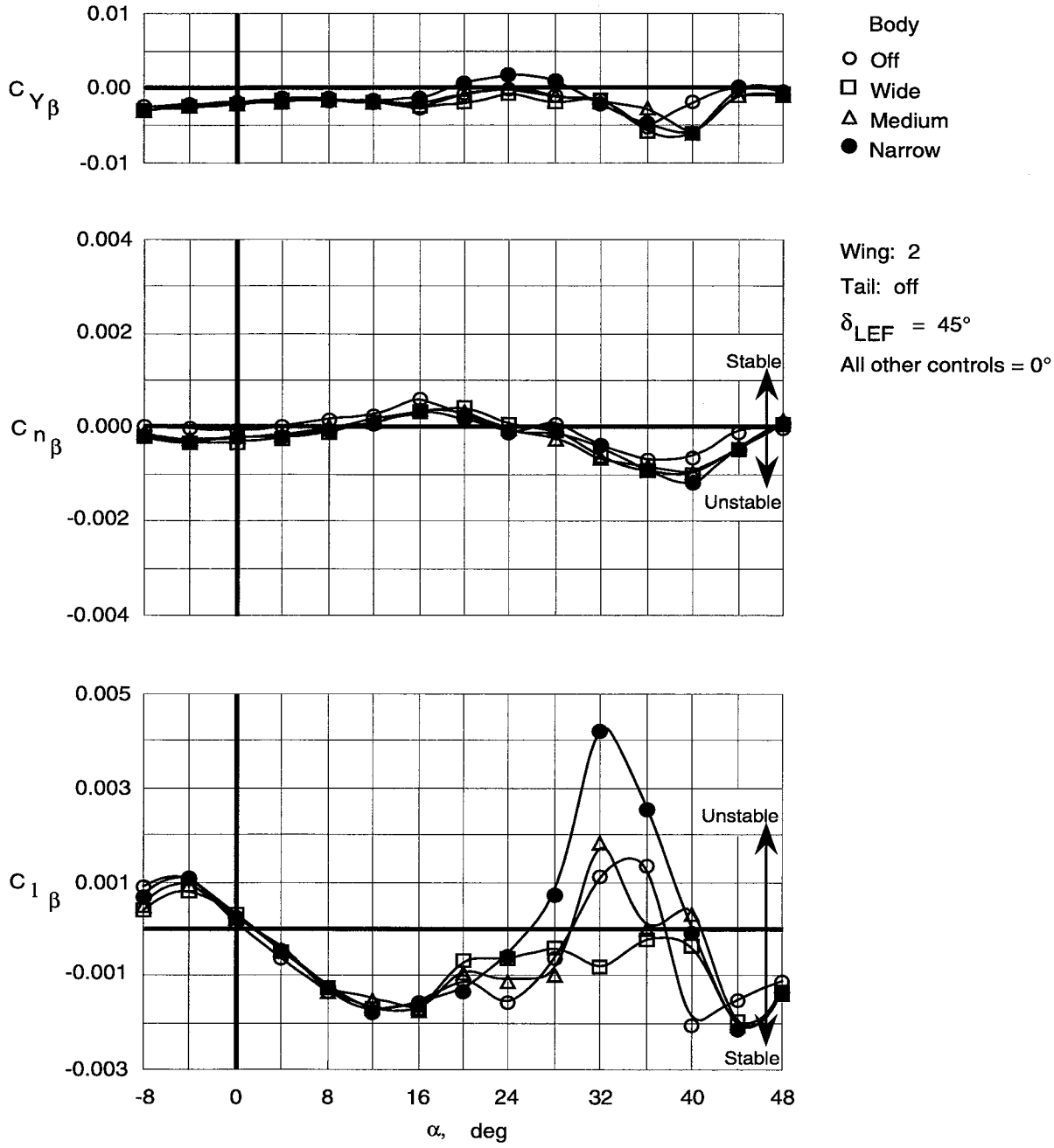

Figure 94. Effect of top body width on lateral-directional stability characteristics of Wing 2 with leading-edge flaps deflected.

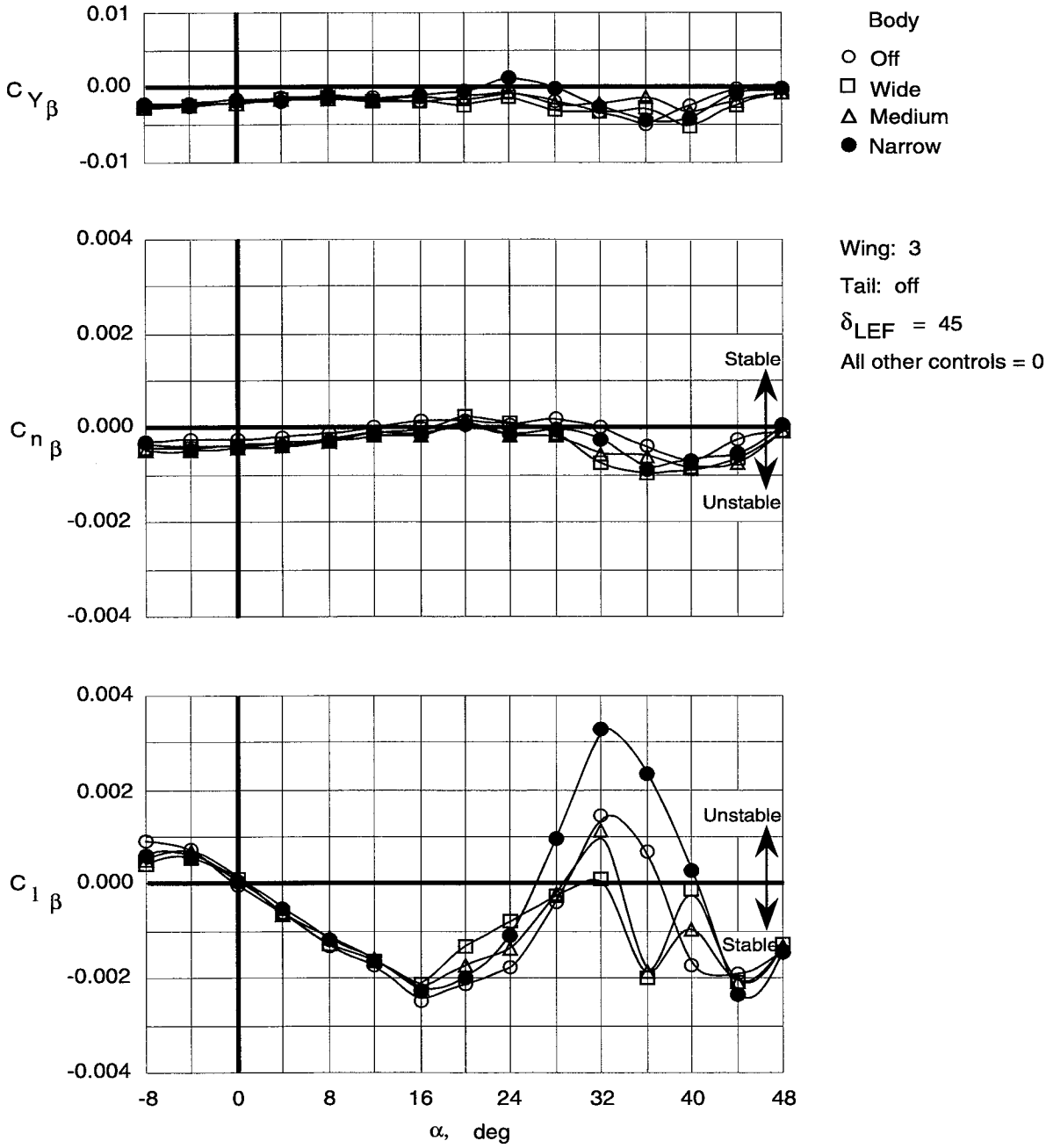

Figure 95. Effect of top body width on lateral-directional stability characteristics of Wing 3 with leading-edge flaps deflected.

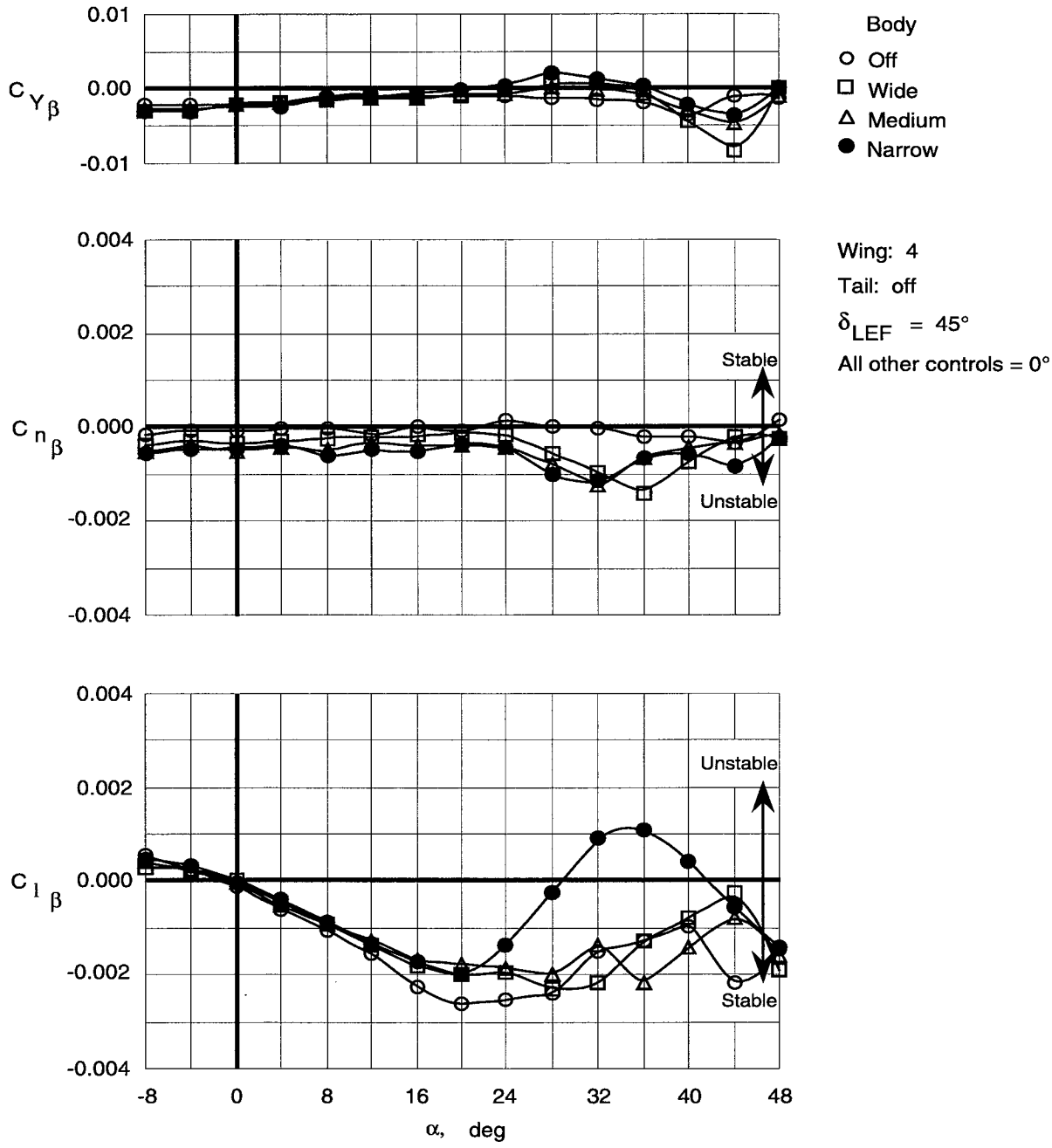

Figure 96. Effect of top body width on lateral-directional stability characteristics of Wing 4 with leading-edge flaps deflected.

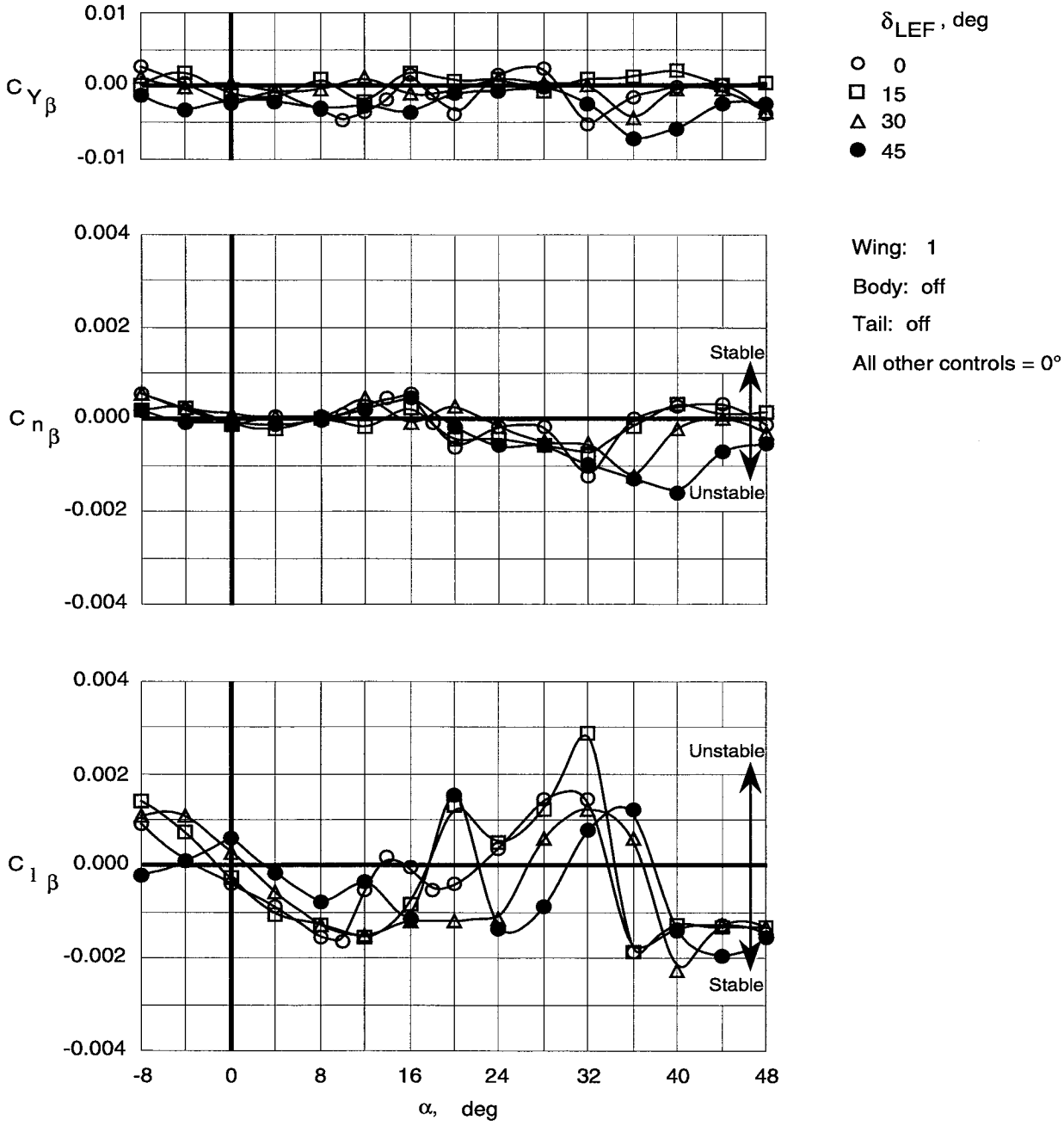

Figure 97. Effect of leading-edge flap deflections on lateral-directional stability characteristics of Wing 1 with top body off.

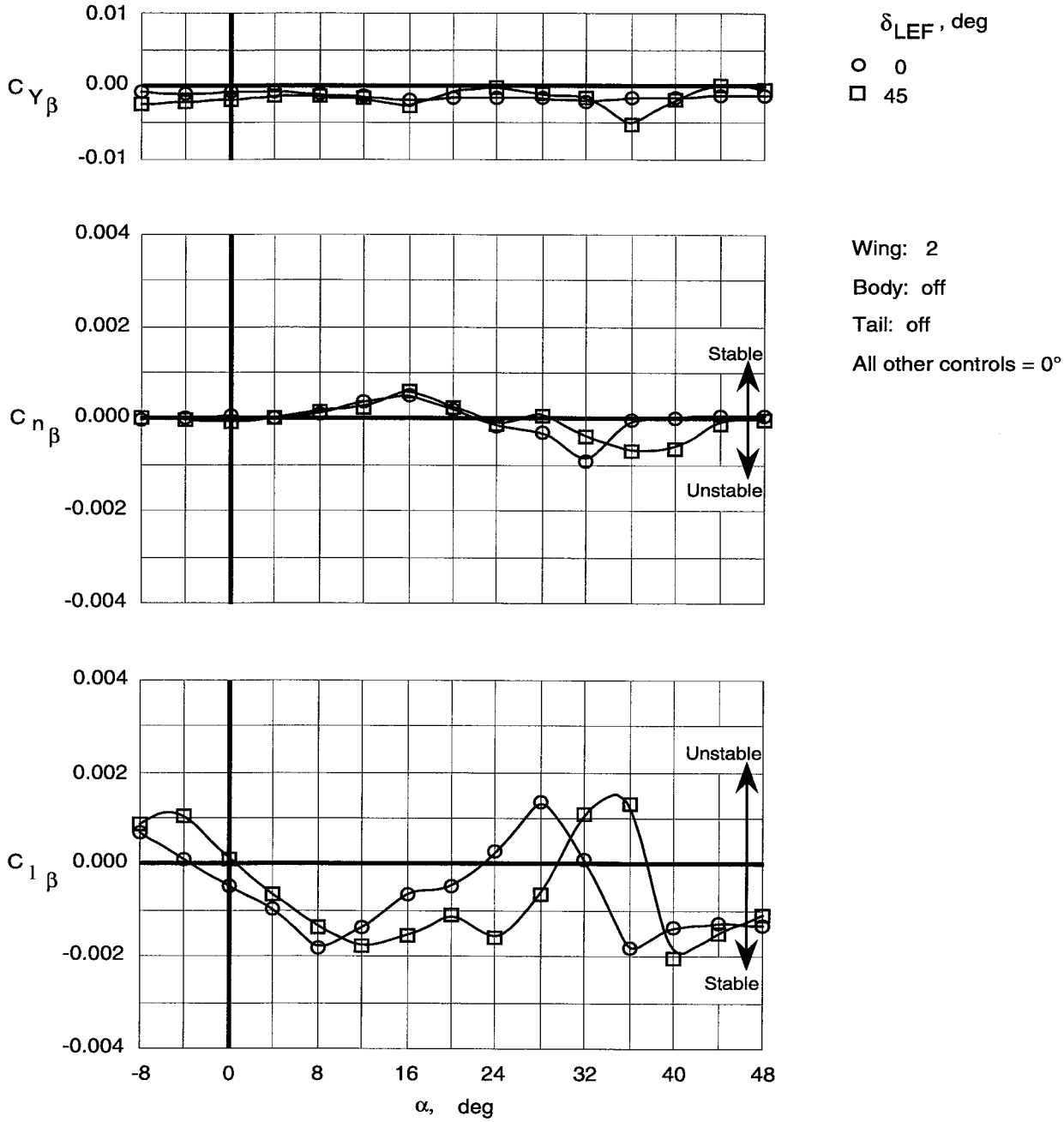

Figure 98. Effect of leading-edge flap deflection on lateral-directional stability characteristics of Wing 2 with top body off.

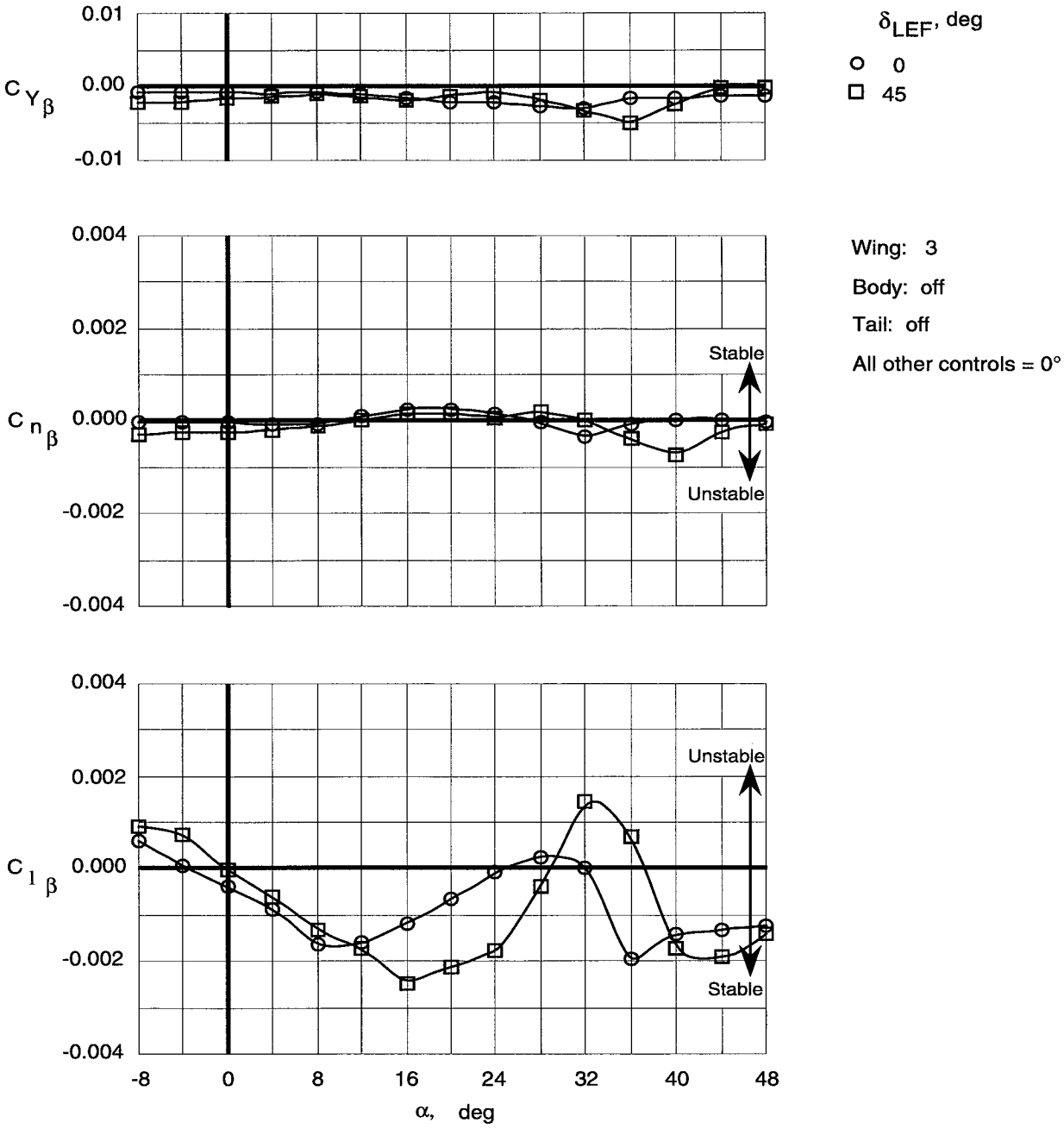

Figure 99. Effect of leading-edge flap deflection on lateral-directional stability characteristics of Wing 3 with top body off.

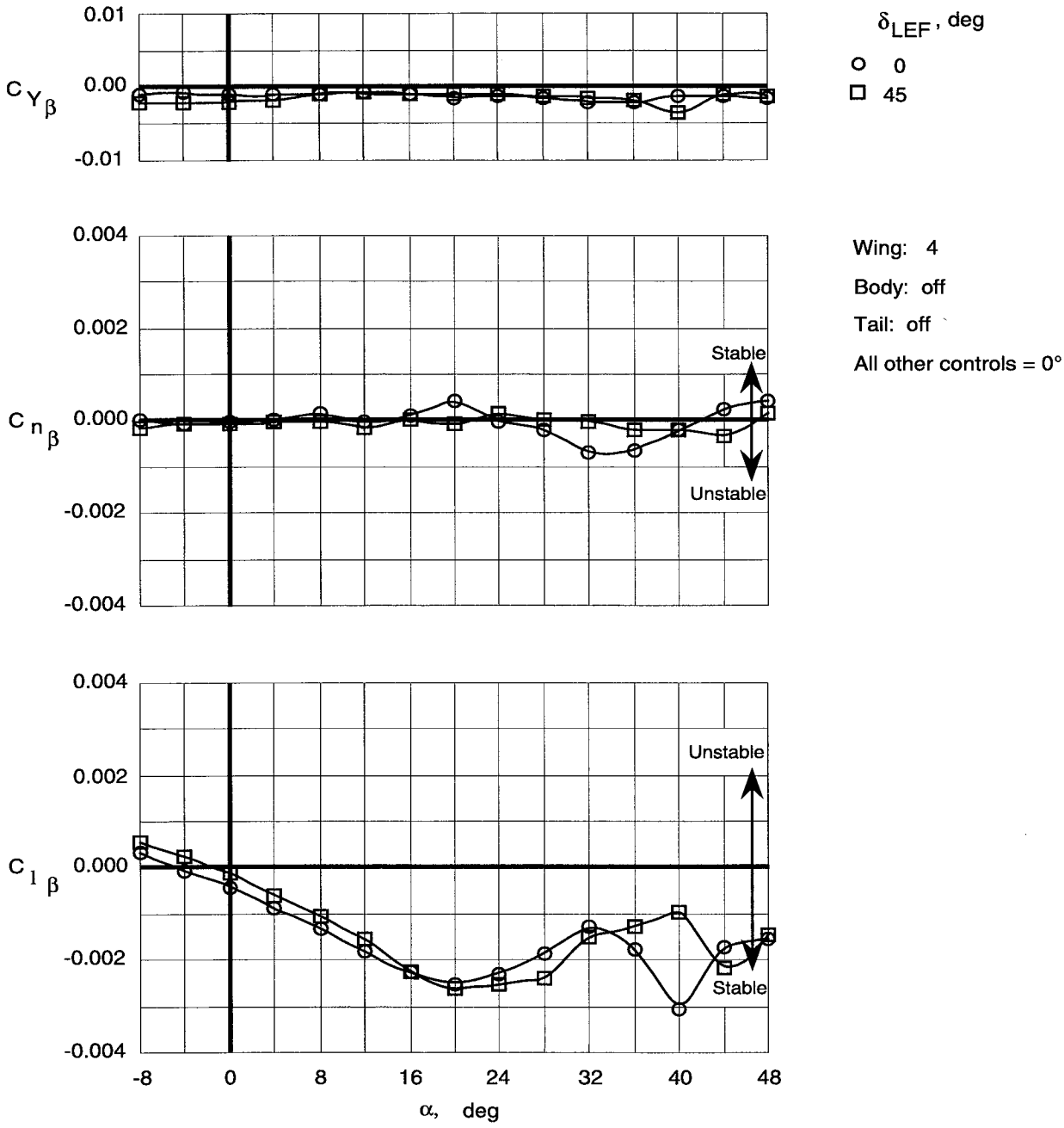

Figure 100. Effect of leading-edge flap deflection on lateral-directional stability characteristics of Wing 4 with top body off.

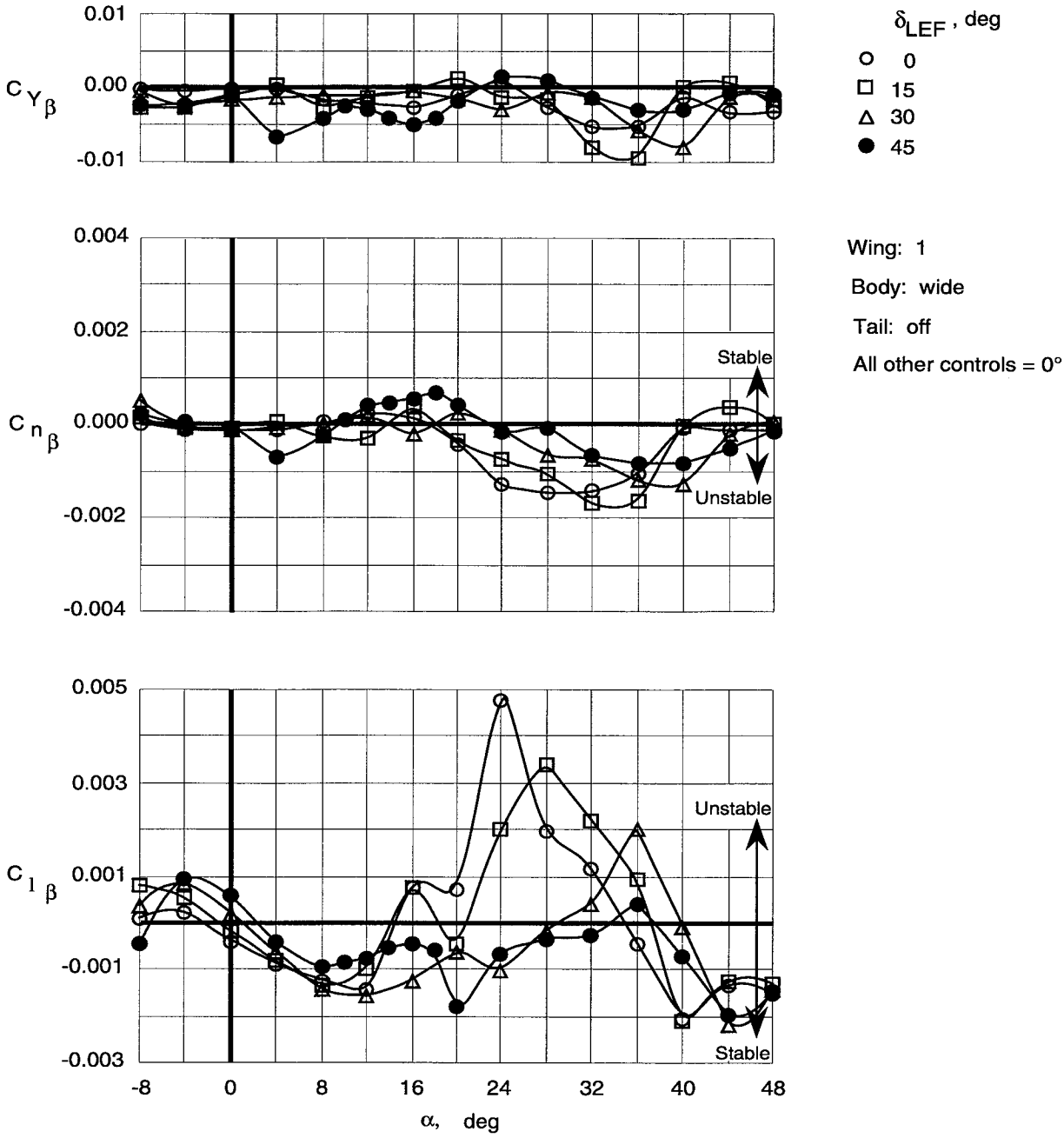

Figure 101. Effect of leading-edge flap deflections on lateral-directional stability characteristics of Wing 1 with wide top body on.

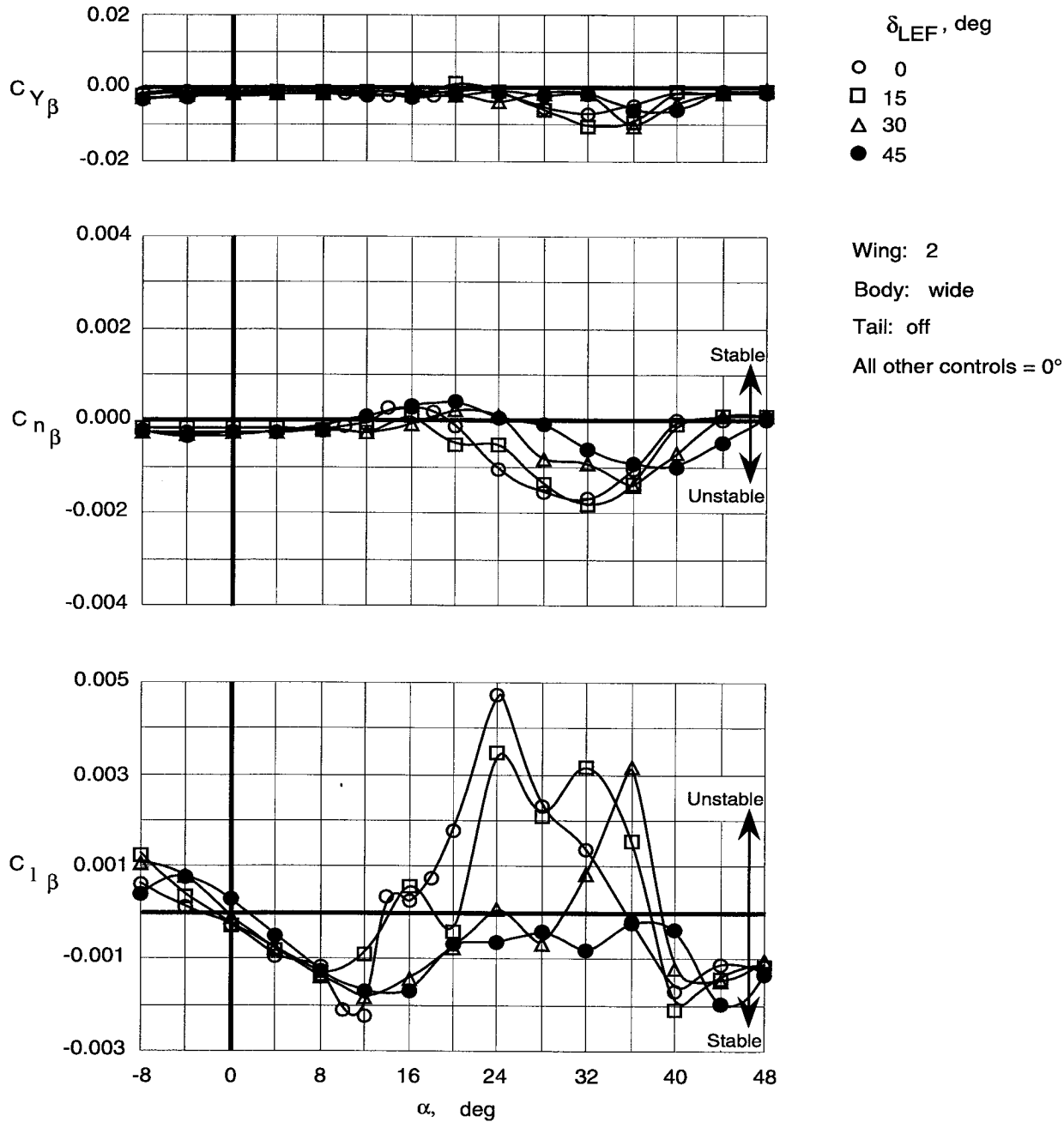

Figure 102. Effect of leading-edge flap deflections on lateral-directional stability characteristics of Wing 2 with wide top body on.

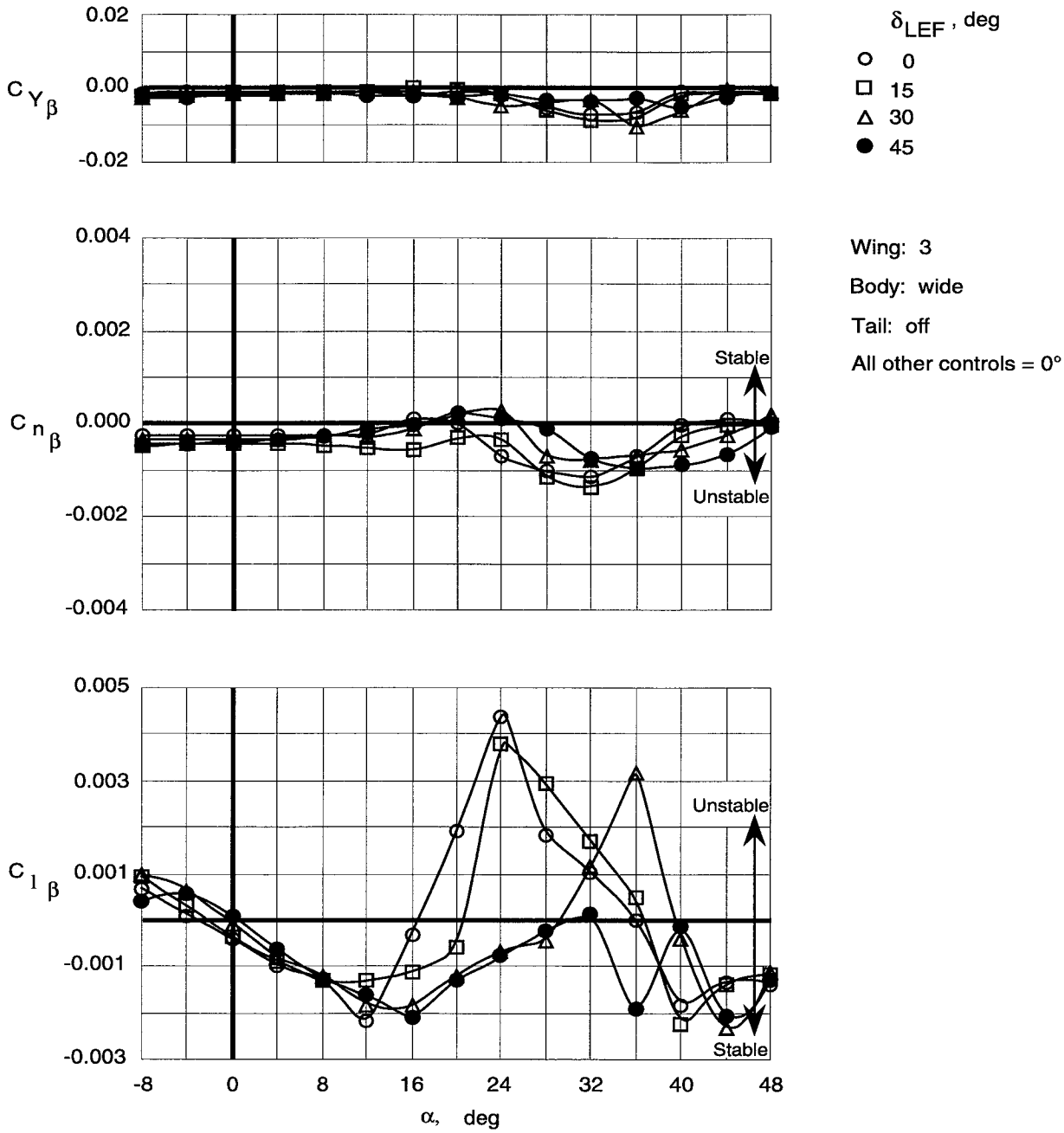

Figure 103. Effect of leading-edge flap deflections on lateral-directional stability characteristics of Wing 3 with wide top body on.

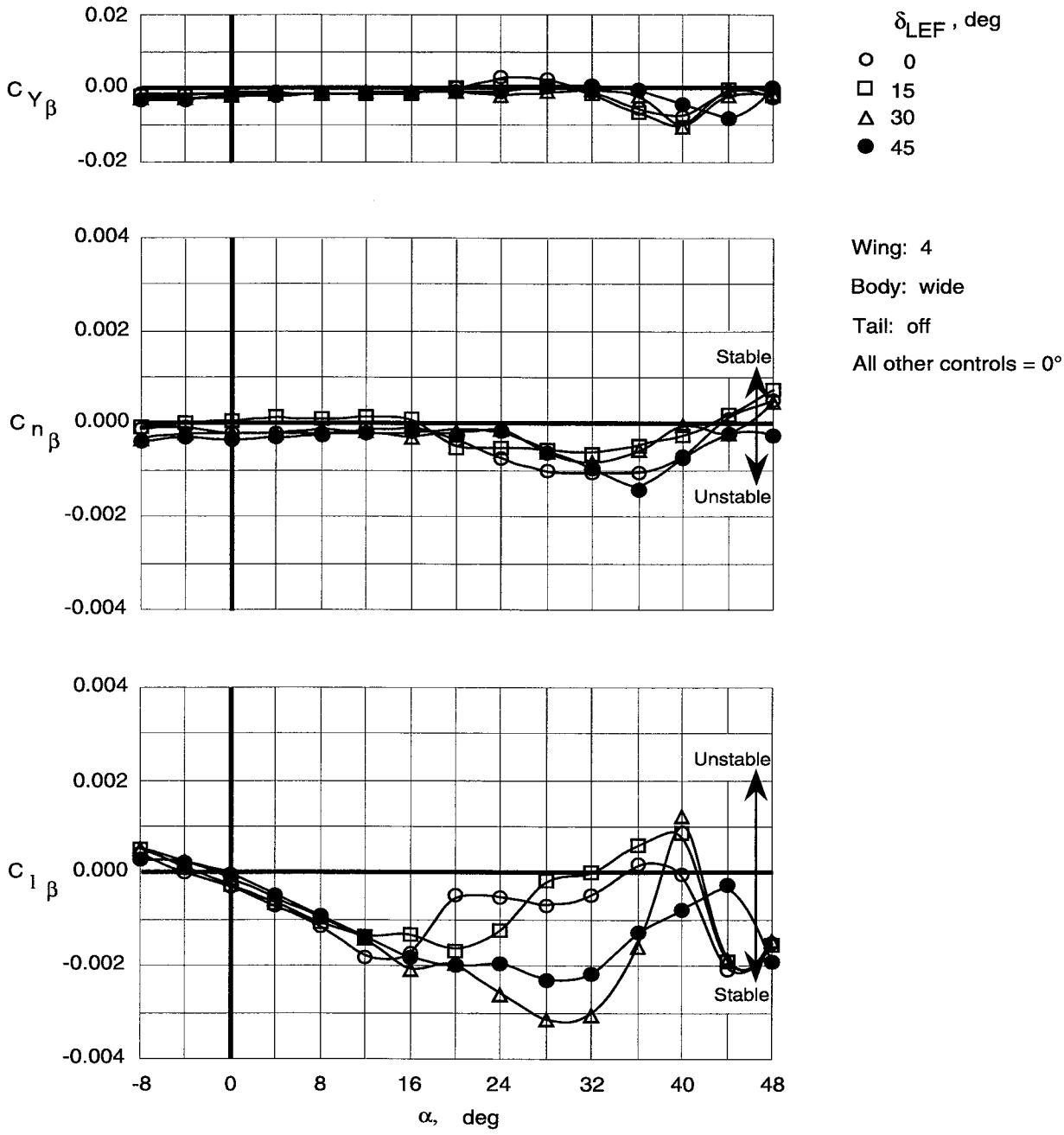

Figure 104. Effect of leading-edge flap deflections on lateral-directional stability characteristics of Wing 4 with wide top body on.

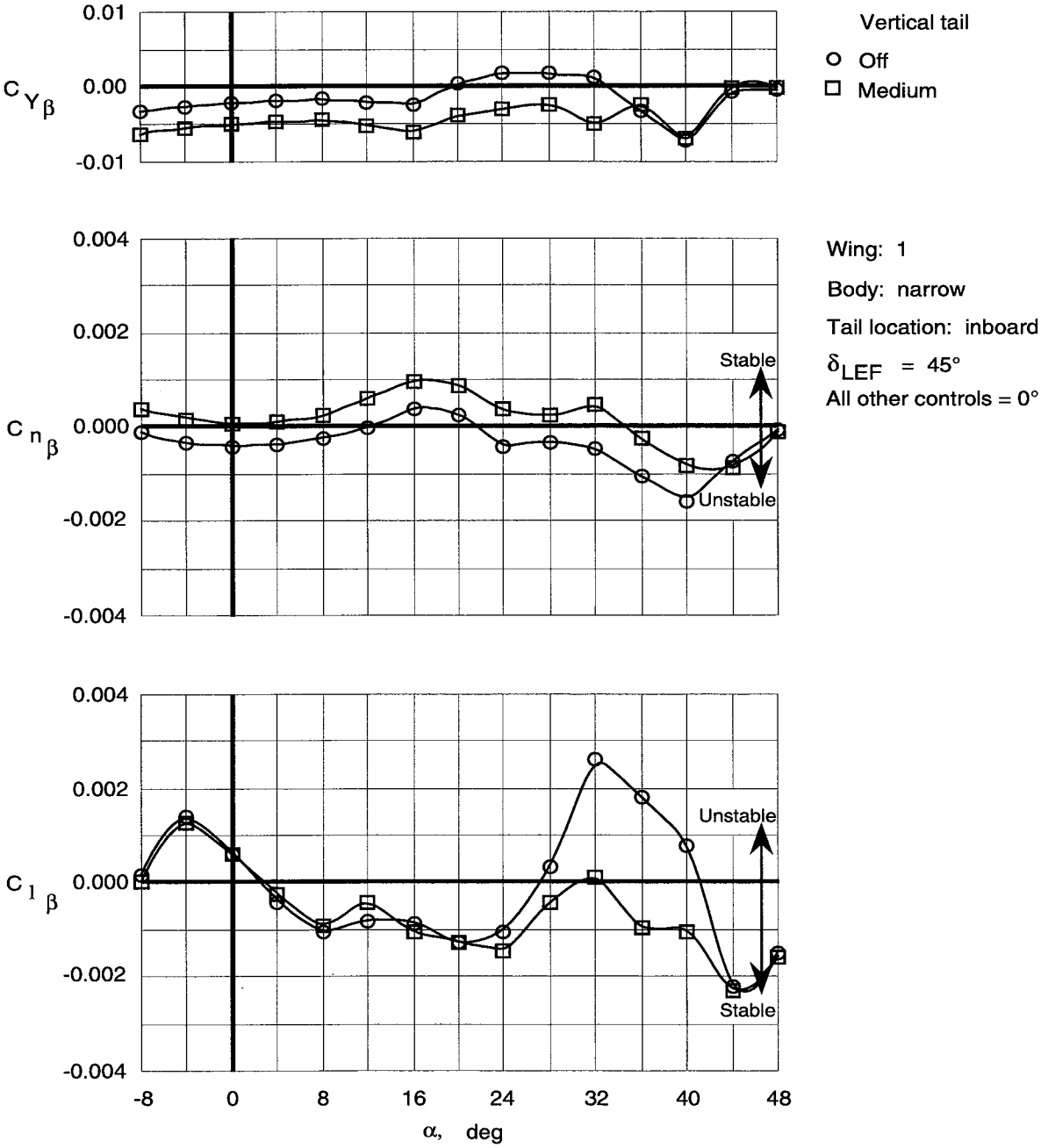

Figure 105. Effect of medium vertical tails on lateral-directional stability characteristics of Wing 1 with narrow top body on and leading-edge flaps deflected.

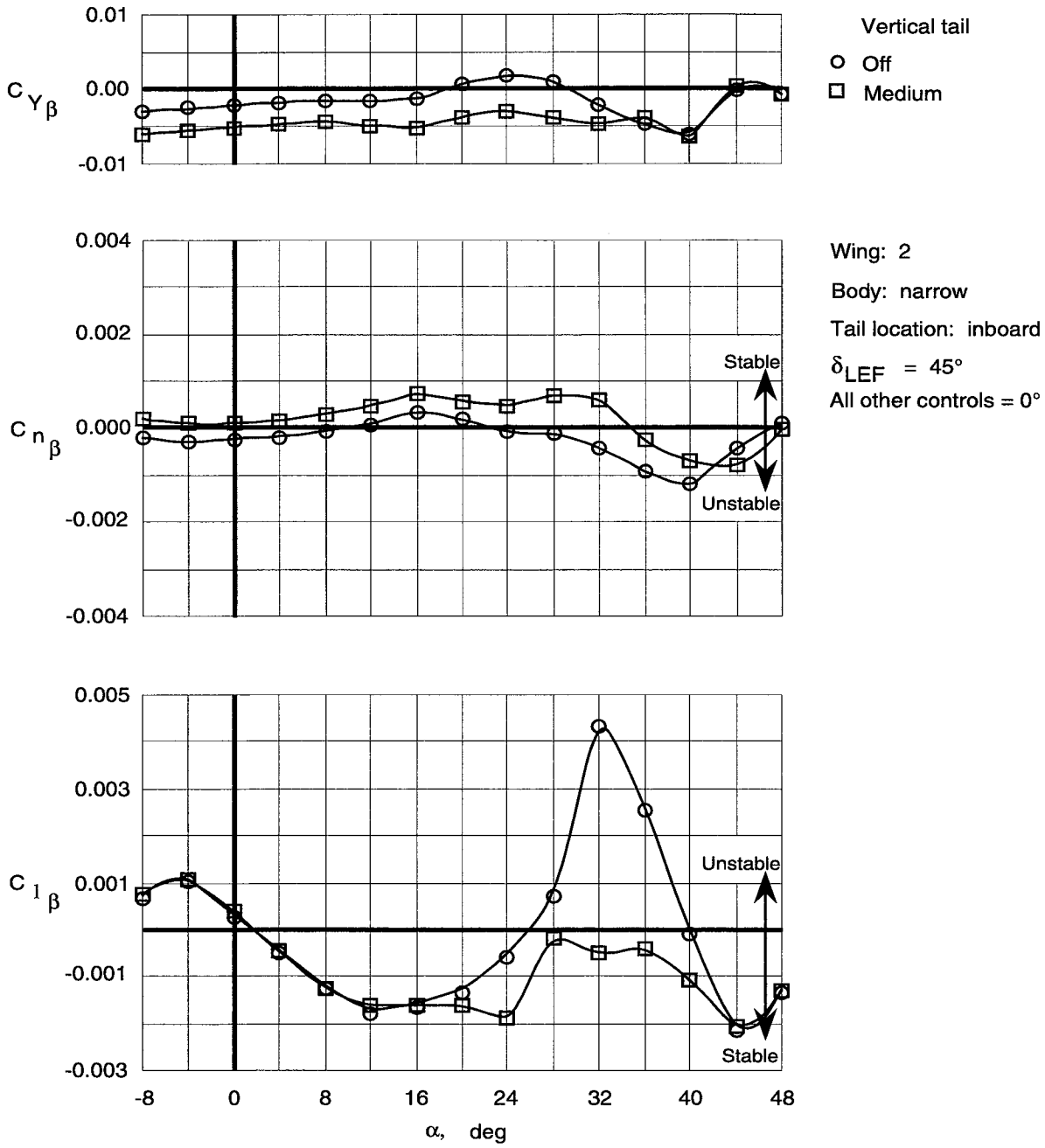

Figure 106. Effect of medium vertical tails on lateral-directional stability characteristics of Wing 2 with narrow top body on and leading-edge flaps deflected.

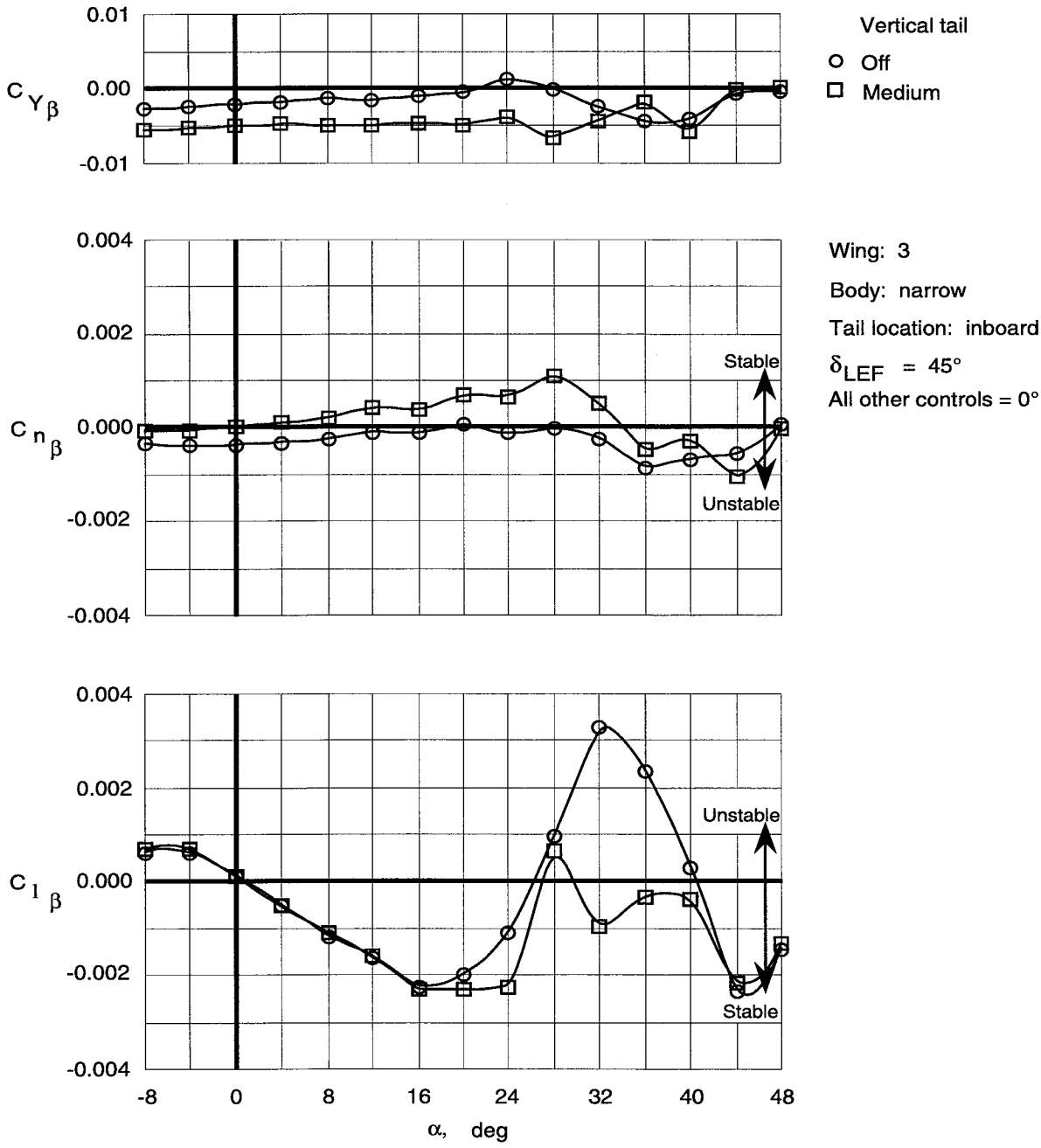

Figure 107. Effect of medium vertical tails on lateral-directional stability characteristics of Wing 3 with narrow top body on and leading-edge flaps deflected.

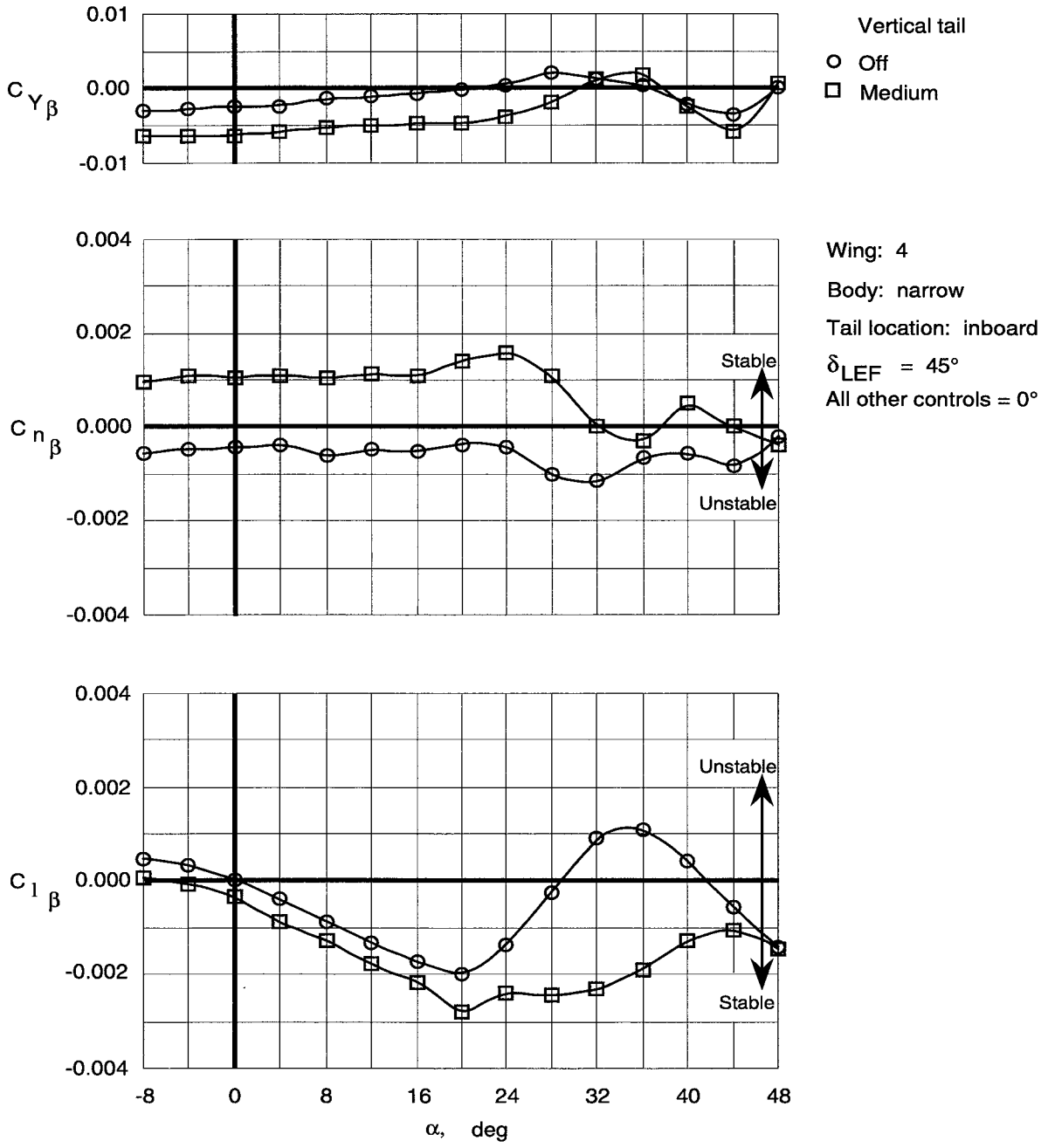

Figure 108. Effect of medium vertical tails on lateral-directional stability characteristics of Wing 4 with narrow top body on and leading-edge flaps deflected.

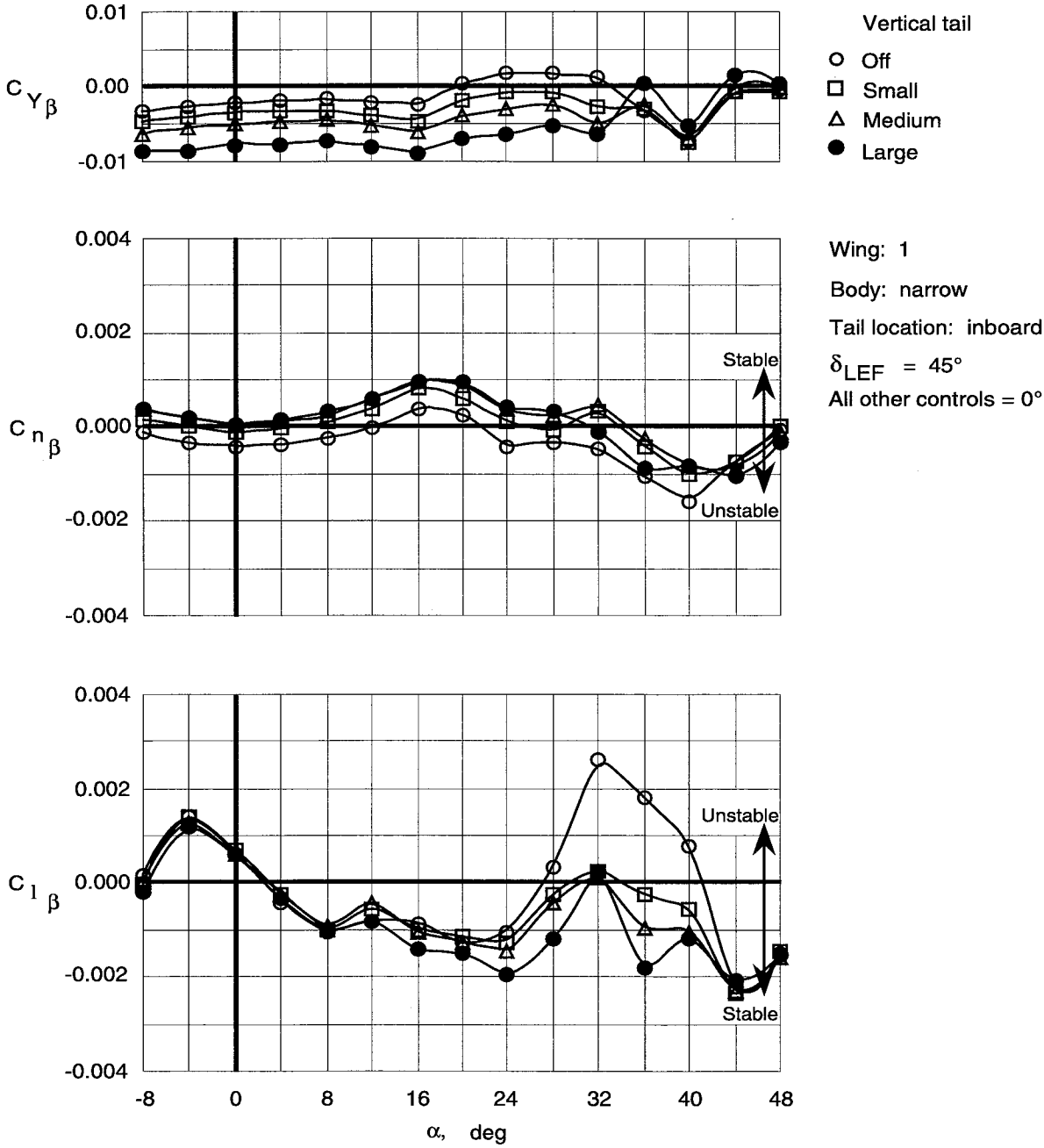

Figure 109. Effect of vertical tail size on lateral-directional stability characteristics of Wing 1 with narrow top body on and leading-edge flaps deflected.

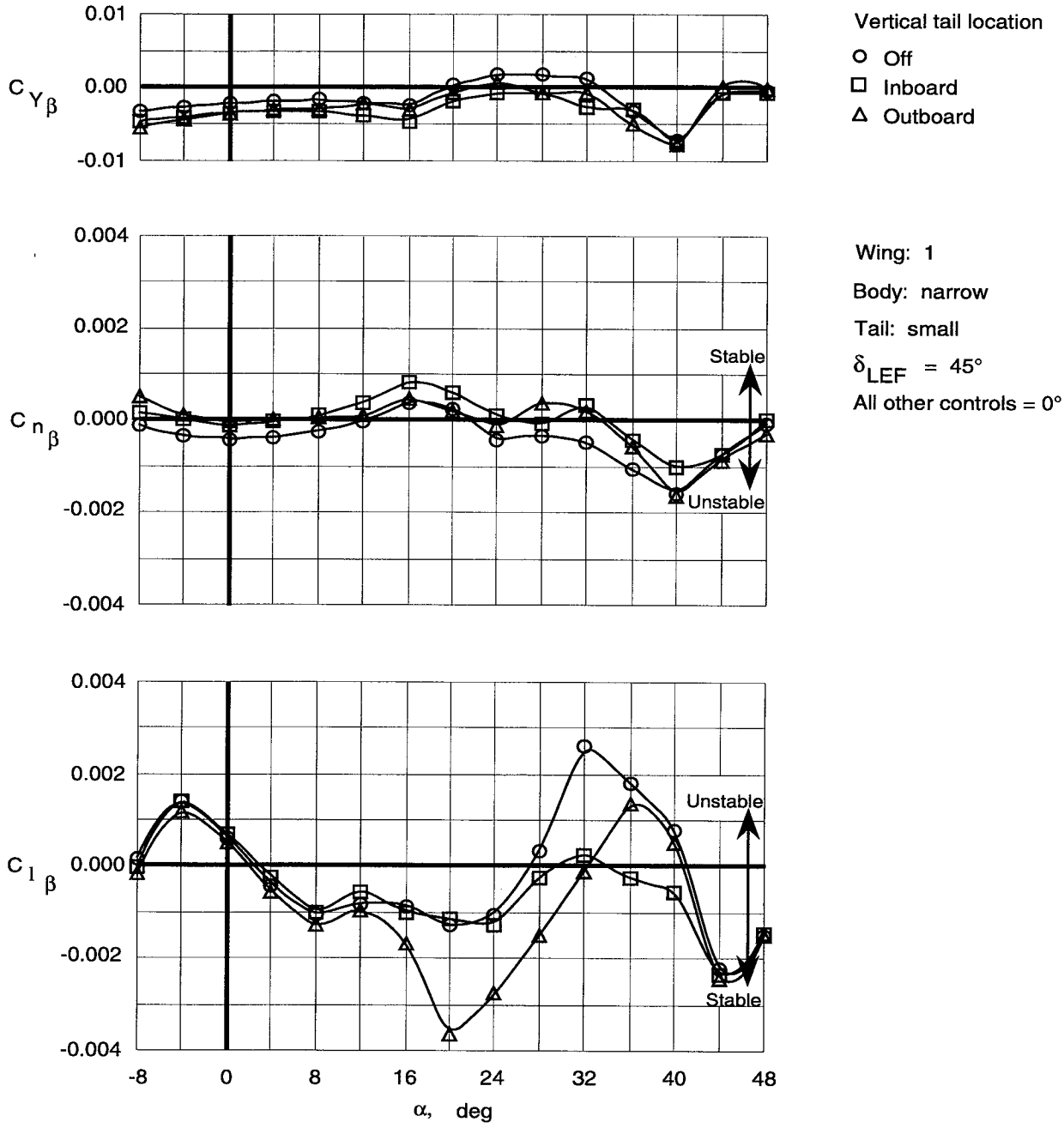

Figure 110. Effect of location of small vertical tails on lateral-directional stability characteristics of Wing 1 with narrow top body on and leading-edge flaps deflected.

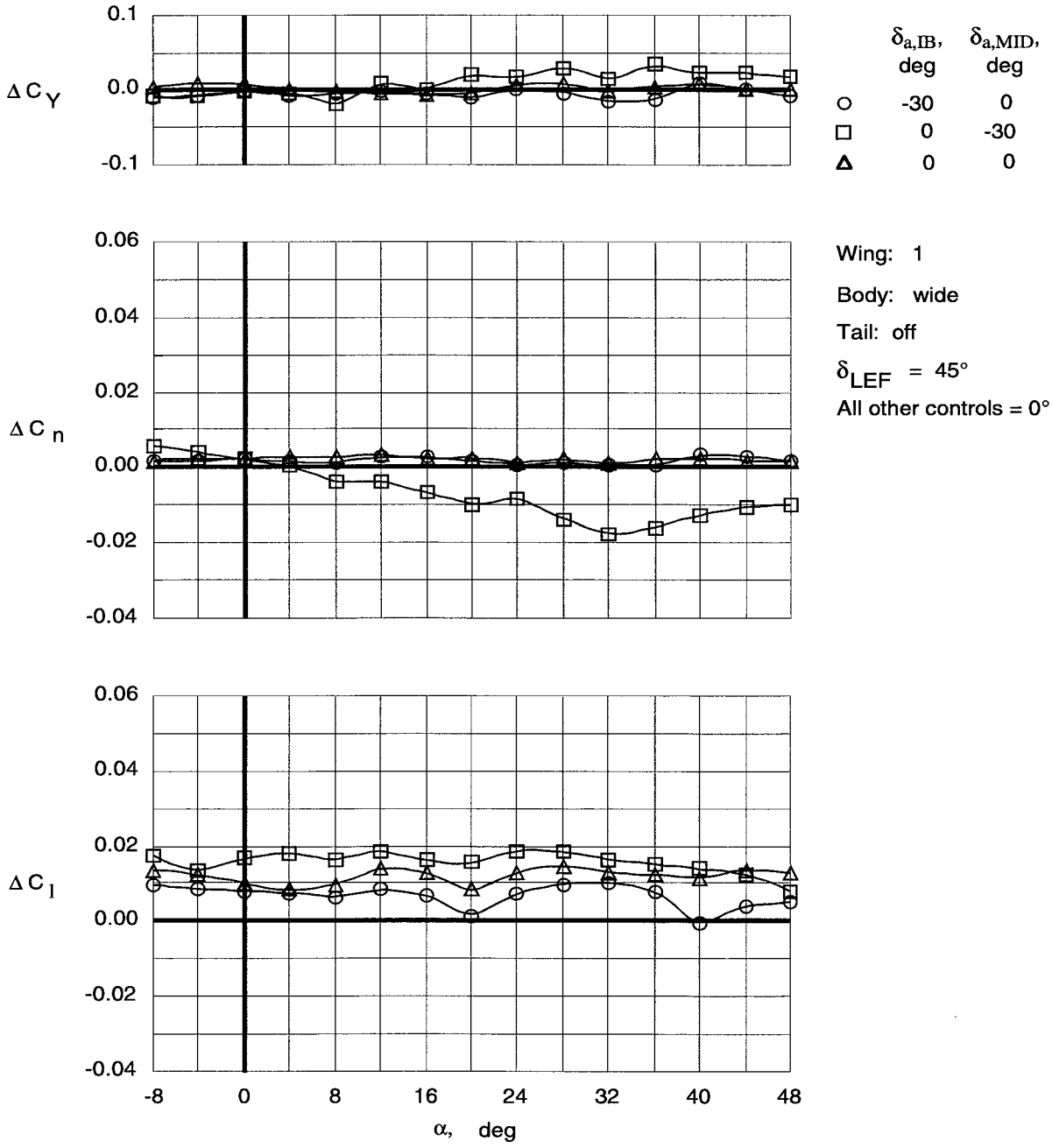

Figure 111. Control effectiveness of differential deflections of trailing-edge flaps on Wing 1 with wide top body on and leading-edge flaps deflected.

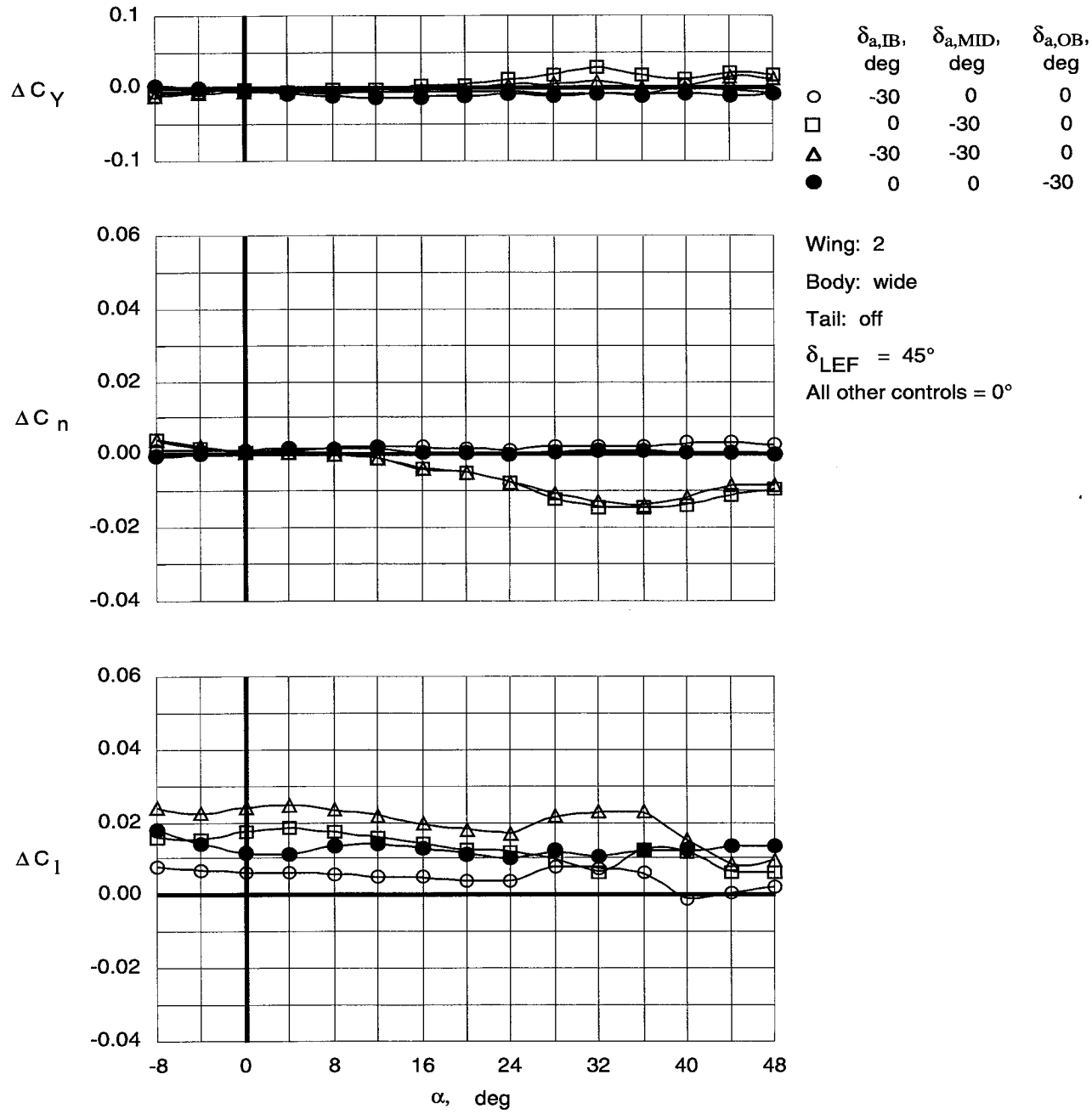

Figure 112. Control effectiveness of differential deflections of trailing-edge flaps on Wing 2 with wide top body on and leading-edge flaps deflected.

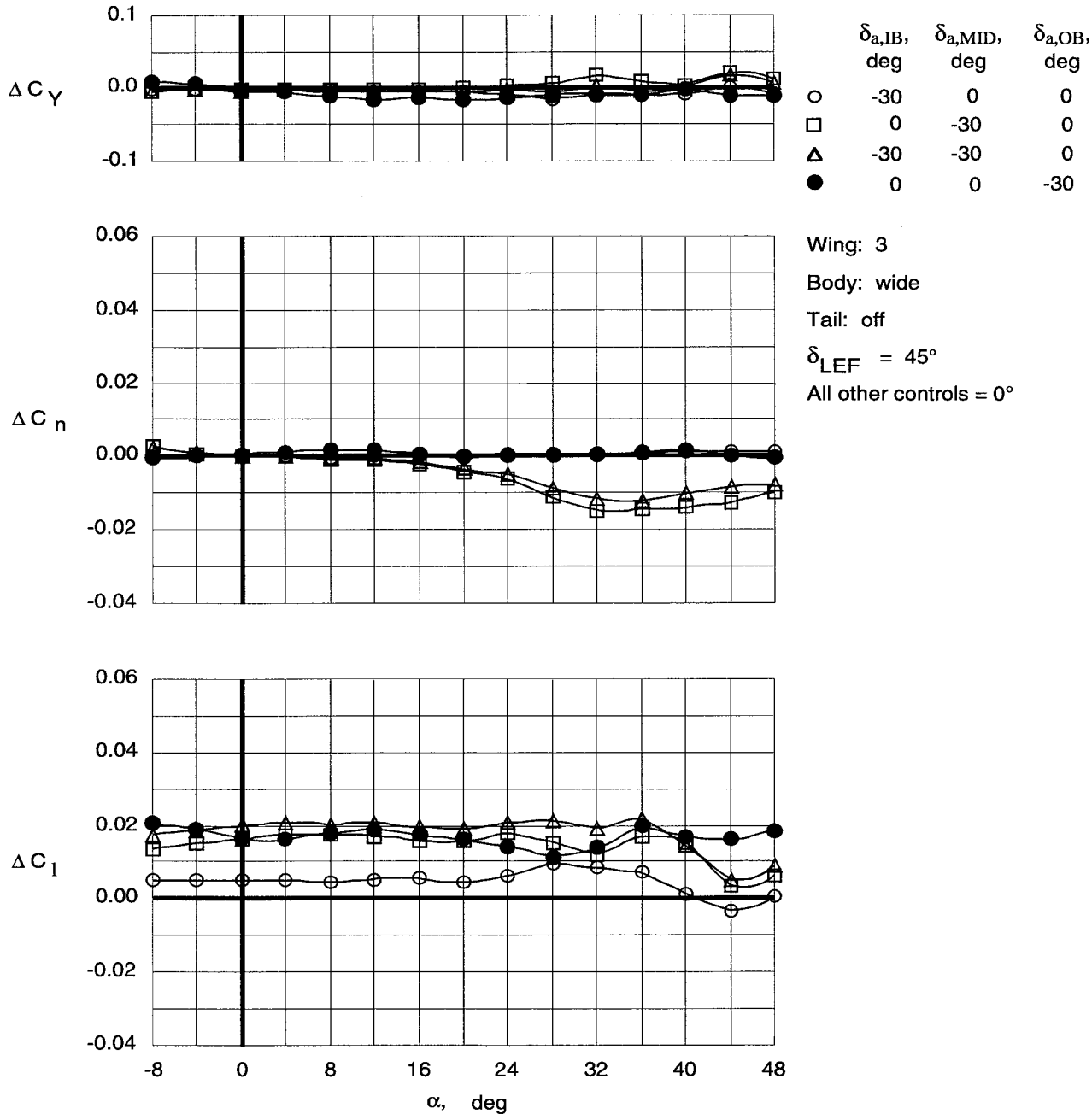

Figure 113. Control effectiveness of differential deflections of trailing-edge flaps on Wing 3 with wide top body on and leading-edge flaps deflected.

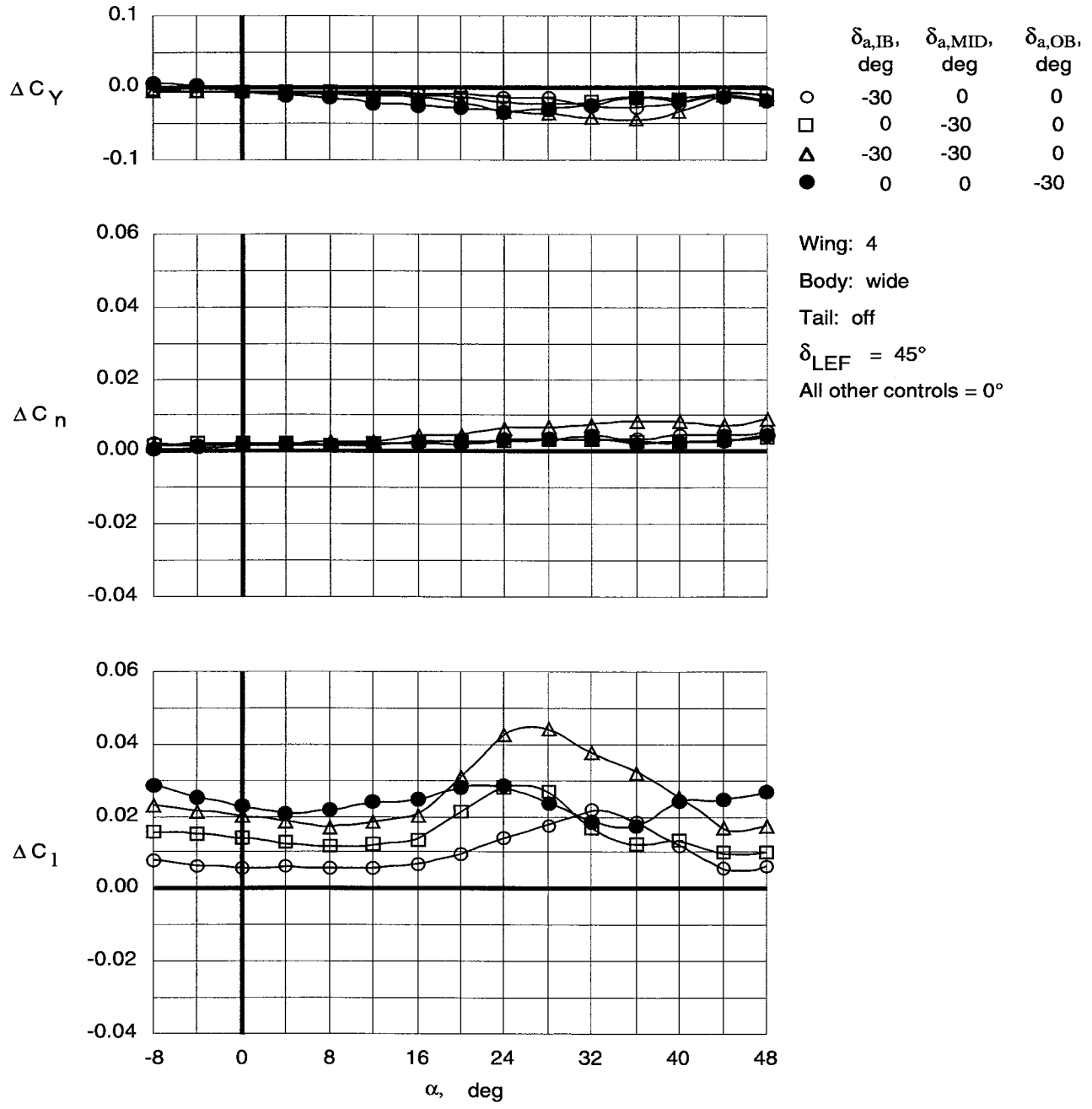

Figure 114. Control effectiveness of differential deflections of trailing-edge flaps on Wing 4 with wide top body on and leading-edge flaps deflected.

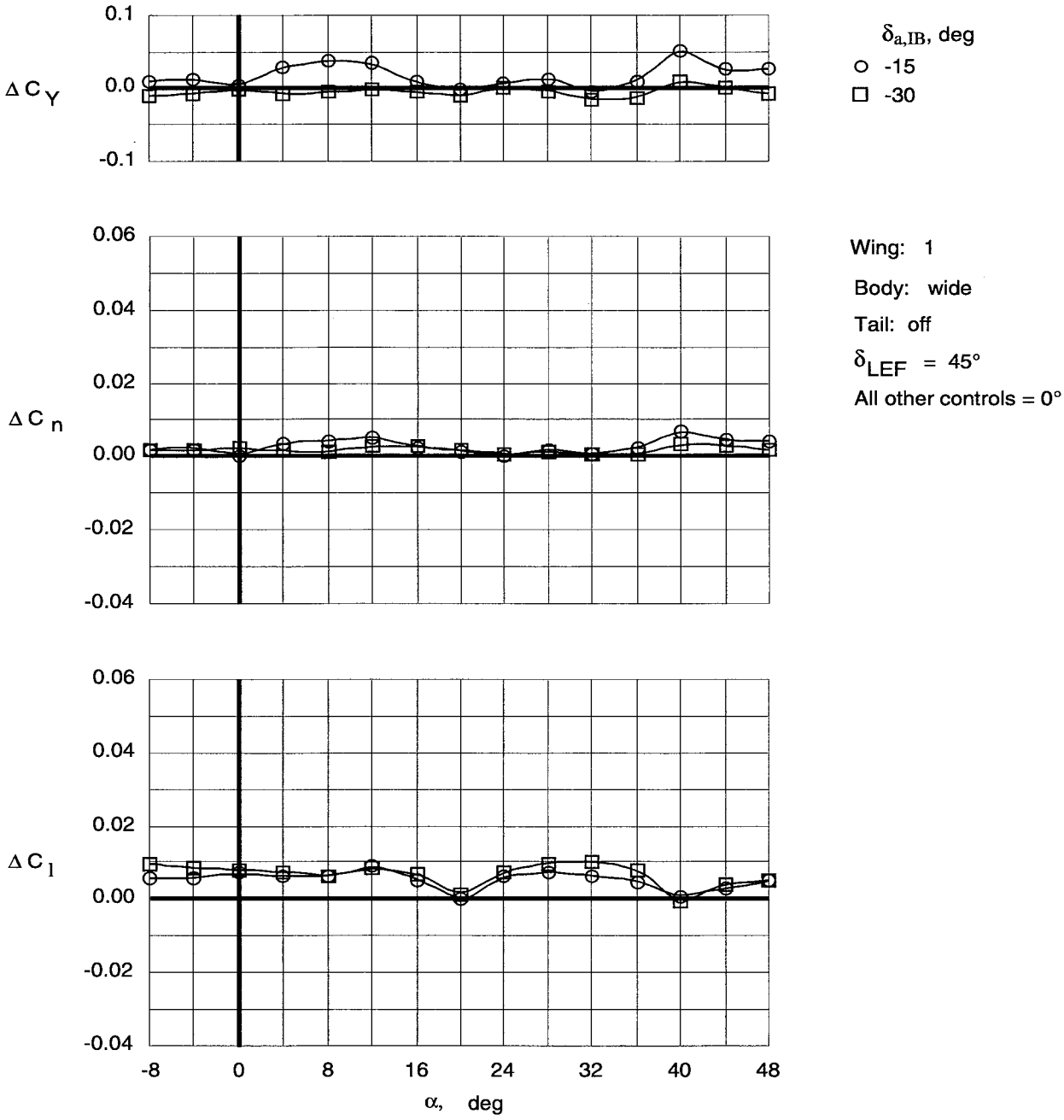

Figure 115. Control effectiveness of differential deflections of inboard trailing-edge flaps on Wing 1 with wide top body on and leading-edge flaps deflected.

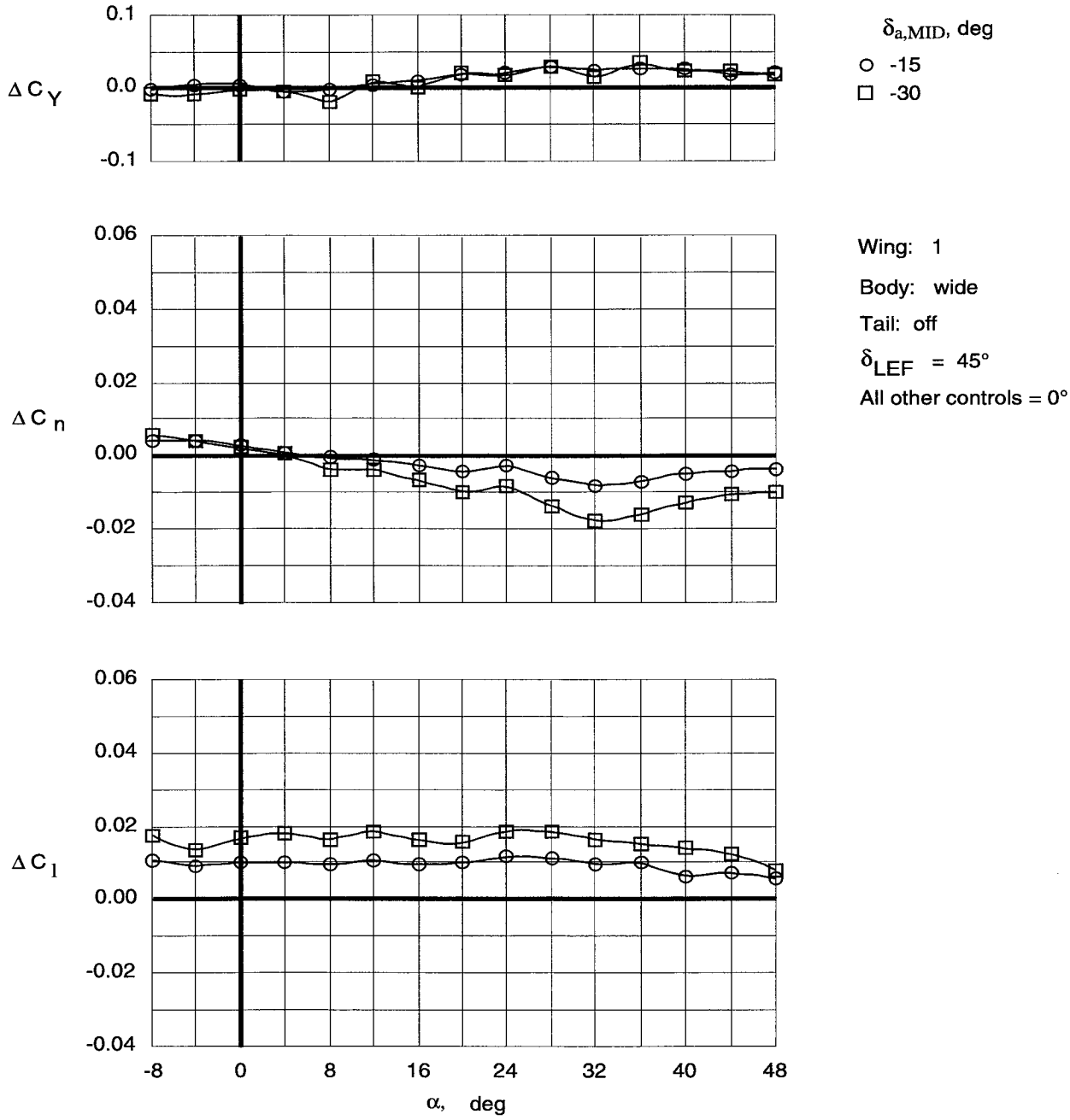

Figure 116. Control effectiveness of differential deflections of middle trailing-edge flaps on Wing 1 with wide top body on and leading-edge flaps deflected.

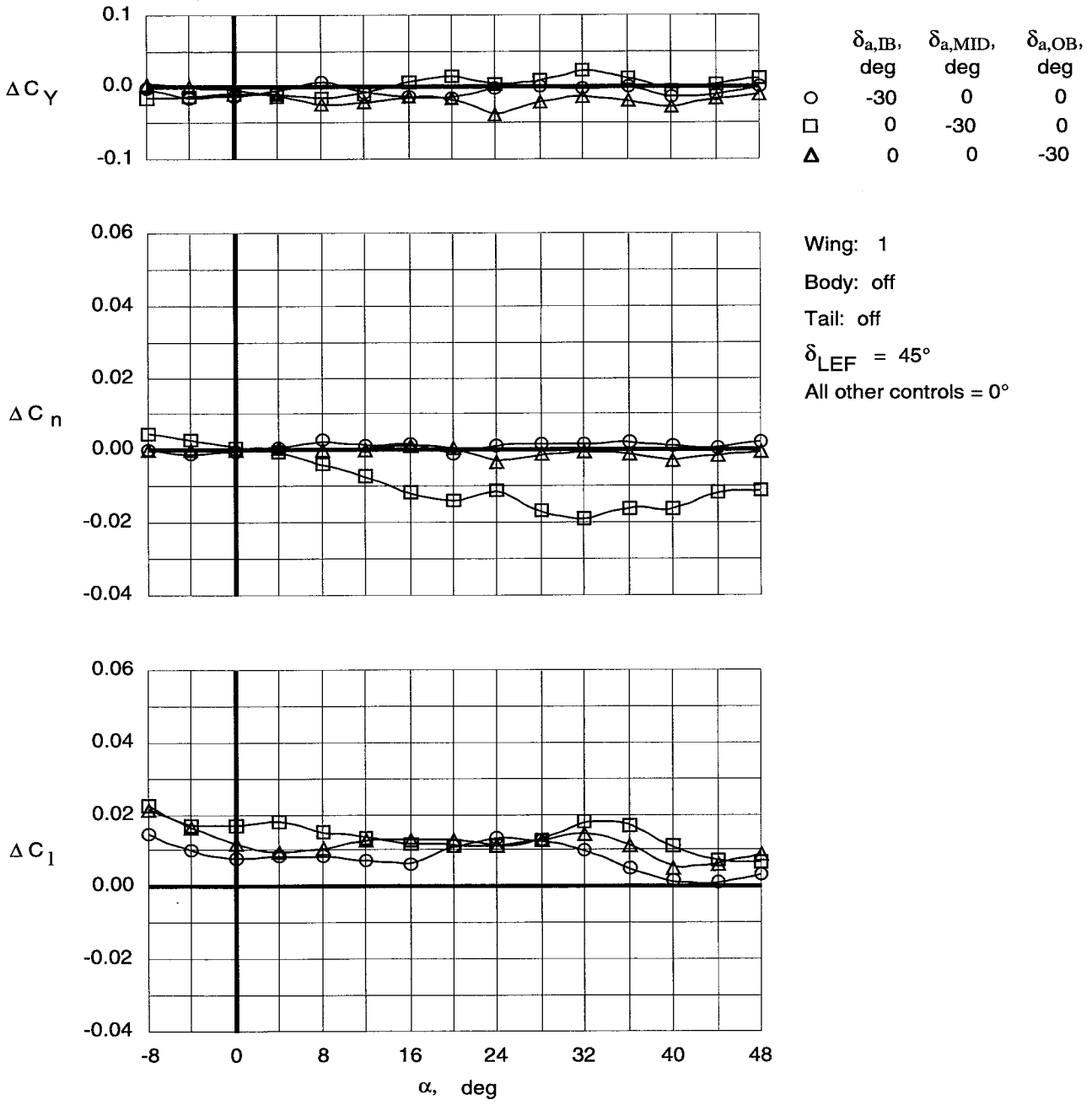

Figure 117. Control effectiveness of differential deflections of trailing-edge flaps on Wing 1 with top body off and leading-edge flaps deflected.

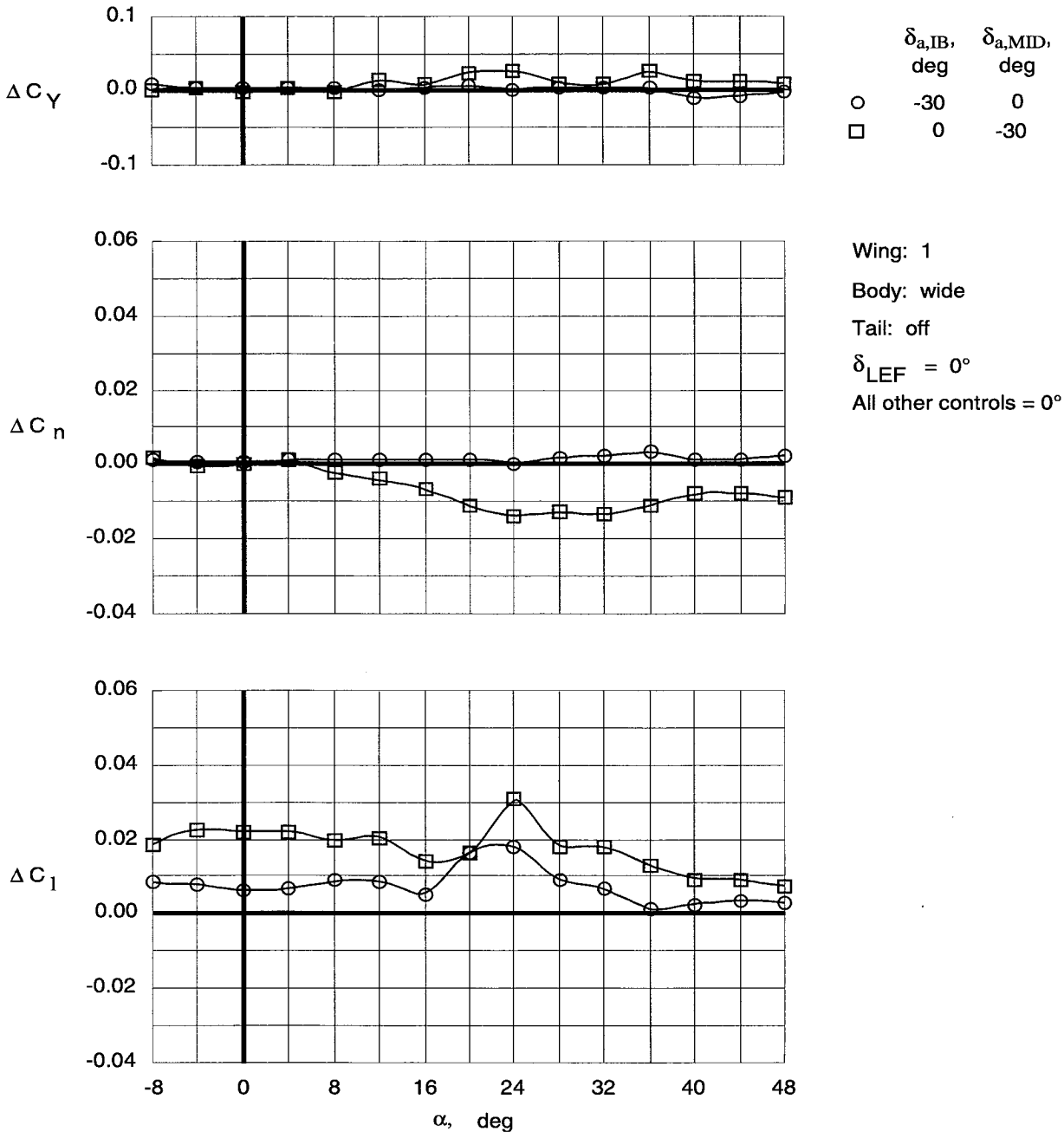

Figure 118. Control effectiveness of differential deflections of trailing-edge flaps on Wing 1 with wide top body on.

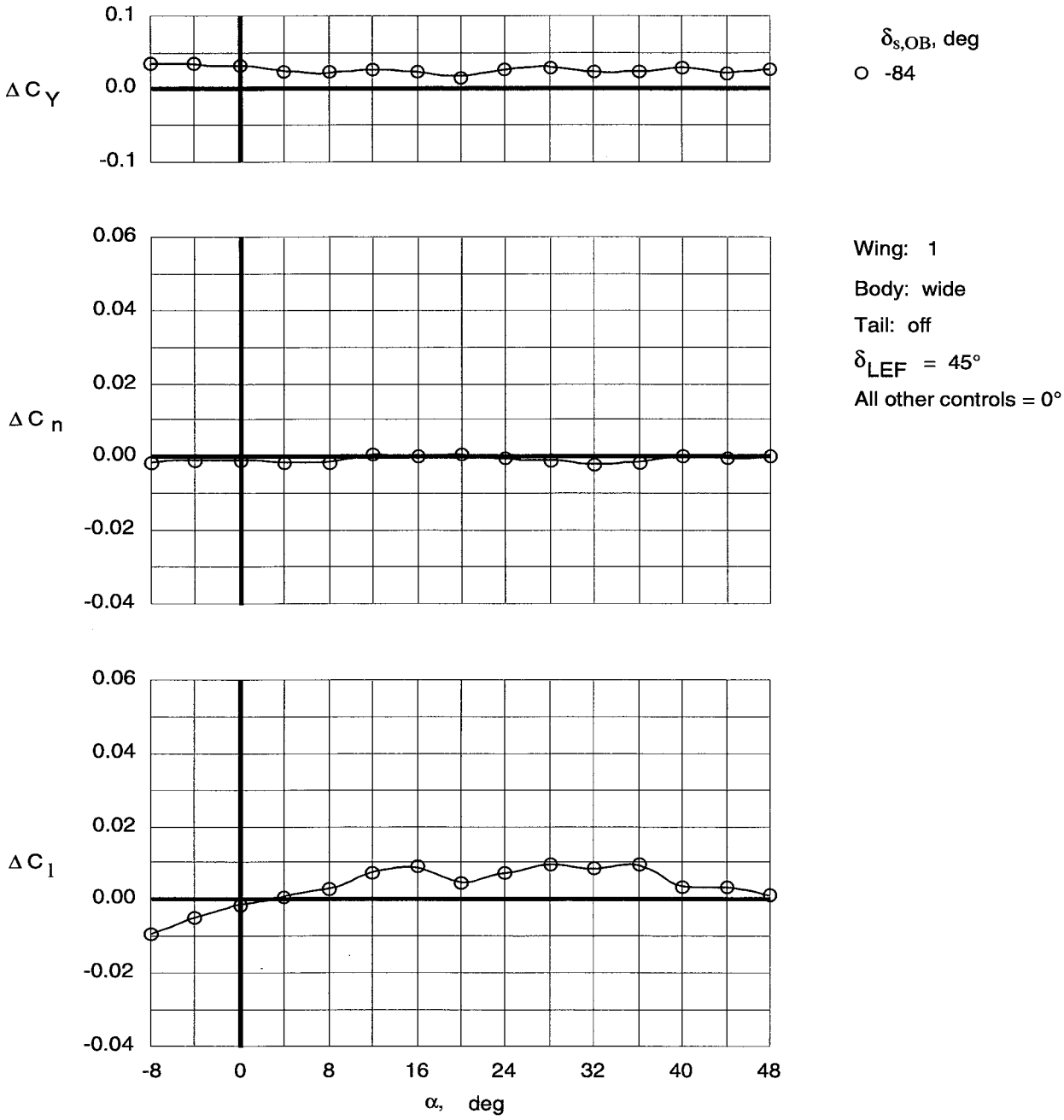

Figure 119. Control effectiveness of split deflection of right outboard trailing-edge flap on Wing 1 with wide top body on and leading-edge flaps deflected.

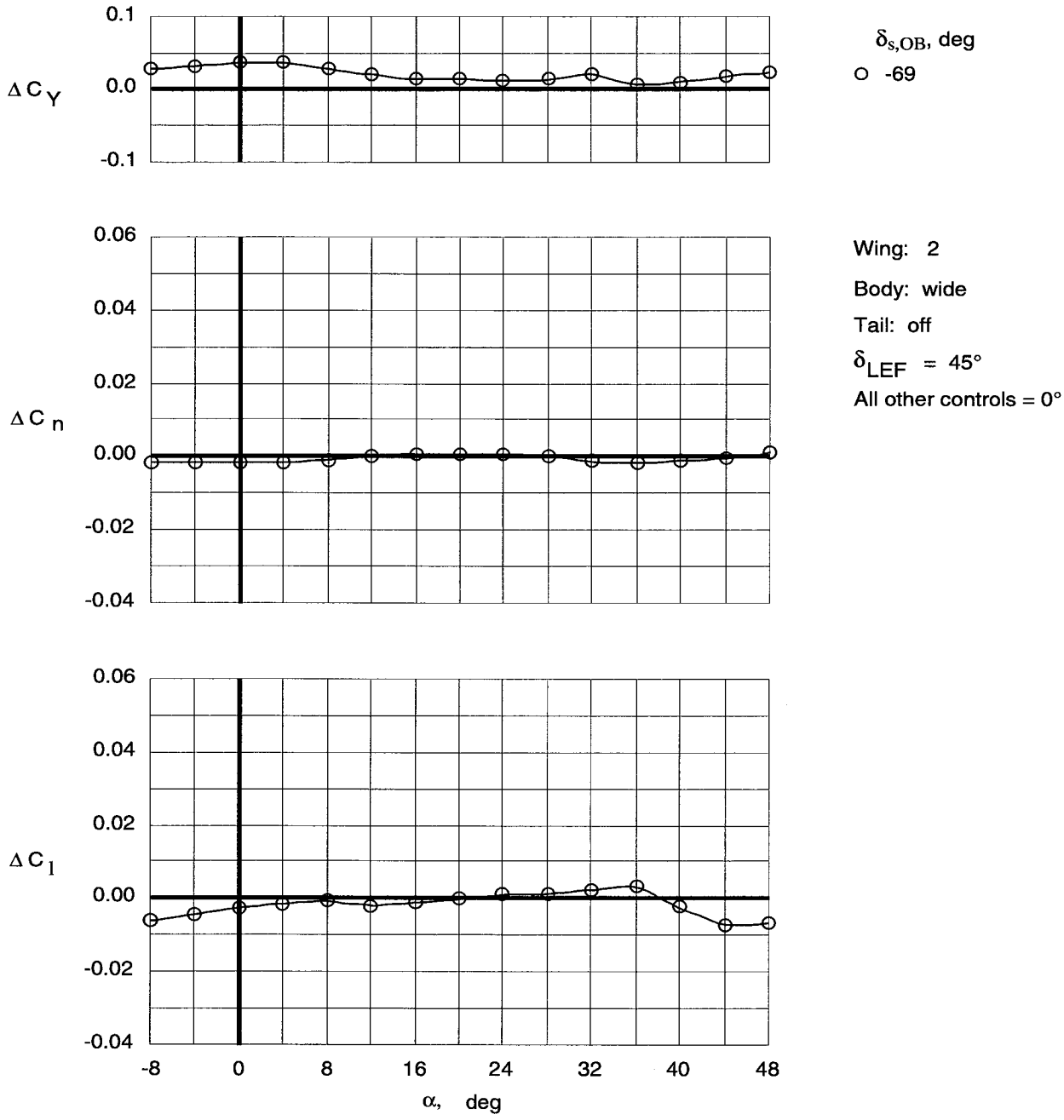

Figure 120. Control effectiveness of split deflection of right outboard trailing-edge flap on Wing 2 with wide top body on and leading-edge flaps deflected.

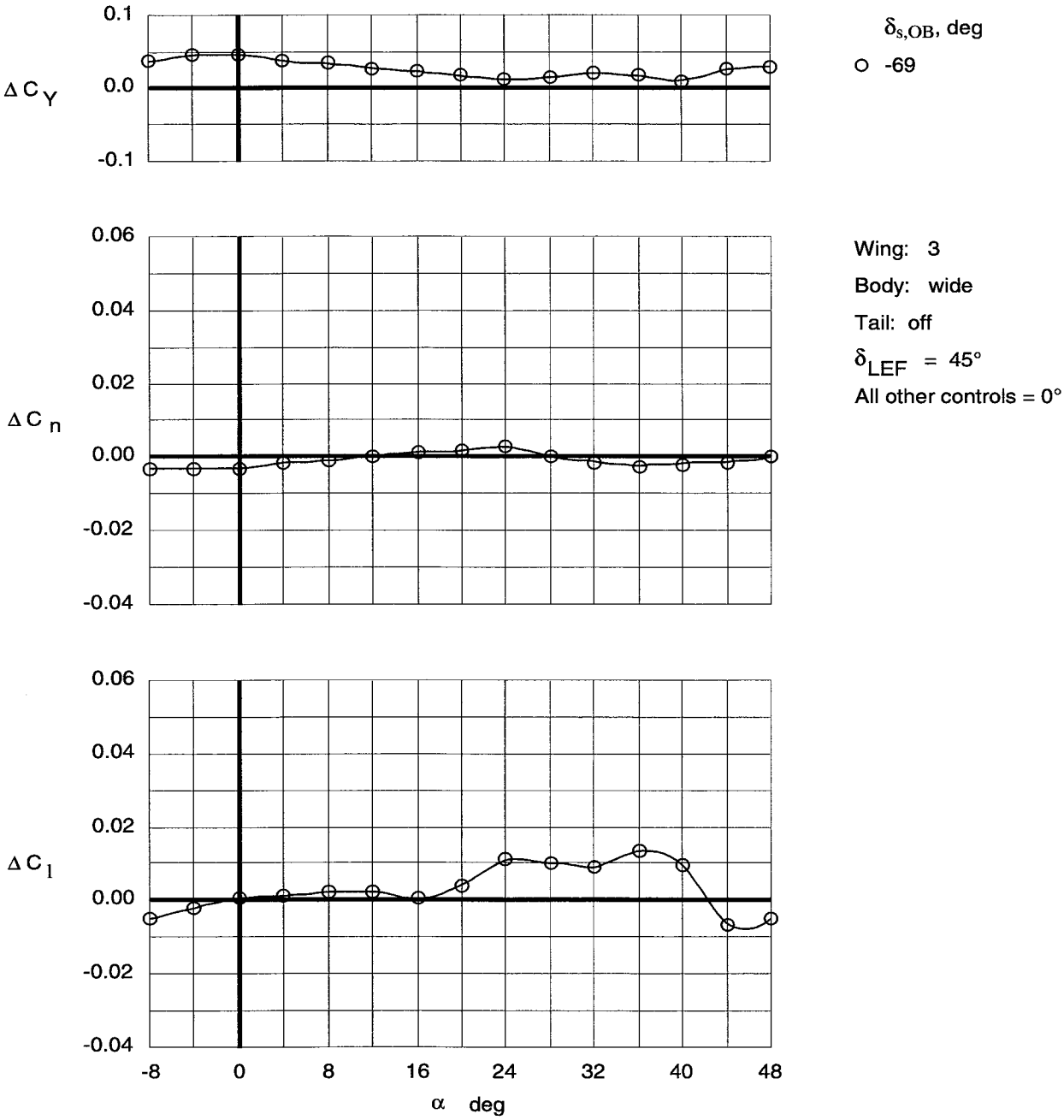

Figure 121. Control effectiveness of split deflection of right outboard trailing-edge flap on Wing 3 with wide top body on and leading-edge flaps deflected.

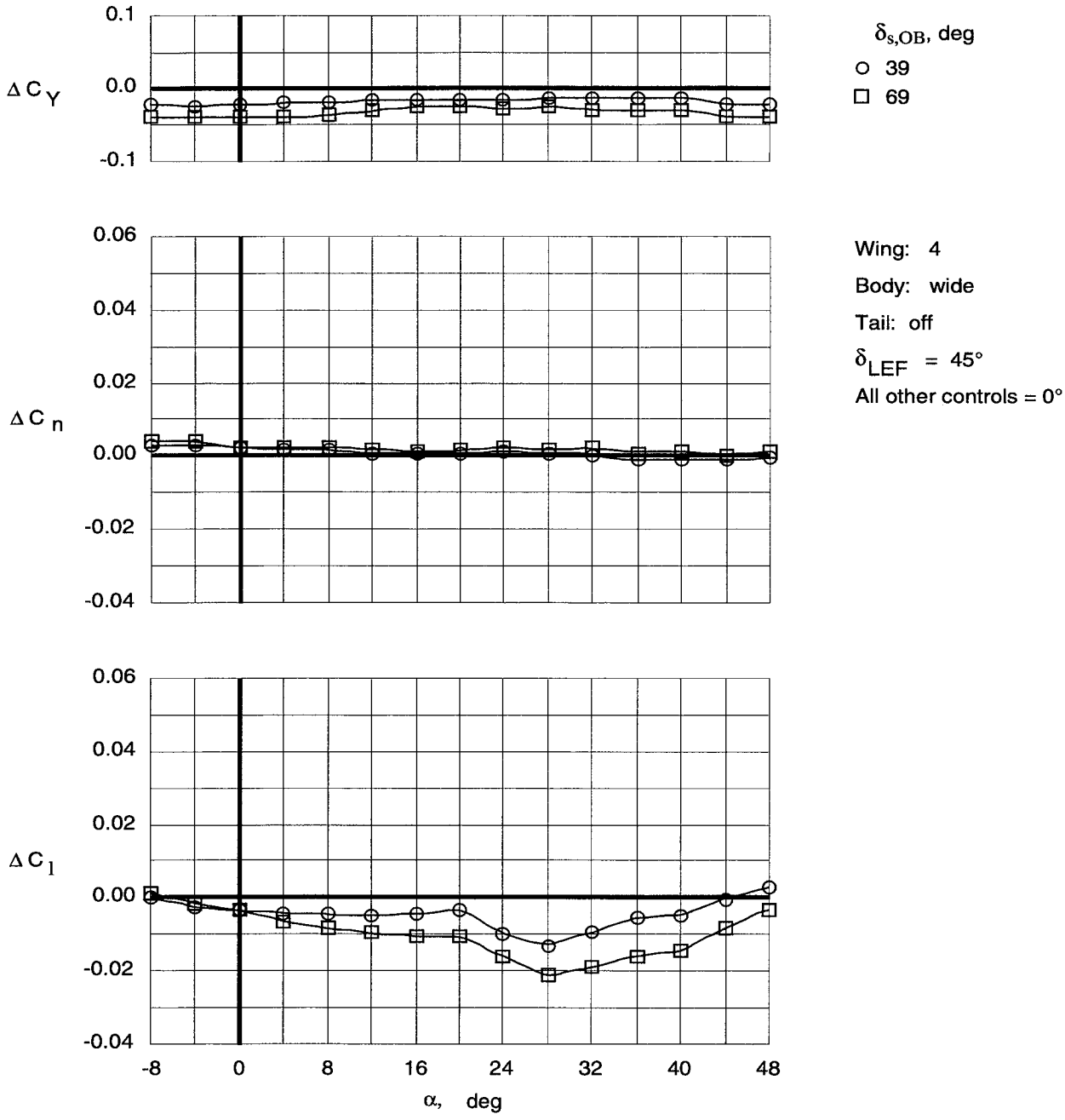

Figure 122. Control effectiveness of split deflections of left outboard trailing-edge flap on Wing 4 with wide top body on and leading-edge flaps deflected.

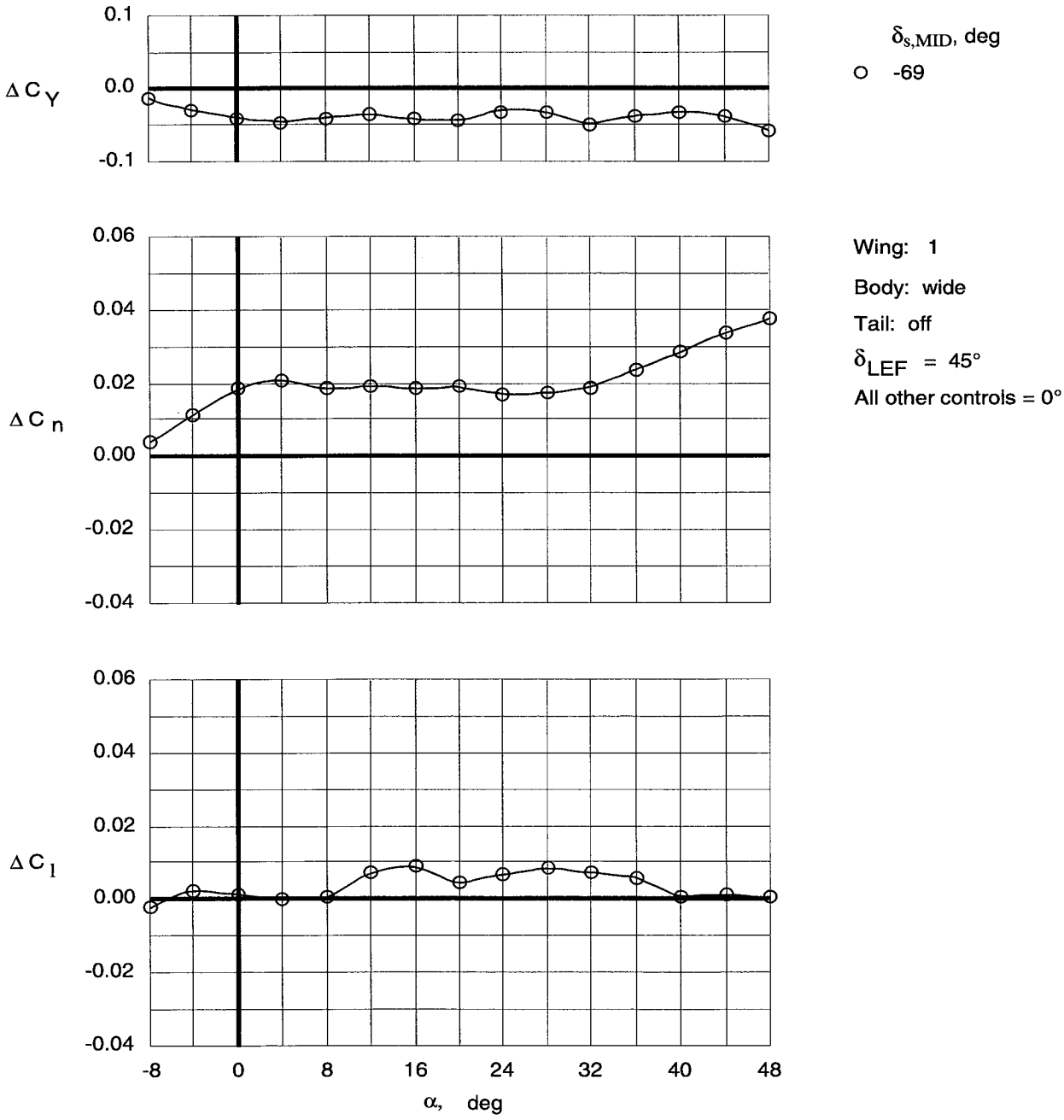

Figure 123. Control effectiveness of split deflection of right middle trailing-edge flap on Wing 1 with wide top body on and leading-edge flaps deflected.

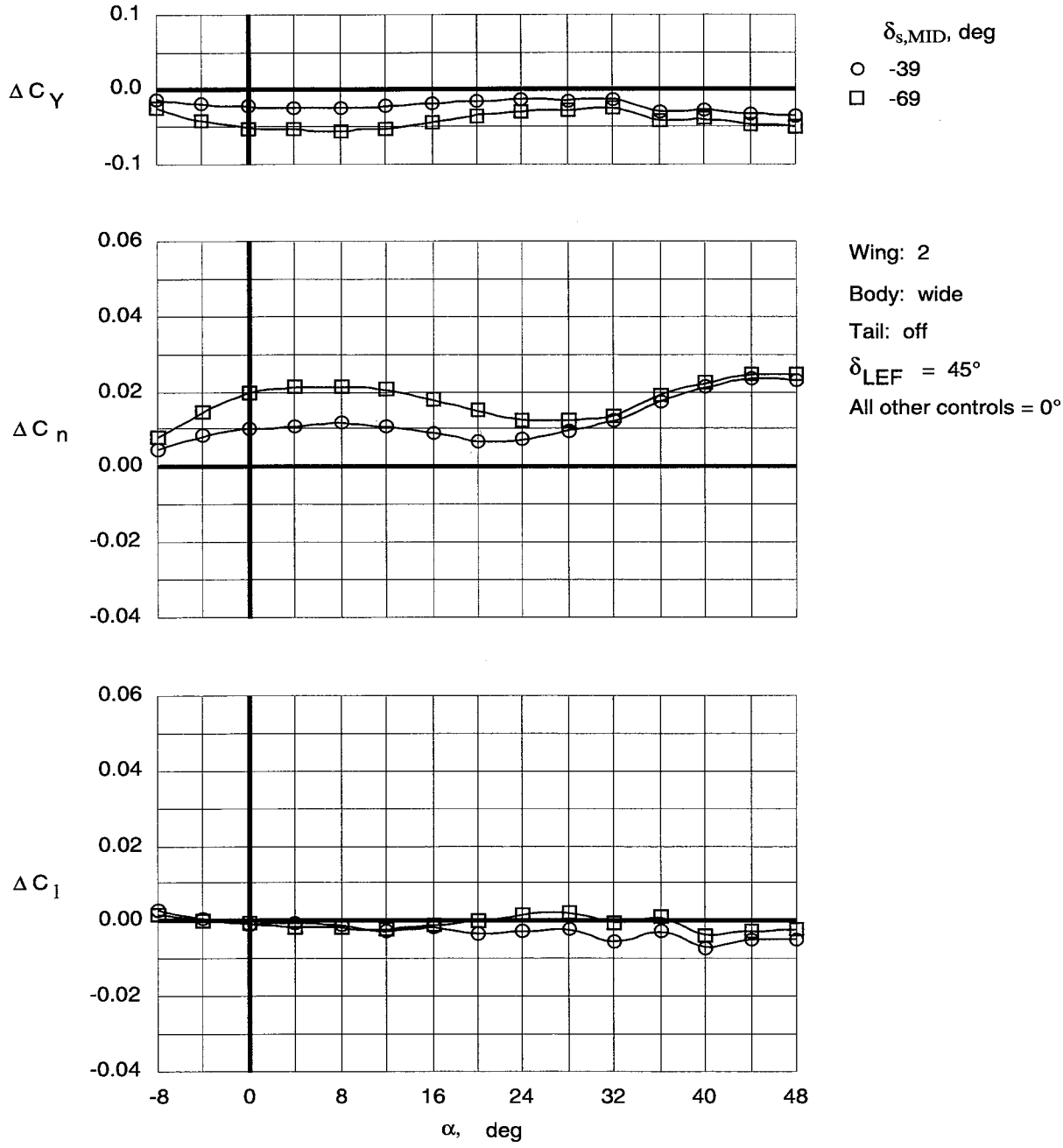

Figure 124. Control effectiveness of split deflections of right middle trailing-edge flap on Wing 2 with wide top body on and leading-edge flaps deflected.

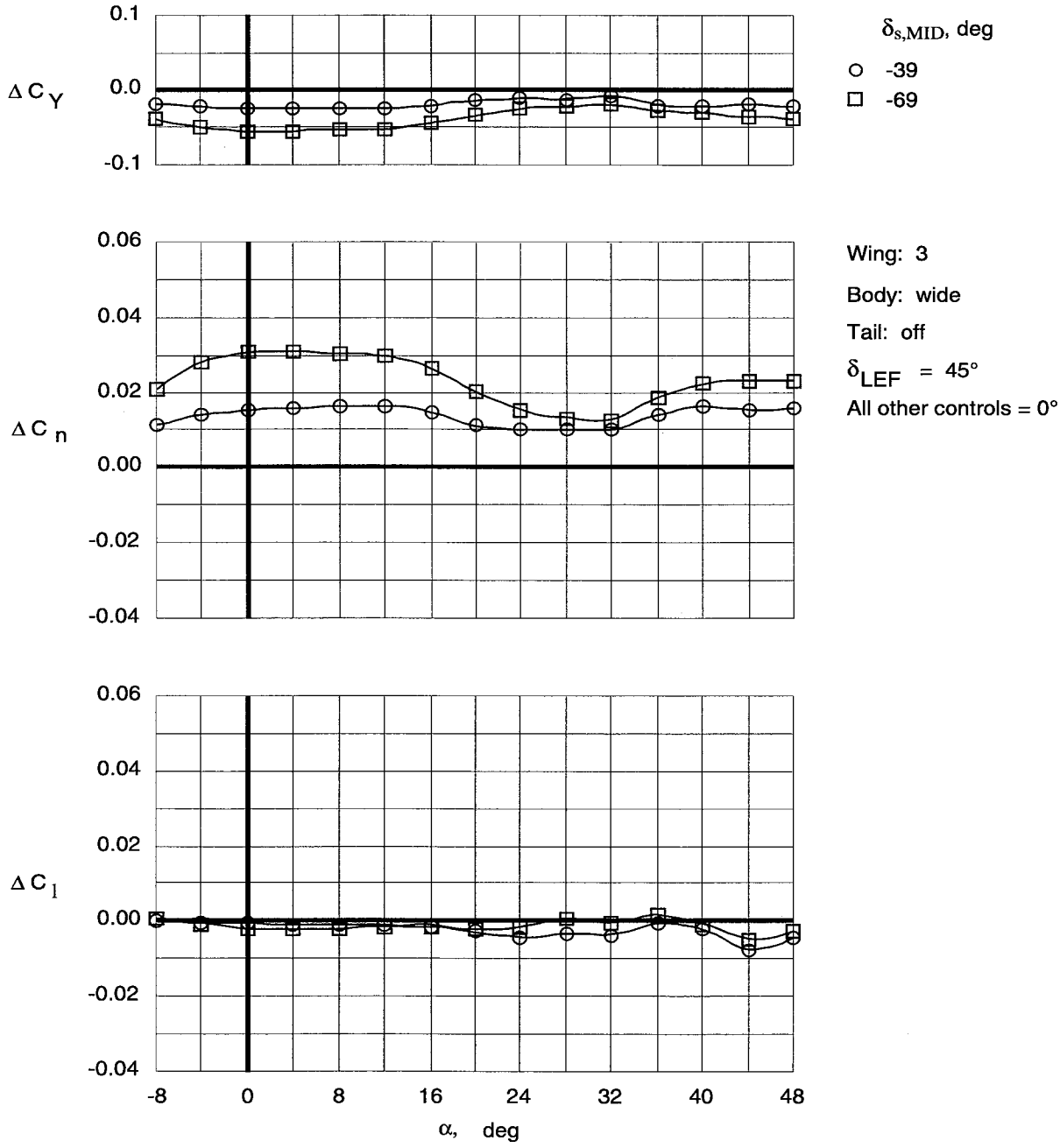

Figure 125. Control effectiveness of split deflections of right middle trailing-edge flap on Wing 3 with wide top body on and leading-edge flaps deflected.

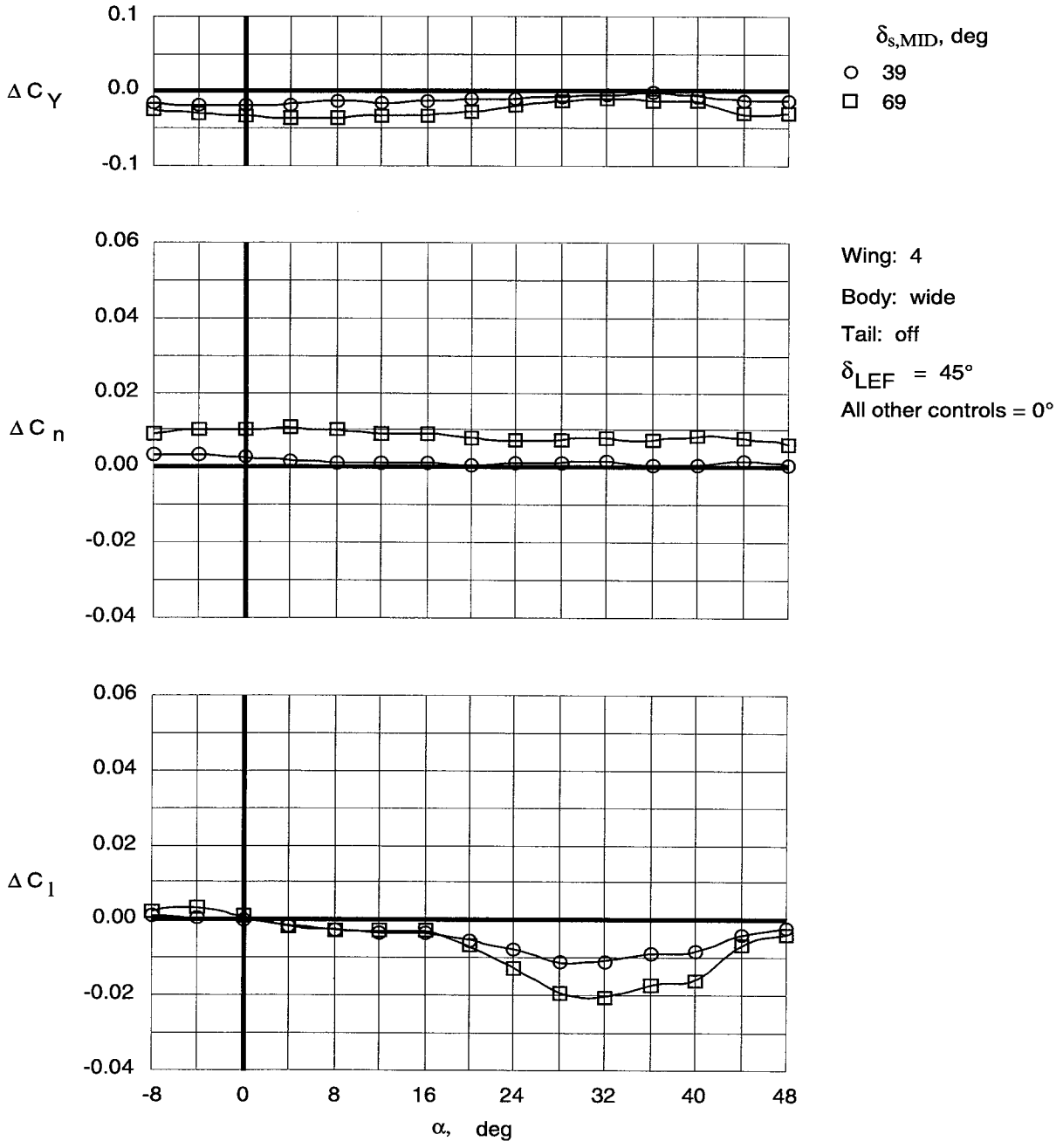

Figure 126. Control effectiveness of split deflections of left middle trailing-edge flap on Wing 4 with wide top body on and leading-edge flaps deflected.

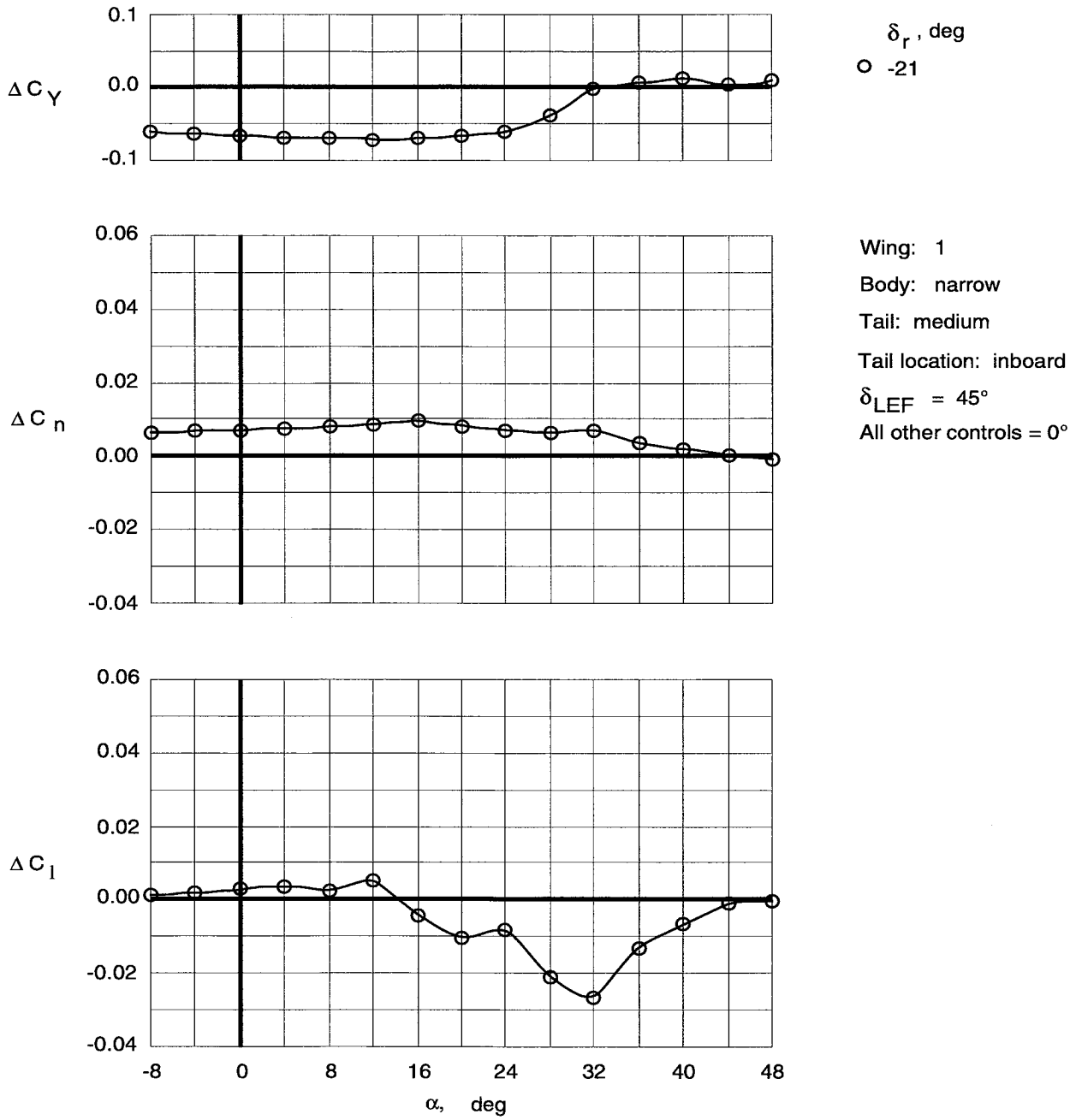

Figure 127. Control effectiveness of deflection of medium vertical tails at inboard location for Wing 1 with narrow top body on and leading-edge flaps deflected.

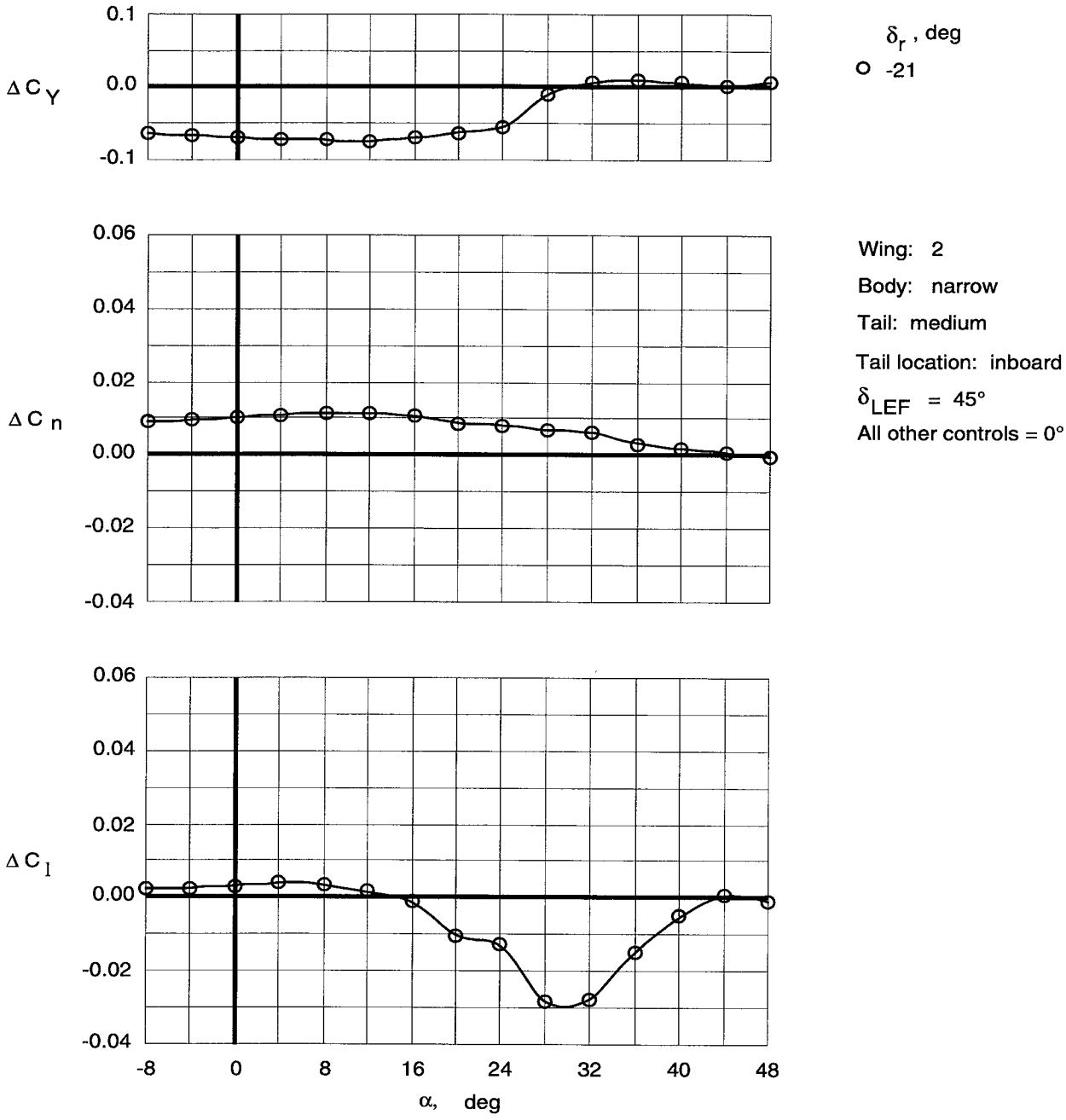

Figure 128. Control effectiveness of deflection of medium vertical tails at inboard location for Wing 2 with narrow top body on and leading-edge flaps deflected.

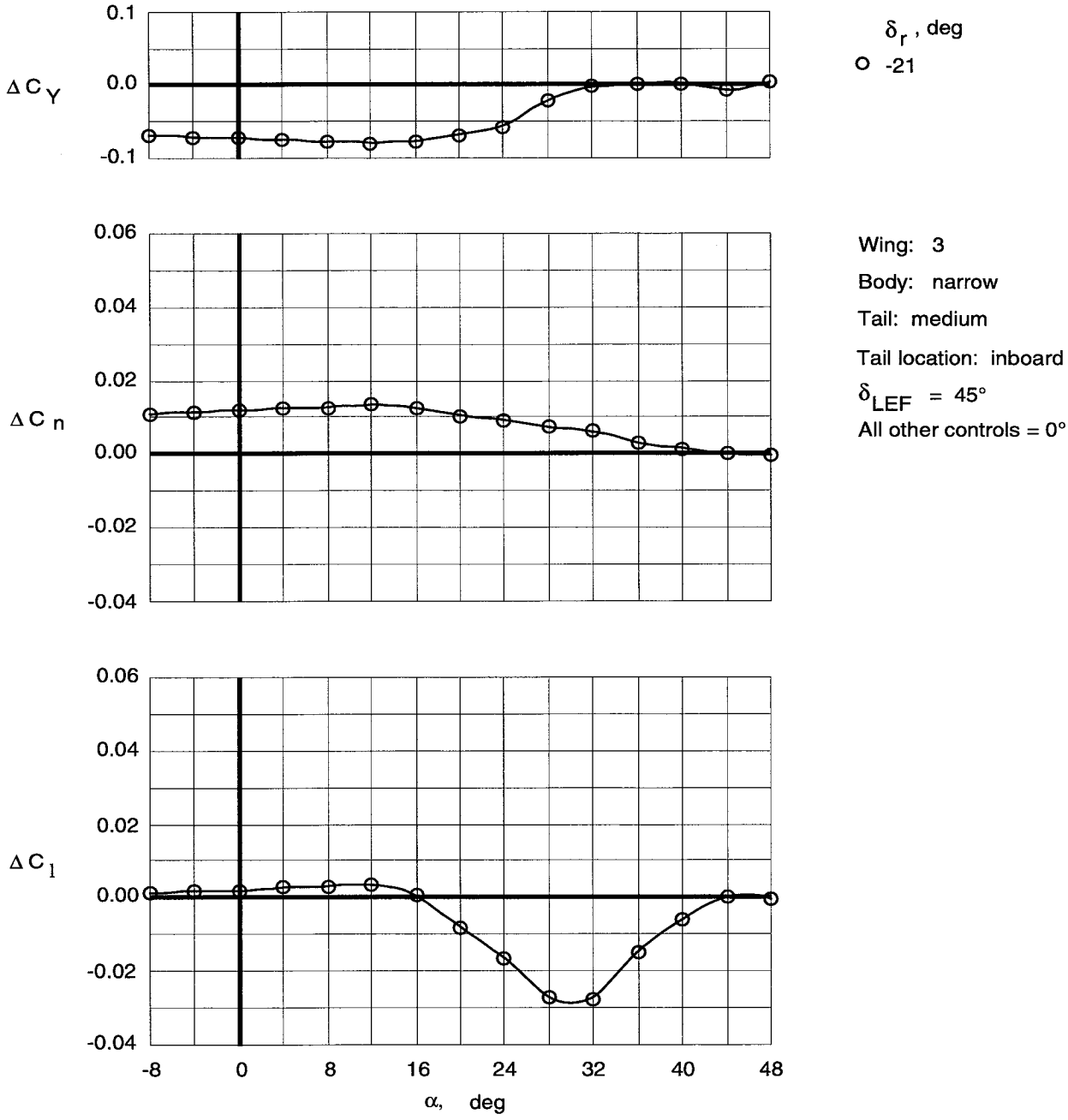

Figure 129. Control effectiveness of deflection of medium vertical tails at inboard location for Wing 3 with narrow top body on and leading-edge flaps deflected.

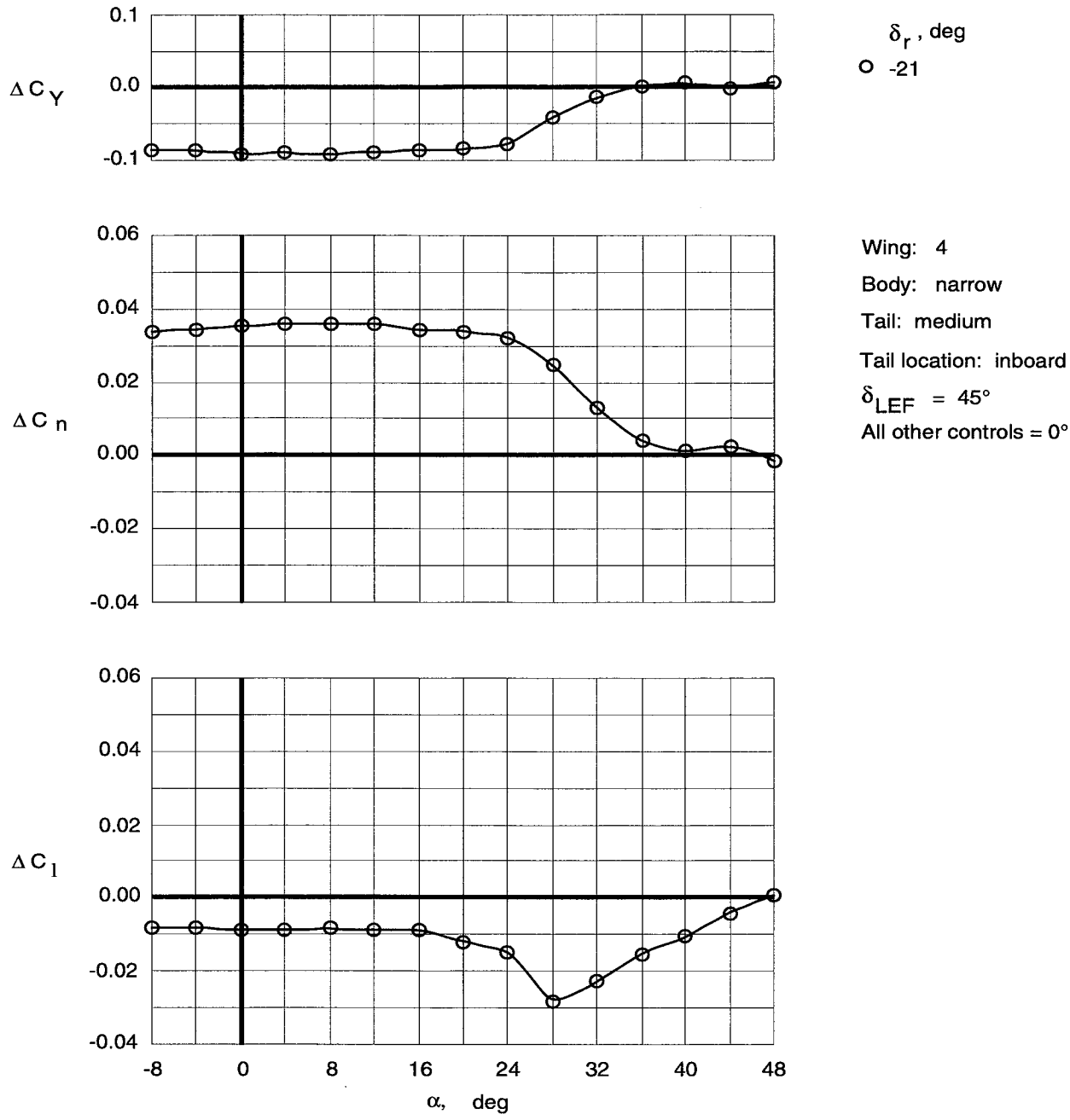

Figure 130. Control effectiveness of deflection of medium vertical tails at inboard location for Wing 4 with narrow top body on and leading-edge flaps deflected.

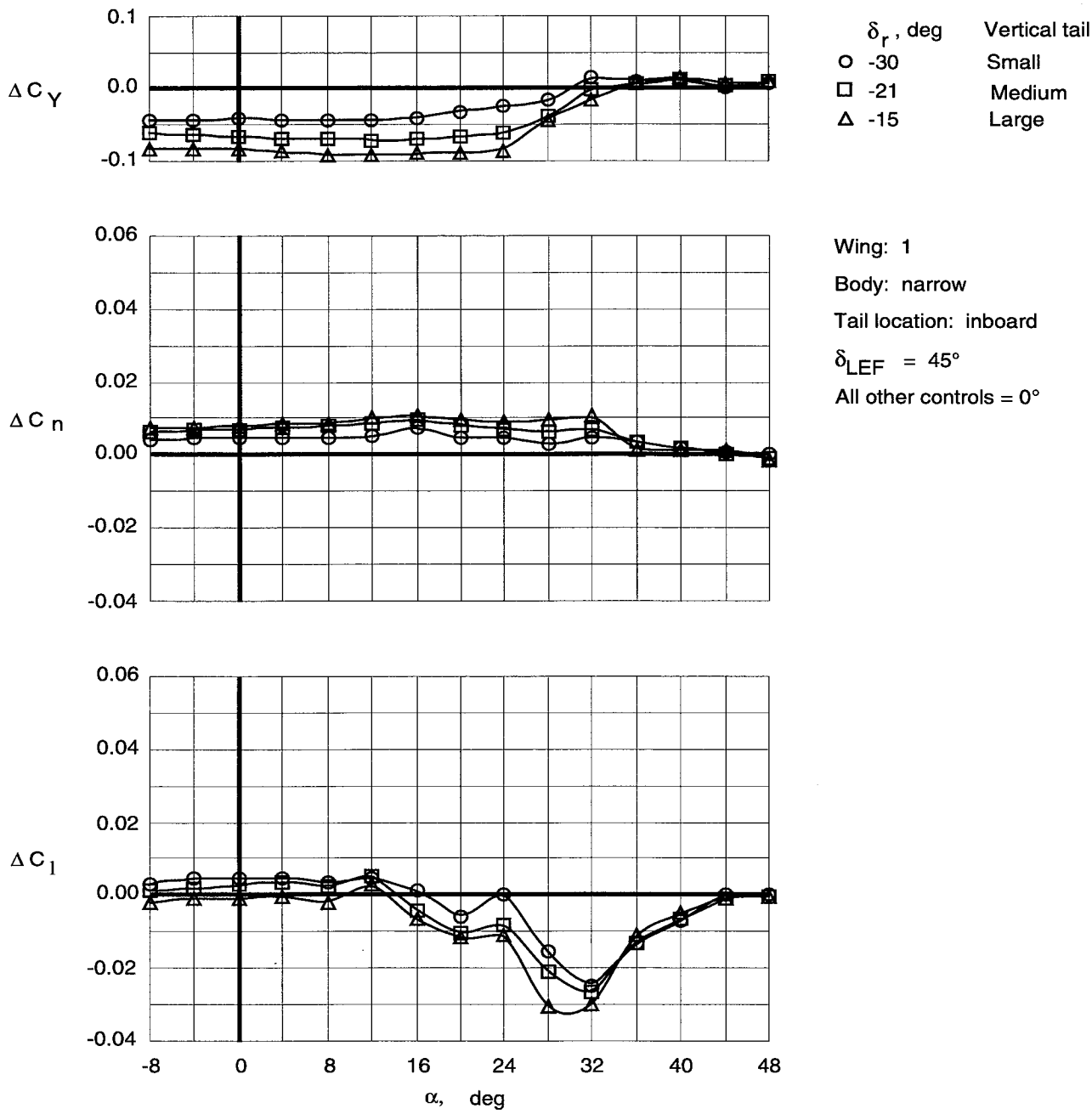

Figure 131. Effect of tail size on control effectiveness of maximum vertical tail deflections for Wing 1 with narrow top body on and leading-edge flaps deflected.

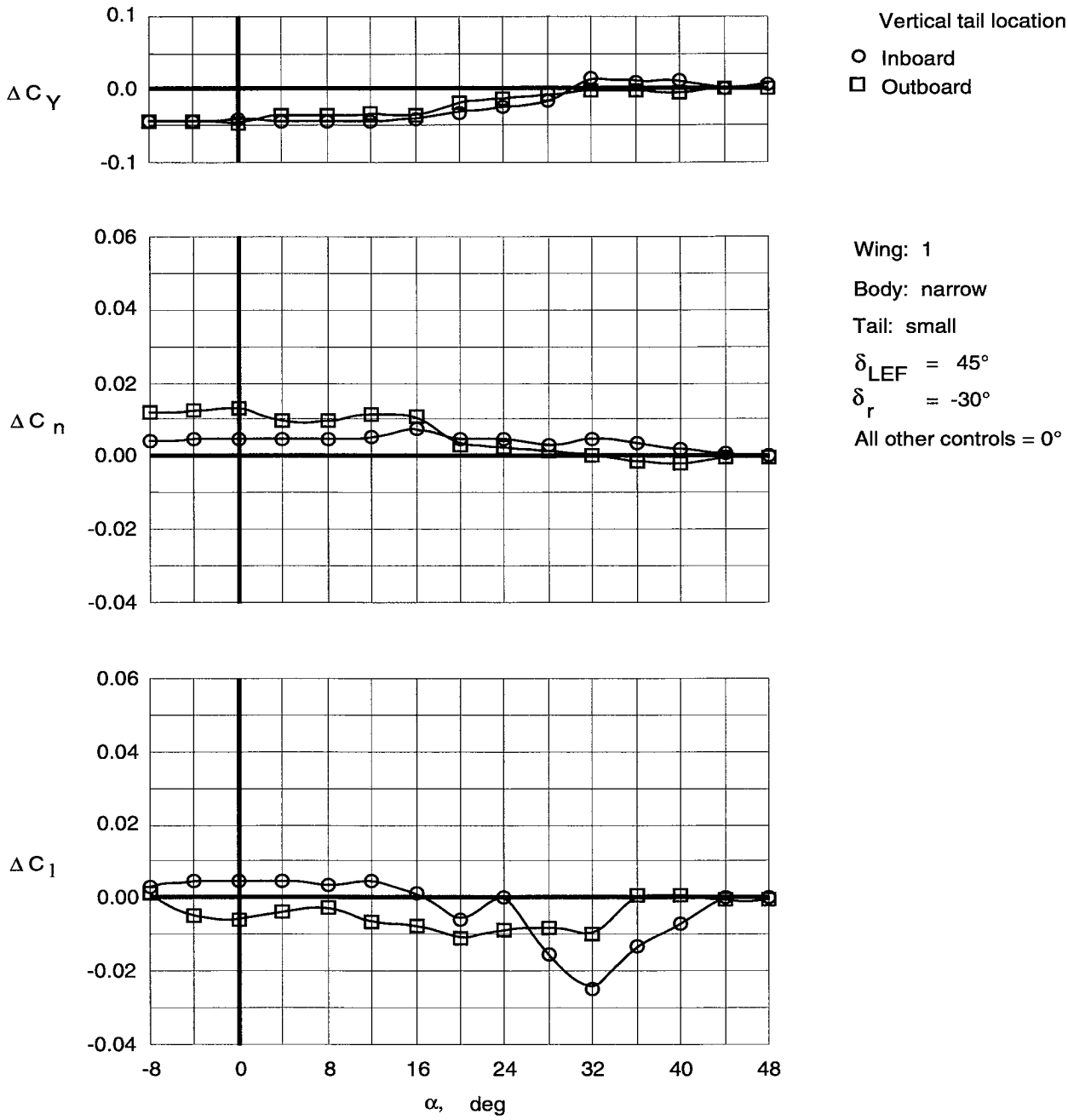

Figure 132. Control effectiveness of –30° deflection of small vertical tails in inboard and outboard locations for Wing 1 with narrow top body on and leading-edge flaps deflected.

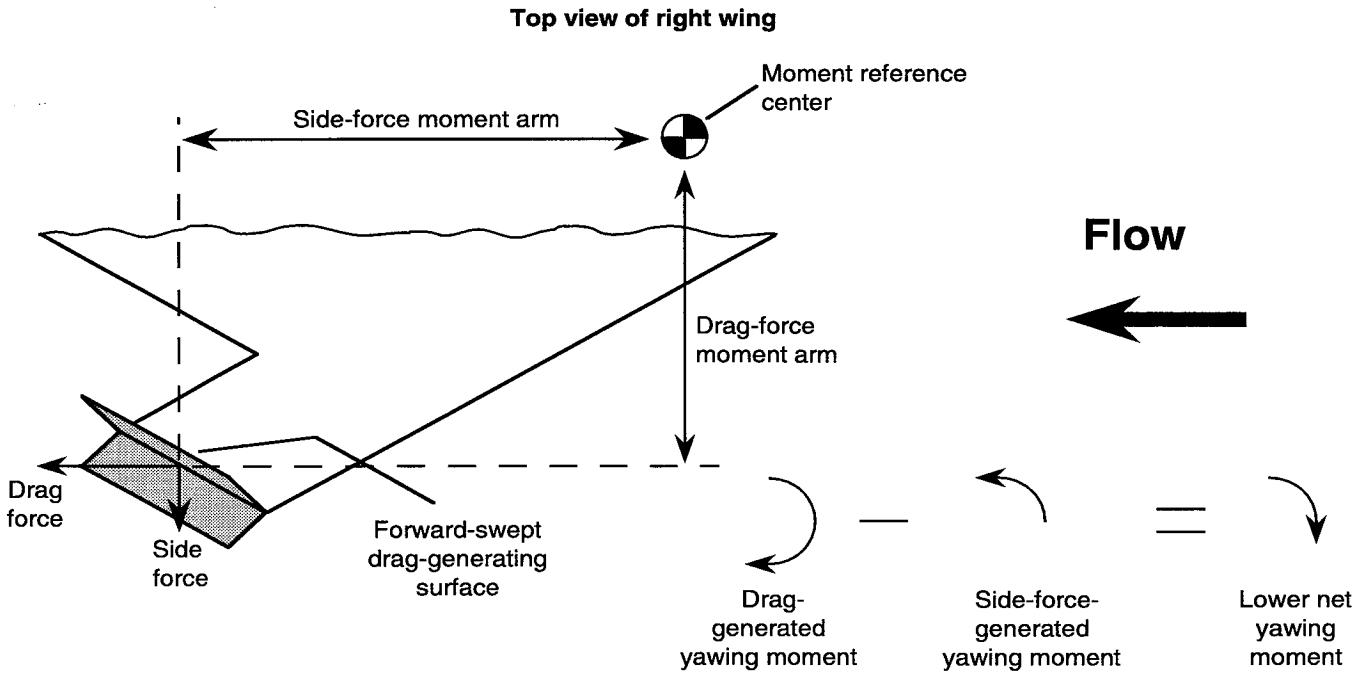

(a) Forward-swept drag-generating surface.

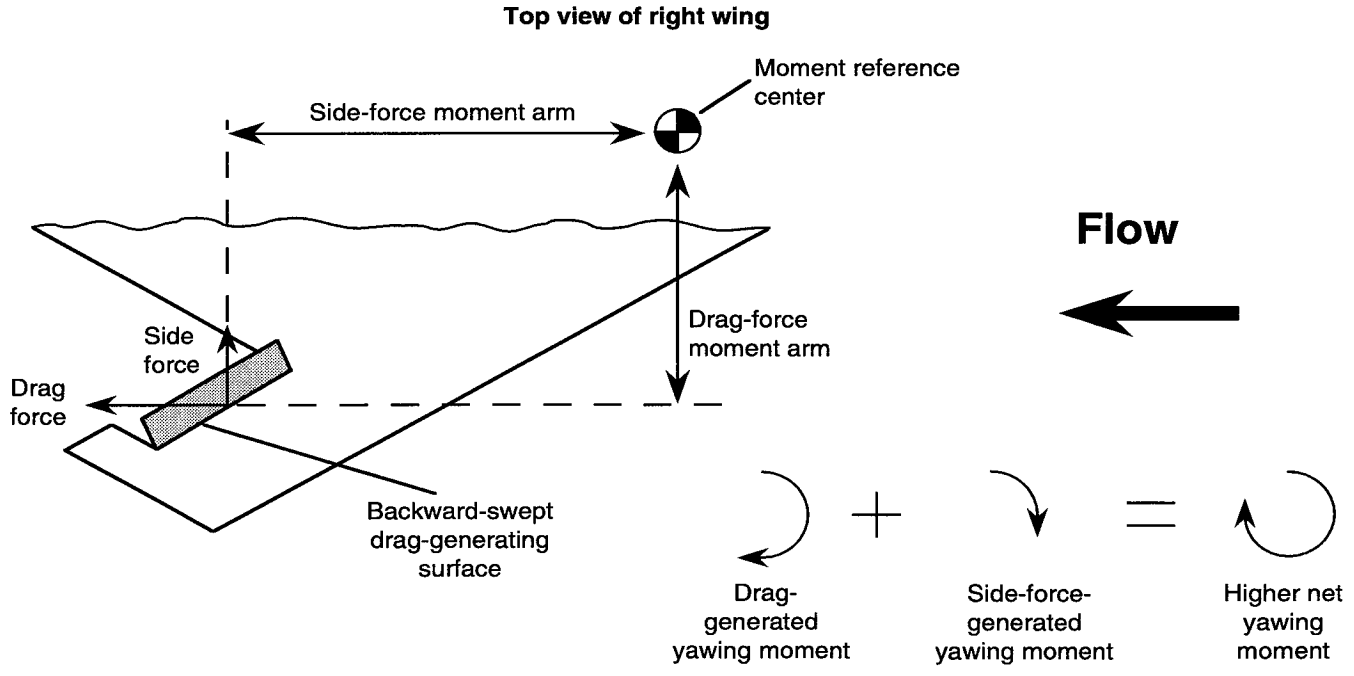

(b) Backward-swept drag-generating surface.

Figure 133. Effect of hinge line sweep of drag-generating yaw control on side force and associated yawing moment generated by control deflection.

REPORT DOCUMENTATION PAGE

Form Approved
OMB No. 0704-0188

1. AGENCY USE ONLY *(Leave blank)*	2. REPORT DATE	3. REPORT TYPE AND DATES COVERED
	August 1995	Technical Memorandum

4. TITLE AND SUBTITLE
Low-Speed Wind-Tunnel Investigation of the Stability and Control Characteristics of a Series of Flying Wings With Sweep Angles of 60°

5. FUNDING NUMBERS
WU 505-68-30-01

6. AUTHOR(S)
Thomas M. Moul, Scott P. Fears, Holly M. Ross, and John V. Foster

7. PERFORMING ORGANIZATION NAME(S) AND ADDRESS(ES)
NASA Langley Research Center
Hampton, VA 23681-0001

8. PERFORMING ORGANIZATION REPORT NUMBER
L-17400

9. SPONSORING/MONITORING AGENCY NAME(S) AND ADDRESS(ES)
National Aeronautics and Space Administration
Washington, DC 20546-0001

10. SPONSORING/MONITORING AGENCY REPORT NUMBER
NASA TM-4649

11. SUPPLEMENTARY NOTES
Moul, Ross, and Foster: Langley Research Center, Hampton, VA; Fears: Lockheed Engineering & Sciences Company, Hampton, VA.

12a. DISTRIBUTION/AVAILABILITY STATEMENT
Unclassified–Unlimited
Subject Category 05
Availability: NASA CASI (301) 621-0390

12b. DISTRIBUTION CODE

13. ABSTRACT *(Maximum 200 words)*
A wind-tunnel investigation was conducted in the Langley 12-Foot Low-Speed Wind Tunnel to study the low-speed stability and control characteristics of a series of four flying wings over an extended range of angle of attack (–8° to 48°). Because of the current emphasis on reducing the radar cross section of new military aircraft, the planform of each wing was composed of lines swept at a relatively high angle of 60°, and all the trailing-edge lines were aligned with one of the two leading edges. Three arrow planforms with different aspect ratios and one diamond planform were tested. The models incorporated leading-edge flaps for improved pitching-moment characteristics and lateral stability and had three sets of trailing-edge flaps that were deflected differentially for roll control, symmetrically for pitch control, and in a split fashion for yaw control. Top bodies of three widths and twin vertical tails of various sizes and locations were also tested on each model. A large aerodynamic database was compiled that could be used to evaluate some of the trade-offs involved in the design of a configuration with a reduced radar cross section and good flight dynamic characteristics.

14. SUBJECT TERMS
Flying wings; Arrow wings; Diamond wings; Reduced radar cross section; Stability and control; High angle of attack

15. NUMBER OF PAGES
156

16. PRICE CODE
A08

17. SECURITY CLASSIFICATION OF REPORT	18. SECURITY CLASSIFICATION OF THIS PAGE	19. SECURITY CLASSIFICATION OF ABSTRACT	20. LIMITATION OF ABSTRACT
Unclassified	Unclassified	Unclassified	